Novel NF-kB mutations in common variable immunodeficiency (CVID)

By

Eunhee (Cindy)

Lee

Supervisors:

Professor Matthew Cook

Professor Carola Vinuesa

Professor Chris Goodnow

Immunology Program

John Curtin School of Medical Research

The Australian National University

Declaration

I hereby declare that this submission is my own work and that to the best of my knowledge and belief, it contains no material previously published nor written by another person nor material which to a substantial extent has been accepted for the award of any other degree or diploma of a university of other institute of higher learning, except where due acknowledgement is made in the text.

(Signed) 

Acknowledgements

I would like to thank my supervisor and mentor, Professor Matthew Cook, for his constant support and push for me to be a better scientist. Furthermore, I would like to emphasize that the research would not have been successful without his creative ideas and thought.

I would like to give thanks to my husband, Rodney Saunders, for supporting my study for the last 5 years and special thanks to my son William Saunders and my daughter Elizabeth Saunders who was born during my PhD period.

I also would like to give thanks to Professor Carola Vinuesa and Professor Chris Goodnow and their post doctoral researchers Dr. Vicki Athanasopoulos and Dr. Keisuke Horikawa for their collaborative work and technical support.

I would like to acknowledge the support provided by all Translational Research Group team members, especially Rochna Chand.

Finally, I would like to express our special appreciation to the participants, patients and their relatives in this project.

Table of Contents

Table of Figures

Table of Tables

Abbreviations

ABIN1	A20 binding inhibitor NF-KB 1
AHD	ABIN homology domain
AICD	antigen inducing cell death
AIHA	autoimmune haemolytic anemia
ANZADA	australian and new zealand antibody deficiency allele
ARD	ankyrin repeat domains
ASK	apoptosis signal regulating kinase1
BAFFR	B cell activating factor receptor
BCL	B cell lymphoma
BCR	B cell receptor
BIR	baculovirus IAP repeat
BLK	B lymphocyte kinase
CARD11	caspase recruitment domain 11
CBM	CARD11, BCL10, MALT1 complex
CC	coiled coil
CCDC50	coiled-coil domain containing 50
CFSE	carboxyfluorescein succinimidyl ester
cIAP	cellular inhibitor of apoptosis
CRISPR	clustered regularly-interspaced short palindromic repeats
CTV	cell trace violet
CVID	common variable immune deficiency
CYLD	cylindromatosis

DAG	Diacylglycerol
DD	death domain
DED	death effector domain
DISC	death inducing signal complex
DLBCL	diffuse large B-cell lymphoma
DR	death receptor
DUB	Deubiquitination
EA	erosive arthritis
ECL	enhanced chemiluminescence
ERK	extracellular signal-regulated kinase
ExAC	exome aggregate consortium
FACS	flourescence- activated cell sorting
FADD	fas-associated protein with death domain
FDC	follicular dendritic cell
GC	germinal centre
GWAS	genome-wide association study
HECT	homologous to the E6-AP carboxyl terminus
HREC	human research ethics committee
HTLV-1	human T-lymphotropic virus Type I
IBD	inflammatory bowel disease
IgAD	IgA deficiency syndrome
IkB	inhibitor of NF-kB
IKK	IkB kinase
IL-1	interleukin-1

IP3	inositol triphosphate
IRAK	interleukin-1 receptor-associated kinase 4
JNK	c-Jun N-terminal kiniase
K48	lysine 48
KO	Knockout
LAC	lymphocyte activation cocktail
LAT	linker ofr activation of T cell
LPS	Lipopolysaccharide
LTβR	lymphotoxin beta receptor
LUBAC	linear ubiquitination chain assembly complex
LZ	leucine zipper motif
MAL	MyD88 adapter-like
MALT	mucosa-associated lymphoid tissue lymphoma translocation protein
MEF	merine embryonic fibroblast
MEKK3	mitogen-activated protein kinase kinase kinase 3
MS	multiple sclerosis
MyD88	myeloid differentiation primary response gene 88
NBD	NEMO binding domain
NEMO	NF-kB essential modulator
NES	neclear export signal
NF-kB	nuclear factor kappa-light-chain-enhancer of activated B cells
NIK	NF-kB inducing kinase
NLR	NOD like receptor

NLS	nuclear localization sequence
NOD	necleotide-binding oligomerization
NRD	NIK responsive domain
OUT	ovarian tumour domain
PB	Plasmablast
PBMC	peripheral blood mononuclear cell
PID	primary immune deficiency
PKC	protein kinase C
PDK1	pyruvate dehydrogenase kinase
PRR	pattern repeat recognition
RA	rheumatoid arthritis
RHD	Rel homology domain
RING	really interesting new gene
RIP	receptor interacting gene
RIPA	radio immunoprecipitation assay
RNF11	ring finger protein 11
RT	room temperature
RTE	recent thymic emigrants
SCF	Skp1, Cdc53/Cullin1, and F box protein
SHARPIN	SHANK-associated RH domain interactor
SLE	systemic lupus erythematosus
SLP-76	SH2 domain-containing leukocyte protein of 76 kDa (SLP-76)
SNP	single nucleotide polymorphism
SOP	standard operating procedure

T1 T2 B CELL	transitional stage 1 /2 B cells
TAB	TAK1-binding protein
TAD	transcription activation domain
TAK	transforming growth factor activated kinase 1
TAX1BP1	Tax1 binding protein 1
TCR	T cell receptor
TEM	effector memory T cells
TEMRA	CD45RA+ effector memory T cells
Tfh	follicular helper T cells
TNFR	TNF receptor
TIRAP	Toll/IL-1 receptor adaptor protein
TLR	toll like receptor
TNF	tumor necrosis factor
TNFAIP3	TNF alpha induced protein 3
TRADD	TNFR1-associated death domain protein
TRAF	TNF receptor associated factor
TRAIL	TNF related apoptosis inducing ligand
TRAM	TRIF-related adaptor molecule
Treg	regulatory T cells
TRIF	TIR-domain- containing adapter-inducing interferon-β
UBC13	ubiquitin-conjugation enzyme 13
UBZ	ubiquitin binding zone
WES	whole exome sequencing
ZAP70	zeta-chain(TCR) associated protein kinase 70kDa

ZnF	zinc finger

List of publications

Lee C. E., Fulcher D., Chand R., Fewings N., Field M., Andrews D., Goodnow C., and Cook M. Autosomal dominant B cell deficiency with alopecia due to a mutation in NFKB2 that results in nonprocessable p100. ***Blood*** 2014 Nov: 124 (19)c 2964-2972

Lee C.E, Athanasopoulos V., Horikawa K., Chand R., Field M., Andrews D., Carola V., Goodnow C., and Cook M. A novel *TNFAIP3* mutation in CVID is rendered pathogenic by a mutation in its interacting partner TAX1BP1. (manuscript in preparation)

Abstract

Common variable immunedeficiency (CVID) is the most common symptomatic primary immunodeficiency. The cardinal manifestations are hypogammaglobulinaemia and recurrent infections. In fact, CVID is a heterogeneous cluster of disorders associated with not only infection but also autoimmune disease, sarcoidosis-like granulomatous inflammation, and neoplasia. In a minority of cases, CVID follows simple Mendelian inheritance, and in other cases, there is familial clustering, with CVID or autoimmunity, and in other cases, CVID is sporadic. The aim of this project was to investigate the genetic and cellular pathogenesis of cases of CVID.

We established a large national cohort of patients with primary antibody deficiencies. First, we discovered a novel heterozygous mutation, S254R in *TNFAIP3* (A20), from two patients with CVID and their family members. Biochemical analysis revealed that the S254R substitution in A20 impairs deubiquitination. Nevertheless, only one patient with the heterozygous (S254R) mutation in *TNFAIP3* exhibited an activated NF-kB and apoptotic phenotype. This patient was also found to carry a mutation encoding an L307I substitution in TAX1BP1, an interacting partner of A20. We investigated this interaction and discovered biochemical evidence that $TAX1BP1^{L307I}$ enhances binding with $A20^{S254R}$. Thus, the A20 phenotype is modified by a TAX1BP1 variant, consistent with non-allelic noncomplementation.

Second, we describe three individuals with complete B cell deficiency within single kindred. We identified a novel heterozygous mutation in *NFKB2* (encoding a D865G substitution) in each affected individual. Mutant p100 is poorly processed, after

activation of the non-canonical NF-kB pathway with CD40L stimulation, both in vitro and in cells isolated from the proband. We discovered that the mutation inhibits p100 phosphorylation. Remarkably, unprocessable p100 exhibits IkB like activity, which serves to sequester p65 in the cytoplasm. In other words, the immune deficiency appears to arise from disruption of both canonical and non-canonical NF-kB pathways.

In summary we have described two novel forms of CVID, one arising from an autosomal dominant mutation in NFKB2, and the other resulting from a low penetrance mutation in TNFAIP3, where the phenotype appears to depend on epistatic interaction with TAX1BP1.

1 Introduction

1.1 NF-kB pathway

NF-kB was discovered by Sen and Baltimore in 1986 as an interacter with the enhancer of kappa light chain. Initially, it was reported that NF-kB was expressed only in the cells that expressed kappa light chains (Sen and Baltimore 1986) and it was therefore named nuclear factor kappa light chain enhance of activated B cells (NF-kB). NF-kB has since been identified in most cells in the immune system and plays a pivotal role in many aspects of immunity. NF-kB is in fact a transcription factor complex. In resting cells, NF-kB complexes are sequestered in cytoplasm in inactive forms by inhibitory proteins of NF-kB. Upon stimulation, NF-kB complexes are liberated from these inhibitory proteins and translocate to the nucleus where they induce gene expression. NF-kB was initially thought to be responsible for acute inflammation but subsequent work has identified many other functions of NF-kB in the immune system. NF-kB regulates expression of many genes including antimicrobial peptides, cytokines, chemokines, stress response proteins and antiapoptotic proteins. Analysis of mice deficient in different NF-kB family members as well as mice lacking different NF-kB inhibitors or IKK subunits demonstrated that proliferation, differentiation, survival and apoptosis of cells in immune responses as well as lymphoid organogenesis require NF-kB. Close regulation of NF-kB appears to be crucial. Reduced NF-kB activation leads to immune deficiency whereas prolonged NF-kB activation leads to inflammation or malignancy associated with tissue damage or uncontrolled cell proliferation (Karin and Greten 2005).

The mammalian NF-kB family consists of 5 members; RELA (p65), c-REL, RELB, NF-kB1 (p50/p105), and NF-kB (p52/p100). Each protein contains conserved Rel-homology domains (RHD) of approximately 300 amino acids length, and dimerization, nuclear-localization and DNA-binding domains (Figure 1.1). Each NF-kB protein can form heterodimers, and all except RELB can also form homodimers. RELA, c-REL and RELB contain a transcription activation domain (TAD), necessary for regulating transcription of target genes after binding to NF-kB binding sites in DNA (Ghosh and Karin 2002; Li and Verma 2002; Ruland 2011).

Expression of some NF-kB subunits is confined to particular types of cells. For example, c-REL was reported to be restricted to haematopoietic cells and lymphocytes and RELB is specifically expressed in the thymus, lymph nodes and peyer's patches. p52 has been reported to be found exclusively in B cells. However, p50 and p65 are expressed widely in various cell types (Li and Verma 2002).

In order to regulate gene expression, p52 and p50 must associate with a TAD-containing NF-kB family member or another protein capable of coactivator recruitment (Hayden and Ghosh 2008). Due to the lack of TAD, homodimers of p50 or p52 were suggested to be the suppressor of transcription (Li and Verma 2002).

In resting cells, homo or heterodimer NF-kB complexes are associated with inhibitors of NF-kBs (IkBs) and sequestered in cytoplasm. They have 6 or 7 ankyrin repeats each containing a 33 amino acid motif, which mediate binding to NF-kB dimers (Figure 1.1). IkBs include IkBα, IkBβ, IkBƐ and BCL-3. p105 and p100, precursors of p50 and p52

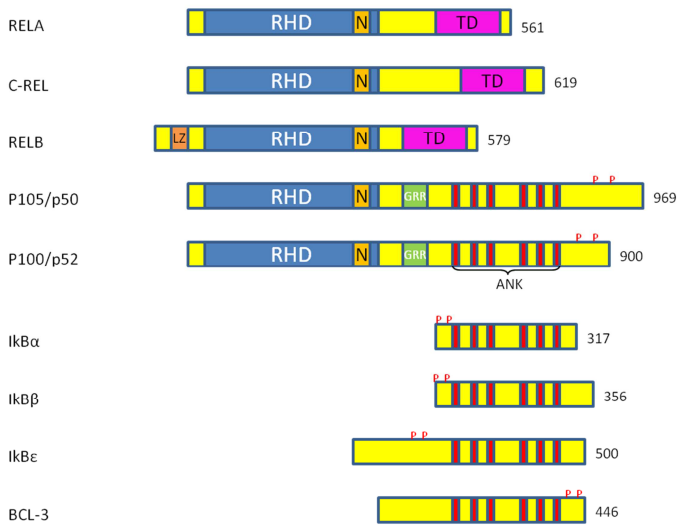

Figure 1.1 Mammalian NF-kB and IkB family members Schematic diagram for different NF-kB members and IkB members are shown. Rel homology domain (RHD), transcription activation domain (TAD), leucine zipper motif (LZ), glycine-rich region (GRR), ankyrin repeats (ANK), nuclear locationzation (N) and phosphorylation site (P) are shown.

respectively, also carry ankyrin repeats, therefore, they are also considered as IkB proteins (Li and Verma 2002). IkB maintains NF-kB proteins in the cytoplasm by masking nuclear localization sequences (NLSs). NLS on NF-kB subunits induces nuclear translocation (Ghosh and Karin 2002). Once NLS are unmasked, dimers can shuttle continuously between the nucleus and the cytoplasm. NF-kB dimers, with exposed NLS, are liberated to enter the nucleus and bind to kB sites to regulate transcription through the recruitment of coactivators and corepressors (Hayden and Ghosh 2008). A strong nuclear export signal (NES) is located at the amino terminus of IkBα. NF-kB complexes containing NES truncated IKBα are found in the nucleus.

After stimulation, IKBα is degraded and therefore the NES no longer exists. As a result, when bound to IkBα, NF-kB-IkBa complexes are expelled from the nucleus and

therefore NF-kB–IkBα complexes are detected mainly in the cytoplasm (Lee and Hannink 2002). Various stimuli result in degradation of IkBs under the action of IkB kinase (Speliotes, Willer et al.) complex activation.

There are two distinct NF-kB signalling pathways designated canonical (or classical) and non-canonical (or alternate) pathways.

1.1.1 Canonical NF-kB pathway

Canonical NF-kB pathway regulates both innate and adaptive immune responses and is activated rapidly in response to a wide range of stimuli such as pathogens, stress signals and pro-inflammatory cytokines. Receptors responsible for activating the canonical pathway include Tumour Necrosis Factor Receptor type 1 (TNFR1), IL-1 receptors (IL-1R), Pattern Repeat Recognition (PRR) such as Toll-like receptors (TLR), NOD like receptor (NLRs) and lymphocyte receptor such as T cell receptors (TCR) and B cell receptors (BCR).

The IkB kinase (Speliotes, Willer et al.) complex regulates the canonical pathway. IKK consists of two catalytically active subunits, IKKα, and IKKβ, and a regulatory subunit IKKγ (also known as regulatory subunit NF-kB essential modulator (NEMO)). While IKKα and IKKβ phosphorylate inhibitors of NF-kB such as IkBα, IkBβ and IkBε, IKKγ regulates IKK complex activation through protein-protein interaction mediated by helix-loop-helix and leucine-zipper motifs (Vallabhapurapu and Karin 2009).

Analysis of *Ikbkb*$^{-/-}$ mice showed that IKKβ is a crucial regulator of the canonical NF-kB pathway. *Ikbkb* deficient mice die prenatally due to TNF dependent liver apoptosis (Li, Chu et al. 1999). Surprisingly, NEMO deficiency is also embryonic lethal. Neither IKBα degradation nor NF-kB activation occurred in NEMO deficient murine embryonic fibroblasts (Romberg, Chamberlain et al.) even though NEMO does not have catalytic activity (Makris, Godfrey et al. 2000; Rudolph, Yeh et al. 2000). By contrast, after TNF or IL-1 stimulation, IKBα degradation and NF-kB activation was similar in IKKα$^{-/-}$ and wildtype MEF.

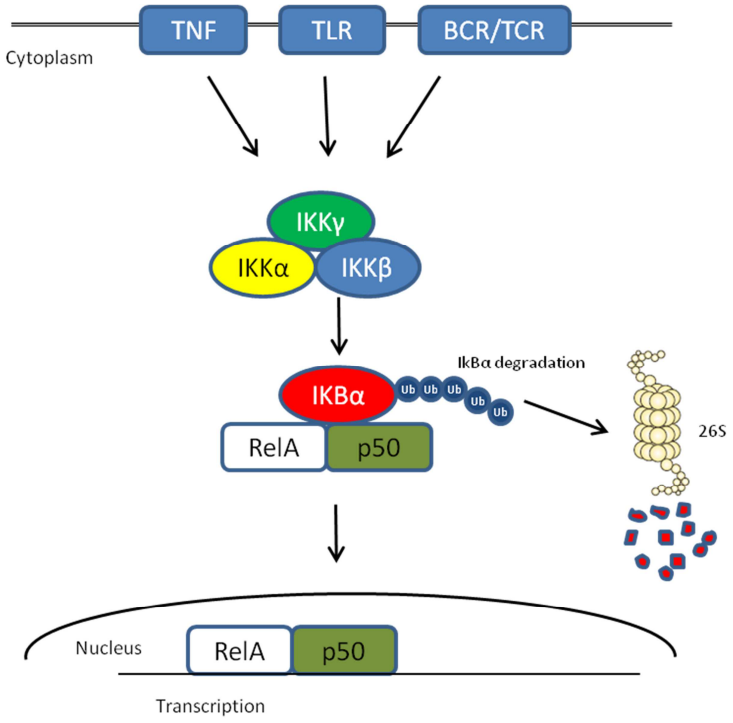

Figure 1.2 Canonical NF-kB pathway. Activation of IKK complex triggers IkBα phosphorylation. Subsequent degradation results in rapid and transient nuclear translocation of the prototypical NF-kB heterodimer such as RelA/p50

These findings indicate that IKKα is dispensable for canonical NK-kB activation, although IKKα can compensate IKB kinase activity in the absence of IKKβ (Hu, Baud et al. 1999; Li, Chu et al. 1999).

Upon stimulation, the IKK complex becomes activated and the IKK complex phosphorylates IkBs at phosphorylation sites (for instance, IKBα on serine 32 and serine 36). Then the Skp1, Cdc53/Cullin1, and F box protein (SCF) containing β transducin repeat containing protein (β-TrCP) E3 ubiquitin ligase complex attaches lysine 48-linked polyubiquitin chains to IKBα at the DSGXXS consensus sequence for ubiquitination. Ubiquitinated IkBs is then degraded by 26S proteosomes (Klionsky, Abdalla et al.). This liberates NF-kB subunits, which enter the nucleus to initiate transcription of NF-kB target genes (Figure 1.2).

After activation by canonical NF-kB stimuli, IkBα is replenished by de novo synthesis of IKBα, which is positively regulated by canonical NF-kB signalling. This represents a negative feedback loop, which prevents prolonged NF-kB activation.

1.1.1.1 A20

Negative regulation of NF-kB regulator by A20 protein encoded by the *TNFAIP3* gene provides another negative feedback loop. A20 was originally identified as a cytokine-induced gene, since robust induction of A20 was seen in human umbilical vein endothelial cells after stimulation with the pro-inflammatory cytokine TNF (hence TNFα induced protein 3, *TNFAIP3*) (Opipari, Boguski et al. 1990). A20 was originally thought to protect cells from TNF-induced cytotoxicity (Opipari, Hu et al. 1992). More

recently, evidence has emerged that A20 is induced not only by TNF, but also by other stimuli including IL-1, CD40, pattern recognition receptors (PRRs), T cell receptors and B cell receptors (Boone 2004; Catrysse, Vereecke et al. 2014).

Evidence from *Tnfaip3*-deficient mice suggests that the principal function of A20 is to terminate exaggerated NF-kB activity. A20 deficient mice died shortly after birth due to multi-organ inflammation and cachexia (Lee, Boone et al. 2000). Embryonic development appeared to be normal. Lee showed that *Tnfaip3*$^{-/-}$ mouse embryonic fibroblasts (Romberg, Chamberlain et al.) failed to terminate prolonged NF-kB activity and were hypersensitive to sublethal doses of TNF and LPS.

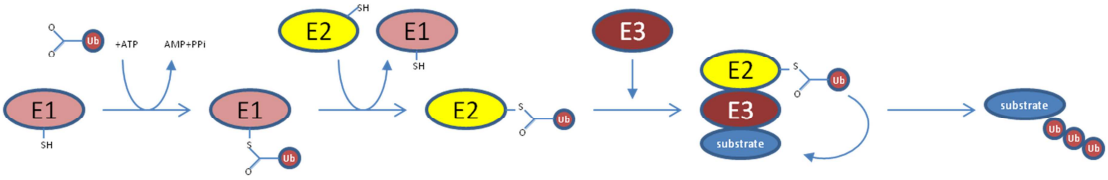

Figure 1.3 Ubiquitination by stepwise ubiquitin enzymes Ubiquitin activating enzymes (E1s) activate ubiquitin in an ATP-Mg2+ dependent manner and form thioester linked complex between the catalytic cystein of the E1 and the C terminus of ubiquitin 96. Activated ubiquitin is then passed from the E1 to ubiquitin conjugating enzymes (E2s) by forming second thioester complex with E2 cysteine. E2s interact with ubiquitin ligases (E3s). E2s and E3s recruit substrates and modify substrates by addition of mono or poly ubiquitin chains.

A20 regulates NF-kB activation by editing ubiquitination. Ubiquitination describes a post translational protein modification in which ubiquitin is covalently attached to a substrate. Ubiquitin is a 76 amino acid peptide (8.5 kDa), which contains 7 lysine residues (K6, K11, K27, K29, K33, K48 and K63). Mammalian ubiquitin is encoded by 4 genes: *UBA52, RPS27A, UBB* and *UBC.*

Ubiquitination proceeds in three steps. E1 enzyme activates ubiquitin by adding ATP, E2 transfers ubiquitin to the substrate protein, and E3 ligase attaches ubiquitin to the substrate (Pickart 2001). Generally, the last amino acid of ubiquitin (glycine 76) binds to a lysine on the substrate protein. Lysine-63 (K63)-linked ubiquitination leads to a protein-protein interaction and consequently regulates signalling whereas K48 linked ubiquitination flags proteins for proteosomal degradation. This process can be reversed by deubiquitination (DUB).

Figure 1.4 Schematic structure of A20 A20 consists of ovarian tumour domain (OTU) and zinc finger domain (ZnF). OTU domain is for deubiquitylating (DUB) activity and catalytic cysteine at position 103 and catalytic histidine at position 256 were known to be critical for DUB activity. A20 contains. While ZnF domain is responsible for E3 ubiquitin ligase activity. Catalytically active ZnF4 introduce K48 linked ubiquitin chains to substrates. NF-kB activity through linear ubiquitin chain can be inhibited through ZnF7.

A20 protein is encoded by the *TNFAIP3* gene located at 6q23 in the human genome. A20 comprises 790 amino acids and weighs approximately 91KDa. A20 is an atypical ubiquitin enzyme (Wertz, O'Rourke et al. 2004). It contains two opposite functions: DUB and E3 ligase at the N- and C-termini, respectively (Shembade, Harhaj et al. 2007). A20 can be located in either cytosol or lysosome membrane (Li, Hailey et al. 2008). It contains an N-terminal ovarian tumour ubiquitin (OTU) domain (1-370aa) and seven zinc finger (ZnF) domains (371-790aa) (Hymowitz and Wertz 2010). The OTU domain has deubiquitylating (DUB) protease activity, which removes K63 linked ubiquitin chains from substrates. The A20 ZnF domain has E3 ligase function, which

catalyzes K48 linkage of ubiquitin chains to substrates, leading to proteasome-dependent degradation (Shembade, Harhaj et al. 2007). DUB and E3 domains of A20 downregulate NF-kB signalling in a two-step process. First K63- linked ubiquitin chains are removed from RIP1 by DUB and then E3 ligase attaches K48- linked ubiquitins to the same substrate (Wertz, O'Rourke et al. 2004).

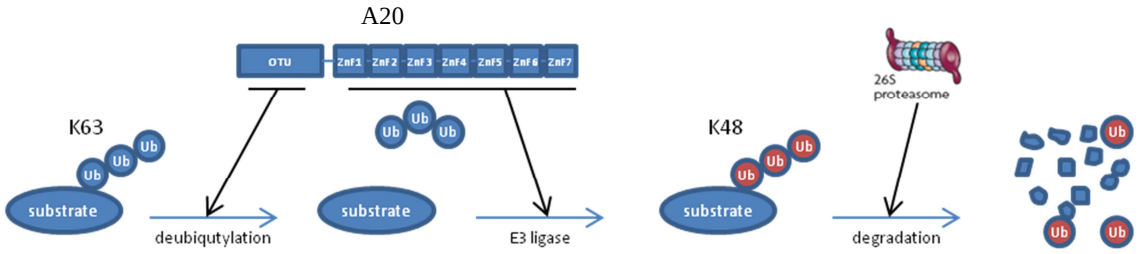

Figure 1.5 Dual functions of A20 modified from Hymowitx and Wertz (2010) Upon TNFa stimulation RIP1 becomes rapidly polyuniquitinated via K63 linkage. A20 then deubiquitinates substrates via OTU domain. RIP1 is then polyubiqutinated via K48 linkage by ZnF domain of A20. K48 linked ubiquitinated RIP1 is subjected to be degradated by proteosome 26S.

The OTU domain contains two active sites, C103 and H256, and amino acid substitutions at either site impairs deubiquitination (Komander and Barford 2008). Even though K63 linked deubiquitinase has been demonstrated in vivo, the isolated OTU domain preferentially deubinquitinates proteins at K48 in vitro (Komander and Barford 2008). This suggests that there are additional factors involved in K63 DUB activity.

The seven cys^2cys^2 zinc finger domain located in the A20 C-terminal has E3 ligase activity. Genetic modification showed that ZnF4 is critical for K48 linked ubiquitin ligase catalytic activity (Wertz, O'Rourke et al. 2004). Recently, it was shown that this ZnF4 was also able to recognise K63 linked polyubiquitin chains (Bosanac, Wertz et al.

2010). In addition, recent evidence suggests that ZnF7 has ligase activity (Skaug, Chen et al. 2011). A20 ZnF7 was shown to inhibit TNF induced NF-kB activation through linear ubiquitin chain assembly complex (LUBAC). Since LUBAC is essential for IKK activation, this mechanism of negative regulation by A20 provides another important feedback loop for NF-kB activation (Tokunaga, Nishimasu et al. 2012; Verhelst, Carpentier et al. 2012).

Recently, $A20^{OTU}$ and $A20^{ZnF4}$ mutant mice, carrying one or two point mutations at active sites, were generated (Lu, Onizawa et al. 2013). These mouse models demonstrated that either DUB or E3 activity alone cannot account for all the functions of A20, since mice remained grossly normal until at least four months of age. Fibroblast from these mice showed decreased NF-kB signalling in response to TNF as compared to A20 deficient cells. Nevertheless, these mouse models demonstrated that OTU and ZnF4 are important motifs that regulate immune homeostasis in vivo, as mutant strains gradually developed splenomegaly and accumulated modestly increased numbers of myeloid cells and lymphocytes (Lu, Onizawa et al. 2013).

1.1.1.2 A20 plays as a negative controller of NF-kB

Canonical NF-kB signalling can be divided into three distinctive pathways according to their activating receptors: TNF, Toll/IL-1R (Speliotes, Willer et al.) and lymphocyte receptor. A20 inhibits NF-kB activation by cleaving K63 linked ubiquitin chains or adding K48 to substrates to block down regulation of signalling. Alternatively, A20 can interrupt NF-kB signalling via non catalytic mechanisms. A20 can interact with E2

enzymes to interrupt E2-E3 interactions which are very important for the down regulation of NF-kB signalling (Shembade, Ma et al. 2010).

1.1.1.2.1 A20 targets canonical NF-kB pathway by TNFa

TNF receptors 1 and 2 are expressed on a wide range of cells. TNFR1 engages with TNF-α and induces receptor trimerization and recruitment of the adapter protein, TNFR1-associated death domain protein (TRADD), to the cytoplasmic tail of the TNF receptor. TRAF2/5 and receptor interacting protein (RIP1) are then recruited and RIP1 is K63 ubiquitinated by TRAF2 (Ea, Deng et al. 2006). Binding of IKKγ to K63-ubiquitinated RIP1 stabilizes IKK interactions with the receptor complex and triggers IKK activation. TRAF2-dependent polyubiquitination of RIP1 recruits transforming growth factor activated kinase 1 (TAK1) and its regulatory subunits TAK1-binding protein (TAB) 1, 2, and 3 to TNFR signalling complex. This results in TAK1 activation, which may phosphorylate the activation loops of the IKK catalytic subunits (Kanayama, Seth et al. 2004; Chen 2005). Mitogen-activated protein (MAP/extracellular signal-regulated kinase (ERK) kinase kinase 3 (MEKK3)) is also recruited to the IKK complex via RIP1, and may be responsible for phophorylation of IKKα and IKKβ (Blonska, You et al. 2004). However, these two kinases are not unequivocally essential for IKK activation in immune cells. It remains possible that IKK activation is induced by autophosphoylation of the IKK complex through conformational change after the interaction between IKKγ and ubiquitinated RIP1 (Yang, Masters et al. 2001; Blonska, You et al. 2004; Vallabhapurapu and Karin 2009) .

K63-ubiquitylation is a pivotal step for IKK recruitment and consequently NF-kB activation. A20 cleaves the K63-linked ubiquitin chain of RIP1 to inhibit signalling and subsequently catalyses the K48-linked ubiquitin chain to RIPK1 to induce proteosomal degradation, which inhibits NF-kB activation (Wertz, O'Rourke et al. 2004). RIP1 is thought to be polyubiquitinated by TRAF2/5 and cIAP1/2. After TNFR ligation, A20 interferes with the interaction between E2 ubiquitin conjugating enzyme, Ubc13, and both E3 ligases TRAF2/5 and cIAP1/2. A20 then catalyses K48 linked ubiquitin chain to Ubc13 and induces the E2 enzyme degradation (Shembade, Ma et al. 2010).

Activation of the canonical NF-kB pathway is also controlled by linear ubiquitin chain assembly complex (LUBAC). LUBAC is composed of SHARPIN, HOIL-1 and HOIP and conjugates the C-terminal Gly76 of a distal ubiquitin moiety to the α-amino group of the N-terminal Met1 of a proximal ubiquitin moiety. NEMO and RIP1 are linearly ubiquitinated by LUBAC upon TNF stimulation. A20 appears to contribute to LUBAC-mediated termination of NF-kB activation. A20 ZnF7 binds to LUBAC and dissociates LUBAC and NEMO to block downregulation of signaling via noncatalytic mechanism (Skaug, Chen et al. 2011; Tokunaga, Nishimasu et al. 2012; Verhelst, Carpentier et al. 2012).

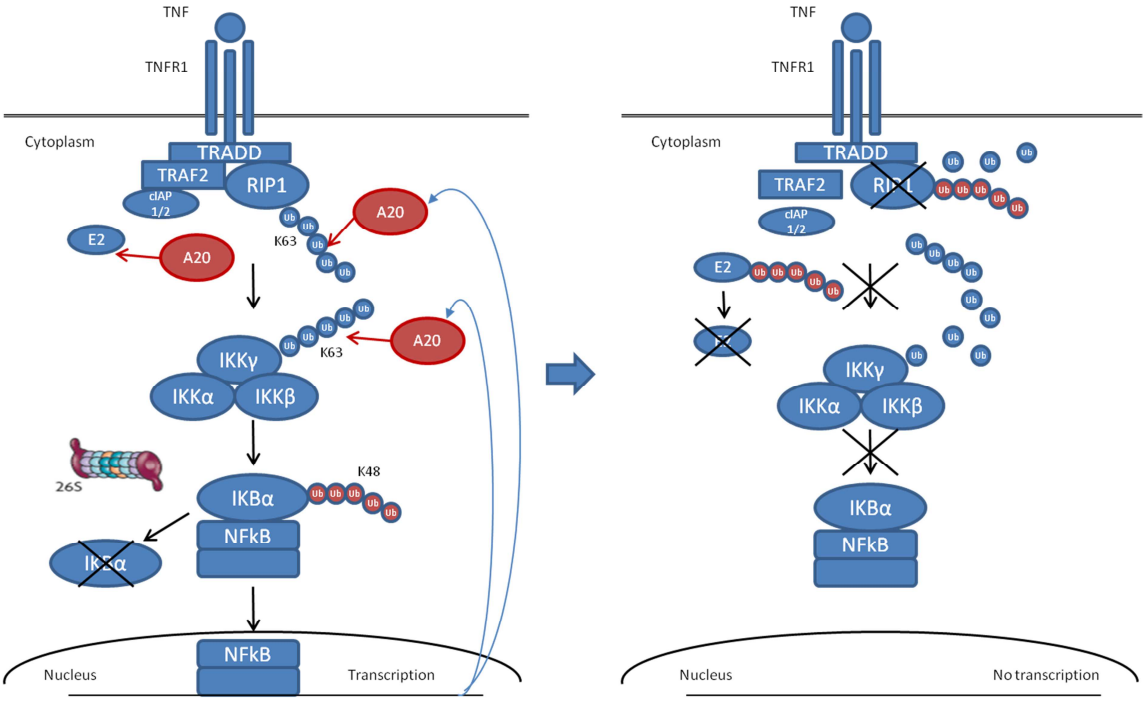

Figure 1.6 NF-kB inhibition by A20 in TNFα induced NF-kB activity Ligation of TNFR1 results in TRAF2/TRF5 and RIP1 recruitment in TRADD dependent manner. TRAF2 ubiquitinates RIP1 and IKK complex is recruited and activated. Activated IKK phosphorylate IKBα and E3 ligase ubiquitilate IKBa via K48 linkage. Proteosome mediated degradation of IkBα releases the NF-kB heterodimers and regulate gene expression. A20 deubiqutinates RIP1 and IKKr and ubiquitinate RIP1 for proteosomal degradation. A20 also target E2 enzymes by introducing K48 linked ubiquitin chains.

1.1.1.2.2 A20 inhibits TLR and IL-1b induced NF-kB

The cytoplasmic regions of the TLR/IL-1R family members share a common motif called the Toll/IL-1 receptor (Speliotes, Willer et al.) domain. TIR domain containing receptors lack intrinsic catalytic activity, therefore, signalling depends on recruitment of adaptor proteins, ubiquitin ligases, and protein kinases. Upon ligand binding, the conformation of TIR domain is altered, and this allows the TIR containing adaptors to interact with the TIR domain (Martin and Wesche 2002). Two major TIR domain containing adaptors are myeloid differentiation primary response 88 (MyD88) and TIR

domain containing adaptor-inducing IFN-β (TRIF). TIR containing adaptor proteins, MyD88 and TRIF, bind to the receptors either directly or via adaptors. Toll/IL-1 receptor adaptor protein (TIRAP, also known as MAL) and TRIF-related adaptor molecule (TRAM) are adaptors for MyD88 and TRIP, respectively. These intermediary adapters are thought to be required for their physical interaction due to electrostatic surfaces. For example, the highly electropositive TIR domain of TLR4 requires electronegative TIRAP to bind highly electropositive TIR of MyD88. Mice deficient in any of these adaptors reveal that they are vital for recruitment of other adaptor proteins, and ubiquitination (Kawai and Akira 2007).

Unlike other TLRs, TLR4 binds to two adaptors (MyD88 and TRIF) and their intermediary adaptors, TIRAP and TRAM, respectively. In the MyD88-dependent pathway, IRAK1, IRAK4 and TRAF6 are recruited, and MyD88 interacts with IRAKs via a death domain. Once IRAK1 and IRAK4 are phosphorylated, they dissociate from MyD88. Phosphorylated IRAK1 and IRAK4 then interact with TRAF6. TRAF6 is an E3 ubiquitin ligase, which polyubiquitinates itself with K63 ubiquitin chains. K63-polyubiquitinated TRAF6, IRAK1, and IRAK4 recruit TAK1 and TAB1, TAB2, and TAB3. TAK1 plus TAB1, 2, and 3 are thought to be responsible for activating the IKK complex. In the TRIF dependent pathway, TRIF recruits TRAF6 by direct interaction, and TRAF6 interacts with Ubc13 and UbcH5c leading to the K63-linked polyubiquitination of TRAF6, and downstream TAK1 and IKK activation. RIP1 is also recruited by TRIF, and might cooperate with TRAF6 to facilitate TAK1 activation (Kawai and Akira 2007).

A20 inhibits NF-kB activation via TRIF pathway by preventing interactions between Ubc13 /UbcH5c and TRAF6. A20 DUB activity removes K63-linked ubiquitin chains from TRAF6 to inhibit NF-kB signaling. In addition, A20 E3 ligase activity catalyses K48 linked ubiquitin chain to Ubs13/ UbcH5c, which leads to their proteosomal degradation (Shembade, Ma et al. 2010).

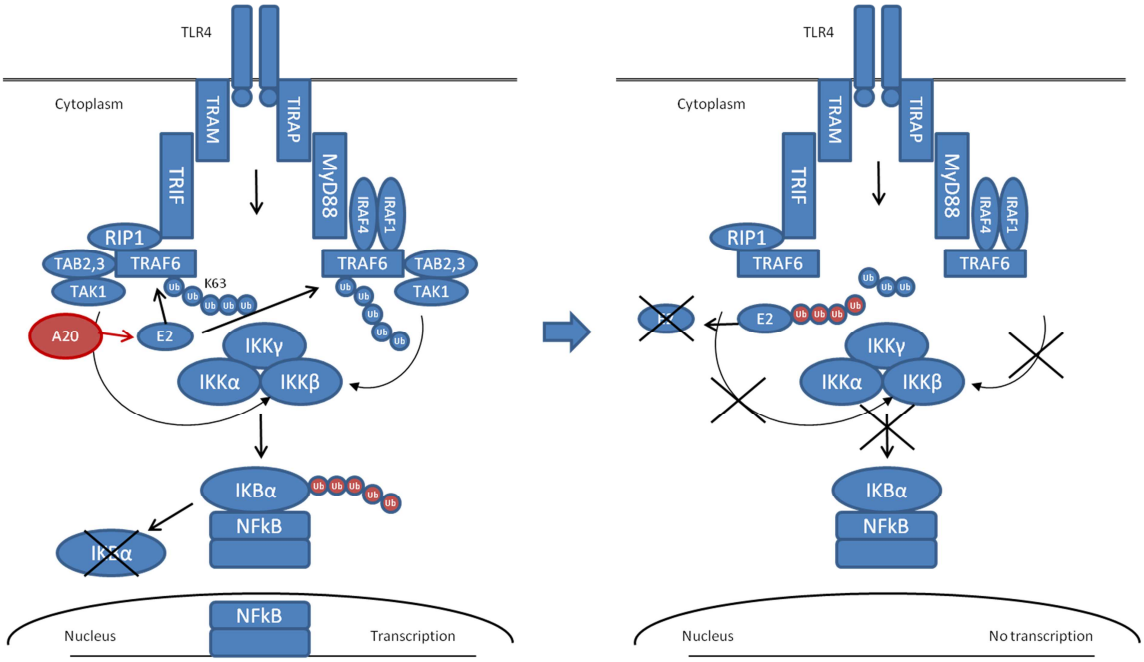

Figure 1.7 NF-kB inhibition by A20 in TLR induced NF-kB activity In TLR4 signalling NF-kB is activated activation via both TRIF and MyD88 dependent pathway with adaptor protein TRAM and TIRAP, respectively. These adoptor proteins recruit TRAF6. Either direct or indirectly with IRAK members, TRAF6 activates TAK1 and TAK1 directly phophorylates IKKβ to activate the IKK complex. A20 deubiquitinates TRAF6 to inhibit its downsignaling. E2 enzymes are targeted by A20 for proteosomal degration.

Besides A20, other inhibitory molecules block TLR4-mediated NF-kB acvtivation. After LPS stimulation, de novo short MyD88 isoform (MyD88s) is generated by alternative splicing (Burns, Janssens et al. 2003; Janssens, Burns et al. 2003).

MyD88s serves as a decoy that inhibits interactions between MyD88 and TRAF6, since MyD88s lacks the intermediate domain essential for the interaction of MyD88 with IRAK4. Dissociation of this complex shuts down LPS induced NF-kB activations. Similarly, IRAK-M is the inactive form of IRAK and interferes with the interaction between IRAK and TRAF6 (Kobayashi, Hernandez et al. 2002)

1.1.1.2.3 A20 inhibits TCR induced NF-kB

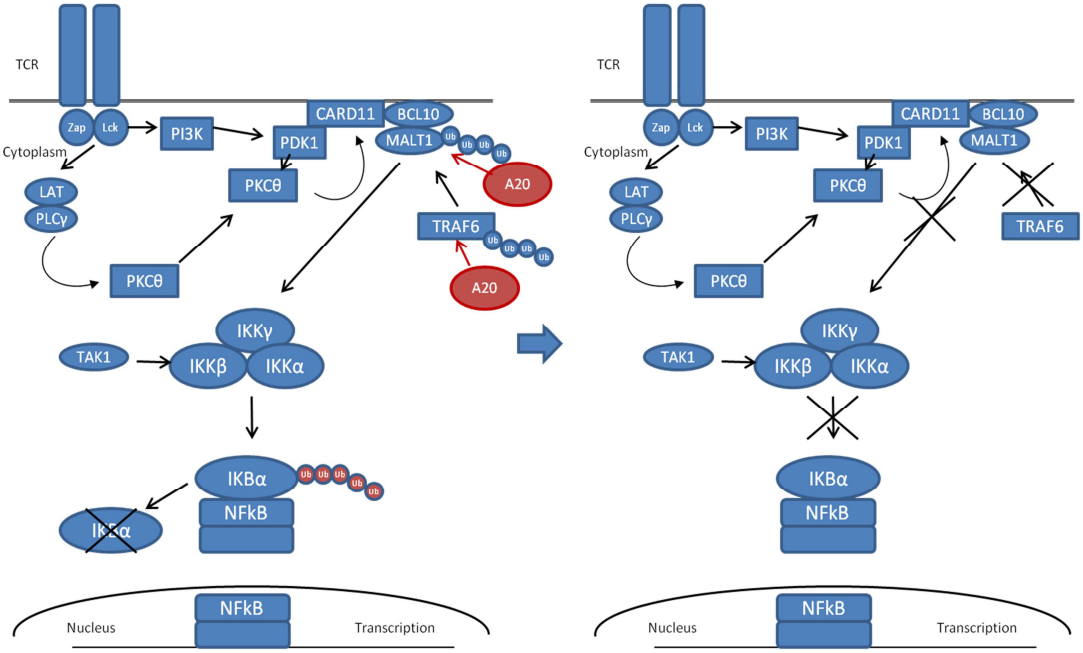

Figure 1.8 NF-kB inhibition by A20 in TCR induce NF-kB activity Src and Fyn and Zap70 are recruited upon TCR stimulation. ZAP70 then pohsphorylates LAT and SLP-76. PLCg1 then becomes activated and leads to PKCc stimulation by generation of IP2, Ca2+ and DAG. PI3K becomes activated through TCR and CD28 signal and facilitates recruitment of PKCc to the immunological synapse. PI3K also phosphorylated phosphoinositides and leads to membrane recruitment of PDK1. Then PKCc becomes activated and recruit IKK and CARD11 into the signaling complex. Phosphorylation of CAR11 then recruits BCL10 and MALT1 and form a stable CBM complex. This complex then activates IKK complex and lead to activation of NF-kB. A20 targets TRAF6 and MALT1 via DUB activity, however, active MALT1 can cleave A20 to terminate its inhibitory function in NF-kB activity.

The protein kinase C (PKC) isoform θ in T cells and β isoform in B cells link TCR and BCR signalling with NF-kB activation. Upon TCR stimulation, Src family kinase Lck, Fyn, and Syk family kinase ZAP70 are recruited and activated. Lck activates PI3K, which in turn activates phosphoinositol and subsequently PDK1. ZAP70 phosphorylation also results in phosphorylation of adapter proteins LAT and SLP-76, which leads to assembly of a multimolecular complex containing phospholipase C gamma (PLCγ) and nucleotide exchange factor, Vav1. PLCγ is then activated resulting in production of inositol triphosphate (IP3), increased intracellular calcium concentration, and formation of diacylglycerol (DAG). DAG activates and translocates PKCθ to the immunological synapse. PKCθ recruitment to the membrane is enhanced by PDK1 after TCR and co-stimulation by CD28 ligation.

PKCθ and PKCβ result in activation of canonical NF-kB signalling via the CARD11, BCL10, MALT1 (CBM) complex. Activation of CARD11 causes a conformational change that allows association with BCL10 and MALT1 (Schulze-Luehrmann and Ghosh 2006). The CBM complex then activates NF-kB via the IKK complex, although the precise mechanism of IKK activation in this pathway remains poorly defined. It has been suggested that TRAF6, an E3 ubiquitin ligase, results in K63 ubiquitylation of MALT1, resulting in activation of the IKK complex. The CBM complex is also thought to ubiquitinate IKKγ via TRAF6 and subsequently activate IKKβ (Sun, Deng et al. 2004). A20 interacts with both MALT1 and TRAF6 to inhibit NF-kB activity by deubiquitylation of K63 from TRAF6 and IKKγ (Duwel, Welteke et al. 2009).

A20 expression is maintained at very low levels in most resting cells. A20 expression is induced when cells are activated by canonical NF-kB stimuli. By contrast, A20 expression is constitutively high in lymphocytes so its NF-kB inhibitory function controls NF-kB activation (Duwel, Welteke et al. 2009). In order to activate NF-kB signalling in lymphocytes, A20 must be degraded or inactivated. In 2008, the Beyaert group discovered that after TCR activation, MALT1 has a specific proteolytic activity and mediates cleavage and inactivation of A20, optimising IKK activation (Coornaert, Baens et al. 2008; Rebeaud, Hailfinger et al. 2008).

1.1.1.3 A20 inhibits apoptosis

Apoptosis, or programmed cell death, is classified as either intrinsic and extrinsic. Intrinsic apoptosis is initiated by the *apoptosome* via mitochondrial signals, and leads ultimately to activation of caspase-9. Extrinsic apoptosis is initiated after extracellular signals lead to receptor-specific activation of signalling pathways involving tumour necrosis factor (TNF) superfamily members. Proapoptotic ligands include FasL and TRAIL, which ligate Fas and DR4/ DR5, respectively (Wagner, Punnoose et al. 2007). Fas recruits Fas-associated death domain (FADD) through homophilic interaction of death domains in the receptor and adaptor. FADD then recruits caspase 8 through a death effector domain (DED) and consequently forms a death inducing signal complex (DISC). DISC then leads to activation of caspase 8 and autocatalytic processing. Cleaved caspase 8 is liberated and moves to the cytosol to target executioner caspases such as caspase 3 and caspase7 to induce apoptosis (Lamkanfi, Festjens et al. 2007).

In 2009, Jin and colleagues reported that DR4 and DR5 simulation induces polyubiqutination of caspase 8 by cullin E3 ubiquitin enzyme. The ubiquitinated caspase 8 binds to the ubiquitin binding protein, p62, and leads to its aggregation and activation (Jin 2009). Polyubiqutination of caspase 8 can be reversed by deubiquitination. Intriguingly, A20 contributes to DISC formation, and physical interaction with DISC has been shown by co-immunoprocipitation (Jin 2009; Bellail, Olson et al. 2012). Apoptosis is inhibited by deubiquitination of caspase 8 and over expression of A20 inhibited apoptosis (Daniel, Arvelo et al. 2004), which is explained by the deubiquitin activity of A20, which can reverse polyubiquitination of caspase 8 (Jin 2009). Further to this, A20 has been reported to inhibit apoptosis via c-Jun N-terminal kinase (JNK) pathways. TNFα induced NF-kB activates JNK pathway through activation of apoptosis signal regulating kinase1 (ASK1) and persistent JNK activation contributes to TNF induced cell death. Interestingly, A20 binds to AKS1 and promotes K48 linked polyubiquitination of ASK1. Proteasomal degradation of ASK1 leads to suppression of JNK activation and eventually blockage of apoptosis (Won, Park et al. 2010).

A20 not only regulates apoptosis directly by actions on apoptotic pathways, but also indirectly, by regulating expression of antiapoptotic genes as a result of NF-kB inhibition. The antiapoptotic actions of A20 are to some extent cell type-specific. In pancreatic β cells, antiapoptotic A20 has been reported (Grey, Arvelo et al. 1999; Liuwantara, Elliot et al. 2006), but in other cell types, proapoptotic functions have been reported for A20, which arise as a consequence of downregulation of antiapoptotic genes through NF-kB inhibition (Tavares, Turer et al. 2010; Kool, van Loo et al. 2011).

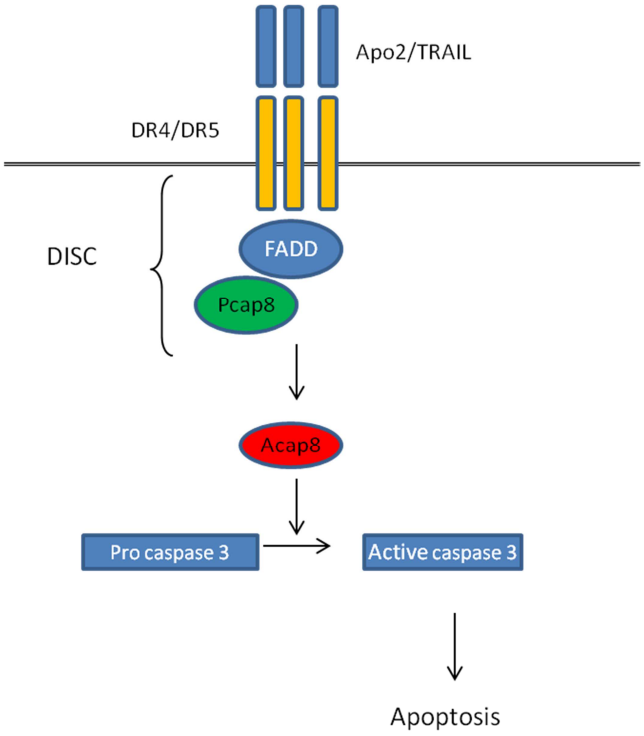

Figure 1.9 Schematic extrinsic apoptotic pathway TRAIL-induced ligation of its cognate death receptors result in recruiting FADD and proactive caspase8 and consequently forming a death inducing signal complex (DISC). The DISC activates capase8 to cleave procaspase3 to become active capase3. Apoptosis is induced by active caspase 3. Pcap8, pro caspase8; Acap8, active caspase8

1.1.1.4 A20 as a disease susceptibility gene

Genome-wide association studies (GWAS) have identified single nucleotide variants in or near A20 that segregate with inflammatory autoimmune diseases including rheumatoid arthritis (RA), juvenile idiopathic arthritis, systemic lupus erythematosus (SLE), inflammatory bowel disease (IBD), coeliac disease, psoriasis, type 1 diabetes, Sjogren's syndrome, systemic sclerosis, and Crohn's disease (Plenge, Cotsapas et al.

2007; Graham, Cotsapas et al. 2008; Han, Zheng et al. 2009; Vereecke, Beyaert et al. 2009; Matmati, Jacques et al. 2011; Ma and Malynn 2012). Two exonic nonsynonymous SNPs, encoding A125V and F127C, have been shown to confer reduced DUB activity of A20. An SNP at a putative 3' enhancer was suggested to alter A20 expression. Taken together, these findings suggest that reduced expression or activation of A20 confers an increased risk of inflammatory and autoimmune diseases. Consistent with this proposition, mice with defects in A20 expression developed SLE or IBD-like phenotypes (Chu, Vahl et al. 2011; Hammer, Turer et al. 2011).

In addition to germline genetic variants, many somatic variants in *TNFAIP3* have been discovered in lymphomas. Biallelic somatic mutations in the coding sequence of *TNFAIP3* that result in stop codons, frame shifts, amino acid changes or splicing alterations have been found in multiple B cell lymphomas, including MALT lymphoma, Hodgkin's lymphoma, diffuse large B cell lymphoma (DLBCL) and follicular lymphoma. A20 acts as a tumour suppressor as reconstitution of A20 in tumour cells showed cell cycle arrest or apoptosis (Compagno 2009; Kato, Ishii et al. 2009).

A20 is considered to be a tumour-promoting factor that supports tumour survival and growth (Vendrell, Ghayad et al. 2007; Hjelmeland, Wu et al. 2010). In addition, normal A20 may be a tumour suppressor (proapoptotic) or tumour enhancer (antiapoptotic) depending on cell type and tumour stage. In summary, loss or reduced A20 function or expression is directly linked to the pathogenesis of human lymphoma or susceptibility to inflammatory diseases such as SLE. A20 is regarded as a disease susceptibility gene and A20 can be a target for therapeutic approach in a broad human diseases.

1.1.1.5 A20 interacting proteins

1.1.1.5.1 TAX1BP1

A20 requires essential contributions from other proteins to exert its functions as a negative regulator of NF-kB. TAX1BP1 was discovered as an A20 interactor in a yeast two-hybrid screen (De Valck, Jin et al. 1999). Interference of TAX1BP1 expression by antisense RNAs attenuated termination of NF-kB activity and promoted apoptosis (De Valck, Jin et al. 1999).

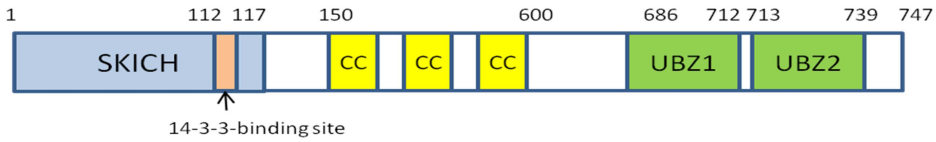

Figure 1.10 Schematic structure of TAX1BP1 It contains SKICH, coiled coil (CC) structures and ubiquitin binding zone (UBZ) domains. SKICH domain contains14-3-3 binding site (RGASTP). The central part contains two helix loop helix (HLH) regions which are responsible for homodimerisation. Two UBZ domains both contain binding motif (PPXY) for WW domain containing proteins. P; proline; X, any amino acid; Y, tyrosine

TAX1BP1 is located at locus 7p15 in the human genome (Nagaraja and Kandpal, 2004). TAX1BP1 localizes in intranuclear speckles, at the Golgi complex, on cytoplasmic vesicles distributed throughout the cytoplasm and near focal adhesion sites in the plasma membrane (Morrison, Reiley et al. 2005; Ulrich, Seeber et al. 2007). Two isoforms of human TAX1BP1 have been reported, and 749 and 783 amino acids are expressed to 86KDa and 90KDa proteins respectively (De Valck, Jin et al. 1999).

TAX1BP1 consists of a novel membrane binding domain, the SKIP carboxyl homology (SKICH) domain, three central coiled-coil regions and two zinc finger domains at the N-terminus. SKICH domains contain 14-3-3 binding sites (RGASTP) but the function of this region is not clear, although SKICH domains have been implicated in membrane localisation (Gurung, Tan et al. 2003). The central coiled-coil domain contains two helix-loop helix regions, and is thought to be responsible for homodimerization and other protein-protein interactions (Chun, Zhou et al. 2000; Ling and Goeddel 2000).

The TAX1BP1 C-terminus contains two zinc finger domains that also bind ubiquitin (UBZ). Both UBZs contain highly conserved motifs PPXY (prolin-prolin-any amino acid-tyrosine), which is thought to bind to WW domain containing proteins (Sudol, Chen et al. 1995). Ubiquitinated substrates such as RIP1 and TRAF6 are thought to bind to TAX1BP1 via the UBZ2. A20 also binds to TAX1BP1 via the same region, suggesting the possibility of TAX1BP1 dimerisation (Iha, Peloponese et al. 2008).

TAX1BP1 inhibits NF-kB induction. Upon TNFα stimulation, TAX1BP1 binds to K63 ubiquitinated RIP1 to block the downstream signalling. Previously, TAX1BP1 was also called T6BP because it was independently discovered as a TRAF6 binding partner. Subsequent studies reveal that TAX1BP1 binds to TRAF6 after IL-1 or LPS stimulation and inhibits NF-kB activity (Shembade, Harhaj et al. 2007). TAX1BP1 lacks ubiquitin editing functions therefore it has been suggested that TAX1BP1 is a scaffold protein that recruits A20 to ubiquitinated substrates to terminate NF-KB signaling (Verstrepen, Verhelst et al. 2011).

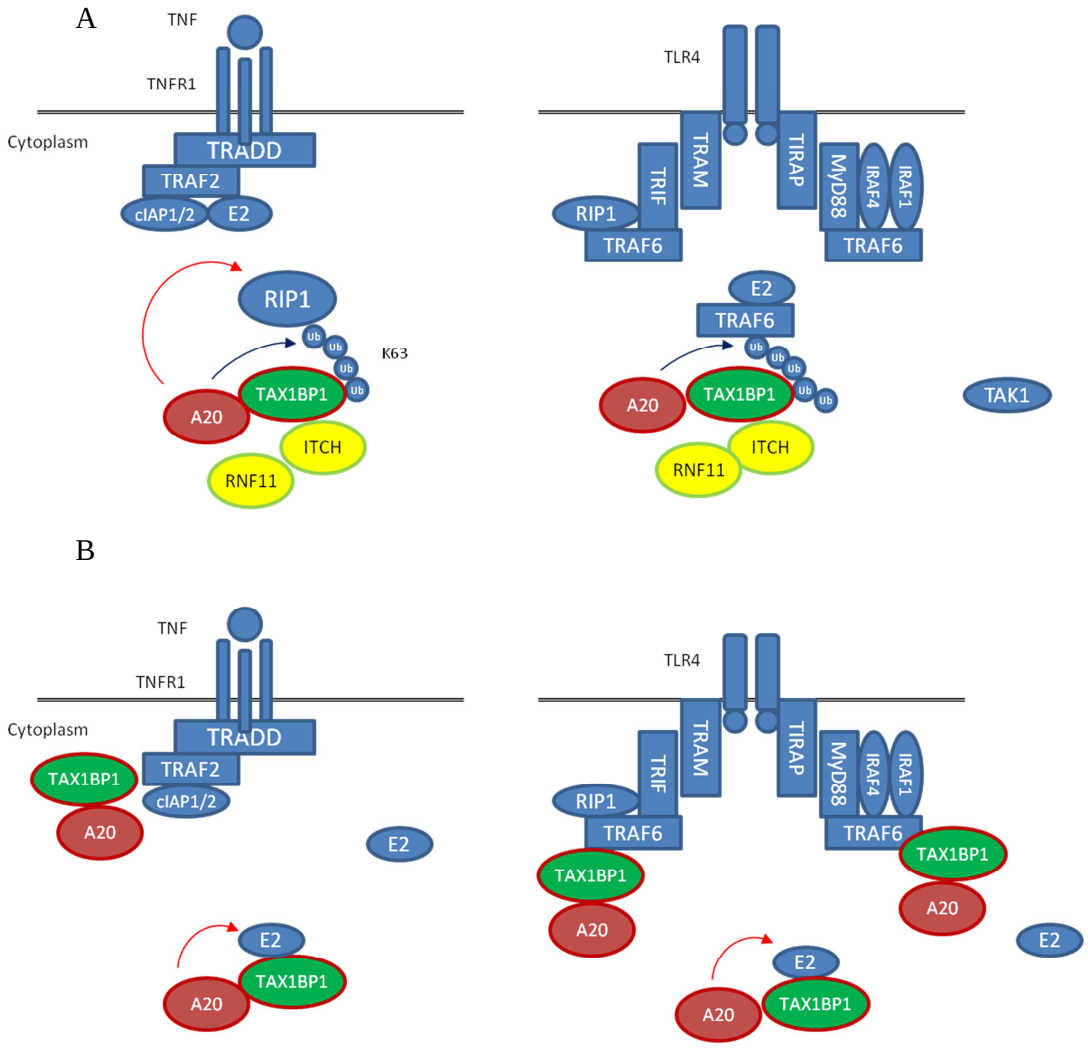

Figure 1.11 Functions of TAX1BP1. (A) TAX1BP1 recognises RIP1 or TRAF6 then recruits A20 to them. A20 then removes K63 linked ubiquitine chains (blue arrow) and attach K48 linked ubiquitin chain (red arrow) for proteosomal degradation. ITCH and RNF11 also exhibit the uniquitin editing process. (**B)** TAX1BP1 binds to E3 emzyme to hinder the interaction with E2 enzyme. TAX1BP1 binds to E2 enzyme directly and recruit A20 to introduce K48 linked ubiquitin chains for proteosomal degradation.

TAX1BP1 also disrupts the interaction between E2 and E3 enzymes. In *TAX1BP1* deficient cells, E2 ligases persist after TNF or IL-1 stimulation while they are degraded

in wildtype cells. Thus, TAX1BP1 may also serve as a scaffold that supports interactions between A20 to the E2 enzymes (UBC13 and UBCH5C), either to permit normal E3 ligase activity or to facilitate K48-ubiquitination of E2s (Verstrepen, Verhelst et al. 2011).

TAX1BP1 controls NF-kB activation by TAX1, a human T-lymphotropic virus type I (HTLV-I) oncogenic protein. Overexpression of TAX1BP1 was shown to inhibit NF-kB activation induced by Tax1, while deficiency of TAX1BP1 enhanced Tax1 induced NF-kB activation. The underlying mechanism of this inhibition is yet to be elucidated, but recently it was demonstrated that Tax1 binds to TAX1BP1-A20 complexes and blocks its inhibitory function.

Overexpression or antisense TAX1BP1 experiments demonstrate that TAX1BP1 has anti-apoptotic properties (De Valck, Jin et al. 1999). It was suggested that TAX1BP1 recruits A20 to a K63 ubiquitylated protein that is involved in apoptotic signalling. Upon TNF related apoptosis inducing ligand (TRAIL) stimulation, Caspase 8 ubiquitylation is an essential for activating 'executioners' Caspase 9 or Caspase 3, which lead to apoptosis. As mentioned previously, A20 is also recruited to this complex and inhibits TRAIL induced apoptosis by deubiquitylating Caspase 8 (De Valck, Jin et al. 1999; Jin 2009).

Tax1bp1 deficiency in mice revealed its essential role in regulation of NF-kB mediated proinflammatory signalling. *Tax1bp1*$^{-/-}$ mice die prematurely from age-dependent hypertrophic cardiac valvulitis (Iha, Peloponese et al. 2008). They also exhibited

hypersensitivity to sublethal doses of TNF and IL-1, a phenotype also observed in *Tnfaip3*$^{-/-}$ mice. After TNF-α, IL-1 and LPS *Tax1bp1*-deficient MEFs show elevated and persistent NF-kB and JNK activation (Shembade, Harhaj et al. 2007). Interestingly, the phenotype of *Tnfaip3*$^{-/-}$ mice was more abnormal than that of *Tax1bp1*$^{-/-}$ mice. It was suggested that A20 might be also contribute to embryonic development independently of TAX1BP1.

1.1.1.5.2 A20 ubiquitin editing complex

A20 and TAX1BP1 also interact with ITCH and RNF11 within a complex that inhibits NF-kB signalling after TNFα, IL-1 or TLR4 stimulation. ITCH was found to coimmunoprecipitate with TAX1BP1 (Shembade, Harhaj et al. 2008; Venuprasad, Zeng et al. 2015). ITCH is a cytoplasmic E3 ubiquitin ligase. Unlike the majority of E3 ubiquitin ligases, which contain really interesting new gene (RING) motifs, ITCH is one of 28 E3 ligases that contain a *homology to the E6 associated protein carboxyl terminus* (HECT) motif. ITCH contains four N-terminal WW domains, which consist of two conserved tryptophans separated by 20-22 amino acids. The HECT domain binds to E2 and transfers ubiquitins to a substrate, and the WW domain binds PPXY motifs to mediate protein-protein interactions (Sudol, Chen et al. 1995).

Itch-/- mice exhibit spontaneous inflammation of lung and stomach, hyperplasia of lymphoid and hematopoietic cell, altered coat colour, and constant scratching (Perry, Hustad et al. 1998; Fang, Elly et al. 2002). Immunological analysis revealed a severe bias to Th2 differentiation, and the majority of their T cells adopt an effector memory T

cell phenotype ($CD44^{hi}$ $CD62^{lo}$) (Fang, Elly et al. 2002). *Itch*$^{-/-}$ cells showed constitutive activation of NF-kB.

RNF11 is RING type E3 ligase of 154 amino acids that also contains an H2 finger domain in its C-terminus, which may facilitate protein-protein interactions (Li and Seth 2004; Shembade, Parvatiyar et al. 2009). RNF11 contains a WW binding domain (PPXY) motif, is predicted to interact with ITCH through this motif, and form a A20 ubiquitin editing complex. *Rnf11*$^{-/-}$ cells showed persistent NF-kB activation upon TNF, IL-1 or LPS stimulation, similar to the signalling defect seen in *Tnfaip3*$^{-/-}$ cells. RNF11 may facilitate termination of NF-kB signalling by ubiquiting substrates, however, the exact function of RNF11 in the complex is yet to be elucidated (Shembade, Parvatiyar et al. 2009).

In summary, A20 interacts with RNF11, ITCH and TAX1BP1, which form an A20 ubiquiting editing complex after cell activation. A20 and substrates bind to TAX1BP1, which together with ITCH, are thought to bind to RNF11 via their WW domains (Hymowitz and Wertz 2010). The details of the physical interaction between TAX1BP1 and ITCH are yet to be determined. TAX1BP1 has been proposed as the scaffold protein of the complex. Scaffolds are normally catalytically inactive but facilitate interactions crucial for efficient signalling. Recently, evidence emerged, however, that the complex depends on TAX1BP1 phosphorylation. After TNFα or IL-1 stimulation, IKKα phosphorylates TAX1BP1 at Serine 593 and Serine 624, promoting interaction among TAX1BP1, A20, ITCH and RNF11 (Shembade, Pujari et al. 2011). It is likely that phosphorylation triggers a conformational change in TAX1BP1, and that the zinc

fingers and PPXY motifs are rendered accessible for recruitment of ITCH, RNF, and A20 and their respective substrates.

1.1.1.5.1 ABIN1

A20 binding inhibitor of NF-kB 1 (ABIN1) was discovered as an A20 binding partner in a yeast two hybrid screen of mouse fibroblasts (A20 as bait) (Heyninck, De Valck et al. 1999). Human *ABIN1* is located on chromosome 5q32. ABIN1 comprises four ABIN homology domains (AHDs), a UBAN domain, a leucine zipper (LZ) structure and a NEMO binding domain (NBD) at its C-terminus containing the YPPM (tyrosine-prolin-prolin-methionine) Src kinase phosphorylation motif. ABIN1 contains four putative nuclear export signals and a nuclear localization, and constitutively shuttles between the cytosol and the nucleus in a Crm1 dependent way (Gupta, Ott et al. 2000).

Overexpression of ABIN1 inhibits NF-kB activation(Verstrepen, Carpentier et al. 2009), while antisense *Tnfaip3* RNA was shown to perturb inhibition of NF-kB activation, leading to the conclusion that the inhibitory function of ABIN1 is mediated by A20. *Abin1* deficient mice exhibit a more severe phenotype than *Tnfaip3*$^{-/-}$mice, suggesting that ABIN1 might regulate NF-kB through additional pathways. ABIN1 is an essential regulator in embryonic development, which is dependent on TNF-induced NF-kB activity. ABIN1 specifically interacts with NEMO via its NBD domain, and facilitates recruitment of A20 to NEMO to exert its deubiqitination activity to the substrate. In addition, ABIN1 inhibits apoptosis by hindering caspase 8 recruitment to FADD.

1.1.1.5.2 CCDC50

CCDC50 (Coiled-Coil Domain Containing 50; YMER) is another A20 interactor, identified by yeast two-hybrid screen (Bohgaki, Tsukiyama et al. 2008). Like other A20 interactors, overexpression of CCDC50 results in termination of NF-kB signalling, whereas reduced expression enhances NF-kB activity. CCDC50 binds directly to its substrate without ubiquitin chains therefore is considered to regulate signalling as an adaptor protein, in a manner similar to NEMO (Bohgaki, Tsukiyama et al. 2008; Tsukiyama, Matsuda-Tsukiyama et al. 2012).

1.1.2 Non-canonical pathway

The non-canonical NF-kB pathway predominantly mediates the activation of RelB/p52. Activation of the canonical pathway is rapid and occurs independently of protein synthesis. By contrast, activation of the non-canonical NF-kB pathway is slow and depends on protein synthesis. Even though NF-kB have been intensively investigated for the past 30 years, the non-canonical pathway is yet to be understood completely, but gene deficient mice indicated that the non-canonical pathway is essential for B cell maturation, lymphoid organogenesis and osteoclastogenesis (Dejardin 2006; Gerondakis and Siebenlist 2010; Zhu and Fu 2010; Novack 2011).

Non-canonical signalling proceeds via processing of p100 (NFKB2) to p52. Unlike constitutive processing of p105 in the canonical NF-kB pathway, p100 processing is tightly regulated by signal induction and is initiated by relatively few stimuli, most notably ligation of CD40, LTβR and BAFF-R.

1.1.2.1 NFKB2

NFKB2 or p100 is a protein of 900 amino acids. Unlike other NF-kB subunits or IkBs, p100 contains both REL homology domain (RHD) and ankyrin repeat domains (ARD). ARDs are thought to inhibit nuclear translocation of transcription factors by covering nuclear localization sequences (NLS), which is located in RHD. ARD has been reported to interact with RHD in p100 and its tight three dimensional structure may prevent p100 processing in unstimulated cells.

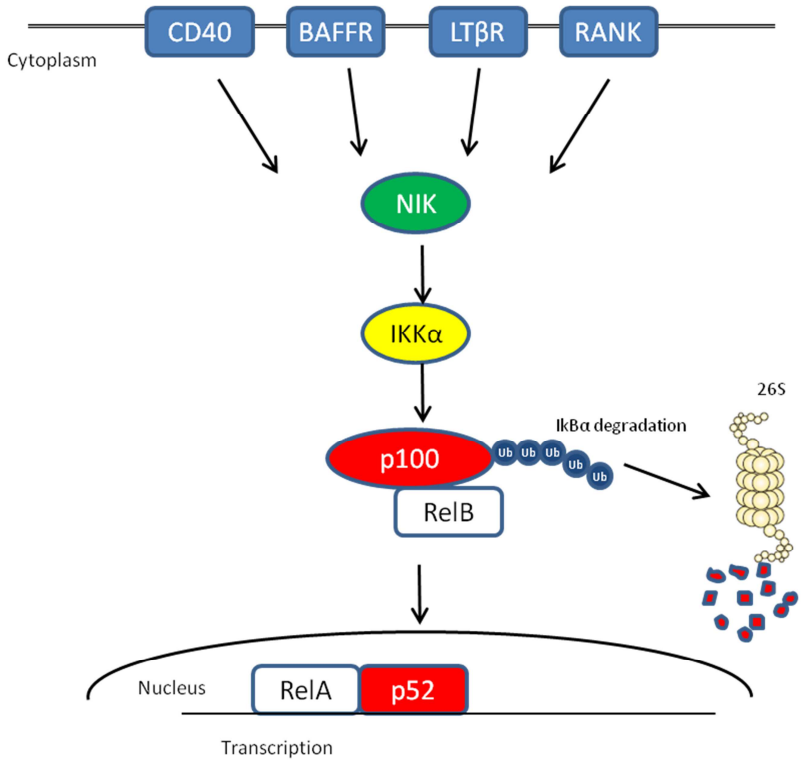

Figure 1.12 Non canonical NF-kB pathway Upon noncanonical stimulation, NIK become stabilized and activated. NIK then activates IKKa and IKKa phosphorylates p100 at the phosphorylation sites. TrCP in SCF E3 liages binds to ubiquitin binding site and ubiquitinates p100 via K48 linkage. C terminal part of p100 is degraded and p52 containing heterodimers enter into the nucleus for gene expression.

The processing inhibitory domain (PID) and NIK responsive domains (NRD are downstream of ARD. The core region of the PID is a death domain (DD), demonstrated to be responsible for inhibition of constitutive p100 processing (Xiao, Harhaj et al. 2001). DD and/or ARD were shown to be negative regulators of p100 processing, as a p100 truncated mutant lacking whole PID or partial ARD underwent constitutive p100 processing (Liao and Sun 2003). The nuclear localization sequence is critical for constitutive p100 processing and location; truncated p100 is translocated into the nucleus. Interestingly, truncated p100 with additional mutations in NLS locate in the cytoplasm and constitutive p100 processing is inhibited, indicating that constitutive p100 processing is dependent on nuclear translocation. One possible explanation for this observation is that the E3 ligases responsible for p100 processing are more abundant in the nucleus (Liao and Sun 2003).

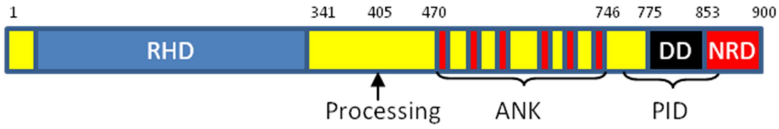

Figure 1.13 Schematic structure of p100 p100 contains Rel homology domain (RHD), ankyrin repeat domain (ARD) processing inhibitory domain (PID), and NIK responsive domain (NRD). PID contains the core inhibitory domain, death domain (DD). NRD is responsible for p100 inducible processing and it contains phorphoylation sites. These sites are phosphorylated by IKKα and bound by βTrCP of SCF E3 ligase upon stimulation.

The NRS is located at the C terminus and is pivotal for p100 processing under normal conditions. Deletion of NRS abolished phosphorylation of p100 and consequently inhibits p100 processing (Xiao, Harhaj et al. 2001). The NRS is phosphorylated by

IKKα in a NIK-dependent manner, tagging the protein for binding by ubiquitin ligase which is necessary for partial degradation in the proteosome.

1.1.2.2 Phosphorylation of p100

Xiao and colleagues discovered that NF-kB inducing kinase (NIK) regulates the processing of NFKB2 (Xiao, Harhaj et al. 2001). NIK is a MAP kinase kinase kinase (MEK3K) and can be activated by both canonical and non-canonical pathways. Originally, NIK was identified as a mediator of TNF/IL-1 induced canonical NF-kB signalling, however, *aly* mice (carrying spontaneous loss of function mutations in *Nik*) and $Nik^{-/-}$ mice showed that NIK was dispensable in the canonical pathway but essential for p100 processing (Shinkura, Kitada et al. 1999).

NIK was initially thought to bind directly to p100 for p100 phosphorylation as a NIK complex isolated from mammalian cells was able to phosphorylate p100. Subsequent studies revealed that IKKα directly phosphorylates p100, and neither IKKβ nor IKKγ are required for p100 processing (Senftleben, Cao et al. 2001; Liang, Zhang et al. 2006).

IKKα can be activated by both canonical and non-canonical stimulation, although in the absence of NIK activation, phosphorylation of IKKα via the canonical pathway fails to phosphorylate p100. This demonstrates that p100 processing depends on NIK through phosphorylation of IKKα. In the absence of NIK, p100 fails to associate with IKKα, which implies that NIK may contribute to this interaction as an adapter protein. Nevertheless, NIK may not simply act as a bridge because only low levels of NIK are required to form relatively high amounts of p100/IKKα complexes. It has been postulated that the three-dimensional conformational structure of p100, formed by both

the DD and the N-terminus, is modified by interactions with recycling NIK, leading to exposure of docking sites for IKKα on p100 (Senftleben, Cao et al. 2001; Xiao, Fong et al. 2004). Finally, IKKα phosphorylates both NIK and p100, which appears to provide a negative feedback loop.

IKKα and NIK result in p100 phosphorylation at serine 866 and serine 870, and phosphorylation at both sites is necessary for p100 processing in vivo, although they appear to be dispensable for p100 phosphorylation by recombinant IKKα in vitro. Serine 872 was also discovered to be a critical phosphorylation site as substitution of this site abolished p100 phosphorylation in vitro (Liang, Zhang et al. 2006).

1.1.2.3 Inhibitory molecules, TRAF2/TRAF3/cIAP1/2 complex

Although NIK mRNA is relatively redundant and undergoes protein synthesis, NIK expression is undetectable in resting cells (Liao, Zhang et al. 2004). This appears to be because of proteasome mediated degradation of NIK mediated by the TRAF2, TFAR3 and cIAP1/2 complex (Zarnegar, Wang et al. 2008). Each of these proteins contains one to three zinc-binding baculovirus IAP repeat (BIR) domain, which has anti- apoptotic activity, and a carboxy-terminal RING domain with ubiquitin ligase activitiy (Salvesen and Duckett 2002; Liston, Fong et al. 2003; Vaux and Silke 2005). BIR domains interact with the N-terminal of TRAF2 (Rothe, Pan et al. 1995). The first two α-helices of the first BIR in the c-IAP1/2 complex are crucial for this interaction (Samuel, Welsh et al. 2006; Varfolomeev, Wayson et al. 2006).

TRAF molecules regulate both canonical and non-canonical pathways. TRAFs were originally identified as adaptor proteins but more recent studies reveal that they have enzymatic function as well. TRAF3/NIK interactions target NIK for continuous degradation by the proteasome. TRAF3 is recruited after different non-canonical stimuli, and is predicted to regulate NIK (Liao, Zhang et al. 2004). Indeed, TRAF3 has been shown to physically interact with NIK. This interaction and subsequent processing of NIK depends on a sequence motif ISIIAQA located between amino acids 78 and 84 of NIK (Liao, Zhang et al. 2004).

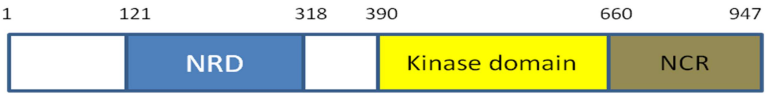

Figure 1.14 Schematic structure NIK It contains negative regulatory domain (NRD), kinase domain, and non-catalytic region (NCR). TRAF3 bins to N terminus of NIK via TRAF3 bindind motif (ISIIAQA) at 78-84 and IKKα and p100 bind to NIK via NCR

Purified TRAF3, however, does not ubiquinate NIK, suggesting that there may be other regulators in the NIK degradation process. (Varfolomeev, Blankenship et al. 2007; Vince, Wong et al. 2007; Vallabhapurapu and Karin 2009). Subsequent evidence has emerged that TRAF2 and the cIAP1/2 complex also regulate NIK abundance.

TRAF2 was originally discovered to be a component of TNFR complexes after TNF stimulation. Two TNFRs, TNFR1 and TNFR2, are present on most cell types and TRAF2 interacts with TNFR1 directly or with TNFR2 through the adaptor protein, TRADD. TRAF2 is itself an adaptor protein in NIK regulation that supports TRAF3 and IAP1/2, yielding the TRAF3-TRAF2-IAP1/2 complex. TRAF2 consists of a highly

conserved TRAF-C domain and a coiled-coil TRAF-N domain. While the C-domain is required for TRAF2 recruitment to the receptor, the N-domain interacts with cIAP1/2 through a baculovirus IAP repeat (BIR) domain (Vallabhapurapu, Matsuzawa et al. 2008). It has been reported that TRAF2 has an anti-apoptotic function and is required to recruit IAPs (Gardam, Turner et al. 2011).

Knock down of TRAF2, TRAF3 or cIAP2 in murine embryonic fibroblasts (Romberg, Chamberlain et al.) resulted in similar phenotypes, with NIK accumulation and abundant p52 production (Grech, Amesbury et al. 2004; Liao, Zhang et al. 2004; He, Zarnegar et al. 2006; Xie, Stunz et al. 2007; Graham, Cotsapas et al. 2008; Gardam, Turner et al. 2011). Thus, it appears that TRAF2, TRAF3 and cIAP2 are all necessary

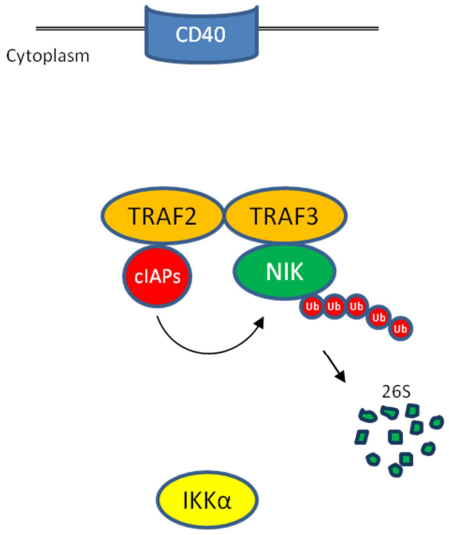

Figure 1.15TRAF2/TRAF3/ cIAP1/2 complex in a resting cell In resting condition, NIK maintains at very low level. NIK is bound by TRAF3 and the cIAP1/2 ubiquitin ligases are recruited to via TRAF3 dimerisation with TRAF2. cIAPs then ubiquitinate NIK via k48 linkage and consequently NIK.becomes degradation by proteosome.

for normal suppression of p100 processing by NIK degradation. While TRAF3 and TRAF2 contribute as adaptor proteins, the cIAP1/2 complex functions mediates K48 ubiquitination of NIK, which leads to its proteasomal degradation (Varfolomeev, Blankenship et al. 2007; Zarnegar, Yamazaki et al. 2008).

1.1.2.4 Degradation of inhibitory molecules upon activation

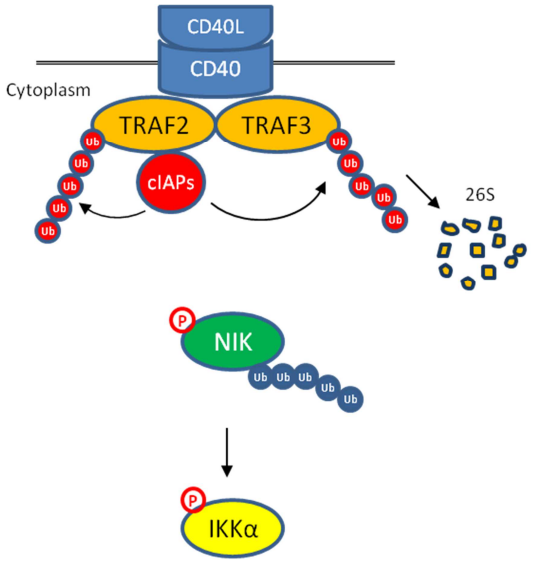

Figure 1.16 NIK activation and stabilization upon stimulation Upon stimulation, TRAF2/ TRAF3 cIAP complex is recruited to the receptor and TRAF2 activate cIAPs to target TRAF2 and TRAF3 for K48 linked ubiquitination. Deradation ofTRAF3 allows NIK to be accumulated and stabilized. NIK then phosphorylates IKKα and IKKα phosphorylates p100 leading to p100 processing

Receptor ligation activates TRAF2, which acts as an E3 ubiquitin ligase to attach K63 to c-IAP1/2. Activated cIAP1/2 complexes are E3 ubiquitin ligases that attach K48 linked ubiquitin chains to TRAF3 molecules, flagging it for proteasomal degradation.

After TRAF3 degradation, activated NIK accumulates. A detailed understanding of the relative preference of IAP1/2 for either TRAF3 or NIK has yet to be elucidated.

1.1.2.5 Ubiquitination of p100

Phosphorylation of the two serine residues at C-terminus of p100 leads to recruitment of the SCF complex E3 ligase. Phosphorylation creates a binding site for β-TrCP, a subunit of the SCF complex. β-TrCP binding site motif was reported as DSGxxxS, a motif that is also found in other proteins including IkBs, p105, β-cat and Vpu (Figure 1.17). β-TrCP of SCF physically interacts with p100 following phosphorylation of serines 866 and 870 in a NIK-dependent manner and stimulates ubiquitination.

IkBα	DDRH**DSGL**D**S**MK
IkBβ	DEWC**DSGL**G**S**LG
IkBε	ESTC**DSGVET**SF
p105	DSVC**DSGVET**SF
β-cat	QSYL**DSGIHS**GA
Vpu	ERAE**DSGNES**EG
p100	EVKE**DS**AYG**S**QS

Figure 1.17 Binding sequences of β-TrCP in human proteins

Physical interaction of β-TrCP with p100 is pivotal for the ubiquitination and processing of p100 (Fong and Sun 2002). The ubiquitin acceptor site of p100 (K856) is located upstream of the phosphorylation site (Amir, Haecker et al. 2004). Polyubiquitinated p100 is then subjected to partial degradation by the S26 proteosome.

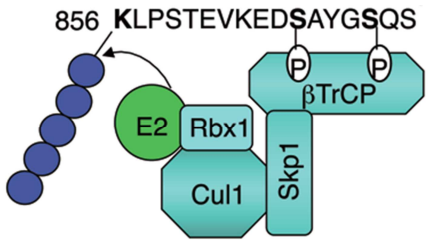

Figure 1.18 SCF E3 ligase complex and binding site of p100 Phosphorylation at serine 866 and serine 870 is a prerequisite for ubiquiting binding. Phosphorylation was thought to create binding docking site for β-TrCP and exhibit E3 ligase activity at K856 (Sun 2011)

1.1.2.6 Degradation of p100 by proteasome S9

The S26 proteasome complex is composed of two subcomplexes: 20S catalytic particle and 19S regulatory particle. S20 forms a cylindrical proteolytic chamber with four stacked heptameric rings. S19 particles are located at both sides and are thought to facilitate 20S by recognizing and recruiting ubiquitinated p100s, unfolding the substrate so that it can enter the proteolytic chamber of the 20S catalytic particle.

The 19S particle is also composed of two subcomplexes: a base and a lid. While the base complex is composed of six AAA families of ATPases and three other proteins, the lid complex is composed of eight non-ATPase proteins. S9 is located in the lid of the 19S subunit and interacts with p100 (Fong, Zhang et al. 2002). The death domain (DD) of p100 appears to be critical for 9S binding, as deletion of the DD of p100 abolished the interaction between DD and S9 (Fong, Zhang et al. 2002). NIK-induced ubiquitination of p100 is a prerequisite for the interaction, however, S9/DD interactions can also be induced in the absence of NIK when the sequences located downstream of the DD of p100 are deleted (Fong and Sun 2002). It was therefore proposed that

ubiquitination induced conformational changes of p100 and rendered DD accessible to S9.

As mentioned above, DD is thought to be a negative regulator of p100 processing as a p100 truncated mutant lacking DD (p100ΔDD) underwent constitutive p100 processing (Xiao, Harhaj et al. 2001). Partial degradation of p100 is required for its constitutive activation, however, it has also been demonstrated that constitutive processing of p100ΔDD is regulated by different mechanism independently of NIK induced ubiquitination (Fong and Sun 2002).

Ubiquitinated p100 binds to S9 and enters the proteolytic chamber of the 20S catalytic particle. P100 is cleaved at residue D415, yielding p52 by partial degradation (Qing, Qu et al. 2007).

1.1.2.7 IKB like function

p100 processing liberates not only p52 but also RELB. p100 /RELB complexes are commonly found in the cytoplasm, and p100 is thought to inhibit RELB translocation to the nucleus, therefore acting as an IkB. The IkB function of p100 is consistent with its structure, which includes an ankyrin repeat domain, commonly seen in other IKBs. The IkB action of p100 was discovered after it was observed that IkBα did not completely abolish retention of p65 in the cytoplasm (Sun, Ganchi et al. 1993; Sun, Ganchi et al. 1994). Subsequent work revealed that p100 bound the p65 complex. (Novack, Yin et al. 2003; Basak, Kim et al. 2007; Tucker, O'Donnell et al. 2007). As a result of this IkB action, p100 processing modulates transcription mediated by both RELB and p52.

More recently, Basak and his colleagues found that p100 interacts with RelA as well as RelB in wildtype MEF, thereby controlling the canonical pathway even in the absence of canonical NF-kB stimuli (Basak, Kim et al. 2007). In 2007, Tucker and colleagues revealed that an ENU strain, *Lym1*, harbours a point mutation in *Nfkb2* that results in a p100 truncation mutant (Y868>X) proximal to the second serine phosphorylation site. In this strain, p100 processing is impaired, and the mice exhibit a more severe clinical phenotype than *Nfkb2* knockout mice. They also showed that unprocessible p100 interfered not only with p52 and RelB translocation, but also canonical NF-kB transcription factor RelA translocation by interacting with RelA (Tucker, O'Donnell et al. 2007). In summary, p100 processing has been demonstrated to control canonical and non-canonical NF-kB pathways.

1.1.3 Crosstalk between canonical and noncanonincal NF-kB pathways

In addition to regulation of canonical NF-kB by p100, other pathways of cross-talk between canonical and non-canonical pathways exist. NIK was originally discovered as a mediator in the TNFα induced canonical NF-kB pathway, however, it is now well known that NIK is an important element in non-canonical NF-kB pathway and accumulation of NIK predominately activates the non canonical pathway. NIK contributes to the activation of canonical pathway when NIK is present in excess. Thus, NIK accumulation seen in TRAF3 deficient cells or in lymphomas resulted in activation of both canonical and non canonical pathways (Zarnegar, Yamazaki et al. 2008; Demchenko, Glebov et al. 2010; Pham, Fu et al. 2011).

RIP1 may be involved in inhibition of non-canonical pathway. RIP1 is an important adaptor protein in TNFR-induced canonical NF-kB pathway. As mentioned above TNFR1 activates the canonical NF-KB pathway. Surprisingly, TNFR1 has an intrinsic activity to activate the non-canonical pathway. However, the non-canonical NF-kB activation is not induced by TNFR1 under normal condition because RIP1 inhibits the non-canonical NF-kB activation by stabilizing TRAF2 and cIAP2 in a manner that the kinase activity of RIP1 is not required. Upon TNF stimulation RIP1 deficient cells induced p100 processing due to degradation of TRAF2 or and cAIP1 (Gentle, Wong et al. 2011; Kim, Morgan et al. 2011). RIP1 may be also involved in inhibition of TRAF2 recruitment to TNFR1.

1.2 Functions of NF-kB signalling in immune system

NF-kB was discovered as a key regulator of inducible gene expression (specifically kappa light chains) in the immune system. Subsequent work has identified many functions of NF-kB in the immune system. The analysis of mice deficient for different NF-kB family members as well as mice lacking different NF-kB inhibitors or IKK subunits demonstrated that they play a major role in differentiation, proliferation, apoptosis and lymphoid organogenesis in immune system (Table 1.1).

NF-kB signalling is involved in primary lymphoid organ development (bone development and thymus architecture) and secondary lymphoid organogenesis (splenic architecture, B cell follicles, marginal zones, lymph nodes, Peyer's patches and germinal centres) (Gerondakis and Siebenlist 2010; Hayden and Ghosh 2011). Several NF-kB knockout mouse models have shown that the non-canonical NF-kB pathway is

crucial for lymphoid organogenesis. These models include mice deficient in RelB or NIK or with compound deficiency in NFKB2 and Bcl-3 or harbouring inactivating mutations of IKKa or NIK (Matsushima, Kaisho et al. 2001; Senftleben, Cao et al. 2001; Weih, Yilmaz et al. 2001; Paxian, Merkle et al. 2002; Yilmaz, Weih et al. 2003; Zhang, Wang et al. 2007). NF-kB regulates lymphoid tissues by inducing mediators of lymphoid organogenesis such as CXCL12, CXCL13, CCL19, CCL21, MadCAM, TNFα and LTα1β2 (Ruddle and Akirav 2009; van de Pavert and Mebius 2010). FDCs produce CXCL13 to attract B cells to form B cell follicles, and abnormal non-canonical NF-kB pathway activation via LTbR inhibits normal formation of B cell follicles (Mebius and Kraal 2005).

NF-kB signalling is also known to be pivotal in lymphocyte development. Pre-B cells or double negative stage IV T cells showed high levels of nuclear NF-kB activity and inhibition of NF-kB by IkB a super-repressor allele results in apoptosis of these cells due to the failure of induction of anti-apoptotic protein A1. In both cases, NF-kB is thought to confer cell survival due to signals that depend on the pre-lymphocyte receptor (Feng, Cheng et al. 2004; Jimi, Phillips et al. 2005). In later stages of T cell development, double positive T cells (CD4+ CD8+) undergo positive and negative selection to become single positive T cells (CD4+CD8- or CD8+ CD4-). In this compartment, NF-kB activity appears to be proportional to lymphocyte antigen receptor binding affinity(Kishimoto, Surh et al. 1998; Hettmann, DiDonato et al. 1999), which in turn contributes to proapoptotic or antiapoptotic responses. During positive selection, NF-kB activity confers survival factors, although NF-KB appears to sensitize thymocytes to apoptosis in negative selection (Kishimoto, Surh et al. 1998; Hettmann,

DiDonato et al. 1999). Genetically modified mouse models reveal that RelA is predominantly expressed in the thymus cortex while Relb and cRel were highly expressed in the medulla. Furthermore, RelB-/- mice showed severely impaired negative selection(Gerondakis, Grumont et al. 2006).

During B cell development, negative selection eliminates B cells which bind to antigen with strong affinity. NF-kB contributes to this response, although by contrast with negative selection in the T cell compartment, NF-kB activity is reduced in during B cell negative selection (Wu, Lee et al. 1996). In mature B cells constitutive low grade nuclear expression of both canonical and non-canonical NF-kB was reported in resting cells and it was thought to be required for B cell survival (Gerondakis and Strasser, 2003; Claudio et al., 2006). Pro- pre B cell maturation require RelA while late B cell maturation from T1to T2 stage of B cells requires BAFFR mediated non-canonical pathway (Klionsky, Abdalla et al.).

NF-KB is also required in lymphocyte differentiation after stimulation by antigen. In the case of CD4+ T cells, T_H0 cells differentiate into T_H1, T_H2, T_H9, T_H17, T_H22 and inducible Treg, and this differentiation is regulated by transcription factors T-bet, GATA3, PU.1 RORγt and FOXP3, respectively. NF-kB was shown to be involved in induction of this transcription factors (Corn, Hunter et al. 2005). NF-kB allows lymphocytes to survive from antigen inducing cell death (AICD) by inducing anti apoptotic genes including A1 and BCL-X_L. c-Rel deficient cells were rescued from apoptosis by transgene expression of antiapoptotic gene BCL2 (Grumont et al., 1998).

Furthermore, NF-kB plays an important role in myeloid differentiation. *c-Rel* and *Rela* were reported to be vital components in erythrocyte differentiation in vivo and monocyte differentiation in vitro (Grossmann, Metcalf et al. 1999; Gerondakis, Grumont et al. 2006). IKKb also negatively control neutrophils proliferation. *Ikbkb*$^{-/-}$ myleloid cells resulted in massive neutrophilia(Greten, Arkan et al. 2007).

Table 1.1 Phenotype of knockout mice for NF-kB signalling components

Type		Mutated gene	Phenotype of Knockout mouse
NF-kB	Single	RelA (p65)	Died at E15.5-E16.5; TNF dependent liver apoptosis; defect in lymphocyte activation, sensitivity to TNF
		NFKB1	Survival to adult; defect in lymphocyte activation
		NFKB2	Survival to adult; disruption of splenic and lymph node architecture; defective T cell response
		RelB	Died postnatally from multi organ imflammation: T cell infiltration of organs, skin inflammation; required for dendritic cell development
		C-Rel	No developmental defects; defects in lymphocyte and macrophage functions; impaired T cell and B cell activation
	Double	RelA and NFKB1	Died at E13.5-E14.5, defects in b LYMPHOPOIESIS
		RelA and c-Rel	Died at E13-E13.5 early liver apoptosis; skin epidermus development
		NFKB1 and c-Rel	Decreased humoral immunity, lack of germinal centres
		NFkB1 and NFkB2	Died postnatally; lack mature B cells and osteoblasts; reduced growth, craniofacial abnormalities
		NFkB1 and RelB	Died postnatally owing to immune deficiency , B cell developmental defects
	Partial deletion	NFKB1 ΔC	Splenomegaly; enlarged lymph nodes; infiltrations of lyung and liver; susceptibilit to pathogens Die postnatally owing to immune deficiency
		NFkB2 ΔC	Died postnatally owing to immune deficiency; multiple organ defects
		C-Rel ΔC	Lymphoid cell hyperplasia
IKK		IKK1	Defects in keratinocyte differentiation, bone and limb development and mammary epithelial proliferation, no mature B cells, impaired RANKL induced NF-kB activation and NIK induces p100 processing
		IKK2	Died at E13.5-E14.5 owing to TNF dependent liver apoptosis, impaired NF-kB activaton by IL-1, TNF and LPS
		NEMO	Died at E11.5-E12.5 owing to TNF dependent live apoptosis, no induced NF-kB activation in MEFs
NF-KB inhibitor		IkBa	Early neonatal lethal inflammatory dermatitis and granulocytosis; constitutive NF-kB activity increased in lymphocytes
		IkBe	NO defect in NF-kB activation; lack severe immune defects; reduction in number of CD44-CD25+ T cells
		Bcl-3	Disrupted splenic architecture; defects in B and T cell responses to antigens
		A20	Died postnatally with multiorgan inflammation and chacasia
		TAX1BP1	Died postnatally with cardiac valvulitis

ΔC, carboxy terminal deletion; E, embryonic day

1.3 Mutations in Human NF-kB

In the past few years, several variants in NF-kB signalling have been identified in humans with various forms of pathology (Geha, Notarangelo et al. 2007). Many of these have been identified by whole exome sequencing.

As described above (refer to 1.1.1.2.3), caspase recruitment domain (CARD) 11 gene encodes a protein that acts as a scaffold for NF-kB signalling downstream of TCR and BCR. Upon TCR activation, PKC θ phosphorylates CARD11 and BCL10 plus MALT1 are recruited to form the CBM complex. Activation of the CBM complex induces IKK activation and consequently NF-kB activation. Five genetic variants (one deletion and four single nucleotide polymorphisms (SNPs)) have been reported in human *CARD11*. Deletion of exon 21 (1377 bp) of this gene and a truncation mutation (Q945X) resulted in complete protein deficiency, while the others were missense mutations in which protein levels were normal. G123D conferred loss-of-function (Greil, Rausch et al. 2013; Stepensky, Keller et al. 2013) mutation while the others (E127G, G116S) conferred gain-of-function (GOF). CARD11 deficiency or LOF mutations result in reduced or no IKK activation due to failure to either form or properly activate the CBM complex. The phenotype of these mutations is reduced or absent T cell proliferation and differentiation. On the other hand, the GOF mutations lead to constitutive NF-kB activation, and the phenotype is accumulation of terminally differentiated B cell (Snow, Xiao et al. 2012; Turvey, Durandy et al. 2014; Brohl, Stinson et al. 2015).

One loss of function germline mutation in BCL10 has been described, in a patient with a combined immunodeficiency. A homozygous splice site mutation affecting the invariant first nucleotide of intron 1 causes complete BCL10 deficiency and confers defects of both hematopoietic and non hematopoietic immunity (Lee, Shin et al. 1999; Willis, Jadayel et al. 1999; Torres, Martinez-Barricarte et al. 2014). Two missense MALT1 mutations have been reported. Deficiency of MALT1 results in combined immune deficiency with abnormal IkB a degradation and IL-2 production (Jabara, Ohsumi et al. 2013; McKinnon, Rozmus et al. 2014).

A nonsense mutation (Q422X) in *IKBKA* has been reported, which causes IKK1 deficiency and results in autosomal lethal Cocoon-like syndrome characterised by multiple fetal malformations. Two genetic variants were described in human *IKBKB,* a nucleotide addition at c.1292 and a nonsense mutation (R272X), which both confer complete IKK2 deficiency. Patients with IKK2 deficiency exhibited severe combined immune deficiency due to impaired responses to various stimuli (Pannicke et al., 2013; Nielsen et al., 2014). Numerous mutations have been described in human *IKBKG* (NEMO). In females, hemizygous *IKBKG* mutations cause incontimentia pigmenti. In males, different mutations result in immunodeficiency with or without ectodermal dysplasia (Lahtela, Nousiainen et al. 2010).

LUBAC is a ubiquitin ligase complex comprising HOIL-1, HOIP and SHARPIN proteins (Gerlach, Cordier et al. 2011; Ikeda, Deribe et al. 2011; Tokunaga, Nishimasu et al. 2012). As described above, LUBAC is important for IKK activation and NEMO recruitment. Several mutations have been described in genes encoding the human

LUBAC complex. Eight genetic variants were discovered in HOIL-1 (Boisson, Laplantine et al. 2012; Boisson, Laplantine et al. 2015). 6 mutations were found in patients with glycogen storage myopathy without immunodeficiency and 2 mutations (Q185X, 2 nucleotides deletion in exon 3) were found in patients with immunodeficiency. Loss or reduced function of HOIL-1 resulted in defects in NF-kB activation. One mutation (L72P) has been reported in HOIP. Although functional analysis has not been reported, the mutation was predicted to cause loss of function (Nilsson, Schoser et al. 2013). ITCH is E3 ubiquitin ligase and a homozygous single nucleotide insertion at 394 in *ITCH* was identified in Amish patients from consanguineous families. This homozygous mutation results in ITCH deficiency and confers multisystem autoimmune disease with morphologic and developmental abnormalities. Physical growth, craniofacial morphology, muscle development and immune function were destructively affected in these patients (Lohr, Molleston et al. 2010).

Table 1.2 Phenotype of gene knockout comparison between humans and mice

gene	Phenotype of knockout mice	Phenotype of loss or reduced function in humans
CARD11	Healthy and fertile defective T cell B cell activation failed to produce specific antibody, IgM high B cells impairment of NF-kB Jnk activation	Pneumonia due to Pneumocystis jirovecii infection, increased numbers of transitional b cells and decreased regulatory T cells, defective NF-kB signaling in lymphocytes upon activation
MALT1	Defective in antigen receptor induced NF-kB activation, cytokine production, and proliferation	Impaired degradation of the NF-KB inhibitor IkBa, decreased IL2, poor antibody response and decreased T cell proliferative responses to mitogens; impaired B cell differentiation, absent proliferation and blast formation in CD3+ cells, decreased phophorylation of p65,
BCL10	Embryonic lethality, severe immunodeficiency defective in antigen receptor induced NF-kB activation reduction in follicular marginal zone B1 B cells	Hypogammaglobulinemia and a profound deficiency of memory B cells and memory T cells with predominantly circulating naïve cells, impaired NF-kB signaling via TLR4 in fibroblasts, impaired development in B cells, and impaired proliferation in T cells
IKBKA	Defects in keratinocyte differentiation, bone and limb development and mammary epithelial proliferation, no mature B cells, impaired RANKL induced NF-kB activation and NIK induces p100 processing	Abnormal cyst in the cranial region, a large defect in the craniofacial area, an omphalocele and immotile and hypoplastic limbs -Cocoon syndrome, the fetuses were terminated at14 and 13 weeks of gestation.
IKBKB	Die at E13.5-E14.5 owing to TNF dependent liver apoptosis, impaired NF-kB activaton by IL-1, TNF and LPS	Hypo/agammaglobulinemia with relatively normal number s of circulating B and T cells. Impaired phosphorylation of IkBa with TNFa stimulation and flagellin via TLR5. B and T cells were of the naïve type and showed poor differentiation o mitogenic responses under certain conditions, impaired phosphorylation of p65 and proliferation of T cells
IKBKG	Die at E11.5-E12.5 owing to TNF dependent live apoptosis, no induced NF-kB activation in MEFs	Ecdermal dysplasia, reduced TNFa and LPS induced NF-kB activation in preB and T lymphocytes
Itch	Inflammation of the lung and stomach, hyperplasia of lymphoid and hematopoietic cells and constant itching	Multisystem autoimmune disease with facial dysmorphism

Human mutations presented are often similar but not identical to phenotypes of mice with engineered deficiencies of the same genes (Table 1.2). There are also some significant differences. For example, *Ikbkb* deficiency is embryonic lethal, whereas in humans, *IKBKB* deficiency, caused by a homozygous duplication (c.1292dupG) in exon 13, showed more restricted functions (Pannicke, Baumann et al. 2013). Thus, analysis of rare human variant alleles provides unique insights into human immunity.

1.4 Common variable immune deficiency

Common variable immune deficiency (CVID) is the most common primary immunodeficiency with an incidence estimated at 1:10000 to 1:50000 (Salzer, Warnatz et al. 2012). CVID was firstly reported in 1953 by Janeway and his colleagues, when they described a 39 year old patient who had a history of recurrent sinopulmonary infections, bronchiectasis and *Haemophilus influenzae* meningitis. The diagnosis of CVID depends on three features: hypogammaglobulinaemia of two or more immunoglobulin isotypes (low IgG, IgA, or IgM), recurrent sinopulmonary infections, and impaired functional antibody responses (Park et al., 2008). The number of B cells in peripheral blood can be normal or reduced, and the proportion of class switched memory B cells is often reduced (Cunningham-Rundles 1989; Cunningham-Rundles and Bodian 1999). Reduction of class-switched memory B cells was shown to correlate with granulomatous disease, splenomegaly and autoimmune cytopenias (Wehr, Kivioja et al. 2008).

Functional abnormalities are often found in T cell compartments, particularly during in vitro analysis, and this is the reason for the inclusion of the *combined* in the name of the syndrome. In older literature, various abnormalities were reported, including abnormal cytokine production, and decreased T helper cell function (Baumert, Wolff-Vorbeck et al. 1992; Holm, Sivertsen et al. 2004). More recently, abnormalities of T cell function have been characterised more precisely in Mendelian version of CVID (Bateman, Ayers et al. 2012). Patients do not usually suffer with opportunistic infections typically seen in patients with T cell deficiency.

The main goal of therapeutic management is to decrease the morbidity and mortality associated with recurrent infections. The low prevalence together with heterogeneous clinical presentations, and recurrent infection with pathogens also encountered in immune competent individuals means that the diagnosis of CVID is often delayed. In 1999, Cunningham-Rundles revealed that the average age of diagnosis was 29 years for males and 33 years for females, while the the average age of onset of CVID was 23 years and 28 years, respectively (Cunningham-Rundles and Bodian 1999).

In addition to recurrent infection, CVID is also associated with an increased risk of autoimmune disease, and sarcoidosis-likev granulomatous inflammation, and neoplasia. Occasionally these complications were diagnosed prior to CVID. Approximately 25-30% of patients with CVID have autoimmune diseases. The most common autoimmune manifestations are thrombocytopenia (ITP), autoimmune haemolytic anaemia (AIHA)(Hermaszewski and Webster 1993; Cunningham-Rundles and Bodian 1999; Cunningham-Rundles 2002).

Granulomas are less frequent, although their presence is harder to ascertain. The risk of non-Hodgkins lymphoma has been estimated to be 400 times greater in CVID pateints than in the general population (Cunningham-Rundles, Siegal et al. 1987).

Intravenous immunoglobulin replacement therapy (IVIG) is effective and is currently the mainstay of therapy for CVID (Park, Lerou et al. 2008). IVIG reduces the incidences of pneumonia and serious recurrent bacterial infections and prevents chronic lung disease and enteroviral menigoencephalitis. However it is not a curative treatment and majority of patients with CVID require a lifelong treatment with Ig replacement. CVID patients with IVIG treatment experience side-effects ranging from minor adverse reactions including headache, nausea, malaise, myalgias, arthralgias, chills, anxiety, flushing, abdominal cramps, rash, low grade fever, and leukopenia to rare but serious reactions, which are anaphylaxis, acute renal failure, stroke, myocardial infarction deep venous thrombosis or pulmonary embolus and aseptic meningitis.

Decades long usage of IVIG treatment may cause deleterious effects and furthermore it is a financial burden for patients. The identification of genetic factors will facilitate appropriate diagnosis and potentially lead to curative therapeutic development (Schaffer, Salzer et al. 2007)

Table 1.3 Genetic defects in patients with CVID

Protein	Gene symbol	OMIM Designation	Reference
Inducible costimulator (ICOS)	*ICOS*	CVID1	(Grimbacher, Hutloff et al. 2003; Salzer, Maul-Pavicic et al. 2004)
Transmembrane activator and CAML interactor (TACI)	*TNFRSF13B*	CVID2	(Salzer, Chapel et al. 2005; Castigli, Wilson et al. 2007; Garibyan, Lobito et al. 2007; Lee, Rauter et al. 2009)
CD19	*CD19*	CVID3	(van Zelm, Reisli et al. 2006)
BAFF receptor (BAFFR)	*TNFRSF13C*	CVID4	(Warnatz, Salzer et al. 2009)
CD20	*MS4A1*	CVID5	(Kuijpers, Bende et al. 2010)
CD81	*CD81*	CVID6	(van Zelm, Smet et al. 2010)
CD21	*CR2*	CVID7	(Wu, Boackle et al. 2007; Thiel, Kimmig et al. 2012)
LRBA	*LRBA*	CVID8	(Alangari, Alsultan et al. 2012; Lopez-Herrera, Tampella et al. 2012; Charbonnier, Janssen et al. 2015)
PRKCD	*PRKCD*	CVID9	(Belot, Kasher et al. 2013; Kuehn, Niemela et al. 2013; Salzer, Santos-Valente et al. 2013)

Nine patients with CVID from four unrelated families showed *ICOS* deficiency. The patients had few peripheral B cells and very few or no class-switched memory B cells and produced very little IL-10 which is important for terminal differentiation of B cells. ICOS mutations appear to be rare (Grimbacher, Hutloff et al. 2003; Salzer, Maul-Pavicic et al. 2004).

TNFRSF13B (TACI) was originally identified in approximately 10% of CVID patients. Several homozygous, heterozygous or compound genetic defects were identified, including mutations encoding Cys104Arg, Ala181Glu, and 204 insAla. Subsequent studies have demonstrated these variants within the healthy population, and also in

healthy relatives of patients with CVID, indicating that TNFRSF13B defects are likely to operate only in epistasis with other variants to confer the CVID phenotype (Salzer, Chapel et al. 2005; Castigli, Wilson et al. 2007; Garibyan, Lobito et al. 2007; Lee, Rauter et al. 2009) (Patrick et al., 2011).

BAFFR deficiency was described in one individual a two related individuals with CVID. A 24 base pair deletion was found from this patient. Reduction of both class switched and non class switched (or marginal zone) B cells, an increase in the transitional B cells and a decrease in plasmablasts were reported (Warnatz, Salzer et al. 2009).

CD19 deficiency was discovered in four patients with CVID from two unrelated families. Homozygous mutations in CD19 introduced a premature stop codon. CD20+ B cell numbers were normal in the patients but CD19 expression was low or undetectable. CD27+ memory B cells were found to be low.

The CD19 complex is formed by three other proteins; CD21 CD81 and CD225. A single nucleotide insertion at a splicing site in *CD81* was discovered from one patient with CVID resulting in a complete lack of CD81 expression. The patient also showed an absence of CD19 expression on B cells and reduced memory B cell numbers. Mutations in *CR2* also showed normal B cells numbers with an absence of CD21 expression and decreased memory B cell numbers (van Zelm, Reisli et al. 2006; Wu and Zhang 2007; van Zelm, Smet et al. 2010; Thiel, Kimmig et al. 2012).

MS4A1 genetic defect was found in a Turkish girl, born of consanguineous parents. 11-bp insertion and 2-bp deletion homozygous mutation in intron 5 of the *MS4A1* gene resulted in loss of CD20 surface expression on B cells. B cell numbers were normal but peripheral memory B cells were reduced (Kuijpers, Bende et al. 2010).

Six different homozygous mutations in the *LRBA* have been discovered from seven patients from six unrelated consanguineous families with CVID. Decreased numbers of switched memory B cells and a failure to differentiate into plasma cells were observed. An increased susceptibility to apoptosis was discovered (Alangari, Alsultan et al. 2012; Lopez-Herrera, Tampella et al. 2012; Charbonnier, Janssen et al. 2015).

Three homozygous mutations in *PRKCD* were discovered in five patients with decreased functional PRKCD protein in patient cells. Hyperproliferation in response to stimulus was shown in the patient B cells. It demonstrated that PRKCD is a crucial factor in B cell tolerance (Belot, Kasher et al. 2013; Kuehn, Niemela et al. 2013; Salzer, Santos-Valente et al. 2013).

In total, nine genetic defects have been identified to account for CVID (Table 1.3). Collectively, these account for 10-15 % of CVID cases. In other words, 85-90% of patients with CVID have no known genetic cause or explanation. The discovery of new genetic defects associated with CVID is required in order to classify the disease and to facilitate diagnosis and prognosis.

2 Methods and Materials

2.1 Materials

2.1.1 Biological materials

2.1.1.1 Patients and participants

The patients, relatives and healthy controls are part of a larger cohort of primary antibody deficiency kindreds enrolled and recruited through the Australian and New Zealand antibody deficiency allele (ANZADA) study. Consents were obtained from all participants. This study has been approved by human research ethics committees at each institution. Blood and saliva were collected according to standard operating procedures (SOP).

The cord blood was obtained through Human Research Ethics committee (Klionsky, Abdalla et al.) approved donations given in the birthing suite of the Centenary Hospital, ACT Health services. Spleen and lymph nodes were donated at time of diagnostic biopsies and therapeutic removal of organ tissue as part of patient treatment plans, and after informed consent was obtained.

2.1.1.2 Other biological materials

HEK293 cell line was purchased from ATCC®. HEK293T, Raji, Daudi and Ramos cell lines were kindly provided by Dr. Vinuesa. *E. coli* strains, JM103and DH5α were purchased from Invitrogen.

2.1.2 Antibodies

The following antibodies were used for flow cytometry analysis; CD3(HIT3A, BD), CD4(SK3, BD), CD8(SK1, BD), CD10 (H110a, BD), CD14 (MφP9,BD) CD19 (SJ25C1, BD), CD27 (L128, BD), CD21(B-ly4, BD), CD23 (EBV CS-5, Biolegend), CD24 (ML5, BD), CD25 (M-A251, BD), CD31(WM59 , BD) CD38 (HB7, BD), CD45RA (H110, BD), CD45RO (UCHL1, Biolegend), CD57 (HNK-1, BD), CD62L (DREG-56, BD), CD69 (FN50, BD), CD84 (H B15e, BD), CD86 (FM95, Miltenyi Biotec), CD127 (A019D5, eBioscience), CCR6 (11A9, BD), CCR7 (3D12, BD), CXCR3(IC6/CXCR3, BD), CXCR5 (RF8B2, BD) FoxP3 (259D/C7, BD), ICOS (ISA3, eBioscience), IFN-γ (25723.11, IL-4 (7A3-3, Miltenyi Biotec), IL-10 (JES3-19F1, BD), IL-17 (SCPL1362, BD), BD), IgA (G20-359, BD), IgD (IgD26, BD), IgG (G18-145, BD), PD1 (J104, eBioscience), 7AAD (BD), and streptavidin (streptavidin, BD) Anti Fas antibody (CH11, Millipore).

The following antibodies were used for western blot; A20 (59A426, Santa Cruz Bio), TNFAIP3/A20 (clone: A-12, sc-166692, Santa Cruz), Ubiquitin (clone: P4D1, sc-8017, Santa Cruz), TAX1BP1 (Abcam), c-Myc (Milipore), Flag (Sigma), NFKB2 (C5, Santa Cruz Bio) NFKB2 p100/52 antibody (cell signaling), Phospho-NFKB2 p100 (ser866/870) antibody (cell signaling), NIK (Santa Cruz Bio), TBP antibody (1TBP18, abcam), and goat anti-mouse IgG HRP antibody (Santa Cruz Bio), GAPDHα (6C5 abcam), Phospho-IKKα/β (16A6, Cell signaling), IKBα (Cell signaling), Phospho-IKBα (Cell signaling), TATA box (ab818, Abcam), sheep polyclonal anti-rabbit IgG (Abcam), goat anti-mouse IgG-HRP (Santa Cruz Bioch), and Anti rabbit IgG HRP-linked antibody (Cell Signaling).

2.1.3 Plasmids

2.1.3.1 pcDNA™3.1(-)/myc-His A, B, & C mammalian expressing vecotr

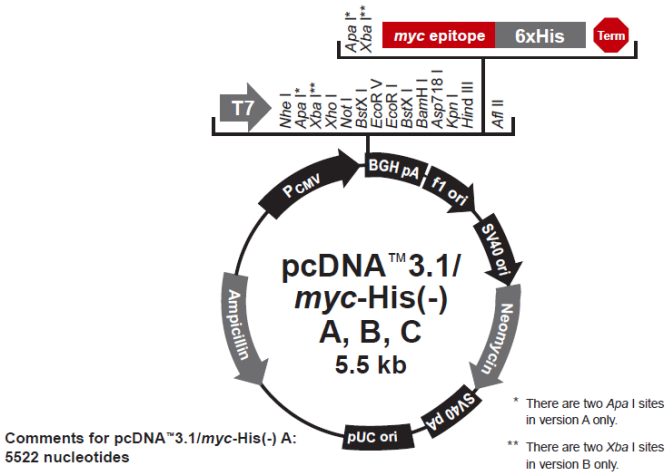

It was purchased from Invitrogen.

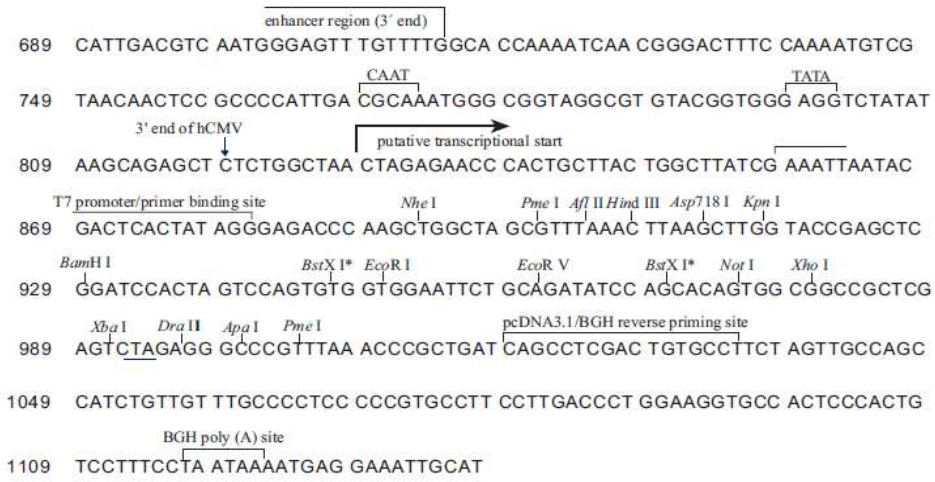

2.1.3.2 pcDNA™3.1(+)/Flag mammalian expressing vector

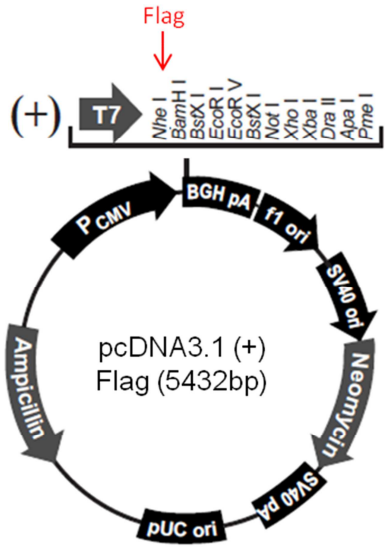

It was kindly provided by Dr Keisuke Horikawa (John Curtin School of Medical Research, Australian National University). Flag gene was inserted between NheI and BamHI

2.1.3.3 pDONR223-NIK vector

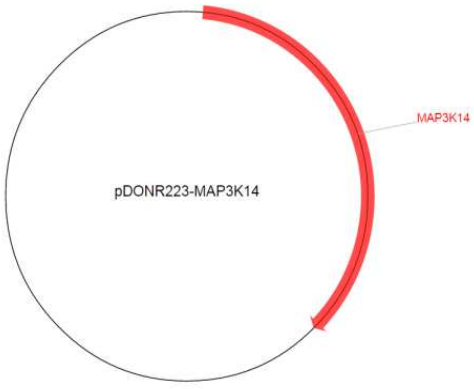

NIK containing pDONR223vector was purchased from Addgene.

2.1.3.4 pX330 U6 chimeric DD CBh hSpCas9 plasmid

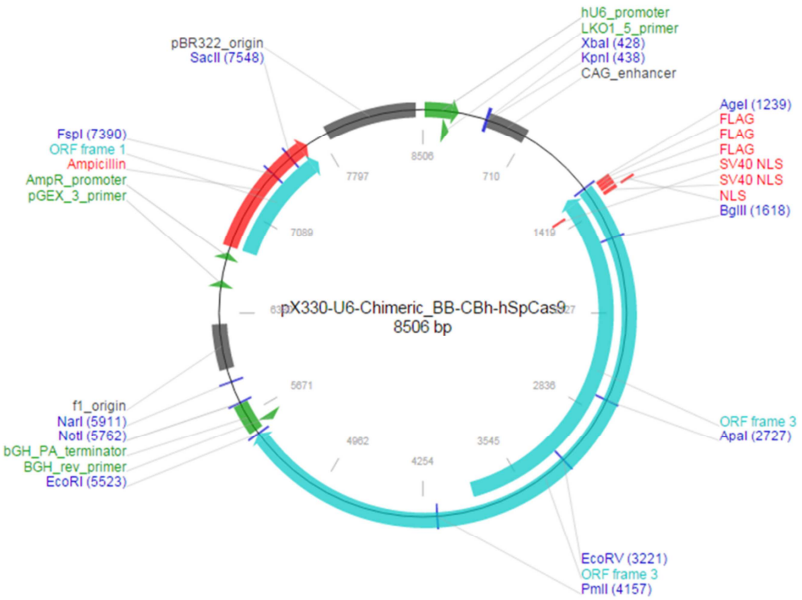

It was kindly provided by Dr. Vicki Athanasopoulos (John Curtin School of Medical Research, Australian National University).

2.1.4 Primers

2.1.4.1 Primers for genotyping by Sanger sequencing

Name	Sequence (5'-3')	Temp*	Size
TNFAIP3gDNAF	AGCCTTATGCCTTGGCTCCTGG	69°C	566bp
TNFAIP3gDNAR	CTGACAGGCGTTTACTTGCTCCA		
TAX1BP1gDNAF	TGTTCTGCTCCTGCATGCTT	69°C	312bp
TAX1BP1gDNAR	ACATAACTGCAGCCTGCCAA		
NKFB2gDNAF	CTTCTCAGCTGGCTGGCGGG	69°C	430bp
NKFB2gDNAR	CTGAGGGGTGGGTGTGGGGT		
TNFSF9gDNAF	GCGCTGTGTCTTCCCGCAGT	69°C	585bp
TNFSF9gDNAR	CTCGTAGCGGGCGCAGGATG		

2.1.4.2 cDNA primers for cloning

Name	Sequence (5'-3')	Temp*	Size
A20cDNAF NotI	aaaGCGGCCGCGCCACCATGGCTGAACAAGTCCTTCC	59°C	2397bp
A20cDNAR KpnI	tttGGTACCcGCCATACATCTGCTTGAACTG		
TAX1BP1cDNA BamHI	aaaGGATCCGCCACCATGACATCCTTTCAAGAAGTCCCA	59°C	2241bp
TAX1BP1cDNAR NotI	tttGCGGCCGCCTAGTCAAAATTTAGAACATTCTGATCAA		
NIKcDNAF NotI	tcatGCGGCCGCGCCACCATGGCAGTGATGGAAATG	59°C	2900bp
NIKcDNAR BamHI	tactGGATCCTTTAGGGCCTGTTCTCCAGCTG		
TNFAIP3 cDNAF1	TTGAATTCGCCACCATGGCTGAACAAGTCCTTCCTCAG		
TNFAIP3 cDNAR1	AAAACTCGAGTTAGCCATACATCTGCTTGAACTG		
TNFAIP3 cDNAF3	TTGGATCCGCTGAACAAGTCCTTCCTCAGG-3'		
TNFAIP3 DA1	AAAACTCGAGTTACTGGGCGTGCCCCTCTCTCCTC		
TNFAIP3 H256AF	CTCGGCTATGACAGCCATGCCTTTGTACCCTTGGTGACCC		
TNFAIP3 H256AR	GGGTCACCAAGGGTACAAAGGCATGGCTGTCATAGCCGAG		
TNFAIP3 S254RF	TGTTCTCGGCTATGACAGACATCATTTTGTACCCTTG		
TNFAIP3 S254RR	CAAGGGTACAAAATGATGTCTGTCATAGCCGAGAACA		

*Temp: optimal annealing temperature; low case: additional nucleotide; red upper case: restriction site sequence; blue upper case: Kozak sequence

2.1.4.3 Primers for sanger sequencing

Name	Sequence (5'-3')
A20cDNA F1	ATGGCTGAACAAGTCCTTCC
A20cDNA F2	AACTGGAATGATGAATGGGAC
A20cDNA F3	GCCGCAAAGTTGGATGAAGCT
A20cDNA F4	GGAAGTGCCAAGCCTGCCTC
A20cDNA F5	CCCTTGGAAGCACCATGTTTG
A20cDNA F6	CAGTTCAAGCAGATGTATGGC
TAX1BP1cDNAF1	AAGTTGGGAGAATGGAAAGAGAAC
TAX1BP1cDNAF2	GAGATTGGCAGGCTGCAGTT
TAX1BP1cDNAF3	AAGCCATCACCTTCTGCAGCA
TAX1BP1cDNAF	CACAATGACATCCTTTCAAGAAGT
TAX1BP1cDNAR	CTCATAATAAAAAGTAACTAGTCAAAATT
T7promoter	AAATTAATACGACTCACTATAGG

2.1.4.4 Guide RNA (sgRNA) primers:

Name	Sequence (5'-3')
sgA20_F2	caccgTGTCATAGCCGAGAACAA
sgA20_R2	aaacTTGTTCTCGGCTATGACAc
sgTAX1BP_F4	caccgATACCAAGCTTATGTCAG
sgTAX1BP_R4	aaacCTGACATAAGCTTGGTATc

2.1.4.5 ssODN repair template

Name	Sequence (5'-3')
A20 S254R C-A Rev	CTCACCAGGCCCACTGTCCTTCAGGGTCACCAAGGGTACAAAATG ATGTCTGTCATAGCCGAGAACAATGGGGTATCTGTAGCATTCCTG GGCAGGCCAG
TAX1BP L307I T-A	CAGAAATAGAAAATACCAAGCTTATGTCAGAGGTCCTAAAAAATAT AGATGGGAACAAAGAAAGCGTGATTACTCATTTCAAAGAAGAGATT GGC

2.1.5 General reagents and commercial kits

Ficoll-Paque plus™ and Amersham ECL ™ western blotting detection reagents were purchased from GE Healthcare. PBS solution, DMEM medium were purchased from GIBCO. RPMI medium 1640, pcDNA™3.1(-)/myc-His A, B, & C, Lipofectiamin LTX with plus reagent, Cell Trace CFSE proliferation kit , Cell Trace Violet cell proliferation kit and PureLink®HiPure Plasmid Filter Midiprep kit were purchased from Invitrogen. SOC medium, L-glutamin , tryptone, yeast extract, penicillin streptomycin solution, and $NaCl_2$, HEPES buffer solution, Dimethyl sulfoxide, L grutamine, Ampicillin sodium salt, protein G agarose were purchased from Sigma Aldrich. Halt Phosphatase inhibitor cocktail (Piercent), Leucosep tube (Greiner Bio One-interpath), Human IL-2 recombinant protein (Thermo Scienctific), Type B CpG oligonucleotide-human TLR9 ligand (ODN2006) (Invivogen), Phusion Hot Start II High-Fidelity DNA polymerase (Finnzymes), Recombinant human TNFα (Biolegend) Nuclease free water (Applied Biosystems), Gel Red nucleic acid gel stain (Omar Bioscience), anti Ig $F(ab)_2$ (Jackson Laborotory), ORAgene-DNA OG-500 kit (DNAgenoTek), Tris-Glycin Mini 12% Gel (Nusep), were purchased. β-mercaptoethanol, isopropanol, absolute ethanol, methanol were purchased from JCSMR store.

Heat inactivated fetal bovine serum, Lipofectamine™ LTX with Plus™ Reagent, Bolt system kit, Neon transfection system 100µl kit were purchased from life Technologies. Protease inhibitor cocktail set III EDTA free and MG-132 were purchased from Calbiochem. Human recombinant CD40 Ligand and Human BAFF were obtained from Peprotech.

Phusion hotstart flex, 100bp DNA Ladder, 1kb DNA Ladder, 6X gel loading dye , Restriction enzyme, KpnI, NotI, BamHI, HindIII-HF, ligase enzyme T4 were purchased from New England Biolabs ®Inc. Human recombinant IL-4, lymphotoxin α/β and human recombinant GM-CSF were purchased from RnD. Fix buffer I and Cytofix/cytoperm kit were purchased from BD. QIAprep spin miniprep mini kit, QIAamp DNA blood mini kit, QIAquick gel extraction kit, RNeasy plus mini kit, Miscript reverse transcription kit SyBr Green PCR Kit were purchased from Qiagen. T-cell activation and expansion beads, CD14 MicroBeads human, CD4 MicroBeads, human recombinant IL-21 and Human GM-CSF were purchased from Miltenyi Biotech Inc. StemSep™ human B cell enrichment kit was purchased from Stemcell™ technologies. Immune-blot PVDF membrane, Precision plus protein™ Dual color standards and Bio-Rad DC™ protein reagent were purchased from Bio-rad.

2.1.5.1 Solutions and media

2.1.5.1.1 FACS wash

2ml of FBS (GIBCO) and 1g of sodium azide (NaN3) were dissolved in ~ 97ml of PBS (1X).

2.1.5.1.2 FACS sorting solution

1ml of FBS was added aseptically in 99ml of sterile PBS (1X)

2.1.5.1.3 Lysis buffer for co immunoprecipitation

120mM NaCl, 50mM HEPES, 1mMEDTA, 0.1%NP40, were dissolved in 1L of dsH_2O. Protease inhibitor and phosphotase inhibitor were added freshly.

2.1.5.1.4 Amplicillin solution (50mg/ml)

10g of amplicillin was added to a final volume of 200ml of dsH_2O and sterilized using a 0.2um filter.

2.1.5.1.5 LB media

10g of trypton, 5g of yeast extract and 5g of $NaCl_2$ were dissoloved in a total volume of 1L of H_2O. the solution was adjusted to pH 7.5 and autoclaved at 121°C for 15 minutes.

2.1.5.1.6 LB agar plate

10g of trypton, 5g of yeast extract and 5g of $NaCl_2$ were dissoloved in a total volume of 1L of H_2O. The solution was adjusted to pH 7.5 and 15g of agar was added and the solution was autoclaved at 121°C for 15 minutes. When the temperature of the solution

reached about 50°C 2ml of Ampicillin solution (50mg/ml) was added and the LB solution was poured into plates and dried overnight at room temperature

2.1.5.1.7 TAE buffer (50X)

TAE buffer was prepared by dissolving 96.8g of Tris base, 13.5g of EDTA and 22.8g of glacial acetic acid in 300 ml of ds H2O. The pH was adjusted to pH8.0 with glacial acetic acid, the solution was autoclaved at 121°C for 15minutes and stored at 4°C.

2.1.5.1.8 Transfer buffer

100ml of Transfer buffer (20X), 200ml of methanol and 1.7Lof ds water were added and chilled overnight at 4°C.

2.1.5.1.9 TBST (10X)

24.23g of Trizma -HCl, 80.06 g of NaCl were added in 1L of water and pH was adjusted to 7.6.

2.1.5.1.10 Blocking buffer (3-5% skim milk or BSA)

3- 5g of skim milk powder or BSA was added in 100ml of TBST (1X) solution. This solution was freshly made.

2.1.6 Bioinformatics

Table 2.1Gene information

Gene			Website address
A20	gDNA	NCBI	http://www.ncbi.nlm.nih.gov/nuccore/NG_032761.1
	cDNA	ensembl	http://asia.ensembl.org/Homo_sapiens/Transcript/Exons?db=core;g=ENSG00000118503;r=6:138188351-138204449;t=ENST00000237289
	gene	uniprot	http://www.uniprot.org/uniprot/P21580
		genecards	http://www.genecards.org/cgi-bin/carddisp.pl?gene=TNFAIP3&search=951aade0b0275b184c6fb29cb8a8ca9f
		OMIM	http://omim.org/entry/191163?search=a20&highlight=a20
TAX1BP1	gDNA	NCBI	http://www.ncbi.nlm.nih.gov/nuccore/NG_029523.1
	cDNA	ensembl	http://asia.ensembl.org/Homo_sapiens/Transcript/Summary?db=core;g=ENSG00000106052;r=7:27778950-27880938;t=ENST00000265393
	gene	uniprot	http://www.uniprot.org/uniprot/Q86VP1
		genecards	http://www.genecards.org/cgi-bin/carddisp.pl?gene=TAX1BP1&search=951aade0b0275b184c6fb29cb8a8ca9f
		OMIM	http://omim.org/entry/605326?search=tax1bp1&highlight=tax1bp1
NFKB2	gDNA	NCBI	http://www.ncbi.nlm.nih.gov/nuccore/NG_033874.1
	cDNA	ensembl	http://asia.ensembl.org/Homo_sapiens/Gene/Summary?db=core;g=ENSG00000077150;r=10:104154229-104162281;t=ENST00000189444
	gene	uniprot	http://www.uniprot.org/uniprot/Q00653
		genecards	http://www.genecards.org/cgi-bin/carddisp.pl?gene=NFKB2&search=e58d9149c970d62be6cab37032bd7e53
		OMIM	http://omim.org/entry/164012?search=nfkb2&highlight=nfkb2
NIK	gDNA	NCBI	http://www.ncbi.nlm.nih.gov/nuccore/555290184
	cDNA	ensembl	http://asia.ensembl.org/Homo_sapiens/Gene/Summary?db=core;g=ENSG00000006062;r=17:45263121-45317040
	gene	uniprot	http://www.uniprot.org/uniprot/Q99558
		genecards	http://www.genecards.org/cgi-bin/carddisp.pl?gene=MAP3K14&search=77113177b98eaff56855e81a429fc8c7
		OMIM	http://omim.org/entry/604655?search=nik&highlight=nik

Table 2.2Predicting functional effect

Name	Website
Polyphen 2	http://genetics.bwh.harvard.edu/pph2/
Mutation taster	www.mutationtaster.org
SIFT	http://sift.jcvi.org

Table 2.3 Analysis tool

Name	Website
Primer design	http://www.ncbi.nlm.nih.gov/tools/primer-blast/index.cgi?LINK_LOC=BlastHome
DNA alignment tool	http://www.ebi.ac.uk/Tools/psa/emboss_matcher/nucleotide.html
Annealing temperature tool	http://www.neb.com/nebecomm/tech_reference/TmCalc/Default.asp
Reverse complementary	http://www.bioinformatics.org/sms/rev_comp.html
Restriction enzyme tool	http://www.restrictionmapper.org/
Searching for overlap	http://www.pangloss.com/seidel/Protocols/venn.cgi
Interacting gene search	http://string-db.org/, http://thebiogrid.org/
Tm Calculator	http://tmcalculator.neb.com/#!/
Gene expression	http://www.immgen.org/index_content.html

2.2 Methods

2.2.1 Cellular phenotypes

2.2.1.1 PBMC isolation from Blood

Whole blood was collected into ACD tubes then diluted with PBS in a 1: 1 ratio then layered onto Ficoll- Paque PLUS solution (GE healthcare, 17-1440-03) before centrifugation at 400*g* for 30 minutes at room temperature then decelerated without the brake. Buffy coats were separated and washed twice in tissue culture media . 2 x 10^6 PBMCs were resuspended with 1ml of freezing medium, which consisted of RPMI, 10% of FBS and 10% of DMSO, and then stored at -80°C overnight and transferred to liquid nitrogen.

2.2.1.2 Cell culture

Frozen PBMC samples were transferred into a 37°C water bath for quick thawing then cells were immediately washed with tissue culture media, followed by centrifugation at

1200rpm for 5 minutes. Cell numbers were counted by haemocytometer and desired cell numbers were maintained in complete RPMI at 37°C with 5% CO_2.

2.2.1.3 Flow cytometry analysis

2.2.1.3.1 Surface staining

PBMCs were thawed and washed with culture media and spun at 350*g* 4°C for 10 minutes. PBMCs were then washed twice with FACS buffer containing 2% of FBS, 1% of NaN_3 in PBS followed by spinning at 300G for 5 minutes at 4^oC. $2X10^6$cells per 200µl were transferred into a well of a 96 well plate with round bottom and centrifuged again at 300*g* for 5 minutes at 4^oC. 30µl of desired antibody cocktail (Appendix II) was added and incubated for 30 minutes on ice. The cells were washed twice with FACS wash then resuspended with 100µl of FACS wash for FACS acquisition.

2.2.1.3.2 Intercellular stain

Intercellular staining was performed after surface staining. Cells were washed with perm wash 1X (BD) twice, then fixed with cytofix solution (BD) for 20 minute on ice. Antibody cocktail (Appendix II), which was prepared with perm wash (1X), was added and incubated for 20 minutes on ice. The cells were washed with perm wash (1X) once and washed with FACS wash once. The cells were resuspended with 100µl of FACS wash for Flow cytometry acquisition.

2.2.1.3.3 Foxp3 staining

Cells were stained with CD4 CD127 and CD25 antibodies by surface staining protocols (Appendix II) then permeabilized and fixed with a FoxP3 staining kit. Cells were stained with Cells were washed with FACS wash twice and fixed with 100µl of 1x human FoxP3 buffer A. After incubating at RT for 10 minutes in the dark, cells were centrifuged at 300*g* for 5 minutes and washed with FACS wash. The pellet was resuspended with 100µl of 1x working solution of Human FoxP3 Buffer C and incubated at room temperature for 30 minutes in the dark. Cells were washed with FACS wash and incubated with Foxp3 antibody cocktail (Appendix II) for 30 minutes at RT in the dark. Cells were then washed with FACS wash twice and 100µl of FACS wash was added for Flow cytometry acquisition.

2.2.1.4 Cell sorting by Flow cytometry, MACS or Stem cell technology

The cells were washed twice with FACS wash at 350*g*, 4°C for 10 minutes. Up to 100 x 10^6 cells were resuspended with 500µl of sorting antibody cocktail (Appendix II). Cells were incubated about 30 minutes in the dark on ice and cells were washed with PBS two times and cells were then flushed through strainers (2µm). Cells were then sorted using BD FACS Aria I into complete RPMI medium, then pelleted and resuspended in tissue culture media.

For MACS sorting, cells were incubated with antibody conjugated MACS Microbeads, then loaded into the MACS column. The column was washed three times with washing buffer (PBS with 1% BSA), then cells were eluted with washing buffer. With Stem cell technology sorting, cells were stained with a stem cell antibody cocktail and the mixture

was added into a tube inserted into Stemcell™ magnet. The mixture was incubated for 5 minute at room temperature and unbound cells were removed by inverting the tube. Cells were then washed twice with culture media.

2.2.1.5 T cell and B cell activation and apoptosis assays

Cells were incubated with various stimuli for 24, 48 or 96 hours. Cells were then stained with the activation antibody cocktail or the apoptosis antibody cocktail (Appendix II).

2.2.1.6 T cell / B cell proliferation

Proliferation of cells was analysed using Cell Trace™ Violet (CTV) Cell Proliferation Kit or Cell Trace™ Carboxyfluorescein succinimidyl ester (CFSE) Cell Proliferation Kit (invitrogen) according to the manufacturer's instructions. Sorted cells or PBMCs were washed twice with PBS and $1x10^6$ cells were resuspended in 1ml of PBS. 1µl of CTV or CFSE was added and cells were incubated at room temperature for 5 minutes and then labelling was quenched with cold complete RPMI on ice for 10 minutes. Cells were centrifuged at 400*g* for 5 minutes at 4°C and washed with complete RPMI.

2.2.1.7 Plasmablast induction

PBMCs were washed twice with complete RPMI and $1x10^6$ cells per 1 ml of complete RPMI were added to each well of a 48 well plate. For plasmablast induction B cells were cultured with various combinations of IL-21 (50ng/ml) and CD40L (1µg/ml) or IL-21 (50ng/ml) and CpG (2µM) or IL-21 (50ng/ml) and CD40L transfectants L-cells for 4 or 5 day at 37°C with 5% CO_2.

2.2.1.8 Monocyte derived human dendritic cell culture

CD14+ cells were isolated from PBMCs using magnetic CD14 microbeads according to the manufacturer's instructions (Miltenyi Biotech, Sydney). Isolated cells were then analysed with Flow cytometry for purity check. CD14+ cells ($1x10^6$ cells/ml) were cultured with GM-CSF (100ng/ml), IL-4 (30ng/ml) and 2-mercaptoethanol (50μM) in complete RPMI1640 for 7 days with replenishment of the media every 2-3 days. The morphology was checked by microscope. The monocyte derived dendritic cells (MDDC) were cultured with various stimuli for desired studies.

2.2.2 Molecular analysis

2.2.2.1 DNA isolation from saliva

Genomic DNA was isolated from saliva using ORAgene-DNA OG-500 kit (DNAgenoTek) according to the manufacturer's instructions. Briefly, saliva samples were mixed in the DNA genotek kit by inversion and gentle shaking for a few seconds. The sample was then incubated at 50°C for 1 hour and 500μl of the sample mix was transferred into a 1.5ml tube. PT-L2P was then added and mixed by vortexing for a few seconds. The sample was incubated on ice for 10 minutes and centrifuged at room temperature for 15 minutes at 13 000 rpm. The supernatant was then transferred into a new 1.5ml tube and 600μl of ?% ethanol was added and mixed. The sample was centrifuged at 13 000 rpm for 5 minutes and the supernatant was removed and 250μl of 70% ethanol was added and incubated at room temperature for 1 minute and centrifuged at 13000 rpm for 5 minutes. The supernatant was then removed completely. 100μl of

H_2O solution was added and the pellet was dissolved by vortexing and pipetting. The DNA solution was stored at -20°C.

2.2.2.2 Whole Exome capture sequencing

The Illumina paired-end genomic DNA sample preparation kit (PE-102-1001, Illumina) was used for preparing the libraries including end repair, A-tailing and ligation of the Illumina adaptors. Each sample was prepared with an index using the Illumina multiplexing sample preparation oligonucleotide kit (PE-400-1001, Illumina) and then pooled in batches of six in equimolar amounts prior to exome enrichment. The Illumina TruSeq exome kit (FC-121-1008, Illumina) was used to capture the human exome for each sample pool. Each 6-plex exome enriched library was sequenced in two lanes of an Illumina HiSeq 2000 with version 2 chemistry as 100bp paired end reads.

Sequence reads were mapped to the GRCh37 or GRCh38 assemblies of the reference human genome using the default parameters of the Burrows-Wheeler Aligner (BWA, bio-bwa.sourceforge.net) [21]. Untrimmed reads were aligned allowing a maximum of two sequence mismatches and reads with multiple mappings to the reference genome were discarded along with PCR duplicates. Sequence variants were identified with SAMtools (samtools.sourceforge.net)(Li and Durbin 2010) and annotated using Annovar (www.openbioinformatics.org) (Wang, Li et al. 2010). A version of PolyPhen2 (genetics.bwh.harvard.edu/pph2) (Adzhubei, Schmidt et al. 2010), was utilized for the calculation of variant effect.

2.2.2.3 Single Nucleotide Variants (SNVs) analysis

SNVs were filtered with sequential parameters for selecting candidate SNVs. Rare or Novel SNVs were the first line of the filtering. The rare or novel alleles were filtered according to the sum of scores for mouse mutant phenotype in the homologous mouse gene, Mendelian disease associations (OMIM), pathway analysis (GO), immune system expression (Immgen) and polyphen2 score, according to the following scheme: mouse mutant phenotype: non-immune=0, nil=1, immune=2; OMIM, non-immune disease=-1, Nil=0, immune disease=1; Gene ontology, non-immune tissue-specific function=0.general cellular process=1, immune-related=2, proven T or B cell function=4; Immgen, high=3, medium=2, low=1, nil=0; Polyphen2 score.

2.2.2.4 RNA extraction

$1x10^6$ cells were washed twice with PBS at 300*g* for 5 minutes at 4°C. 1ml of Trizol was added to the cell pellet and mixed well by pipetting several times and incubated for 5 minutes at room temperature. 0.2ml of chloroform was added and mixed well by shaking tubes vigorously by hand for 15 seconds. After 2-3 minutes incubation at room temperature, the mixture was centrifuged at 12000g for 15 minutes at 4°C and the aqueous phase was carefully transferred into a 1.5ml tube. 0.5ml of 100% isopropanol was added to the aqueous phase and incubated for 10 minutes at room temperature. It was centrifuged at 12000g for 10 minutes at 4C and supernatant was removed. The pellet was washed with 1 ml of 75% ethanol and mixed by vortexing and centrifuged at 7500g for 5 minutes at 4°C. The wash was discarded and the pellet was air dried for 5-10 minutes. The pellet was resuspended with 30µl of RNase free water and mixed by passing the solution up and down several times through a pipette tip. The solution was

incubated in 55-60°C heat block for 10 minutes. RNA concentration was measured by nano drop and RNA was stored at -80°C.

2.2.2.5 Reverse Transcriptase PCR to cDNA

Frozen RNA, 5X miScript RT buffer and RNAse free water were thawed at room temperature. The reverse transcription master mix was prepared on ice as blew.

Component	Volume
miScript RT buffer 5X	4µl
RNase-free water	15µl-RNA volume
miScript Reverse transcriptase mix	1µl
Template RNA	1µg
Total volume	20µl

The mixture then was incubated for 60 minutes at 37°C then further 5 minutes at 95°C to inactivate miScript Reverse Transcriptase Mix. The cDNA was then stored at -20°C.

2.2.2.6 RT PCR

Commercial primers were purchased from Promega and real time PCR was run with Sybr green. 10pmol of forward and reverse primers were added to cDNA and Sybr green master mix (Promega). The PCR was initiated at 94°C for two minutes for DNA denaturation, and ran 35 cycles of denaturation at 94°C for 30 seconds, primer annealing at 55-70°C for 30 seconds and extension at 72°C for 1minute. This was followed by the final extension step, 5 minutes of 72°C and PCR products were then stored at 4°C or -20°C.

2.2.2.7 PCR primer design

Whole DNA sequences were obtained from DNA data base (NCBI). 1000bp of genomic DNA sequence surrounding mutations (500pb forward and 500bp backward) were subjected for Primer-BLAST (http://www.ncbi.nlm.nih.gov/tools/primer-blast/index.cgi?LINK_LOC=BlastHome). The primer set was selected after analysis for possible off-target amplification (BLAST).

2.2.2.8 PCR

The standard PCR solution was prepared with 2X Arbiter master mix (TrendBio) with forward and reverse primers on ice. (Table 2.4)The PCR was initiated at 94°C for two minutes for DNA denaturation, and ran 35 cycles of denaturation at 94°C for 30 seconds, primer annealing at 55-69°C for 30 seconds and extension at 72°C for 1minute. This was followed by the final extension step of 5 minutes of 72°C, and PCR products were then stored at 4°C or -20°C. 10µl of the products were loaded onto a 1.5% agarose gel with GelRed Nucleic Acid Gel Stain (Omar Bioscience) and electrophoresis was performed in 1XTAE buffer at 100 voltages for 30 minutes. The GelRed stained PCR products were visualised under UV light with Gel Doc XR+ system (Bio-Rad). The optimal annealing temperature was determined by gel photograph.

Component	Volume
DNA (100ng/µl)	1µl
Primers (10pmol)	1 µl
Arbiter 2x Master mix®	10µl
H_2O	8µl
Total volume	20µl

Table 2.4 PCR set up

The conditional PCR was prepared with Phusion hotstart Flex polymerase (NEB). 10pmol of forward and reverse primers and 10-100ng of DNAs, 0.3µl DMSO and up to

20µl of ds H_2O were added into a PCR tube. The PCR was initiated at 98°C for three minutes followed by 35 cycles of denaturation at 98°C for 10 seconds, primer annealing at optimal temperature (55°C -70°C) for 30 seconds, and extension at 72°C for 1~2 minutes. The final extension step was 5 minutes of 72°C. Products were loaded onto a 1~2% of agarose gel containing 1X GelRed and electrophoresis was performed in 1XTAE buffer at 100V for 30 minutes. The gel red stained PCR products were visualised under UV light with Gel Doc XR+ system (Bio-Rad).

2.2.2.9 Purification of PCR products- Gel extraction, Exo SAP

The PCR products were purified using QIAquick Gel Extraction Kit (QIAGEN) to remove polymerases, dNTP and the germline DNA. Alternatively, primers were removed from PCR product by ExoSAP-IT (usb®). 5µl of PCR products were mixed with 2µl of ExoSAP-IT. The mixture was incubated at 37° C for 15 minutes and 80° C for 15 minutes by thermocycler.

2.2.2.10 Sanger sequencing

2pmol of primers and 30ng of PCR products were submitted to Biomolecular Resource Facility at John Curtin School of Medical research, Australian National University.

2.2.2.11 Analysis of sequencing results

The sequencing results were aligned with a reference DNA to identify mutations using http://www.ebi.ac.uk/Tools/psa/emboss_matcher/nucleotide.html. Reference

sequences were obtained from NCBI or ensemble. Forward and reverse primers were used for conforming mutations.

2.2.2.12 Microarray

Naïve B cells were isolated by positive selection. Naïve B cells were CD19+, CD27-, CD10- and $CD21^{high}$. After sorting, the cells were incubated with anti Ig stimulus (5ug/ml) overnight at 37°C with 5% CO2. The activated naïve B cells were then used for RNA extraction. RNAs were extracted by either trizol method or RNA kit method. The RNA pellets were then resuspended with RNase free water and stored at-80°C for overnight. The RNA solution was then delivered to Ramaciotti Centre for Genomics (Sydney) for microarray analysis. Duplicate biological samples were prepared for the assay. The microarray was done in Affymetrix platform with gene array. The data were analysed by Partek analyser gene array was qualified for the assay.

2.2.3 Biochemical analysis

2.2.3.1 Gene expressing vector construction

2.2.3.1.1 Design primers for desired genes

In order to generate mammalian expressing vectors containing target genes, cDNA nucleotide sequences of the gene of interest were found through Ensembl and NCBI (Table 2.2). Using restriction enzyme mapper; http://www.restrictionmapper.org/; http://66.155.211.155/nebecomm/DoubleDigestCalculatorIntl.asp. We idenified appropriate restriction sites with the multicloning locus.

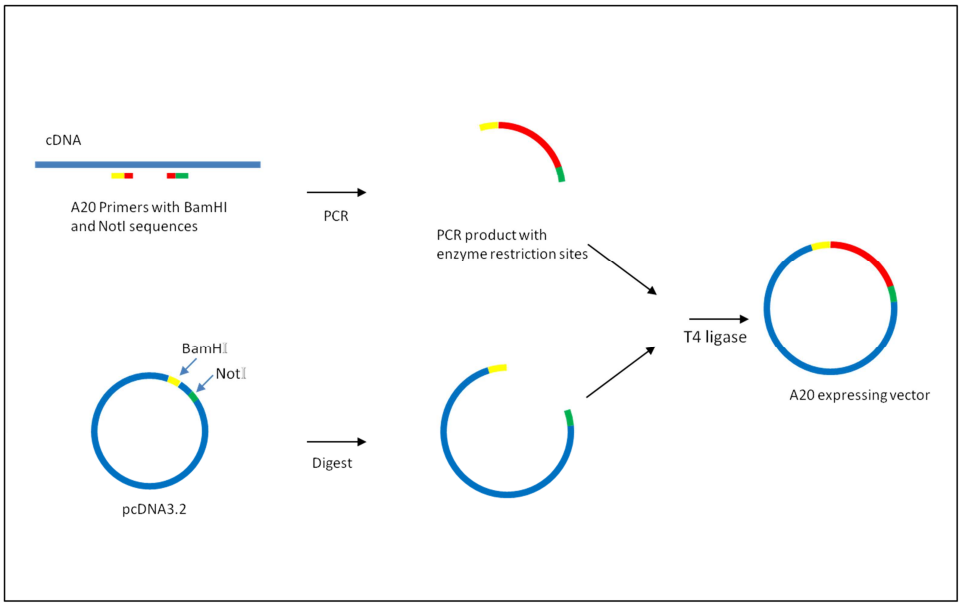

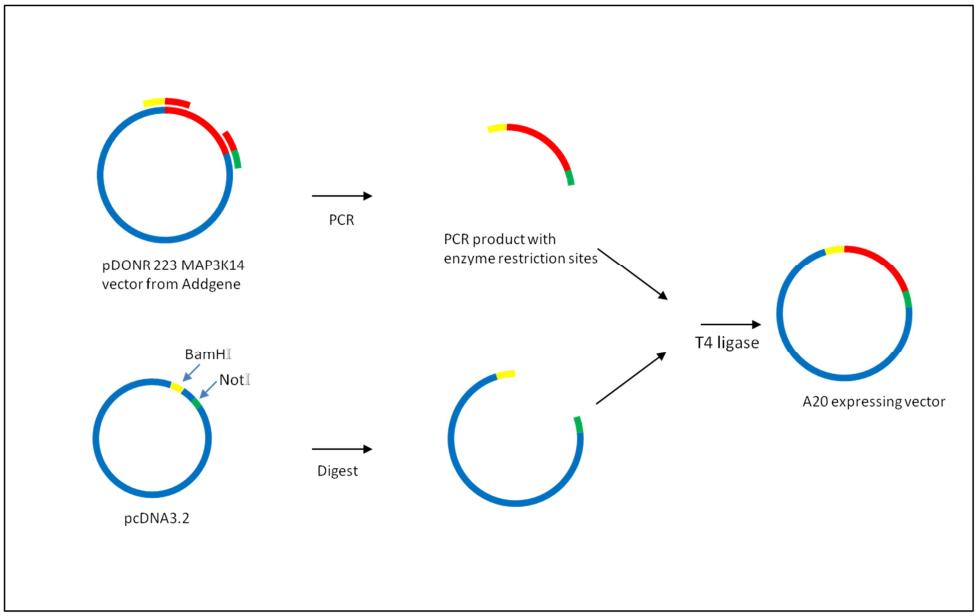

The primers contained approximately 15 nucleotides of the gene of interest and restriction site and additional nucleotides which were added for codon reading frame or

assistance of digestion. In forward primers Kozak sequence was added to help initiating transcription.

eg. A20cDNAF NotI

additional nucleotides restriction sequence

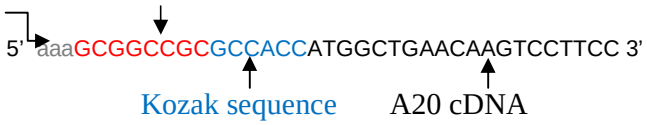

2.2.3.1.2 Digestion of DNAs

The genes of interest were amplified by polymerase chain reactions (2.2.2.2.). The PCR products were visualized by DNA staining with GelRed after electrophoresis. PCR products and vectors were set up with the following digestion enzyme reactions. The PCR product and vector were digested with restriction enzymes for 4 hours at 37°C.

1. A20-pcDNA vector (-c version)

Name	DNA	DNA (1ug)	NEBuffer2	KpnI	NotI	BSA	water	Total volume (µl)
A20 digestion	A20 pcr product	42.5	5	1	1	0.5	-	50
pcDNA digestion	pcDNA (-c)	3.6	5	1	1	0.5	38.9	50
+ control Single cut	pcDNA (-c)	3.6	5	1	-	0.5	39.9	50
+ control Single cut	pcDNA (-c)	3.6	5	-	1	0.5	39.9	50
-control No cut	pcDNA (-c)	3.6	5	-	-	0.5	40.9	50

2. TAX1BP1-Flag tagged pcDNA(+)

Name	DNA	DNA (1ug)	Buffer 3	BamH I	NotI	BSA	water	Total volum e (µl)
TAX1BP1 digestion	TAX1BP1 Pcr product	42.5	5	1	1	0.5	-	50
pcDNA digestion	pcDNA-Flag (+)	3	5	1	1	0.5	39.5	50
+ control Single cut	pcDNA-Flag (+)	3	5	1	-	0.5	40.5	50
+ control Single cut	pcDNA-Flag (+)	3	5	-	1	0.5	40.5	50
-control No cut	pcDNA-Flag (+)	3	5	-	-	0.5	41.5	50

3. NIK-pcDNA vector (– c version)

Name	DNA	DNA (1ug)	NEBuf fer3	BamHI	NotI	BSA	water	Total volume (µl)
NIK digestion	NIK	16.4	5	1	1	0.5	26.1	50
pcDNA digestion	pcDNA (-c)	3.6	5	1	1	0.5	38.9	50
+ control Single cut	pcDNA (-c)	3.6	5	1	-	0.5	39.9	50
+ control Single cut	pcDNA (-c)	3.6	5	-	1	0.5	39.9	50
-control No cut	pcDNA (-c)	3.6	5	-	-	0.5	40.9	50

2.2.3.1.3 Ligation of two products

Digested products were purified by gel extraction (protocol 2.2.2.). The amount of PCR product was determined according to the following formula (Klionsky, Abdalla et al.).

$$\frac{\text{Molar size of insert} \times \text{Concentration of vector (ng/µl)}}{\text{Molar size of vector}} \times (\text{ratio}) = \text{Conc of insert (ng/µl)}$$

1:3, 1:5, and 1:7 ratios were used for optimal results. The reactions were set up as below.

	Standard reaction (1:3)	Standard reaction (1:5)	Standard reaction (1:7)	Positive control	Negative control
5X rapid T4 ligation buffer	2µl	2µl	2µl	2µl	2µl
Digested vector (~5kb)	1µl (50ng)	1µl (50ng)	1µl (50ng)	-	1µl
Digested PCR product (~2kb)	1.2µl (60ng)	2µl(100ng)	2.8 (140ng)	-	1µl (60ng)
Single cut vector	-	-	-	1ug (50ng)	-
T4 DNA ligase	1µl	1µl	1µl	1µl	-
Deionized water	14.8µl	14µl	13.2µl	16µl	16µl
Total	20µl	20µl	20µl	20µl	20µl

The reactions were then mixed by pipetting and incubated overnight at 4°C.

2.2.3.1.4 Transformation

The ligation reactions were briefly centrifuged and 2µl of each ligation reaction was transferred to a new tube. 0.1ng of uncut plasmid was added to separate 1.5ml tubes and incubated with DH5α cells on ice for 20 minutes. The tubes were then warmed in a 42°C heat block for 45 seconds and then immediately placed into an ice bath for a further 2 minutes. 950µl of SOC medium (sigma) was added into the tubes. The tubes were then incubated for 1.5 hours at 37°C with shaking at about 150rpm. 50µl or 100µl of each transformation culture was plated onto an LB agar plate containing Ampicillin

(100ug/ml). The plates were then incubated overnight (16-24hours) at 37°C and the number of colonies were recorded from each plate.

2.2.3.1.5 Plasmid isolation

A single colony was inoculated with 5ml of LB medium containing ampicillin (100ng/ml) and incubated at 37 °C overnight with shaking. 1ml of each culture was stored with glycerol to a final concentration of 20% at -80°C. QIAprep Spin Miniprep Kit (QIAGEN) was used to isolate plasmids. Briefly, bacterial cell pellets were obtained by centrifugation at 13000rpm for 5 minutes and were resuspended in the manufacturer's lysis buffer (QIAGEN). Denatured and precipitated cellular components were removed by centrifugation (at 13000rpm, 1 minute) and filtration using the QIAprep columns. The columns were washed with PE buffer which contained 70% of EtOH and then were eluted with H2O by centrifugation at 13000rpm for 2 minutes and the plasmid concentration was measured by nanodrop and the DNA solution was stored at -20°C.

2.2.3.2 Transfection

2.2.3.2.1 Lipofectamine

HEK293 or HEK293T cells were seeded at $1x10^6$ cells per well in 6 well plates and incubated overnight at 37°C with 5% CO_2. When cells were reached approximately 70-90% confluence, transfection was performed using 2ug of mammalian expression vectors was added in 250 µl of incomplete RPMI with 2µl of PLUS™ reagent (Life technologies), incubated at room temperature for 5 minutes while 10µl of lipofectamine® LTX (Life technologies) was added in 250µl of incomplete RPMI and

incubated at room temperature for 5 minutes. Next, these two solutions were combined and incubated at room temperature for 30 minutes. The overnight culture media was replenished with 1.5ml of fresh complete media without antibiotics. 0.5ml of transfection solution was added dropwise onto the cell culture and mixed gently by rocking the plate. The transfected cells were incubated for an additional 1-2 days at 37°C with 5% CO_2.

2.2.3.2.2 Neon Transfection

Neon ™ Transfection System was used for electroporation. Raji cells were washed with PBS and 1 x 10^6 cells were pelleted and mixed with 50µl of R buffer. 10µg of DNA mixer was separately prepared with 50µl of R buffer. The DNA mixed was mixed with the cell solution and aspirate d into Neon™ pipette. The pipette was inserted into Neon tube containing 3ml of Electrolytic buffer. The electroporation was completed by pressing start button with appropriated protocols. The sample was then added in prewarmed complete media without antibiotics and incubated at 37°C in humidified CO_2 incubator.

2.2.3.3 Bradford protein assay

Total protein content was determined by serial dilution of the cell lysate in PBS, and addition of 20µl of Bradford regent (Sigma) was added to each wells and the plate was incubated for 30 minutes, then analysed for absorbance at 570nm, and compared to the standard curve.

2.2.3.4 Immunoblotting

Cell lysates were prepared in RIPA buffer (Sigma) or CytoBuster ™ protein exraction reagent (Novagen) with protease inhibitor cocktail (Dong, Strome et al.) and Halt phosphatase inhibitor (Piercent) and the lysates were subjected to SDS-PAGE. After protein estimation, equal amounts of proteins were mixed with 2X SDS sample loading buffer containing 10% of β-mercaptoethanol freshly and boiled at 100°C for 5 minutes. The samples were then loaded in precast polyacrylamide gels with precision plus protein™ dual color standards (Bio-rad). The gel was run at 120V for 1 hour, then transferred to PVDF membrane by wet transfer method. 20X transfer buffer was diluted with H_2O and chilled overnight. The transfer sandwiches were prepared with transfer buffer (- charge cassette- sponge- gel-PVDF membrane- sponge- cassette + charge), run at 120V for 2 hours. Membranes were blocked for 1 hour 3~5% of BSA in TBST or 5% of skim milk in TBST. Primary antibodies were added with blocking buffer and incubated at 4°C overnight with gentle shaking. The membranes were washed with washing buffer (TBST 1X) for 10 minutes three times. HRP-conjugated secondary antibodies were added with blocking buffer and incubated at 4°C for 1 hour. The membranes were washed with washing buffer for 10 minutes three times anf analysed using the Amersham ELC western blotting system (GE healthcare) and band intensity was quantified with Fujifilm multi gauge software and normalized to loading control.

2.2.3.5 Immunofluorescence

HEK293 cells were transfected with indicated constructs and treated with TNF or left unstimulated. Cytospins were fixed with 4% paraformaldehyde in phosphate buffered saline, and permeabilized with 1% Triton X, then blocked with 3% skim milk and

stained with primary antibodies at 4°C overnight. Slides were washed three times with PBST for 5 minutes each before secondary immunofluorescent antibodies were added. The slides were then washed another three times with PBST and mounted with anti fade mounting media containing Dapi. Images were acquired by Leica SP5 confocal microscope with a 63x oil immersion objective.

2.2.3.6 Deubiquitination assay

Human *TNFAIP3* were amplified with AccuPrime *Pfx* DNA polymerase (Invitrogen) from cDNA pool obtained from human peripheral blood. The full-length coding sequence of TNFAIP3 was cloned into the pcDNA3.1+ vector and confirmed with sequencing. PCR-based mutagenesis was used to introduce the mutations (H256A and S254R) in this study. The OTU domains of human *TNFAIP3* (encoding 2-370 residues) were cloned between BamHI and XhoI sites in pGEX-6P-1 vector (GE Healthcare). GST-fused TNFAIP3 OTU protein was expressed in *E. coli* BL21 (BIOLINE) cells at 30ºC for 12-16 hrs with 200 µM IPTG. Cells were lysed by sonication in 50 mM Tris (pH8.0), 100 mM NaCl, and 1 mM EDTA, followed by the addition of Triton-X100 (1% w/v). The lysates were cleared by centrifugation, and then incubated with glutathione agarose (SIGMA). Precipitated complex was washed three times with lysis buffer, followed by washing with Prescission buffer (50 mM Tris [pH 7.5], 150 mM NaCl, 1 mM EDTA, and 1 mM DTT). TNFAIP3OTU protein was excised with Prescission protease (GE Health) and collected from supernatant. The purified A20 OTU domain was tested for hydrolysis of Lys 63 linked tetraubiquitin chains in a time course experiment *in vitro*. Purified TNFAIP3OTU proteins were incubated in 100 µl of

DUB buffer (25 mM HEPES [pH 8.0], 5 mM DTT, 5 mM MgCl2) containing 2.5 µg of K48- or K63- linked polyubiquitin chain (#UC-230, #UC-330 from BostonBiochem). At the indicated time, 20 µl of reaction mixture was collected and enzymatic reaction was stopped by the addition of SDS sample buffer. Negative control was known mutation A20 H256S, which contains an amino acid substitution at 256 from histidine to serine.

2.2.3.7 Co Immunoprecipitation

HEK293T cells were co-transfected with A20 and TAX1BP1 expressing vectors. Cells were washed with PBS and 250µl of lysis buffer was added to each well on a 6 well plate and incubated on ice for 30 minutes. Lysed cells were collected into 1.5ml tubes. A 50% protein G agarose slurry was prepared with lysis buffer. Lysed cells were spun down at 13000rpm for 15 minutes at 4°C. Total protein was measured in the supernatant. For preclearing, 50µl of 50% slurry protein G was added into the sample tube with an isotype control antibody (2µg). The mixture was incubated at 4^{o}C overnight with gentle rotation. The mixture was spun down at 1300rpm for 1 minute at 4^{o}C, and the supernatant was transferred into 3 new tubes and anti Myc, anti Flag or anti Isotype antibody (2µg each) and 30µl of protein G agarose slurry were added. The mixture was incubated at 4°C for 2 hours with gentle rotation. The protein agarose slurry was spun down and supernatant was discarded. Approximately 1ml of lysis buffer was added and the slurry was washed 3 times at 1300rpm, 4°C. 30µl of 2XSDS sample buffer was added and the protein solution was boiled at 100°C for 5 minutes. The denatured samples were stored at -20°C for further immunoblotting experiments. Anti c-Myc and anti FLAG antibodies were used for western blot.

2.2.3.8 CRISPR CAS9

pX330 U6 chimeric DD CBh hSpCas9 plasmid was obtained from Addgene.

Guide RNA containing target cutting site (CCG) was constructed. In order to introduce desired mutations, DNA repair template was also synthesized (approximately 100bp). Cells were then transfected with these nucleotides by either Neon transfection or Lipofectimine transfection. Cells were then incubated at 37°C for 24 hours in humidified with Co_2 incubator. The following day single cells were isolated by reporter gene expression such as GFP and mCherry and the single cells were cultured for 3-4 weeks. Sanger sequencing and western blot were conducted to confirm knockout of the gene of interest.

3 Pedigree I

3.1 Results

3.1.1 Discovery of rare mutations in patients with CVID

This chapter describes results from two kindreds recruited to the Australian and New Zealand Antibody Deficiency Allele (ANZADA) study. So far, more than 150 individuals have been investigated by whole exome sequencing (WES) to identify causative genetic variants. Analysis of this dataset has revealed that mutations within the same gene is exceptionally uncommon in CVID, once variants in known CVID-associated genes have been excluded. For our discovery programme, we hypothesized that a subset of CVID is caused by rare, highly penetrant genetic variants within the coding region of the genome.

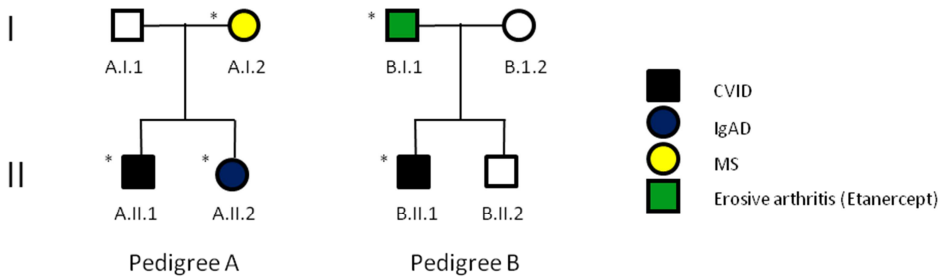

Figure 3.1 Pedigree of the family. Two affected individuals and their relatives were recruited through part of the ANZADA study. Circles represent female subjects and squares represent male subjects. Colour filled symbols denote clinical features; Black, common variable immune deficiency (CVID); blue, IgA deficiency syndrome (IgAD); yellow, multiple sclerosis (MS); green, Erosive Arthritis (EA). * denotes A20 ^{S254R} carrier.

First, we analysed novel mutations and then filtered the mutant genes according to immune relatedness. After this analysis, only one specific novel mutation was identified

in more than one pedigree, a missense mutation in *TNFAIP3*. *TNFAIP3* encodes the deubiquitinase A20, which is already known to be an important immune regulator.

3.1.2 A20 mutations and functional analysis

3.1.2.1 *TNFAIP3* sanger sequencing results

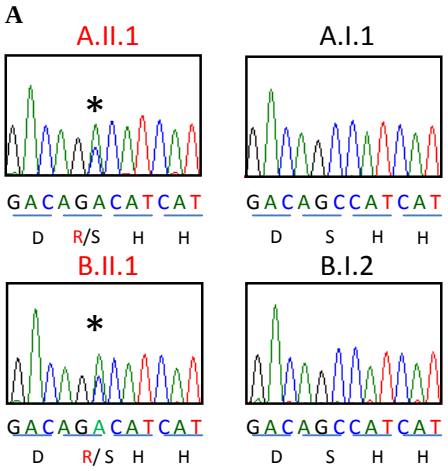

B

cDNA		Protein	
Position	**Allele change**	**Position**	**Residue change**
828	AGC ⇒ AGA	254	S [Ser] ⇒ R [Arg]

C

D

```
                                    *
Human       IYLPLHWPAQECYRYPIVLGYDSHHFVPLVTLKDSGPE
Mouse       IYLPLHWPAQECYRYPIVLGYDSQHFVPLVTLKDSGPE
Macaca      IYLPLHWPAQECYRYPIVLGYDSHHFVPLVTLKDSGPE
Bovine      IYLPLHWPAQECYRYPIVLGYDSQHFVPLVTMKDSGPE
Horse       IYLPLHWPAQECCRYPIVLGYDSHHFVPLVTLKDSGPE
Opossum     IYLPLHWPAQECYKYPIVLGYDSQHFAPLVTLKDSGPE
Platypu     IYLPLHWPAHECYRYPIVLGYDSQHFVPLVTLKDSGPE
Xenopus     IYLPLHWPAKECYKYPVVLGYDSQHFAPLVTMKDSGPE
Danio       IYLPLHWPPGECYKYPIVLGYDSQHFAPLITIKDSGPE
```

Figure 3.2 S254R *TNFAIP3* mutation A. Sanger sequencing of S254R *TNFAIP3* heterozygous mutation. **B.** The position of the missense mutation. **C.** Schematic representation of human A20 structure contains ovarian tumour (OTU) domain and seven zinc finger (ZF) domain. The mutation S254R in OTU domain is denoted. **D.** Conservation of amino acid at the residue. * denotes A20 S254R and A shows active site.

Using WES, we identified an identical missense mutation (g.8910C>A) in probands from two separate unrelated kindreds (A.II.1, A.II.2 and A.I.2, Figure 3.1). In each case, the *TNFAIP3* mutation was confirmed by Sanger sequencing. We went on to genotype other members of each kindred. We concluded that the mutation in family A may have been transmitted from the proband's deceased maternal grandfather (Figure 3.3).

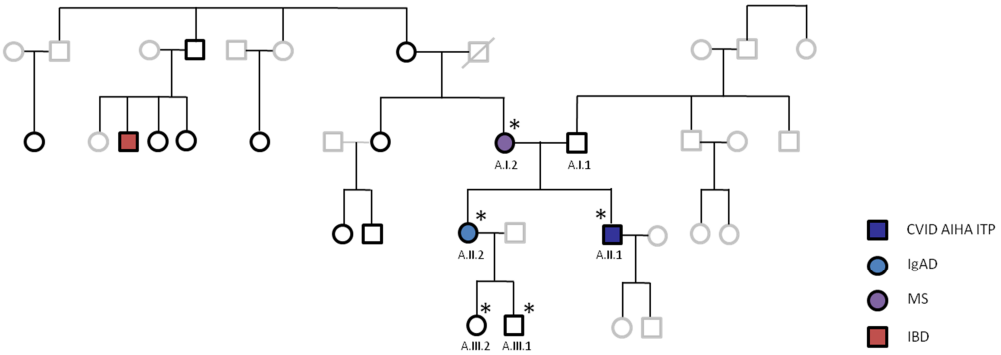

Figure 3.3 Pedigree of Family A Sanger sequencing of *TNFAIP3* heterozygous mutation. Circles represent female subjects and squares represent male subjects. Subjects with bold lines were Sanger sequenced. CVID, common variable immune deficiency; AIHA, autoimmune haemolytic anemia; ITP, immune thrombocytopenic purpura; IgAD, IgA deficiency syndrome (IgAD); MS, multiple sclerosis, IBD, inflammatory bowel disease; green. * denotes A20 ^{S254R} carrier.

In family B, B.II.1 and his father B.I.1 were carriers of the mutation. Genomic DNA from both saliva and lymphocytes was tested and yielded similar findings. The heterozygous mutation (C→A) encodes an amino acid substitution of serine with arginine. This mutation remains novel according to 1000 genomes, dbSNP, and the Exome aggregate consortium (ExAC). Three major mutation prediction algorithms,

Polyphen2, MutationTaster and SIFT, predicted that it is a damaging mutation. S254 is conserved from human to danio.

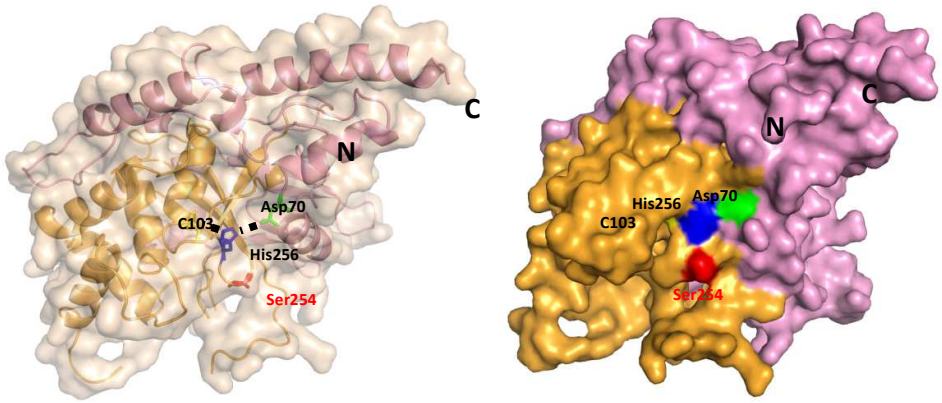

Figure 3.4 Crystal structure of A20 and location of S254R residue. C103 and His256 are active sites in DUB. Asp70 is a supporter of the active sites.S254R is adjacent to the active sites

Crystal structures of A20 predict that the mutation disrupts the catalytic triad preventing nucleophilic hydrolysis or steric hindrance of substrate (Figure 3.4) Figure 3.2C shows the structure of A20. It has an ovarian tumour domain (OTU) at its C terminal and a zinc finger domain at the N terminal. In the DUB region there are two residues critical to function (103 and 256); substitutions of either of these amino acids leads to loss of its DUB function. Thus, the S254R mutation is located two amino acids away from one of the residues thought to be critical for DUB activity. Taken together, these findings led us to hypothesize that S254R alters the conformational structure to alter A20 function.

3.1.2.2 In vitro A20 ubiquitination assay

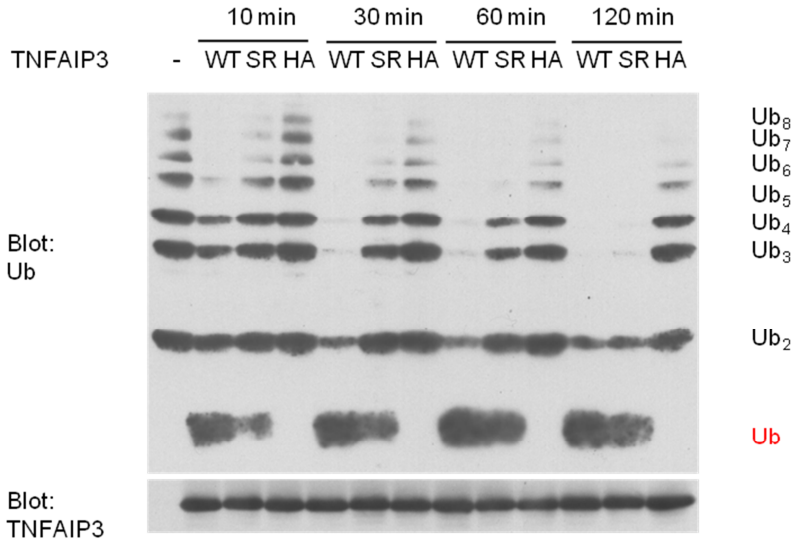

Figure 3.5 Catalytic activity of the mutation. Wildtype or R254S A20 OTU domain was incubated with K48 linked polyubiquitin. At indicated times, enzyme reaction was stopped and hydrolysis of polyubiquitin chains was examined by immunoblotting ubiquitin chains. SR-OTU domain contains amino acid substitution at 254 from serine to arginine; HS-OTU domain contains an amino acid substitution at 256 from histidine to serine; Ub-Ub8, monomeric to heptameric ubiquitin chains

We began by testing the deubiquination activity of the mutant protein. Wild type or mutant versions of the A20 OTU domain were expressed in *E.coli* and purified by the GST fusion system from GE healthcare. GST fusion proteins containing the A20 OTU domain were precipitated with glutathione agarose (SIGMA) followed by cleavage of the GST proteins bound to glutathione sepharose. Purified OTU domains were tested for their capacity to hydrolyse Lys48-linked heptameric ubiquitin chains in an in vitro time course experiment. Polyubiquitin chains were incubated with either wild type OTU domain, a catalytically inactive OTU domain (His256>Ala), or the S254R OTU domain. Polyubiquitin chains were detected by western blotting using anti-ubiquitin antibodies. The mutant S254R OTU domain showed reduced catalytic activity compared to the wildtype polypeptide (Figure 3.5). After 30 minutes incubation,

wildtype A20 OTU cleaved most of the polyubiquitin chains and generated dimeric or monomeric ubiquitin chains, whereas mutant S254R OTU domain cleaved only octameric and heptameric ubiquitin chains, similar to catalytically inactive H256A OTU. After 60 minutes, S254R OTU failed to lyse tetrameric ubiquitin chains while wild type OTU cleaved most of the polyubiquitin chains and resulted in monomeric ubiquitin chains. Thus, the catalytic activity of S254R appears to be intermediate between H256A and wildtype OTU. At the 2 hour incubation time point, S254R produced di- or mono-meric ubiquitin chains while H256A resulted in UB5 and UB6 chains.

3.1.2.3 pIKBα activation

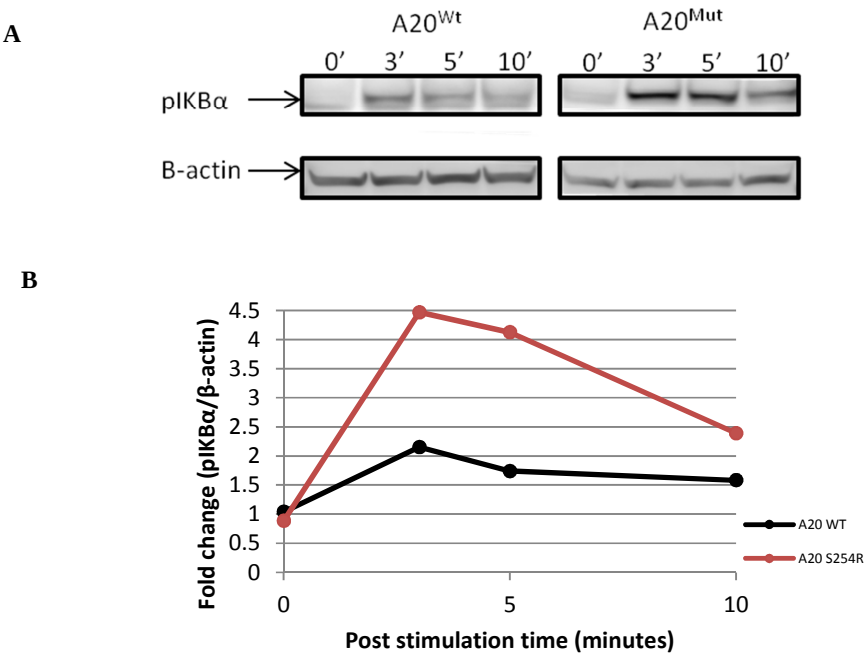

Figure 3.6 Immunoblot analysis for phosphorylated IKBα A. Constructs for wildtype or S254R A20 were transfected into HEK293T. pIKBα was analysed at 0, 3, 5, 10 minute after TNFα stimulation. β-actin was assessed as a housekeeping gene. A20 S254R, A20 containing an amino acid substitution at 254 from serine to arginine; **B.** Summary plot.

A20 is a negative regulator of the NF-kB pathway that acts on many target proteins. We examined NF-kB activation in the presence of mutant A20. We expressed wildtype or S254R mutant A20 by transient transfection in HEK293T, then cells were stimulated with TNFα for various times (as shown). Cell lysates were analysed by western blot for pIKBα. We observed that $A20^{S254R}$ resulted in enhanced and prolonged pIkBα activity compared to wildtype (Figure 3.6). This difference was evident at 3 minutes after the stimulation, and persisted at 5 minutes after the stimulation. By 20 minutes, pIKBα was similar in both mutant and WT transfectants, and to baseline. These findings indicated that $A20^{S254R}$ exhibits robust and prolonged NF-kB activity compared to its wildtype. DUB and IkB activation assays demonstrated that the S254R mutation results in loss of function.

3.1.3 Summary of clinical phenotypes

A.II.1 is a 41 year old male who was diagnosed with CVID after presenting with autoimmune thrombocytopenic purpura and panhypogammaglobulinaemia at age 19 years. As a result of refractory thrombocytopenia (platelets 2 x 10^9/L) he underwent a splenectomy at age 20. At age 30 he was diagnosed with autoimmune haemolytic anaemia (AIHA). He has a history of recurrent sinopulmonary infection, campylobacter enteritis, and intestinal giardiasis. He was commenced on intravenous immunoglobulin replacement after the diagnosis of hypogammaglobulinaemia was made. He suffered several further bouts of AIHA, which were managed with high-dose corticosteroids. He continued to suffer with recurrent bacterial sinusitis despite adequate antibody replacement. He has developed symptoms of colitis, with diarrhoea, weight loss, abdominal pain and abdominal lymphadenopathy.

The proband (A.II.1) is the son of a healthy father (A.I.1). His mother (A.I.2) reports a history of multiple sclerosis, although she is currently well in the absence of immune modulating medication. A.II.1 (sister (A.II.2) of the proband) has IgA deficiency. She gives no history of recurrent infection.

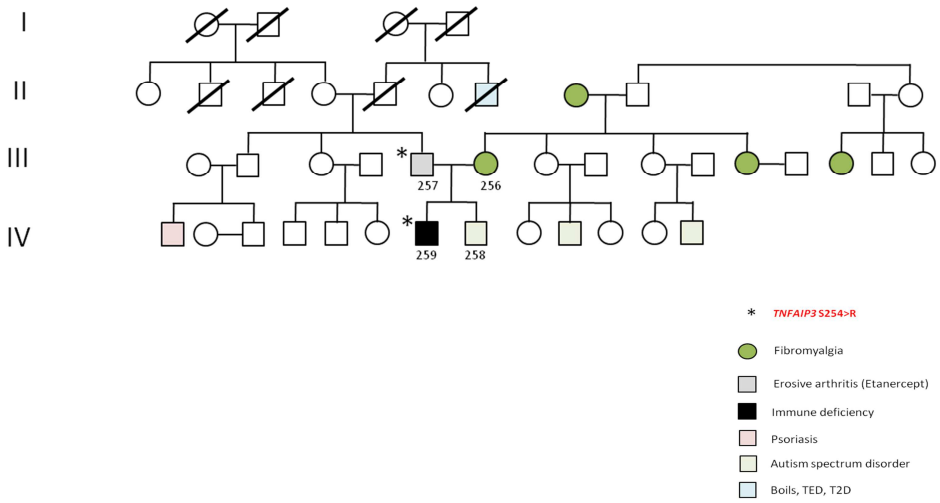

Figure 3.7 Pedigree of Family B Sanger sequencing of *TNFAIP3* heterozygous mutation. Circles represent female subjects and squares represent male subjects. * denotes A20 ^{S254R} carrier. TED, thyroid eye disease; T2D, type 2 diabetes

The proband (B.II.1) presented with recurrent bacterial respiratory tract infections in the first decade of life and was diagnosed with hypogammaglobulinaemia at age 8 years. He was commenced on intravenous immunoglobulin replacement therapy. He has one sibling, who has been diagnosed with autistic spectrum disorder. B.II.1 gives no history of autoimmune disease. The proband's father has refractory seronegative arthritis with joint erosions. He failed to respond to methotrexate or sulfasalazine, but made an excellent response to TNF antagonist (etanercept).

3.1.4 Cellular phenotype

3.1.4.1 B cell phenotype

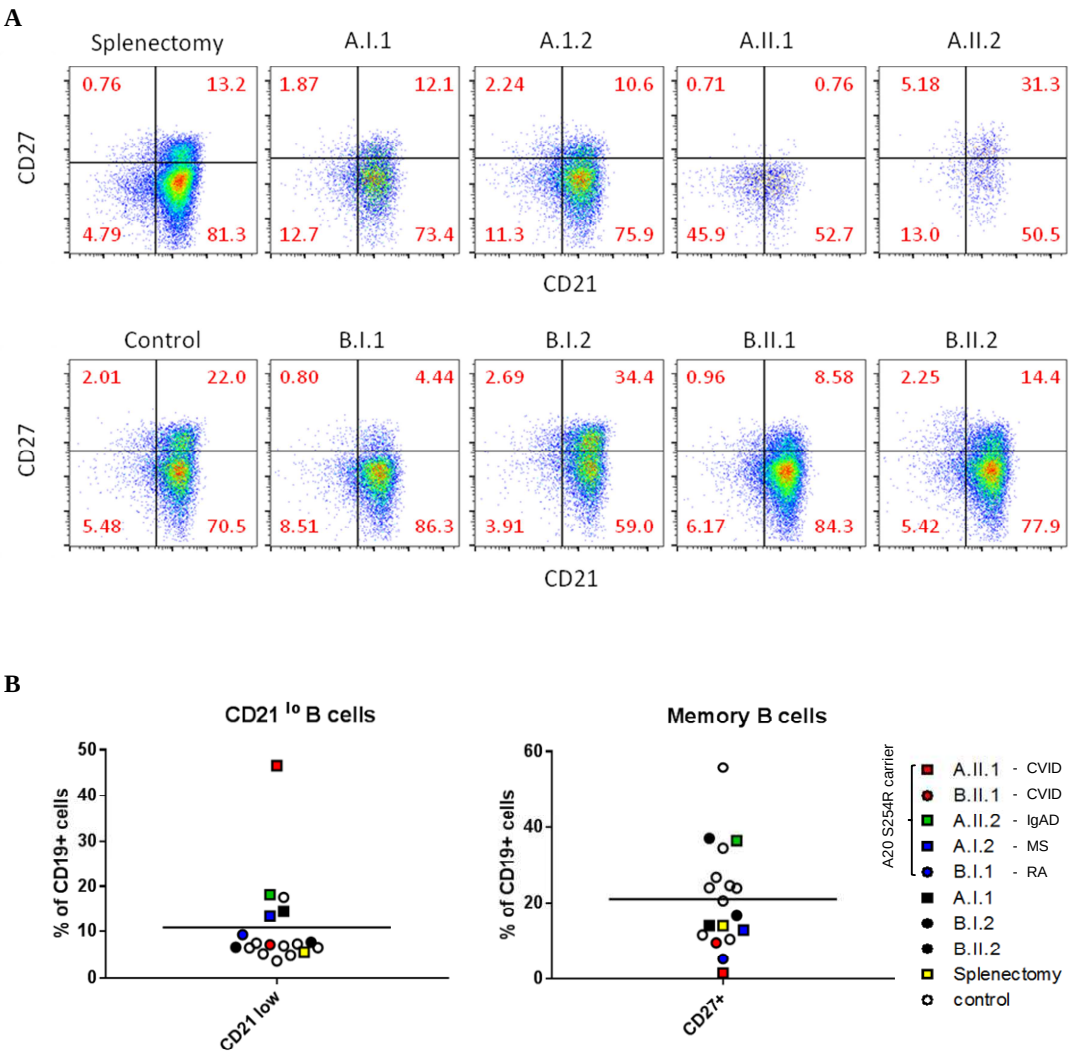

Figure 3.8 Flow cytometric analysis of B cells. A. CD19+ cells were analysed for CD21 and CD27 expression. Memory cells ($CD27^{+}$, $CD38^{+}$) and $CD21^{lo}$ B cells were identified. A representative sample from an unrelated splenectomised patient is shown. **B.** Summary plot of $CD21^{lo}$ cells and memory B cells. Coloured symbols indicate S254R carriers. Clinical phenotypes are indicated. CVID, common variable immune deficiency; IgAD, Immunoglobulin A deficiency; MS, multiple sclerosis; RA, rheumatoid arthritis. Square presents family A and circle presents family B.

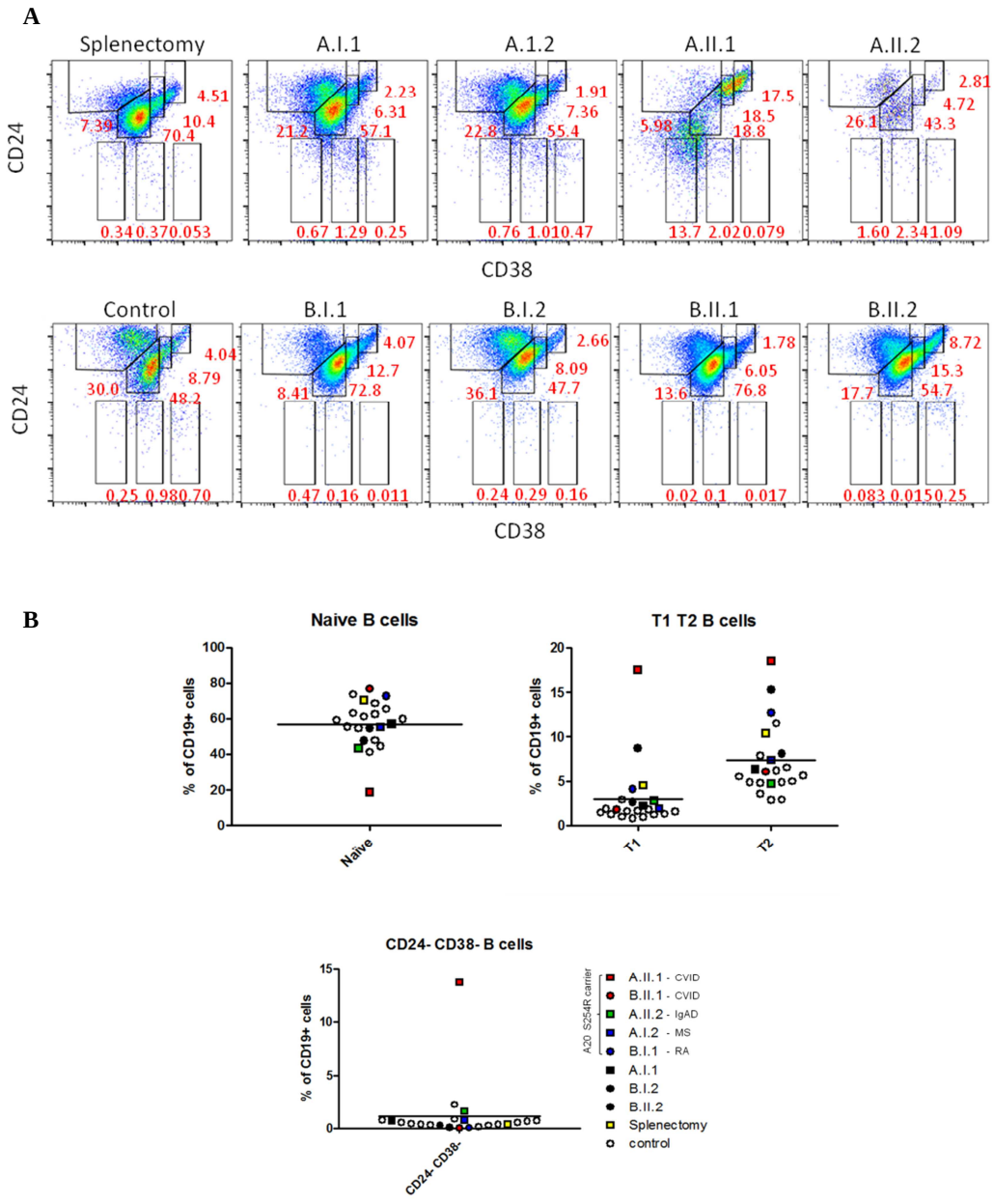

Figure 3.9 Flow cytometric analysis of B cells $CD19^{+}$ $CD3^{-}$ cells were analysed for CD24 and CD38 expression. Naïve B cells ($CD24^{+}$, $CD38^{+}$), transitional stage 1 B cells ($CD24^{+++}$, $CD38^{+++}$), transitional stage 2 B cells ($CD24^{++}$, $CD38^{++}$), memory B cells ($CD24^{++}$, $CD38^{+}$), anergic B cells ($CD24^{-}$, $CD38^{-}$), and plasma cells ($CD24^{-}CD38^{+++}$) were identified. Healthy individual and a patient that underwent a splenetomy were used as controls. **B.** Summary plot of naïve, T1, T2, and anergic B cells ($CD24^{-}$, $CD38^{-}$). T1 B, transitional stage 1 B cells; T2 B, transitional stage 2 B cells; PB, plasmablast/plasma cells. $A20^{S254R}$ carriers are identified by coloured symbols. Clinical diagnoses are shown. Squares indicate family A and circles indicate family B.

Initial flow cytometric analysis of circulating B lymphocytes showed that A.II.1 has normal numbers of $CD19^{+}$ cells but very few memory B cells (1%), and little evidence of either class-switched or non-switched memory B cells ($CD19^{+}CD27^{+}$). CD21 and CD27 expression analysis showed that approximately 40% of $CD19^{+}$ cells of A.II.1 were $CD21^{lo}$ B cells (Figure 3.8). He is therefore classified as Freiburg class Ia, defined as < 0.4% of class switched memory B cells and more than 20% of $CD21^{lo}$ B cells (Warnatz, 2009).

B cell analysis by CD24 and CD38 expression reveals that A.II.1 has a deficiency of mature naïve B cells ($CD24^{++}$, $CD38^{++}$) compared to healthy controls (Figure 3.9). In addition, A.II.1 showed abnormally high proportions of transitional T1 ($CD24^{+++}$, $CD38^{+++}$) and T2 B cells ($CD24^{+}$, $CD38^{++}$), which was confirmed by CD10 analysis. Approximately 30% of his B cell compartment was $CD10^{+}$, which represents a 5-fold increase relative to controls (Appendix IV). We also identified a prominent population of B cells that are CD24- CD38- in A.II.1. In contrast, the other A20 carrier A.I.2 showed a normal range of memory, naïve and transitional B cells. $CD21^{lo}$ B cells accounted for approximately 5% of $CD19^{+}$ cells. A.II.2 showed that slight deficiency in memory B cells and increase in transitional B cells.

Since A.II.1 underwent a splenectomy we also analysed B cells from several individuals who had undergone splenectomies for autoimmune thrombocytopenia (ITP) in the absence of hypogammaglobulinaemia. None of those individuals had a similar B cells phenotype to that of A.II.1. A representative flow cytometric plot is shown in Figure 3.9, and this individual showed reduced memory B cells but normal naive, transitional

and $CD24^{-}CD38^{-}$ B cells. Thus, the B cell profile of A.II.1 is not obviously accounted for by splenectomy. In conclusion, A.II.1 exhibits a B cell phenotype that is quite different from both healthy controls and other $A20^{S254R}$ mutation carriers.

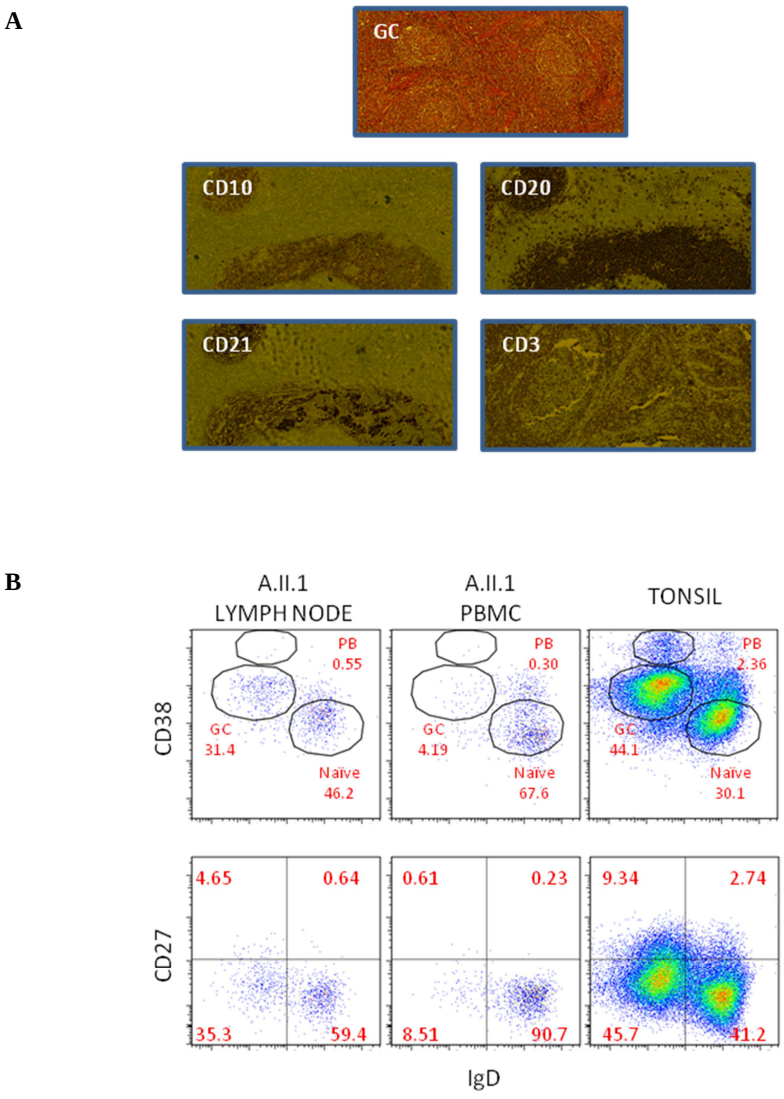

Figure 3.10 Analysis of lymph node from the proband A.II.1. A. Photomicrographs of lymph node analysied by Haematoxylin and Eosin staining, or by immunohistochemistry with indicated antibodies. **B**. Flow cytometric analysis of B cells from lymph node biopsy. CD38 and IgD or CD27 and IgD were analysed on CD19+ cells. Analysis of tonsil from an unrelated donor is shown for comparison. GC, Germinal centre B cells; PB, plasmablast cells.

B.I.1 and B.II.1 carry the identical *TNFAIP3* S254R mutation. Both have high proportions of mature naïve B cells (approximately 70%) with slightly reduced memory B cells ($CD24^{+++}$, $CD38^{+}$). Nonetheless, we found no evidence of expansion of the $CD24^{-}$ $CD38^{-}$ population or increased $CD21^{low}$ B cells.

At age 39, A.II.1 underwent a diagnostic mesenteric lymph node biopsy, as part of investigation for diarrhoea, weight loss and intra-abdominal lymphadenopathy on imaging. By haematoxylin and eosin staining, the architecture of the node was preserved, except for the absence of plasma cells. Immunohistochemical analysis revealed germinal centres $CD10^{+}$, $CD20^{+}$ and $CD21^{+}$ cells (Figure 3.10), which were also $Bcl6^{+}$. Consistent with these findings, flow cytometric analysis revealed that GC B cells accounted for approximately 31% of his $CD19^{+}$ cells. Remarkably, despite abundant GC B cells, neither memory B cells nor plasmablasts were identified.

3.1.4.2 T cell phenotype

Analysis of circulating T cells (Figure 3.11) revealed that the majority of CD4 T cells in A.II.1 adopted an effector memory phenotype ($CD45RA^{-}$, $CCR7^{+}$). Strikingly, there were very few naïve T cells ($CD45RA^{+}$, $CCR7^{+}$) (Figure 1.7). By contrast, the majority of CD4 T cells in A.I.2, B.I.1, A.II.2 and B.II.1 were naïve ($CCR7^{+}$, $CD45RA^{+}$), and their effector memory T cells ($CD45RA^{-}$, $CCR7^{+}$) were comparable to healthy controls. In A.II.1, CD8+ T cell analysis revealed a skewing to effector memory cell formation (TEM, $CD45RA^{-}$, $CCR7^{-}$) or $CD45^{+}$ effector memory T cells (TEMRA, $CD45RA^{+}$, $CCR7^{-}$) with very few naïve T cells.

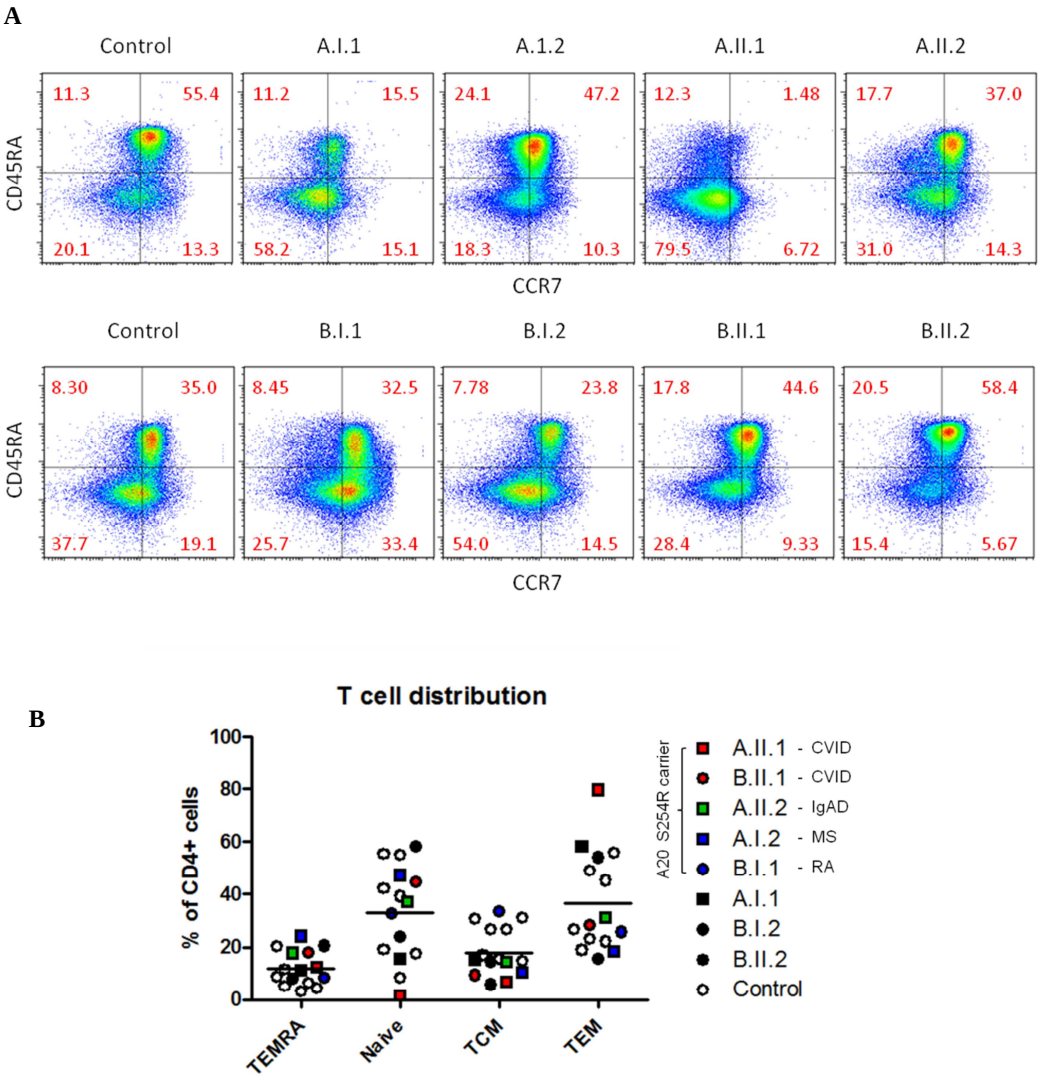

Figure 3.11 Flow cytometric analysis of T cell distribution. A. CD45RA and CCR7 expression were analysed for CD45+ effector memory T cells ($CD45RA^+$, $CCR7^-$), naïve T cells ($CD45RA^+$, $CCR7^+$), central memory T cells ($CD45RA^-$, $CCR7^-$), and effector memory T cells ($CD45RA^-$, $CCR7^+$). **B.** Summary plot, $A20^{S254R}$ carriers are shown with coloured symbols. TEMRA, $CD45RA^+$ effector memory T cells; TCM, central memory T cells;TEM, effector memory T cells

Next, effector CD4 T cells subsets were examined for chemokine receptor expression (Figure 3.12). The majority of effector helper T cells in A.II.1, A.I.2 and A.II.2 adopted a Th2 phenotype ($CXCR3^-$, $CCR6^-$). By contrast, effector T cells

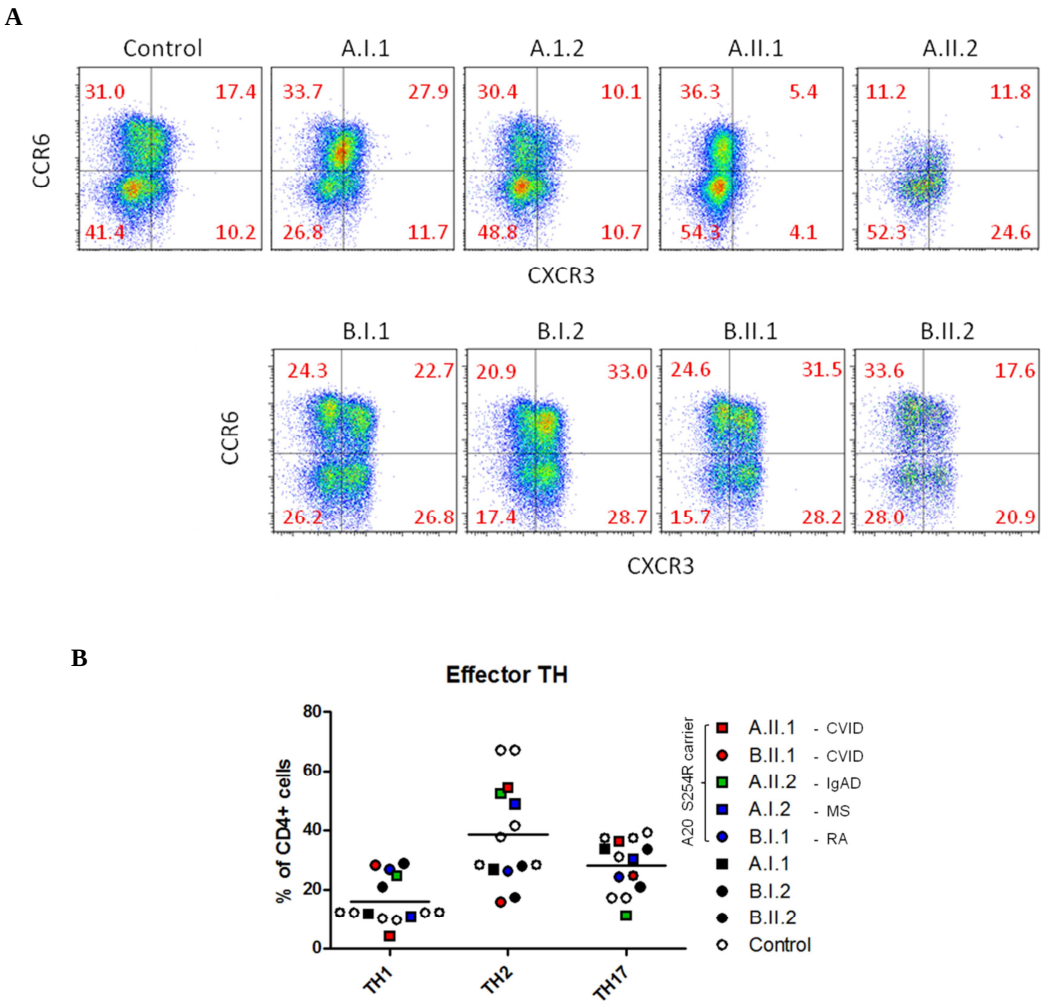

Figure 3.12 CD4+ T cell subsets. A. Flow cytometric plots of CCR6 and CXCR3 expression. TH1 (CXCR3- CCR6+), TH2 (CXCR3- CCR6-), TH17 (CXCR3+ CCR6-) were shown. **B.** Intercellular expression of cytokine IFN-g, IL-4, and IL-17 were analysed and represent TH1, TH2 and TH17 respectively.

from B.I.1 and B.II.1 were evenly distributed into effector subsets according to chemokine receptor expression. The proportion of Th1 ($CXCR3^+$, $CCR6^-$) in A.II.1 and A.I.2 were reduced compared to controls, whereas they were increased in B.I.1 and B.II.1. The relative proportion of Th17 cells ($CXCR3^-$, $CCR6^+$) in A.II.1 was reduced, whereas in B.I.1, B.II.1 and A.II.2 Th17 cells were increased compared to controls (Figure 3.12 B).

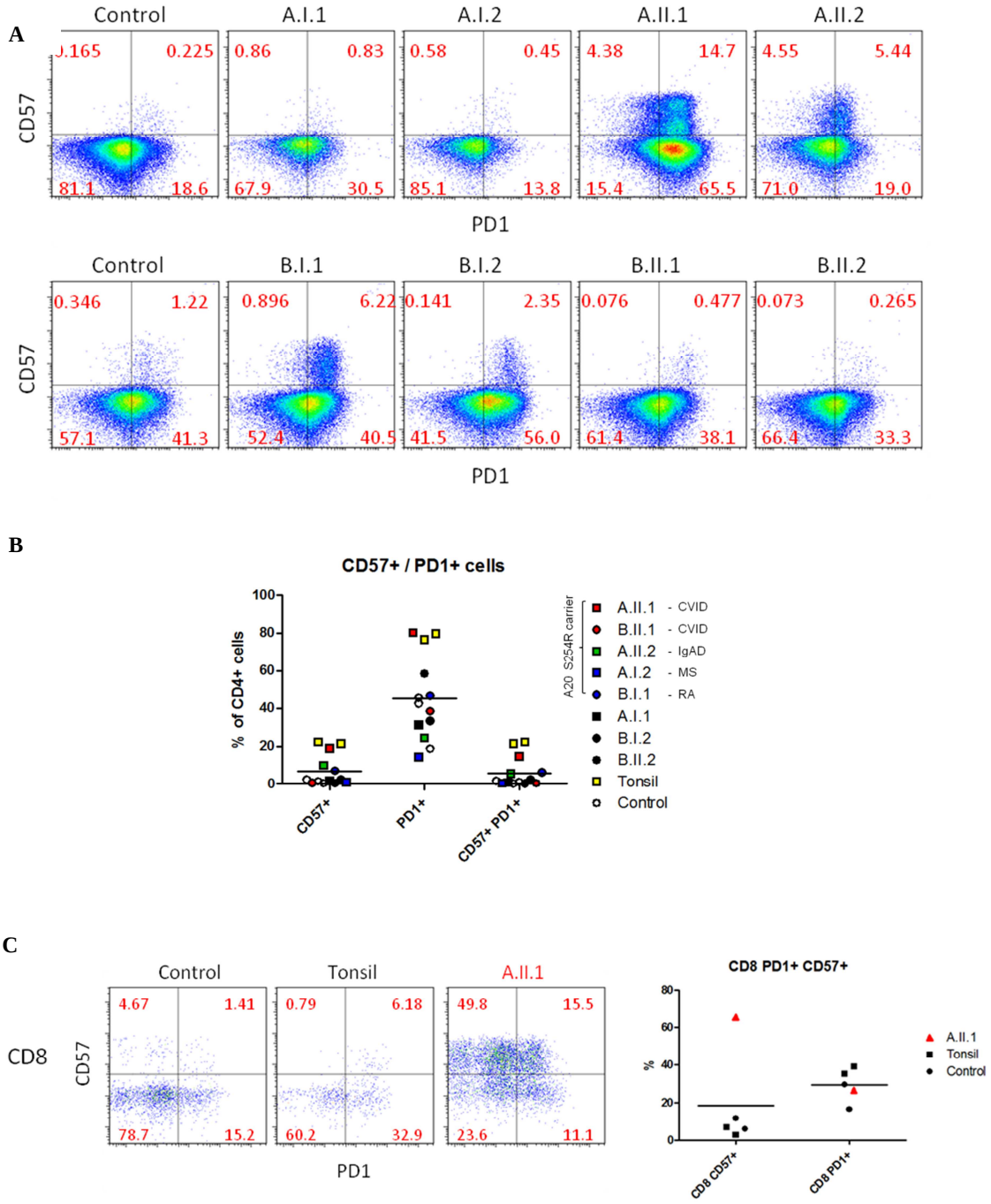

Figure 3.13 Exhaustion markers. CD57 and PD1 were used as exhaustion markers on $CD4^{+}$cells. Tonsils are shown for comparison. **A.** Flow cytometric dot plots and **B**. summary plot of CD4 T cells **C**. $CD8^{+}$ cells. black filled circle, healthy control; black filled square, tonsil; red triangle, A.II.1

A

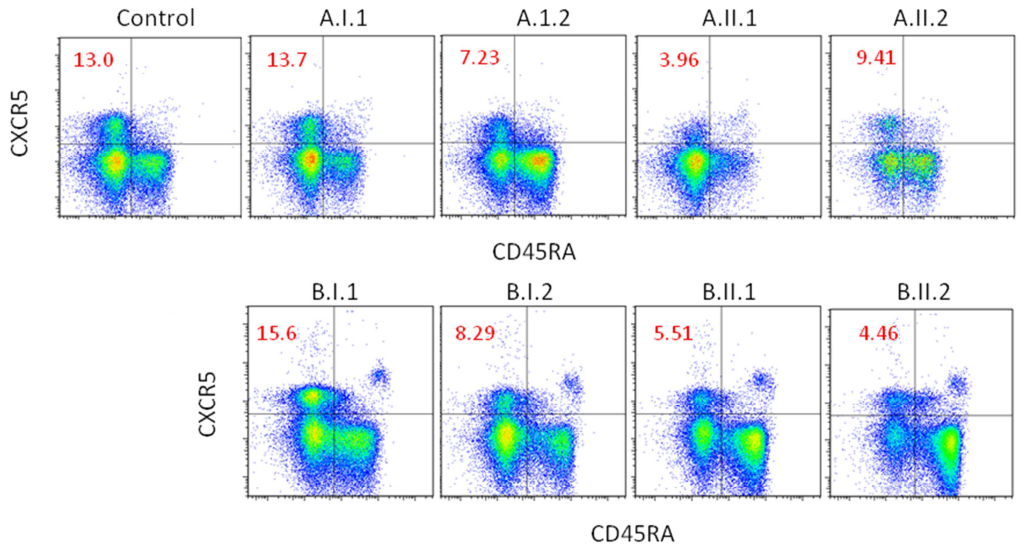
Control
A.I.1
A.1.2
A.II.1
A.II.2
13.0
13.7
7.23
3.96
9.41
CXCR5
CD45RA
B.I.1
B.I.2
B.II.1
B.II.2
15.6
8.29
5.51
4.46
CXCR5
CD45RA

B

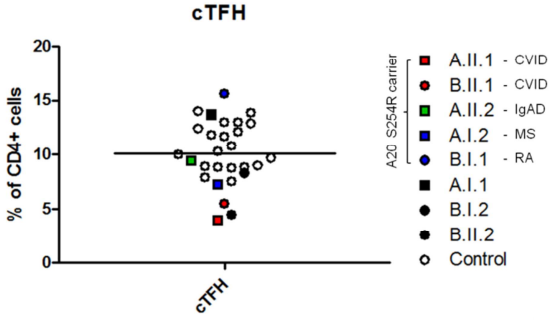
cTFH
% of CD4+ cells
20
15
10
5
0
cTFH
A20 S254R carrier
A.II.1 - CVID
B.II.1 - CVID
A.II.2 - IgAD
A.I.2 - MS
B.I.1 - RA
A.I.1
B.I.2
B.II.2
Control

C

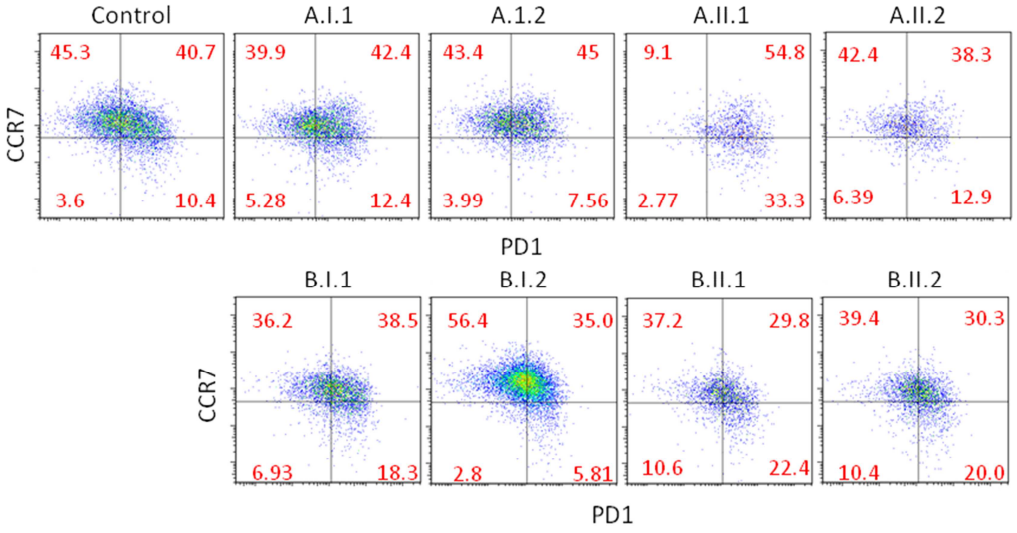
Control
A.I.1
A.1.2
A.II.1
A.II.2
45.3
40.7
3.6
10.4
39.9
42.4
5.28
12.4
43.4
45
3.99
7.56
9.1
54.8
2.77
33.3
42.4
38.3
6.39
12.9
CCR7
PD1
B.I.1
B.I.2
B.II.1
B.II.2
36.2
38.5
6.93
18.3
56.4
35.0
2.8
5.81
37.2
29.8
10.6
22.4
39.4
30.3
10.4
20.0
CCR7
PD1

Figure 3.14 Flow cytometric analysis of circulating follicular helper T cells CXCR5 and CD45RA were analysed on $CD3^{+}CD4^{+}$ cells. CXCR5 $CD45RA^{-}$ cells represent cTfhs. **A.** Dot plot **B.** Summary plot **C.** PD1 and CCR7 expressions were analysed on cTfhs and active ($CCR7^{lo}$ $PD1^{hi}$) and resting effector cells ($CCR7^{hi}$ PD^{lo}) are shown

In view of the large number of TEM and TEMRA cells, we proceeded to further analysis for evidence of T cell exhaustion according to expression of CD57 and PD1 (Figure 3.13). This revealed expansion of CD57 and $PD1^{+}$ $CD4^{+}$ T cells in A.II.1 (80% of $CD4^{+}$ T cells were $PD1^{+}$, and 22% were $CD57^{+}$). This is abnormal when compared with peripheral blood from healthy controls, but similar to the distribution of T cells observed in human tonsil (Figure 3.13C). Two $A20^{S254R}$ carriers, A.II.2 and B.I.1 showed slightly increased CD57 expression. $CD8^{+}$ T cell compartment, where approximately 65% were $CD57^{+}$, which represents a 7-fold increase relative to controls.

Memory T cells can be further subdivided according to CXCR5 expression. $CXCR5^{+}$ CD4 T cells are often referred to as circulating Tfh cells (cTfh) (Fazilleau, Mark et al. 2009). A.II.1 exhibits a relative reduction of cTfh (cTfh: 3.96% of $CD4^{+}$ $CXCR5^{+}$ $CD45RA^{-}$), approximately 2.5 fold decrease relative to controls. B.II.1 presents a relative reduction of cTfh (5.51%, 1.8 fold decrease). By contrast, B.I.1 exhibits a 1.6 fold increase relative to controls.

PD1 and CCR7 expression was used for further analysis to distinguish effector ($CCR7^{lo}$ $PD1^{hi}$) and memory Tfh cells ($CCR7^{hi}$, $PD1^{lo}$) (Ye et al, Immunity). A.II.1 exhibits a 3-fold increase in $CCR7^{lo}$, $PD1^{hi}$ cells and a 4 fold decrease in $CCR7^{hi}$, $PD1^{lo}$ cells (Figure 3.14). B.II.1 exhibits a 1.8-fold increase in effector phenotype ($CCR7^{lo}$, $PD1^{hi}$) and a 1.3-fold decrease in resting phenotype ($CCR7^{hi}$, $PD1^{lo}$) Tfh cells. B.I.1 shows a 1.1-fold increase and a 1.9-fold decrease in $CCR7^{lo}$, $PD1^{hi}$ cells and $CCR7^{hi}$, $PD1^{lo}$, respectively.

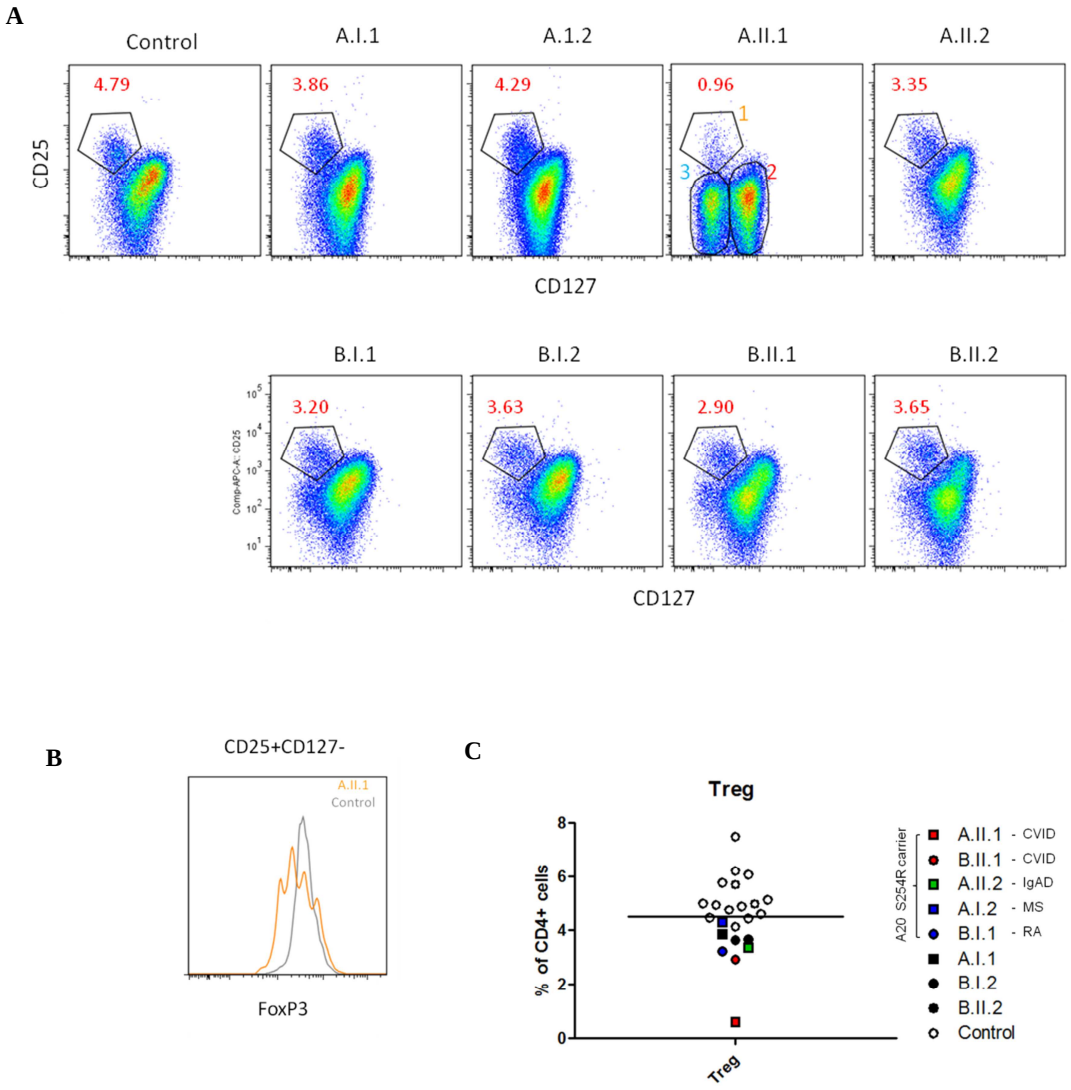

Figure 3.15 Flow cytometric analysis of regulatory T cells A. CD127 and CD25 expression was analysed on $CD4^+$ $CD3^+$ cells. Potential regulatory T cells are shown in the region. **B**. Foxp3 expression of the populations from region shown in A. Grey line represents controls and red line represents the proband. **C**. Summary plot of Tregs with a mean (4.6%). $A20^{S254R}$ carriers are indicated with coloured symbols. Clinical diagnoses are shown. Squares, family A; Circles, family B.

Analysis of regulatory T cells revealed A.II.2, B.II.1 and B.I.1 have a slight reduction of putative regulatory T cells ($CD25^+$ $CD127^-$ cells) compared to controls (from 0.96 and 3.65%). However, A.II.1 has a deficiency of regulatory T cells. Normally, the $CD25^+$ $CD127^{lo}$ phenotype identifies $FOXP3^+$ regulatory T cells, however, approximately 40%

of putative regulatory T cells from A.II.1 were Foxp3 negative. Thus, he exhibits a relative deficiency of regulatory T cells (approximately 9-fold decrease) compared to the mean (4.6%) of controls.

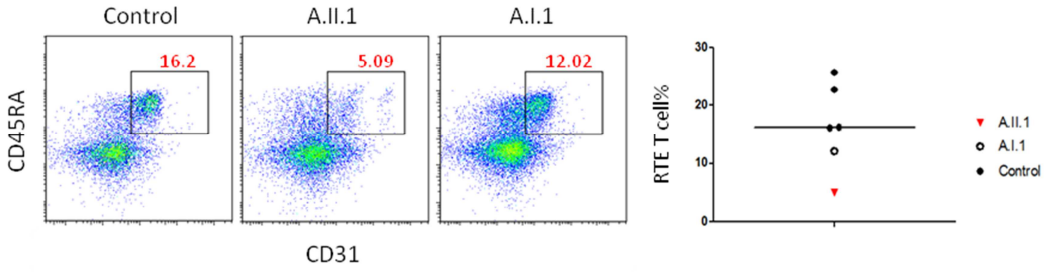

Figure 3.16 Flow cytometric analysis of recent thymic emigrants (RTE) CD31 and CD45RA expressions were analysed on $CD4^+$ $CD3^+$ cells. $CD31^+$ $CD45RA^+$ cells represents recent thymic emigrants **A.** Flow cytometric dot plot **B.** summary plot for RTET cells in $CD4^+$ $CD3^+$ cells inverted red triangle, A.II.1; open circle, A.I.1; black filled circle, healthy controls

Finally we enumerated recent thymic emigrant cells according to expression of CD31 and CD45RA (Figure 3.16). 5% of $CD4^+$ cells were recent thymic emigrant ($CD31^+$, $CD45RA^+$) T cells, compared with a mean of 18.5% in healthy controls.

3.1.5 Functional phenotypes

3.1.5.1 Plasmablast induction

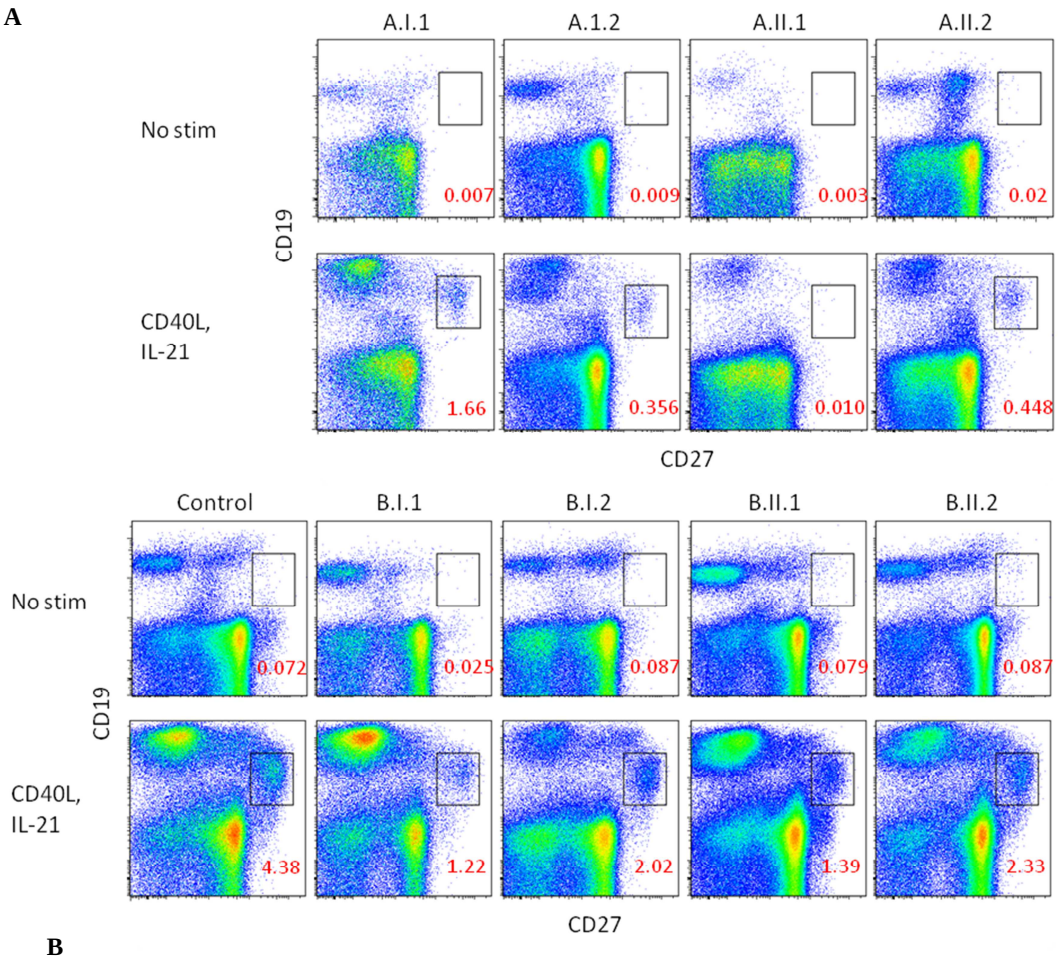

Figure 3.17 Flow cytometric analysis of plasmablast induction in vitro A. PBMCs were cultured with CD40L transfectant cells (1:50 ratio) and IL-21 (50ug/ml) for 5 days. Plasmablasts are $CD27^{++}$ $CD19^{lo}$ cells. **B**. Summary plot shows PB proportion out of B cells PB.

Analysis of a lymph node isolated from A.II.1 was noteworthy for the absence of plasma cells. We proceeded to analysis of plasmablast induction in vitro to investigate that the absence of plasma cells resulted from an intrinsic B cell defect.

PBMC were stimulated with CD40L + IL-21 for 5 days and plasmablast (PB) induction was examined according to CD19 downregulation and high level expression of CD27. We observed a consistent and significant defect in plasmablast formation in B cells from A.II.1, relative to controls and the other $A20^{S254R}$ carrier (Figure 3.17). Plasmablasts expressed as a percentage of CD19 cells show a significant deficit in plasmablast formation in A.II.1. This result was expected, since AII.1 has very few memory B cells, and we observed no plasmablasts in vivo (LN biopsy). Interestingly, B.II.1 also exhibited relative reduction in plasmablast formation in vitro. We observed approximately 2-fold and 4-fold reductions in plasmablast induction in B.II.1 (4.2%) and B.I.1 (2.2%), respectively, when compared to healthy controls (Figure 3.17B).

3.1.5.2 B cell activation

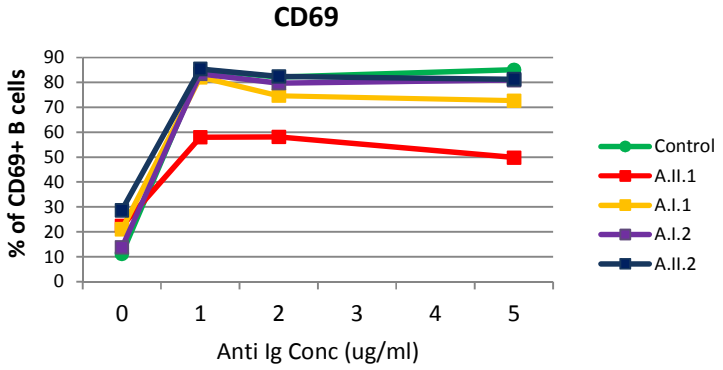

Figure 3.18 B cell activation PBMCs were activated with a range of anti Ig F(ab)2 for 24 hours and cell activation marker, CD69 was analysed. Percentage was out of $CD19^{+}$ cells.

We examined B cells for expression of NF-kB-dependent activation marker, CD69 as a control for activation after stimulation in vitro (Figure 3.18). B cells were stimulated with anti-Ig $F(ab)_2$ for 24 hours. We observed a reduction in expression of CD69 by B cells from A.II.1 across the dose range of anti-Ig $F(ab)_2$. 40~50% of the B cells from A.II.1 became CD69 positive while 70%~80% of the B cells from controls became CD69 positive. Interestingly, approximately 25% of B cells expressed CD69 in the absence of simulation although he has massive transitional and anergic B cells and very few memory B cells. These data suggest a possible B cell intrinsic defect in activation.

3.1.5.3 T cell activation

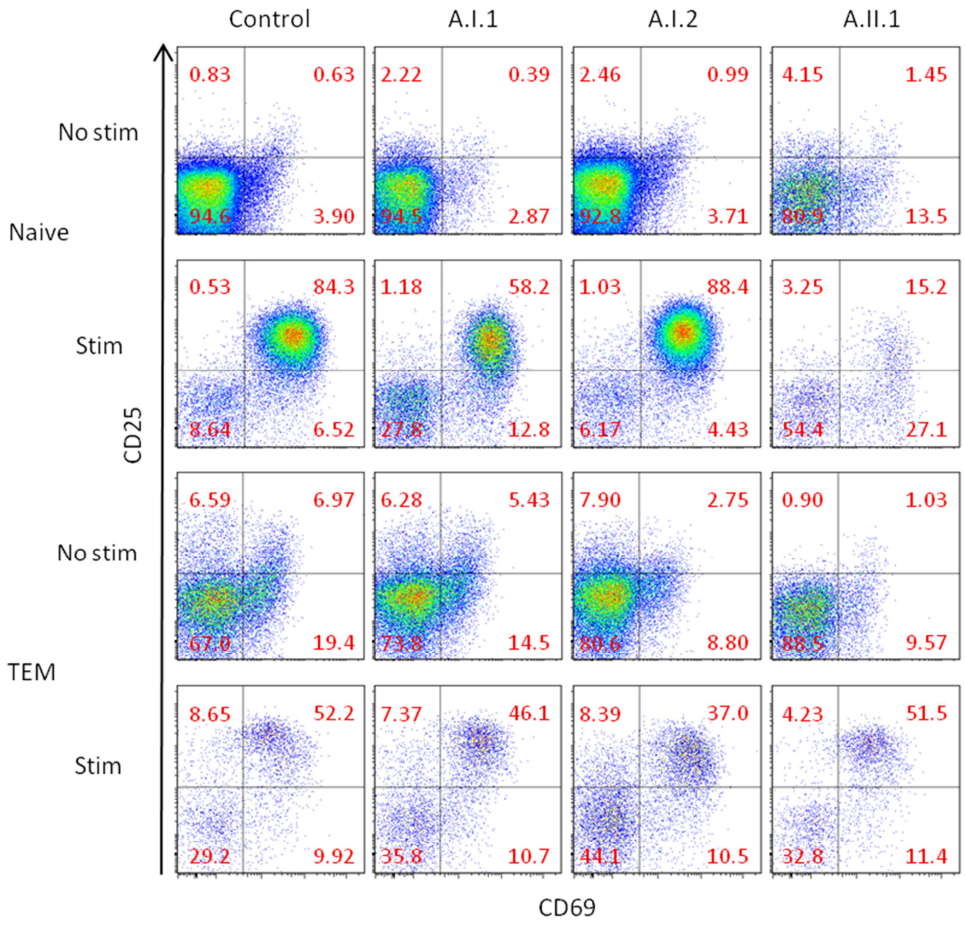

Figure 3.19 Flow cytometric analysis of CD25 and CD69 expression in response to T cell activation beads. Naive T cells ($CD4^+$, $CD3^+$, $CD45RA^+$, $CCR7^+$) and TEM ($CD4^+$, $CD3^+$, $CD45RA^-$ $CCR7^-$) were purified and incubated with T cell activation beads (Miltenyi Biotec) according to the manufacture's instruction. After 24h of incubation, CD25 and CD69 expressions were analysed. This is representative of two separate experiments.

Next we examined T cell activation in vitro. Naïve ($CD3^+$, $CD4^+$, $CD45RA^+$, $CCR7^-$) or effector memory ($CD3^+$, $CD4^+$, $CD45RA^-$, $CCR7^-$) T cells were positively sorted (BD FACSAria™) and stimulated in vitro with T cell activation beads containing anti CD2/CD3/CD28 antibodies (Miltenyi Biotec) for 24 hours. We examined up regulation of T cell activation markers CD69 and CD25 in the presence or absence of T cell activation beads. Unexpectedly, approximately 18% of A.II.1's naïve T cells were

CD69 positive cells in the absence of in vitro stimulation, which represents a significant difference from controls ($p<0.0001$) (Figure 3.20). This suggests that naïve T cells from A.II.1 were activated in vivo. By contrast, after stimulation in vitro, A.II.1 exhibited impaired activation of naïve $CD4^+$ T cells. In this experiment (representative of two), 54.4% of CD4 naïve T cells remained negative for CD69 and CD25 ($p=0.0125$, $p=0.0142$ respectively, n= 8).

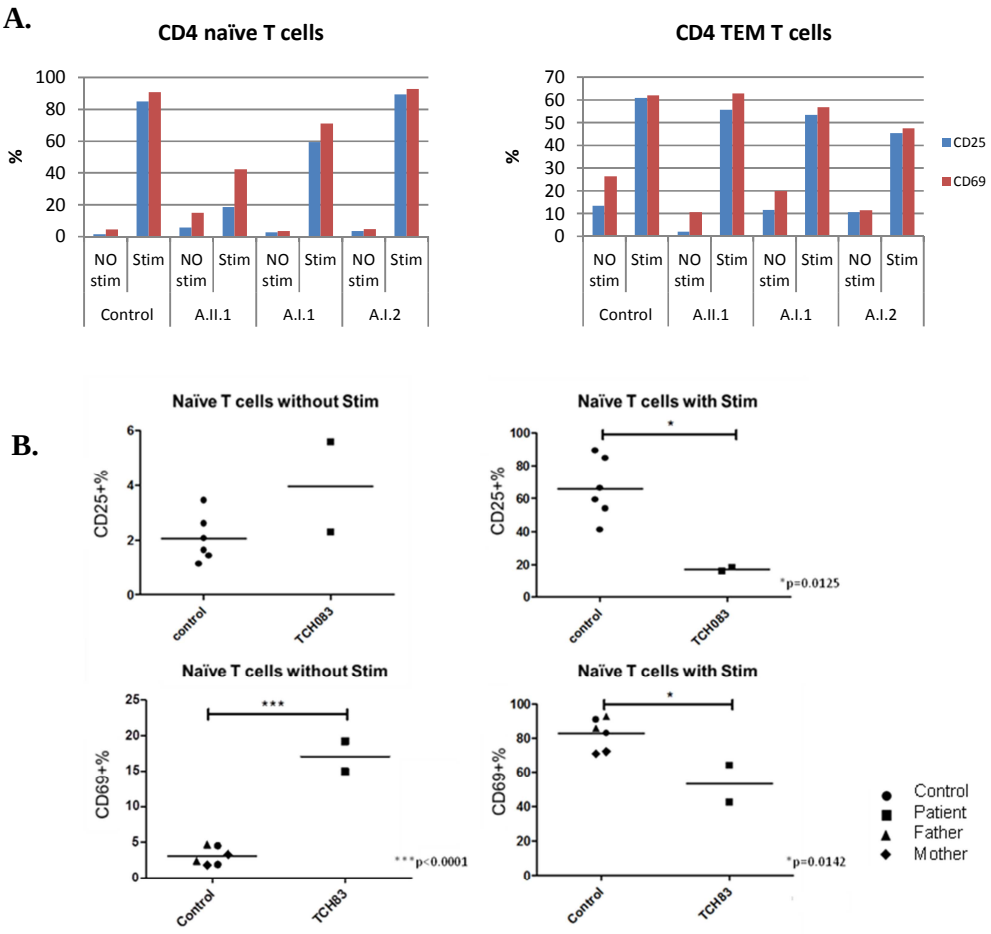

Figure 3.20 Summary of CD69 and CD25 expression on naïve $CD4^+$ T cells and effector memory $CD4^+$ T cells. Percentage was obtained from live $CD4^+$ T cells and **A.** the experiment is representative of two separate experiments. **B.** Statistical analysis was done with two tailed T-tests.

It is noteworthy that these findings are very similar to those described in caIKKβ mice, where a gain-of-function mutation in IKKβ results in constitutive activity of the IKK complex (Krishna, 2012), a similar biochemical defect to that expected and observed as a result of a defect in A20. As in A.II.1, caIKKβ exhibit spontaneous $CD4^+$ T cell activation even in the absence of TCR crosslinking in vitro, while T cell activation is impaired after stimulation in vitro.

3.1.5.4 B Proliferation

We also examined B cell proliferation in vitro after 5 days incubation with CD40L transfectant cells (1:50 ratio) and IL-21 (50ng/ml). A.II.1 and A.I.2 showed obvious defects in B cell proliferation (Figure 1.16.A). B.II.1, B.I.1 and B.II.1 showed relatively normal proliferation compared to controls after 5 days activation (Figure1.21). We observed a significant reduction in live B cells in the A.II.1 cultures during the proliferation assay (Figure 3.21), suggesting increased apoptosis within the B cell compartment as well as the T cell compartment.

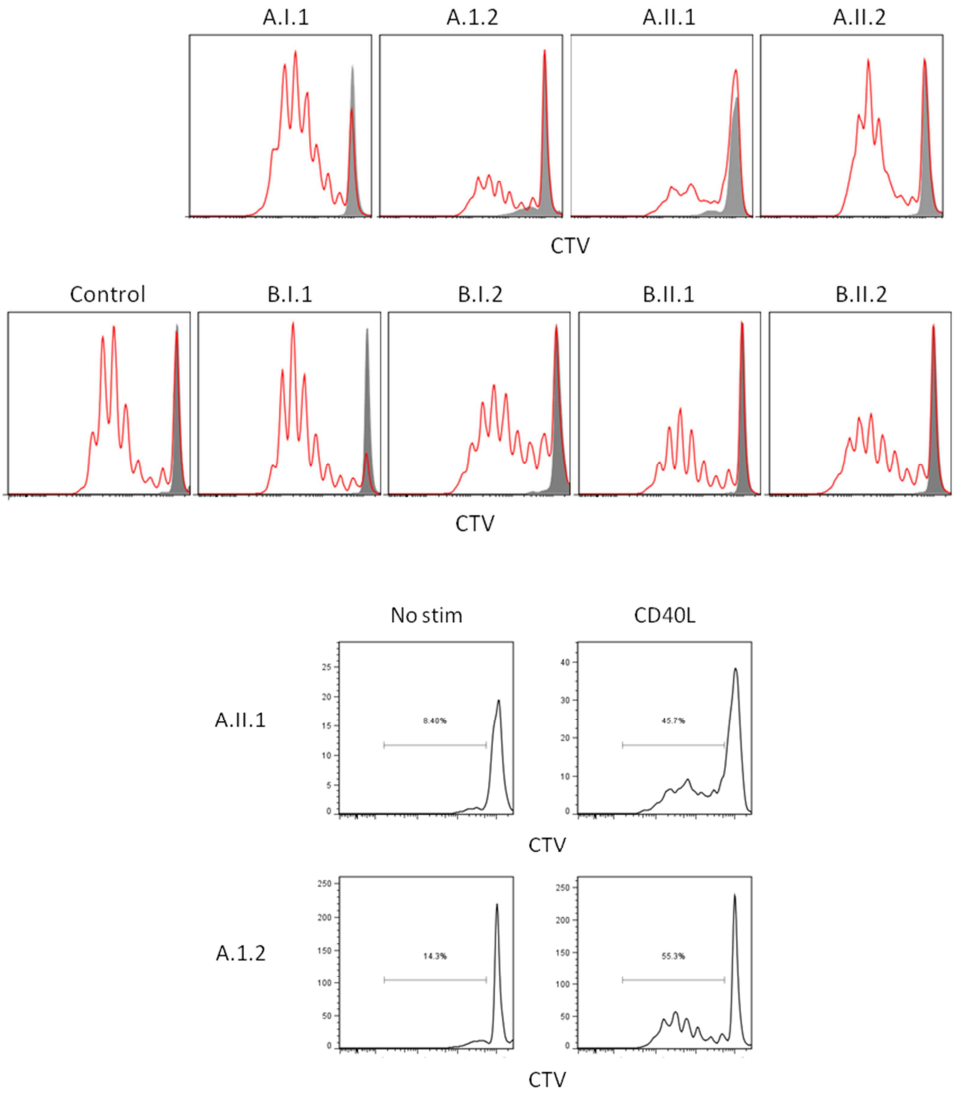

Figure 3.21 Proliferation of B cells in response to CD40L. PBMCs were labelled with cell trace violet (CTV) and incubated with CD40L transfected cells for 5 days. Viable B lymphocytes were gated and analysed according to CTV expression.

3.1.5.5 T cell proliferation and T cell survival

We also examined T cell proliferation in vitro (Figure 3.22). Both PBMCs and sorted naïve T cells were examined for proliferation, determined by dilution of CFSE or CTV label, respectively, after 5 days incubation with T cell activation beads. $CD4^+$ T cells

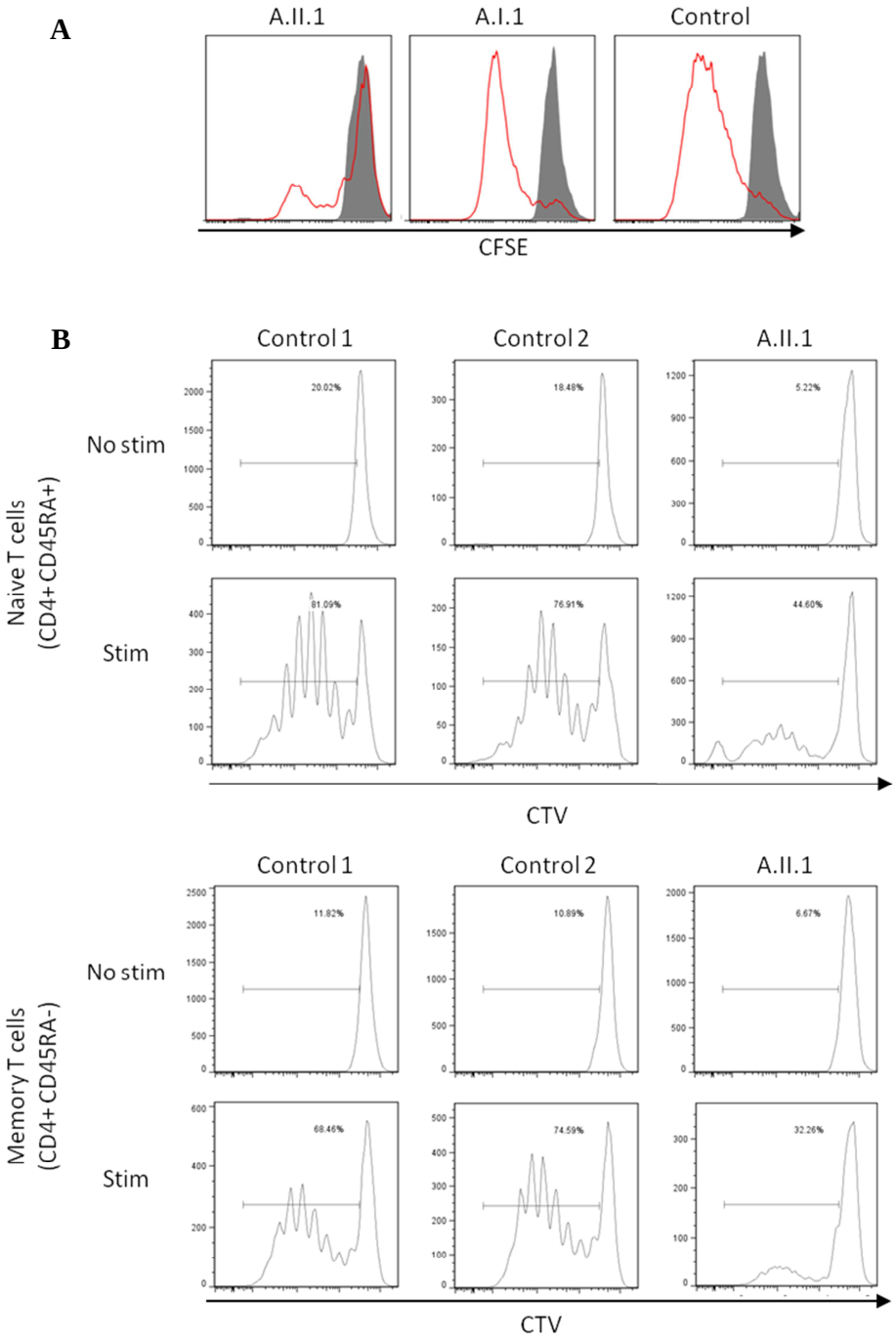

Figure 3.22 Proliferation of T cells in response to T cell activation. PBMCs or sorted T cells were labelled with CFSE or cell trace violet (CTV) and incubated with T cell activation beads (Milteni Biotech) for 5 days. Viable lymphocytes were analysed according to CTV or CFSE.

from A.II.1 showed a defect in proliferation. Both unfractionated PBMCs and sorted T cells divided less than cells from healthy controls. In PBMC cultures, the majority of A.II.1's T cells remained undivided. Sorted T cells also showed similar results: ~60% of naïve T cells and ~70% of memory T cells remained undivided.

3.1.5.6 Cell survival

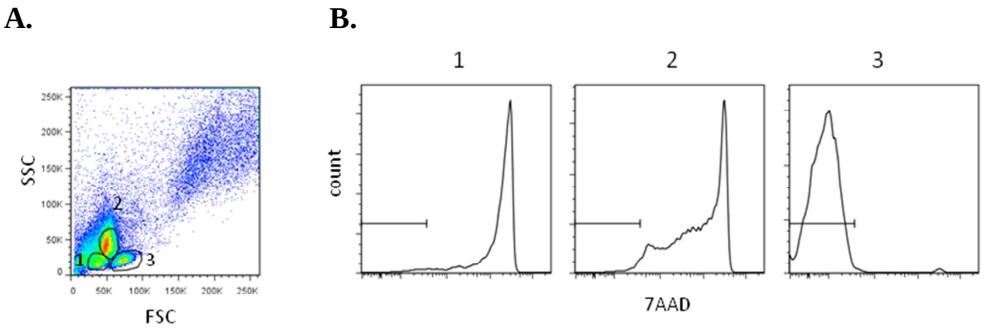

Figure 3.23 Position of live cells in forward and side scatter flow cytometry data with 7AAD staining. A. Forward and side scatter dot plot. **B**. 7AAD profile from 3 populations. PBMCs from healthy controls were used for this experiment.

In addition to an abnormality of proliferation, we observed a consistent reduction in the total number of cells remaining in culture of PBMCs from A.II.1, raising the possibility of increased cell death. We proceeded to more formal analysis of cell survival using 7AAD to identify apoptotic cells. In Figure 3.23, population 1 is $7ADD^{high}$, which are late apoptotic cells. Population 2 contained both $7AAD^{high}$ and $7AAD^{intermediate}$ cells, indicating both late and early apoptotic cells. Population 3 contained only $7AAD^{negative}$ (viable) cells. These results demonstrate concordance with cell viability determined by forward and side scatter.

Survival of the sorted T cells was then analysed by forward and side scatter and this revealed a significant loss of viable cells (approximately 70%) from A.II.1 culture of after 24 hours without stimulation. By contrast, approximately 80% of naïve T cells from healthy control and his family members remained viable. After stimulation, approximately 40% of cells remained viable in cultures of naïve T cells from healthy controls. In cultures of naïve T cells purified from A.II.1, less than

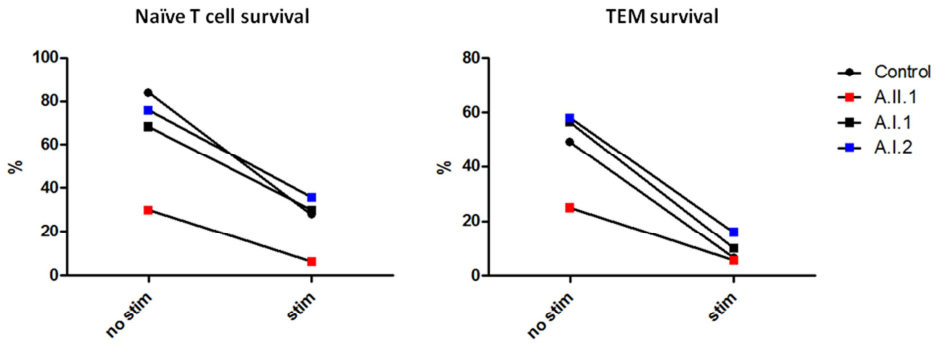

.

Figure 3.24 Viability of sorted T cells with T cell activation beads for 24 hours. Live cells were measured using viable cell gating (population 3) from Figure 3.23. Proportions of live cells were analysed with or without the stimulation. A.II.1, red filled square symbol; controls, black filled triangle symbol; A.I.1, black filled square symbol; A.I.2, blue filled square symbol.

5% of cells survived in the presence of TCR stimulation. Analysis of effector memory T cells (TEM) also showed similar results. Approximately 30% of TEMs from A.II.1 survived after a 24-hour incubation in the absence of simulation, whereas approximately 70% of TEMs from controls survived. After stimulation, the survival percentage was similar in A.II.1 and controls. Two separate experiments showed very similar results. In other words, the survival of *unstimulated* naïve T cells from A.II.1 was similar to that observed after in vitro stimulation of control naïve T cells, and in vitro survival of naïve and memory T cells from A.II.1 was similar as well. We considered the possibility that

naïve T cells from A.II.1 are partially activated (in vivo) to explain this propensity to apoptosis. This had been suggested by our earlier observation of increased CD69 expression at baseline. Furthermore, a similar in vitro survival defect has been reported in T cells from caIKKβ mice (S2012).

We also re-examined the proliferation assay to investigate further T cell survival. First, live cells were identified according to forward and side scatter plot then a cell trace violet histogram graph was used to analyse proliferation in each subset. After 5 days of activation, cells had undergone up to 8 cell divisions. The total cell number from each cell division was divided by the 2 to the power of cell division number to obtain the proliferation precursor frequency. All the precursor cell numbers were combined and

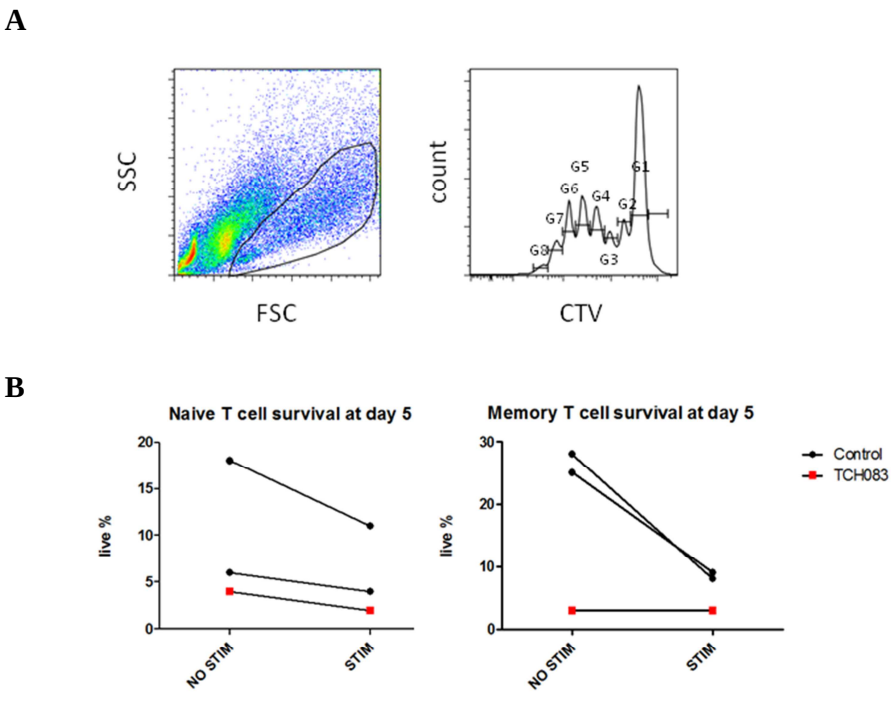

Figure 3.25 Viability of precursor cells after 5 days with T cell activation beads. Live cells were measured using viable cell gating (population 3) from Figure 3.23. **A**. Live cells on forward and side scatter dot plot. **B.** CTV analysis on live cells. **C.** Viability of precursor cells after 5 days stimulation.

the total live precursor cells then were divided by total cell number to get the proportion of survival. In both memory and naïve T cells cultures, there was significant cell loss by apoptosis without stimulation. Less than 5% of memory T cells from A.II.1 survived, compared with control memory T cells, this represents a >8-fold deficit (Figure 3.25). While this experiment suggests that apoptosis is enhanced even in naïve T cells, one caveat of this experiment is that naïve cells were positively sorted using CD3 and CD4.

3.1.5.7 Apoptosis

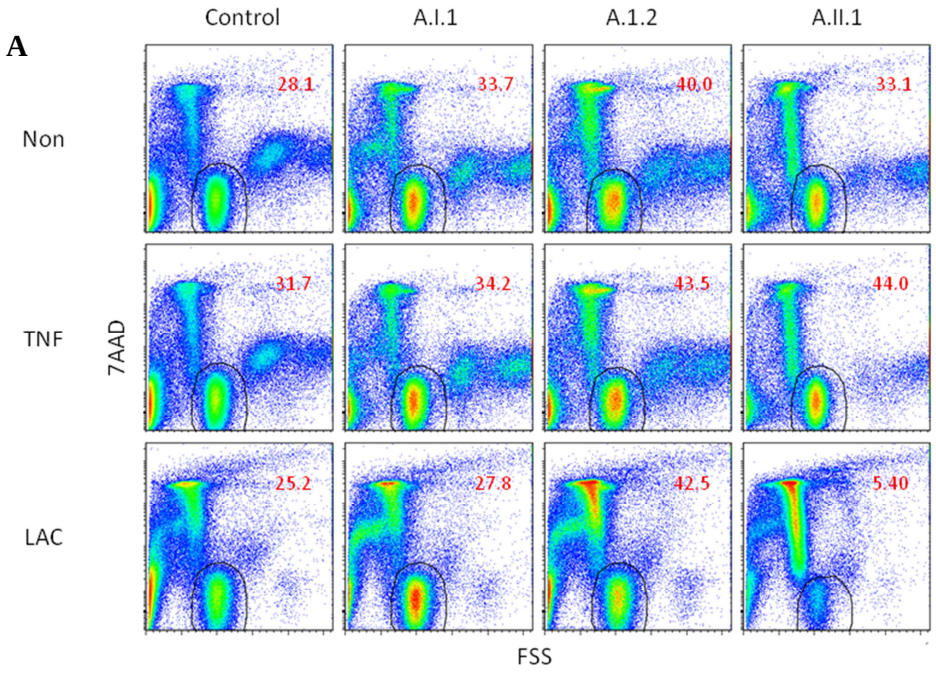

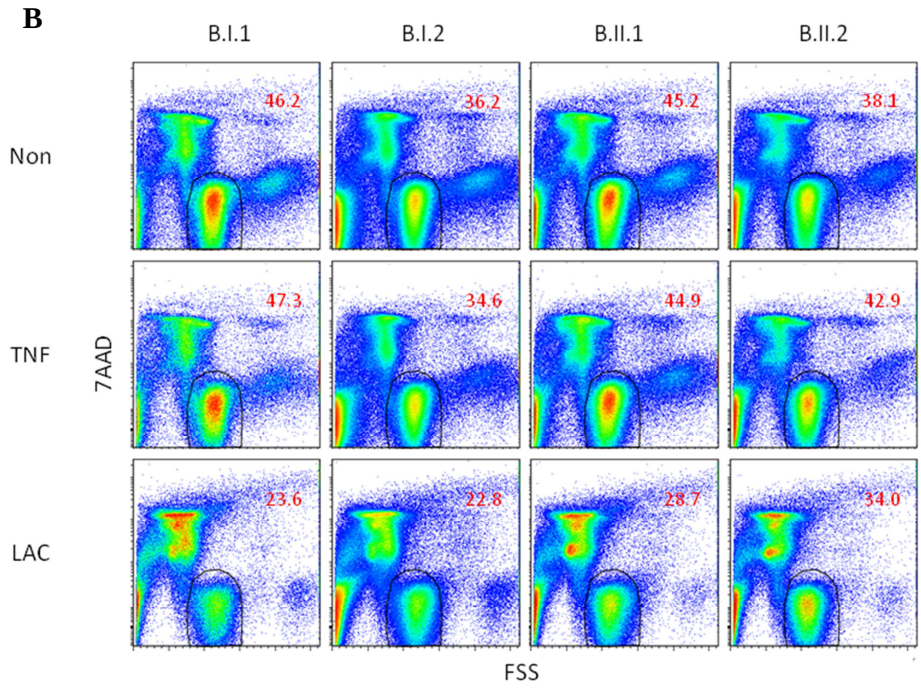

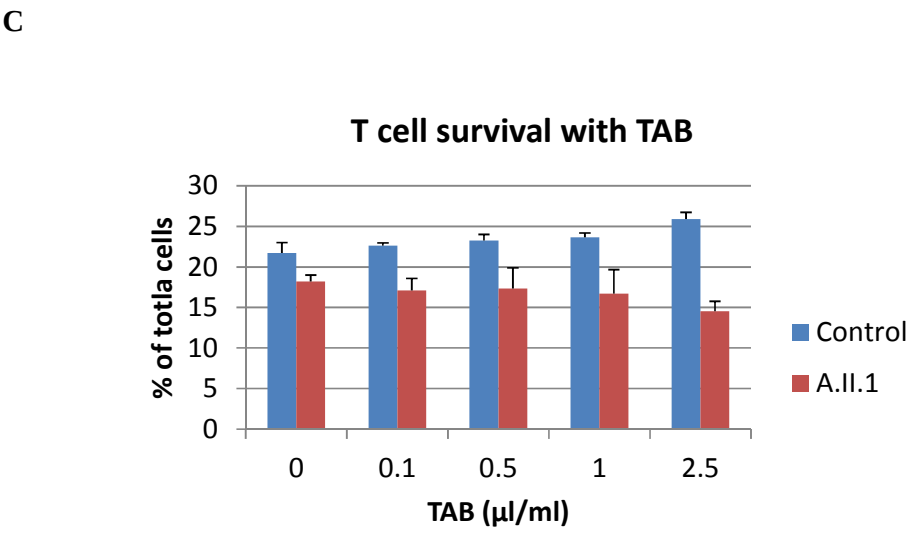

Figure 3.26 Analysis of cell survival after various stimuli. PBMCs were stimulated with LAC, TNFα or nil for 24 hours. **A.** Family A. **B.** Family B **C.** PBMCs were stimulated with a range dosage of TAB and live cells were analysed. LAC, lymphocyte activation cocktail; TAB, T cell activation beads.

Next, we examined apoptosis in response to various additional stimuli. First, T cells were stimulated with either TNF or a lymphocyte activation cocktail (LAC) containing

PMA, ionomycin and brefeldin A. The most substantial defect in survival was observed after 24 hours stimulation with LAC. 5.4% of total patient cells remained viable compared with 25% from the control (Figure 3.26). In this experiment, we did not observe apoptosis in unstimulated cultures. The discrepancy between this result and that described above (1.1.5.6) may be explained by a difference in the absence of positive selection in this experiment.

In PBMC cultures, we did not observe evidence of apoptosis after T cell activation beads. To exclude insufficient stimulation, the experiment was repeated with increasing amounts of T cell activation beads. Figure 3.26C shows that apoptosis was induced in a T cell activation bead dose-dependent manner while the there was no induction of apoptosis in control cultures, even with the highest doses of T cell activation beads (2.5ul/1M cells). Remarkably, the enhanced apoptosis observed with A.II.1 was stimulus-specific, and was not seen after stimulation with either anti-FAS or TNFα. This specificity provided us with a possible clue about the underlying defect.

3.1.5.8 Gene expression signature

3.1.5.8.1 B cells

So far, we have established that the defect in A.II.1 consists of baseline activation of T cells, reduced proliferation in vitro, increased T cell exhaustion, and enhanced apoptosis in vitro in response to TCR ligation, and PMA/ionomycin. These findings would be consistent with a defect in NF-kB conferred by a mutation in *TNFAIP3*. To explore this

possibility further, we examined global gene expression in lymphocytes isolated from A.II.1 and controls.

Naïve B cells were sorted according to $CD21^+$, $CD19^+$, $CD10^-$, $CD27^-$ and were stimulated with anti Ig $F(ab)_2$ for 24 hours, and global gene expression was determined by microarray. One patient and one control with two technical replicates were used for B cell gene expression Approximately 20000 transcripts were identified by Partek analysis software.

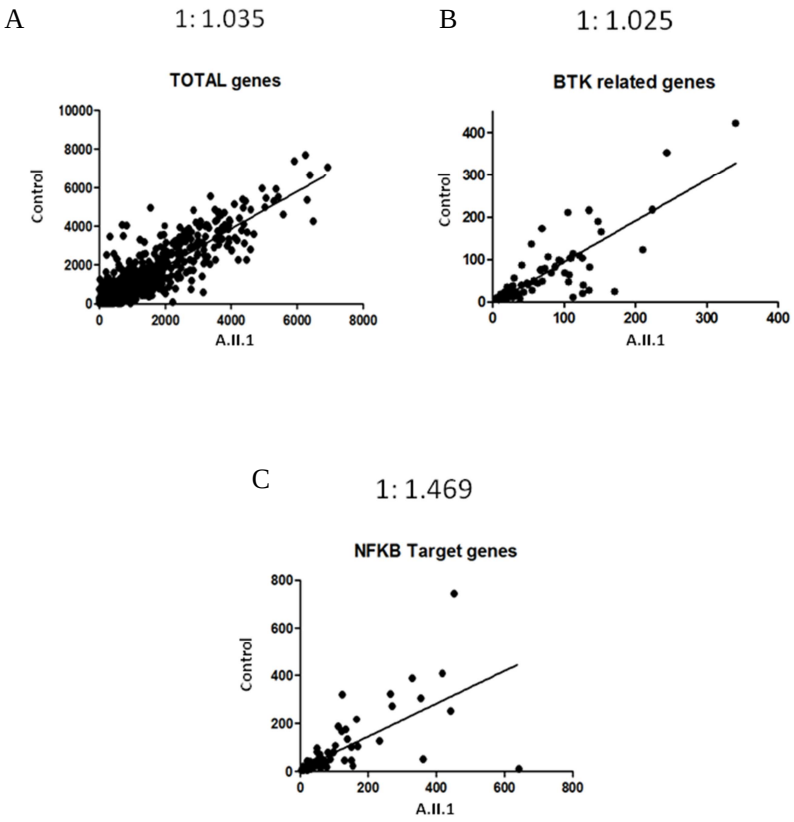

Figure 3.27 Gene expression of control vs. the proband from Microarray gene analysis A. total gene expression of the proband vs. age matched healthy control. **B**. BTK related gene expression of the proband vs. age matched healthy control **C**.NF-kB target gene expression of the proband vs. age matched healthy control.

Overall gene expression was similar between patient and control (Figure 3.27A), but we observed a bias towards overexpression of NF-kB target genes in A.II.1 (Figure 3.27C). For comparison, we analysed target gene expression downstream of the BTK pathway and found no difference between proband and control (Figure 3.27B).

Heat map projections of approximately 120 genes are shown in Figure 3.27A. Overall, higher expression of signature NF-kB target gene transcripts was found in the patient's B cells compared to the control (Figure 3.27C).38 NF-kB target genes were upregulated or downregulated >2-fold ($p<0.05$). 33 were upregulated in A.II.1 (Figure 3.28).

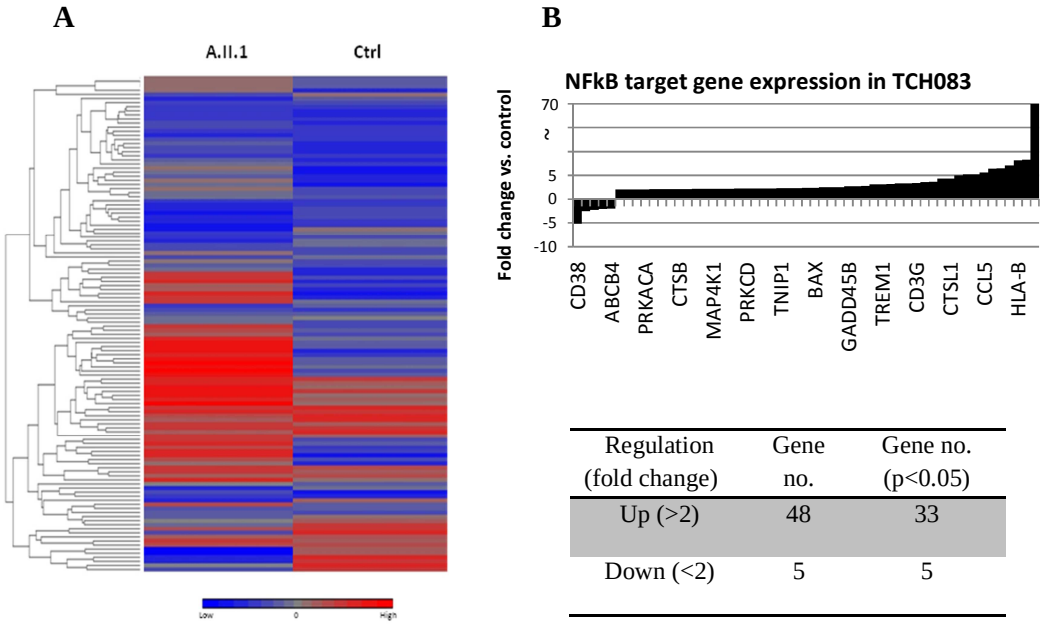

Regulation (fold change)	Gene no.	Gene no. ($p<0.05$)
Up (>2)	48	33
Down (<2)	5	5

Figure 3.28 NF-kB target gene expression of stimulated naïve B cells by microarray. A. Heat map projection of 120 selected NF-kB target genes are shown. **B**. 38 genes which have more than 2 fold different from control are listed with their relative expression to control .33 genes were upregulated and 5 genes were downregulated.

Genes whose expression differed most were *IL8* and *CCL2* (8-fold and a 61-fold increase, respectively). Recently it has been demonstrated that apoptotic cells secrete soluble factors which promote chemotaxis of phagocytotic cells toward dying cells (Gregory and Pound, 2011; Ravichandran, 2011). Both IL-8 (CXCL8) and MCP1 (CCL2) are chemokines and it has been found that they are produced from Fas or TNF induced apoptotic cells to guide phagocytes to apoptotic cells (Cullen et al., 2013). The gene expression signature would therefore be consistent with the observation that B and T cells from A.II.1 exhibit an increased propensity to apoptosis.

3.1.5.8.2 T cells

Since naïve T cells showed an active phenotype in an absence of stimulation, we performed an independent analysis of T cell gene expression. Naïve T cells (CD3+CD4+ CD45- cells) were sorted by positive selection and RNA was prepared for gene expression in the absence of stimulation. RNAseq data were analysed by voom after normalisation by sequencing depth.

Hierarchical cluster analysis shows that the two controls clustered closely together indicating that their expression profiles are similar, and significantly different from the expression signature observed in T cells from the proband. As in the B cell compartment, heat map projections reveal higher expression of signature NF-kB target gene transcripts from the patient's naïve T cells compared to the controls (Figure 3.29).

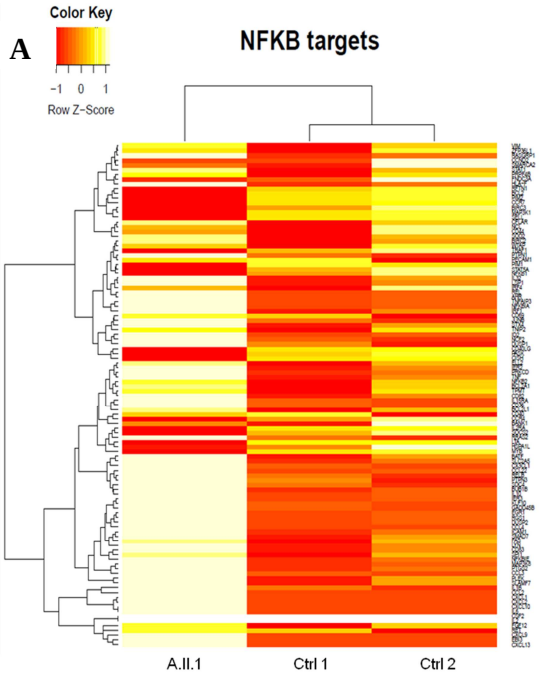

B

Regulation (fold change)	Gene no.	Gene no. (p<0.05)
Up (>2)	40	31
Down (<2)	4	4

Figure 3.29 NF-kB target gene expression of naïve T cells by RNAseq. A. Hierachical cluster analysis of RNA-Seq and Heat map projection of 100 selected NF-kB target genes are shown. **B**. 31 genes were upregulated and 4 genes were downregulated with p<0.05. one patient and two aged matched control with two technical replicate were used for T cell gene expression.

Thus, independent gene expression analyses reveal concordance for results obtained from T and B cells. Specifically, we observed upregulation of NF-kB regulated genes in both compartments. 35 NF-kB regulated genes were either upregulated or downregulated at least 2-fold (p<0.05). 31 genes (88.6%) were shown to be upregulated in A.II.1 relative to controls. Remarkably, IL-8 and CCL2 were most highly expressed in both naïve T cells and naïve B cells. Taken together analysis of global gene expression in both T and B cell compartments points to aberrant over-activity of NF-kB activity, and would be consistent with loss of function *TNFAIP3* mutation.

3.1.5.9 IkBα analysis

In view of these results, we examined NF-kB signalling specifically. IKK activation leads to phosphoralytion of IKBα and consequently rapid degradation of IKBα upon cell stimulation. We stimulated T cells with TNFα and examined IKBα expression by flow cytometry over a brief time-course.

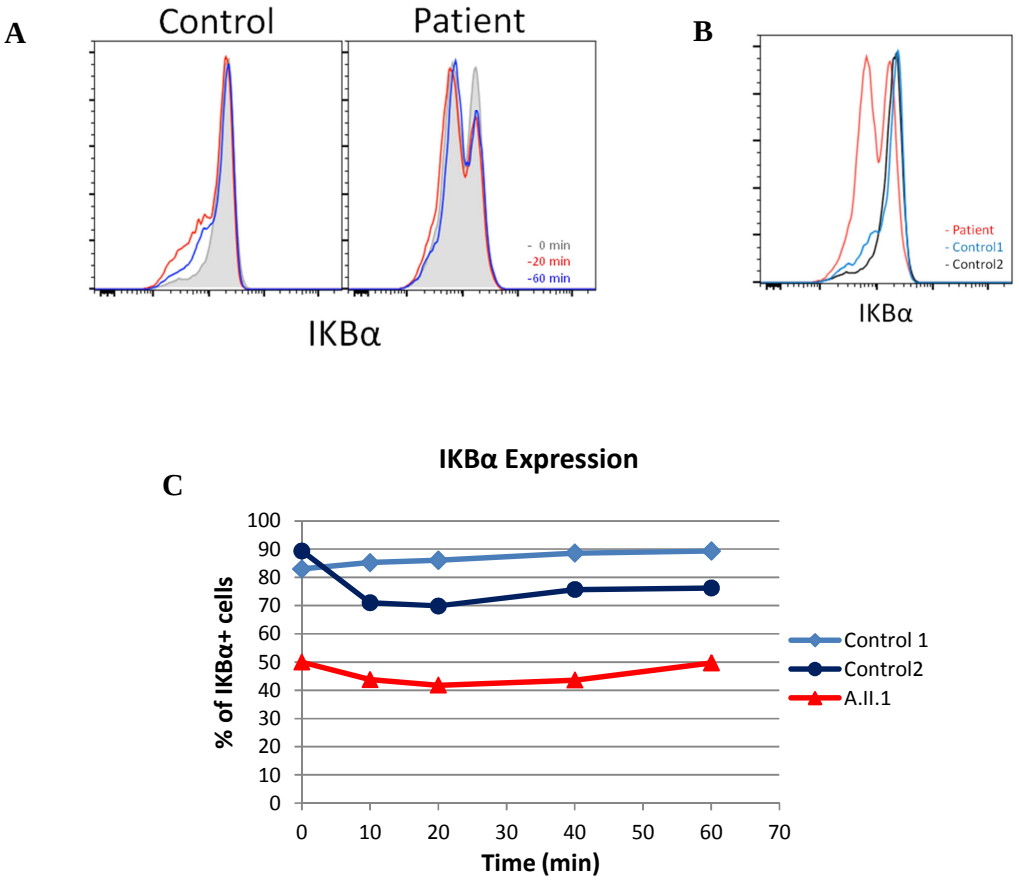

Figure 3.30 IkBα expression after TNFα stimulation. PBMCs were thawed and incubated at 37°C for 2 hours prior to the stimulation. Cells were then incubated with TNFα (50ng/ml) for various time points. CD3+ cells were analysed for IkBα expression by intracellular staining. **A.** Histogram of IkBα expression at 0, 20, and 60 minutes after the stimulation. **B.** Comparison of IkBα expression between A.II.1 and controls without stimulation. **C.** MFI of IKB**α** expression in time course stimulation with TNFα.

We observed that IkBα expression decreased at 20 minutes and its expression increased back to baseline at 60 minutes after stimulation in A.II.1 and one of the controls (Figure 3.30). Changes in IKBα expression were similar in A.II.1 and controls. We did observe, however, that 50% of T cells from A.II.1 lacked IKBα even in the absence of stimulation (compared with less than 15% in controls), consistent with constitutive NF-kB activation.

3.1.6 A20 interacting gene search

It has been reported that mutations in NF-kB genes including *CARD11*, *MALT1*, *IKBKA*, and *IKBKB* cause defects in T and B cell differentiation, activation and/or proliferation (Lahtela, Nousiainen et al. 2010; Snow, Xiao et al. 2012; McKinnon, Rozmus et al. 2014; Nielsen, Jakobsen et al. 2014; Turvey, Durandy et al. 2014; Brohl, Stinson et al. 2015). A.II.1 showed defects in activation of T cells and B cells, proliferation of T cell and B cell, and plasmablast differentiation. The cellular phenotype of A.II.1 is similar to one from primary immune deficiency patients with *CARD11* mutations. Furthermore, a mouse model, which carries a constitutively active form of IKKβ shows a very similar phenotype including a high percentage of effector T cells, irresponsive T cell activation, spontaneous naïve T cell activation, abnormal T cell proliferation, high PD1 expression and poor survival (Krishna, 2012). This suggests that the cellular phenotype of A.II.1 is caused by activated NF-kB resulting from defects in negative regulation of NF-kB and A20 ^{S254R}. On the other hand, the cellular and functional changes observed in kindred B, and indeed in other carriers within kindred A, are far less significant than those observed in the proband from kindred A. We therefore

investigated A.II.1 for a second genetic variant that might modify A20 to cause a more severe NF-kB signalling defect, and explain this function and phenotypic discrepancy.

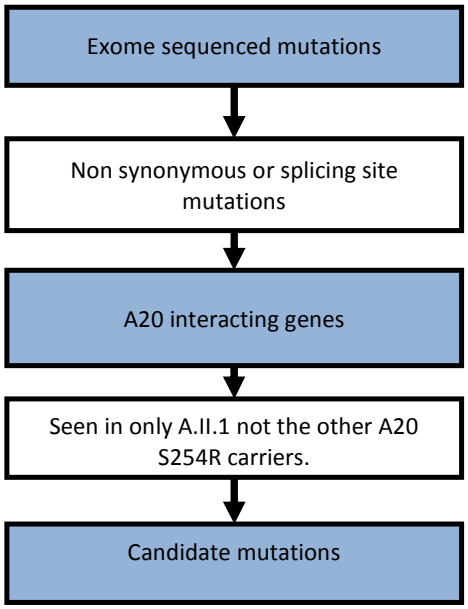

Figure 3.31 Schematic diagram for mutation selection

First, we examined lymphocytes from A.II.1 for a somatically acquired second mutation in *TNFAIP3.* RNA was isolated from PBMCs, from which we generated cDNA. We analysed transcripts for splice variants, and for sequence variation by Sanger sequencing. No somatic variants in *TNFAIP3* were identified, although we found a previously unreported splice variant of TNFAIP3 (between exon 7 and exon8), which was present in A.II.1 and several healthy controls) .

Second, we interrogated the A.II.1 genome for variants in *TNFAIP3* interacting genes. Using the String and BioGrid software tools, we identified 89 interacting genes (listed

in Appendix III). We identified 13 nonsynonymous or splice site mutations of these genes in A.II.1's exome. We excluded variants found in other A20^{S254R} carriers, since we had shown through exhaustive analysis that other carriers are phenotypically distinct. This left us with just one variant, a heterozygous missense SNP in *TAX1BP1* (L307I). We confirmed the *TAX1BP1* polymorphism by Sanger sequencing from lymphocytes and saliva and also confirmed that among all S254R carriers, only A.II.1 caries the *TAX1BP1* variant, which was transmitted paternally (A.I.1). *TAX1BP1*^{L307I} is not novel. According to dbSNP, the MAF is 0.069. Analysis by Polyphen2 and SIFT tests showed 0.278 and 0.78 scores, respectively, scores consistent with possible damage.

3.1.6.1 *TAX1BP1*^{L307I}

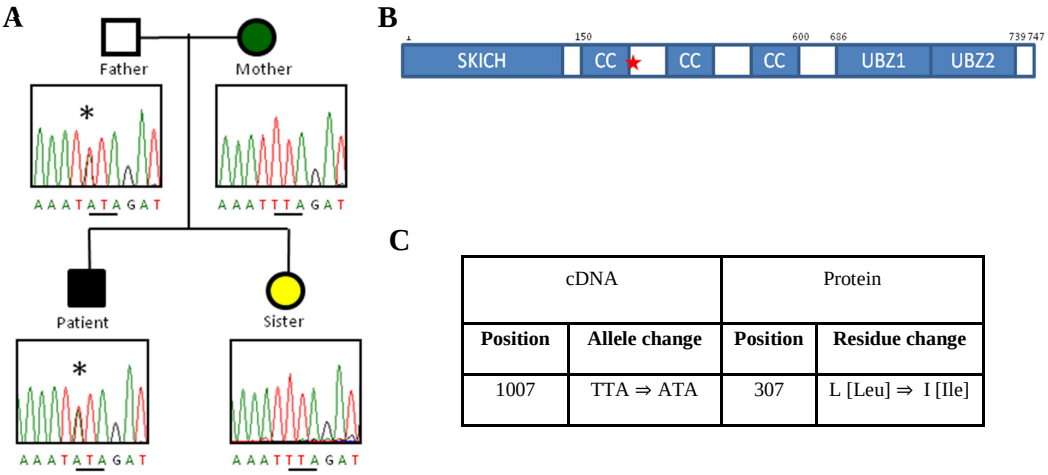

cDNA		Protein	
Position	**Allele change**	**Position**	**Residue change**
1007	TTA ⇒ ATA	307	L [Leu] ⇒ I [Ile]

Figure 3.32 L307I TAX1BP1 mutation. A. Sanger sequencing of *TAX1BP1* showing heterozygous mutation (*). **B.** Schematic representation of human *TAX1BP1* structure showing SKICH domain, three coiled coil (CC) domains and two ubiquitin binding zone (UBZ) domains. The mutation encoding L307I is next to the first coiled-coil domain (star). **C**. Summary of the mutation

TAX1BP1 is a scaffolding protein that is crucial for assembly of the macromolecular complex containing A20, ITCH, RNF11, and RIP1. We investigated TAX1BP1 as a potential modifier of A20 to explain the severe NF-kB phenotype of A.II.1. Since L307 is located in a coiled coil region of TAX1BP1, which is responsible for protein interactions (Figure 3.32), we hypothesized that this mutation might affect interaction between A20 and TAX1BP1.

3.1.7 Biochemical analysis

3.1.7.1 NF-kB activation

To investigate the effects of both A20 and TAX1BP1 variants in the absence of endogenous normal genes, we generated a *TAX1BP1* and *TNFAIP3* double-deficient RAJI cell line ($A20^{-/-}$, $TAX1BP1^{-/-}$) by CRISPR/Cas9. The deletion of two nucleotides (GT) at g.8910 in *TNFAIP3*, and the insertion of one nucleotide (T) at g.48154 in *TAX1BP1* were confirmed by Sanger sequencing and frameshifts were predicted to result in premature termination of expression due to the appearance of a stop codon (TGA) at 252 in *TNFAIP3* and at 331 in *TAX1BP1*. Absence of endogenous protein expression was confirmed by western blot.

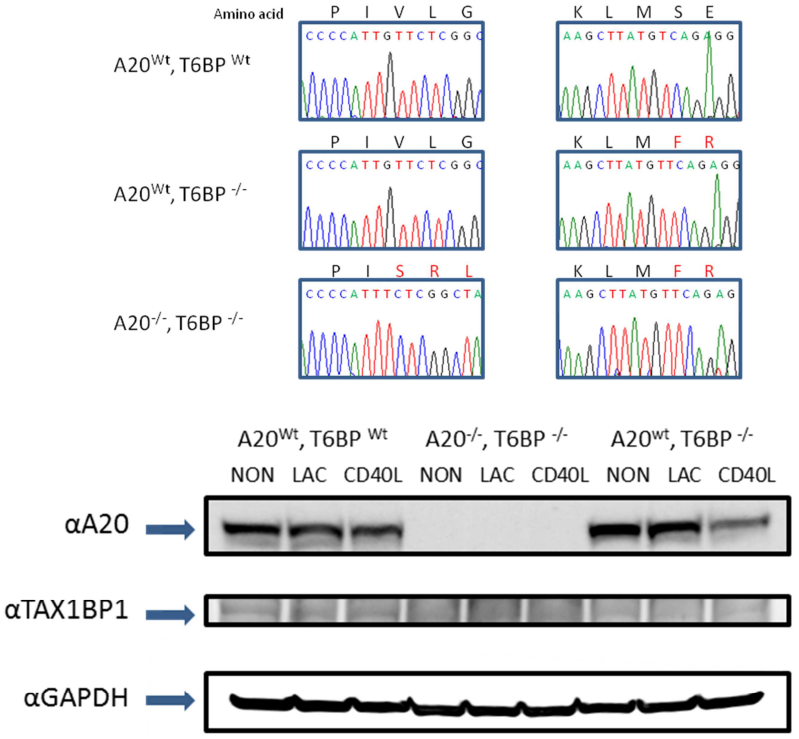

Figure 3.33. *TNFAIP3*$^{-/-}$ *TAX1BP1*$^{-/-}$ Raji cells were generated by CRISPR/CAS9. **A**. Sanger sequencing of *TNFAIP3* and *TAX1BP1* germline DNA. Amino acids changed are shown in red. **B.** A20 and TAX1BP1 expression was analysed by western blot. T6BP, TAX1BP1; Wt, Wildtype, LAC, lymphocyte activation cocktail

Wildtype or mutant *TNFAIP3* vectors were co transfected into double knockout Raji cell line (*TNFAIP3* $^{-/-}$, *TAX1BP1*$^{-/-}$) with wild type or mutant type TAX1BP1 and an mCherry vector. The positively transfected cells were isolated using by FACS according to mCherry expression and sorted cells were then activated with various stimuli for 24 hours and 48 hours and cells were analysed for CD69 expression.

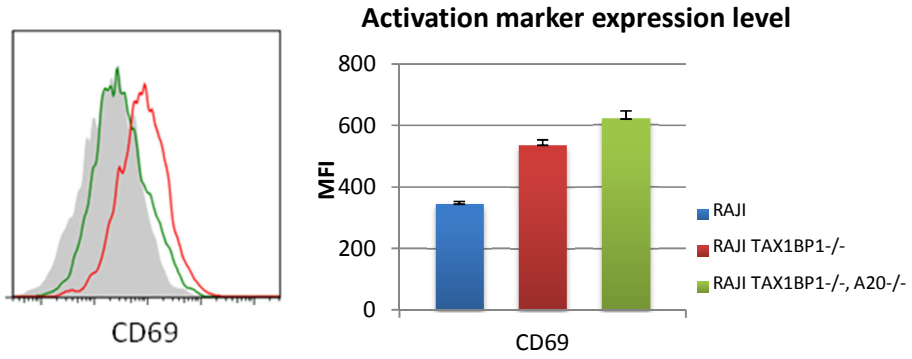

Figure 3.34 The expression of B cell activation markers in knockout cell lines created by CRISPR CAS9 system. Mean fluorescence intensities (MFI) of CD83, CD86 and CD69 expressions were obtained. Three experiments were conducted.

Before transfection, CD69 expression was increased in Raji cells deficient in TAX1BP1, and expressed at even higher levels when rendered doubly deficient in *TNFAIP3* and *TAX1BP1*, when compared with WT cells (Figure 3.34).

A

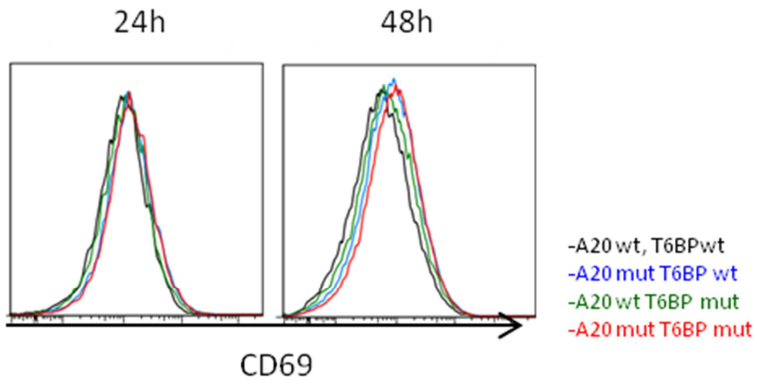

B

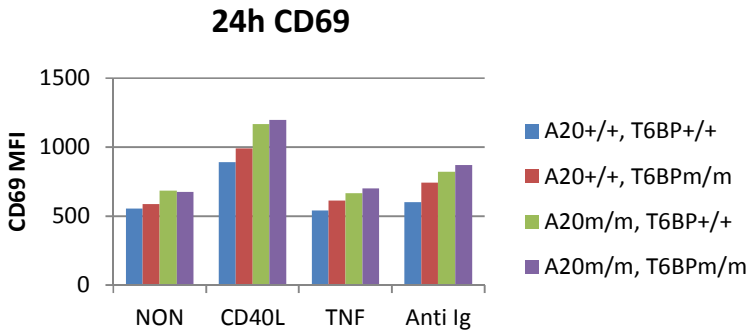

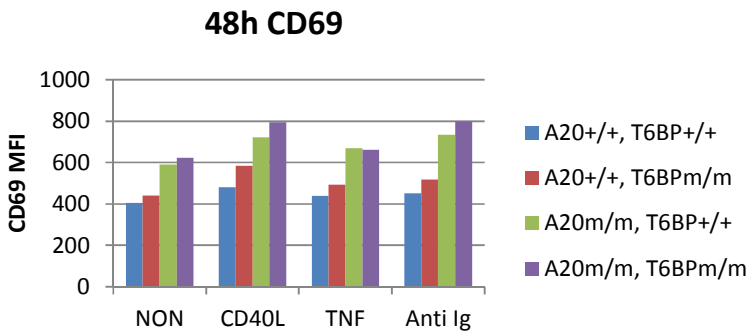

Figure 3.35 Analysis of CD69 expression. Constructs encoding either wildtype or S254R A20 and wildtype or L307I TAX1BP1 were transfected into ***TNFAIP3***-/- ***TAX1BP1***-/- Raji cells. **A.** Histogram of CD69 expression from cultures incubated with CD40L(1ug/ml) for 24h and 48h **B.** Bar graphs of CD69 expression at 24 hours and 48 hours.

Next, we examined the action of genetic complementation of double-deficient Raji cells with either mutant or wild type alleles of *TAX1BP* and *TNFAIP3*, either together, or with their wildtype interacting partners. CD69 expression was determined by flow cytometry. Wild type or mutant A20 mammalian vectors were cotransfected with wildtype or mutant TAX1BP1 mammalian vectors into Raji *TNFAIP3-/- TAX1BP1-/-* cells by electroporation using the NEON system.

mCherry vectors were used for selecting transfectants and mCherry positive cells were sorted and activated with CD40L, TNFα or anti-Ig for 24 hours or 48 hours. CD69 expression was measured by flow cytometry. TNFAIP3^{S254R} and TAX1BP1^{L307I} transfection resulted in increased CD69 expression, relative to cells transfected with wildtype constructs. Significantly, transfection of either mutant *TAX1BP1* or *TNFAIP3* with wild type interacting partner resulted in phenotypes intermediate between those found after transfection of mutant versions of both *TAX1BP1* and *TNFAIP3*, although cells containing the mutant allele of *TNFAIP3* and those homozygous for both mutant

genes exhibited similar phenotypes. Mutant T*AX1BP1* cells expressed less CD69. CD40L stimulation induced enhanced CD69 expression in all cultures however TNFα and anti Ig did not significantly stimulate the expression levels. Nonetheless, this was shown in all stimulations and the difference between wildtype and mutant types was more pronounced after 48 hours.

3.1.7.2 Co-immunoprecipitation

A20 and TAX1BP1 are known to form a macromolecular complex in order for A20 to perform its normal catalytic function. We investigated the possibility of physical interaction between mutant A20 and TAX1BP1 to explain the putative epistatic interaction between *TAX1BP1* and *TNFAIP3*. We generated constructs of wildtype and point mutants of each gene with tag proteins. A20 was conjugated with a C-terminal cMyc and TAX1BP1 was FLAG-tagged at its N terminal.

HEK293T cells were transiently co-transfected with wild type A20 and wild type TAX1BP1 or $A20^{S254R}$ and $TAX1BP1^{L307I}$ expressing vectors. After 36 hours, cells were stimulated with TNFα to induce A20 complex formation and cells were harvested and lysed.

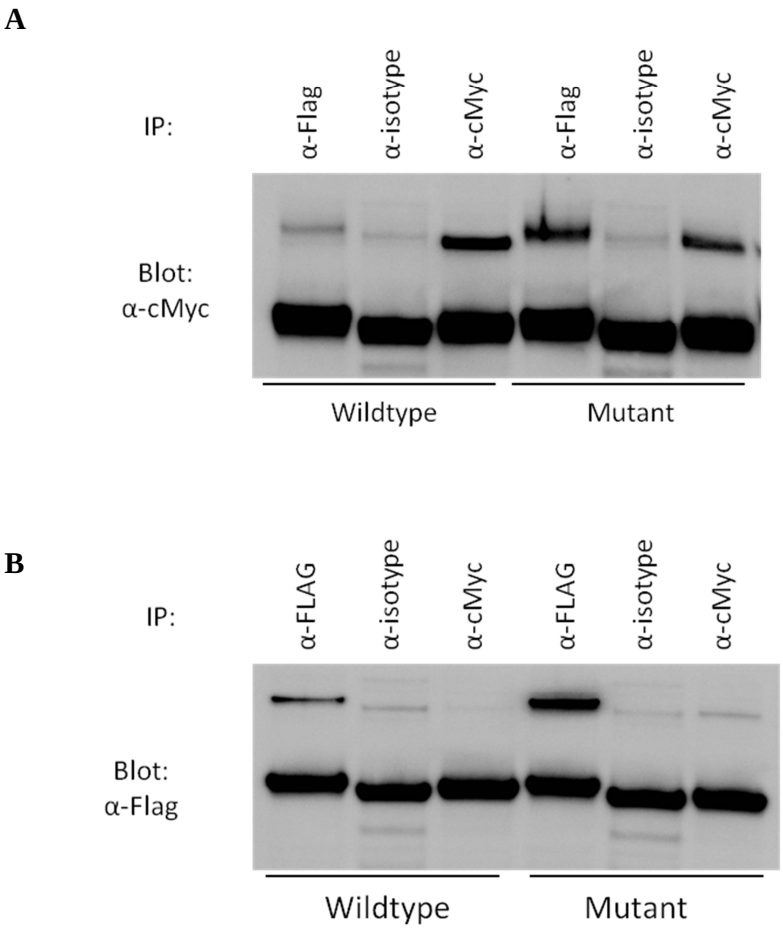

Figure 3.36 Co-immunoprecipitation of A20 and TAX1BP1. Wildtype A20 and wild type TAX1BP1 or $A20^{S254R}$ and $TAX1BP1^{L307I}$ cell lyates were precipitated with anti-Flag, anti-cMyc or isotype control antibodies. **A.** Immunoblotting with anti c-Myc **B.** Immunoblotting with anti FLAG antibodies. A20-cMyc fusion; TAX1BP1-Flag fusion.

A20 was immunoprecipitated with anti-cMyc and the interaction was analysed by immunoblotting with anti-Flag for TAX1BP1. We also analysed cells after immunoprecipitaion of TAX1BP1 followed by immunoblot analysis with anti cMyc.

Anti-cMyc (A20) precipitated a small amount of anti FLAG (TAX1BP1)-containing complex in cells transfected with $A20^{WT}$ and $TAX1BP1^{WT}$. By contrast, we observed

more FLAG (TAX1BP1)-containing complexes after anti-cMyc (A20) precipitation of cells transfected with $A20^{S254R}$ and $TAX1BP1^{L307I}$ (Figure 3.36A). Similar results were obtained with the converse strategy, in which we precipitated protein complexes with anti cMyc (A20) (Figure 3.36B).

These findings suggested preferential assembly of mutant TAX1BP1 and A20, and this would be consistent with the observed severe phenotype in A.II.1. In the absence of any interaction, we would expect approximately 50% of A20-containing molecular complexes to contain mutant A20. In the presence of this perturbed interaction, greater that 50% would contain the A20 with reduced function. These findings potentially explain why simple *TNFAIP3* heterozygosity confers a mild phenotype, but combined *TNFAIP3* and *TAX1BP1* mutations confer a severe phenotype. In other words, our results are consistent with non-allelic non complementation, in which two mutations within separate genes, combine to cause a phenotype that might be expected with damaging homozygous mutations of either gene alone.

3.2 Discussion

We discovered a novel mutation in *TNFAIP3* (g.8910C>A) by whole exome sequencing, from two unrelated patients with common variable immune deficiency (CVID) recruited to the Australian and New Zealand Antibody Deficiency Allele (ANZADA) study. By genotyping their family members we found three additional carriers of the mutation.

A20 is an important negative regulator that terminates signalling via the canonical NF-kB pathway. In most cells, A20 expression is maintained at very low levels in resting cells, but its expression is induced when cells are activated by canonical NF-kB stimuli. This is thought to providea negative feedback loop for regulating NF-kB signalling (Catrysse, Vereecke et al. 2014). The mutation we report here is located at S254 proximal to an active site, H256, and it was predicted to alter the conformation of the A20 structure to perturb catalytic activity by crystallization and in silico tests.Indeed, the deubiquitination experiment reveals that the mutation *TNFAIP3*^{S254R} impairs deubiquitination. Consistent with previous reports we also found that the OTU domain cleaves K48 linked ubiquitin chains rather than K63-linked ubiquitin chains in vitro. While the wildtype OTU domain was able to generate dimeric or monomeric ubiquitin chains within 30 minutes of activation, S254R attenuated DUB activity to generate di- or mono-meric ubiquitin chains. This biochemical defect was, however, not as severe as that observed with an OTU harbouring a H256R substitution.

Our NF-kB activation experiment reveals a substantial effect of A20^{S254R} on NF-kB activity (Figure 3.6). A20^{S254R} exhibits robust and prolonged NF-kB activity compared

to its wildtype. Two distinct domains of A20 function in a stepwise manner so DUB function facilitates the E3 ligase function of A20 (Wertz, O'Rourke et al. 2004), and therefore, the S254R mutation may influence not only DUB activity but also E3 ligase of A20.

Lu and colleagues generated *Tnfaip3* $^{OTU/OTU}$ mice, which carry a cysteine to alanine mutation at amino acid residue 103, and demonstrated that the OTU domain accounts for some of A20 functions (Lu, Onizawa et al. 2013), although the phenotypes of these mutant mice were less severe than that of *Tnfaip3*$^{-/-}$ mice, which die prematurely from multi-organ inflammation and cachexia (Lee, Boone et al. 2000; Lu, Onizawa et al. 2013)(Lee et al., 2000 Lu, 2013).

Interestingly, mice carrying mutations in the OTU domain do not exhibit defects at birth but exhibit splenomegaly and dextran sulphate sodium (DSS) induced colitis by 6 months of age (Lu, Onizawa et al. 2013). These abnormalities are similar to those observed in proband A.II.1.

TNFAIP3$^{S254R/+}$ carriers have various defects in immune function, but both probands, from two independent kindreds, exhibit primary antibody deficiency. Proband from kindred A (A.II.1) presented with severe haematological autoimmunity. Detailed immunological phenotyping revealed increased numbers of T cells but a normal number of B cells. Further analysis of the B cell compartment, however, revealed a high proportion of transitional B cells and a deficiency of memory B cells. We found no evidence of plasma cell formation either in vivo or in vitro.

We found evidence of constitutive cellular activation, based on analysis of cell surface phenotype, an increase of propensity to apoptosis. Consistent with this, biochemical analysis revealed enhanced IKBa activity. Furthermore, global gene analysis revealed an active NF-kB signature, that was remarkably concordant between T and B cells. Taken together, these findings are consistent with a defect in termination of NF-kB signalling as a result of the A20 S254R mutation (Figure 3.5-6, 3.30).

Several individuals who presented with persistent B cell lymphocytosis have been found to harbour gain of function mutations in *CARD11* (Snow, Xiao et al. 2012). While our proband had normal total B lymphocyte numbers, the defects in lymphocyte activation, and proliferation were very similar. The mutations in *CARD11* may be associated with regulating A20 functions. MALT1 has been reported to have a specific proteolytic activity that cleaves A20 upon TCR activation (Coornaert, Baens et al. 2008). CARD11 mutations confer activation of MALT1 and consequently lead to inactivation of A20. This could explain the similarity between the patient with A20 S254R and patients with *CARD11* mutations.

The mutant CARD11 and A20 S254R both result in activation of IKKβ. Remarkably, the phenotype of our patient is very similar to one of the constitutively active IKKβ mice (caIKKβ) which carry a gain of function mutation in *Ikbkb* (Krishna, Xie et al. 2012). Analysis of circulating CD4+ T cells revealed that the majority adopted an effector memory type (T_{EM}), with very few naïve T cells in either CD4 or CD8 compartments. A similar defect in T cell differentiation, with increased formation of T_{EM} cells was also observed in caIKKβ mice.

Since A20 is constitutively expressed to inhibit activation of NF-kB in lymphocytes, any defect in A20 would be expected to enhance activation of lymphocytes. In the absence of stimulation, lymphocytes from caIKKβ mice express increased CD69. Similarly, we observed spontaneous activation in T cells from proband A.II.1.

Chronic activation is thought to impair responsiveness to repeated stimulation of lymphocytes. In caIKKβ mice, there is a reduced response to TCR stimulation. We reported impaired upregulation of both CD69 and CD25 after T cell stimulation of cells from A.II.1. A similar result was reported in patients *CARD11* gain-of-function mutations. Absence of responsiveness may reflect cloncal exhaustion, and consistent with this, we observed high expression of exhaustion marker PD1 was seen in A.II.1, and similar findings were reported in T cells from caIKKβ mice (Krishna, Xie et al. 2012).

Activation and proliferation experiments both showed that the majority of the patient's cells failed to survive. Apoptosis experiments confirmed that cells from A.II.1 were prone to apoptosis after stimulation with PMA and ionomysin, or TNFa. Remarkably, global gene expression showed that both T and B cells expressed very high levels of IL-8 and CCL2. They chemokines are known to facilitate phagocytosis. In 2013, Cullen and colleagues discovered that TNFα or CD95 induced apoptotic cells secreted various signals, particularly IL-8 and CCL2 to induce phagocytosis (Cullen, Henry et al. 2013).

A20 is physically associated with the DISC complex, and inhibits the DISC formation by removing ubiquitin chains of caspase 8 through DUB activity (Jin 2009). Thus, impaired DUB function may result in an enhanced propensity to apoptosis.

Increased cell death was observed in caIKKβ mice, as well as high levels of expression of both active caspase 8 and active caspase 3. Intriguingly, patients with gain-of-function mutations in *CARD11* did not show cell apoptosis. Although CARD11 is crucial for lymphocyte activation, CARD11 is restricted to lymphocytes. By contrast, A20 and IKKβact more broadly to regulate canonical NF-kB pathways such as TNF or TLR-induced NF-kB, which might explain why A20 S254R more closely resembles the phenotype of caIKKb mice than *CARD11* patients.

We observed a severe phenotype in A.II.1, with evidence of increased cell activation, enhanced apoptosis, and clinical features of autoimmunity and immune deficiency. Other carriers of the TNFAIP3 mutation were phenotypically normal. Recent evidence has emerged that truncated mutations in *TNFAIP3 resulting in A20* haploinsufficiency is sufficient to cause a florid inflammatory phenotype (Zhou, Wang et al. 2016). The discrepancy could be explained because A20 S254R still contains a functional E3 ligase domain and haploinsufficient DUB activity may be compensated by E3 ligase domain.

The severe phenotype observed in the proband from kindred A, however, appears to be due to the combined action of the A20 variant, and a variant in its interacting partner, TAX1BP1. A20 forms macromolecular complexes that function in NF-kB inhibition and apoptosis (Shembade, Harhaj et al. 2008; Shembade, Parvatiyar et al. 2009). The discovery of an increasing number of A20 interacting partners indicates that A20 is involved in a broad range of immune regulation. We hypothesized that an additional mutation in interacting partners would alter A20-containing complexes to impair A20 functions. We identified 13 nonsynonymous or splicing mutations from A20 interacting

genes in the A.II.1 genome. Among them a mutation in *TAX1BP1* was the only unique mutation that was found in A.II.1 but not in the other A20S254R carriers.

TAX1BP1 was discovered in a yeast two–hybrid screen for A20 binding partners (De Valck et al., 1999). TAX1BP1 is also an essential regulator. TAX1BP1-deficiency in mice results in premature death due to age-dependent hypertrophic cardiac valvulitis. These mice also exhibit hypersensitivity to sublethal doses of TNF and IL-1, which had also been observed in A20-/- mice (Iha, Peloponese et al. 2008). Inhibition of NF-kB is attenuated in *Tax1bp1* deficient cells, due to impaired ubiquitin editing, although TAX1BP1 does not possess the ubiquitin editing activity. Therefore TAX1BP1 is thought to be a scaffolding protein that recruits A20 to ubiquitinated substrates, enabling A20 to perform its ubiquitin editing function to terminate NF-kB signalling (Verstrepen, Verhelst et al. 2011). Recently, it has been reported that phosphorylation of TAX1BP1 is required to form A20 editing complexes, and mutations in active sites of TAX1BP1 impair the formation (Shembade, Pujari et al. 2011). This observation confirms that functional TAX1BP1 is important for the normal operation of the A20 editing complex, and that mutations on TAX1BP1 could impair the A20 ubiquitin editing functions.

We went on to confirm both the functional consequence of TAX1BP1 deficiency, and the defect on function conferred by combined mutations in TAX1BP1 and TNFAIP3. In order to exclude endogenous gene expression, we generated RAJI $^{A20-/-\ TAX1BP1-/-}$ and RAJI $^{TAX1BP1\ -/-}$ were by CRISPR/cas genetic engineering. We observed high level expression of CD69 in RAJI $^{A20-/-\ TAX1BP1-/-}$ and RAJI $^{TAX1BP1\ -/-}$ cells, confirming that

TAX1BP1 and A20 inhibit NF-kB activation. RAJI $^{A20-/-\ TAX1BP1-/-}$ showed enhanced CD69 expression compared with RAJI $^{TAX1BP1-/-}$. Consistent with previous reports, this suggests that A20 has additional functions independent of TAX1BP1. The effect of $A20^{S254R}$ and $TAX1BP1^{L307I}$ was tested in RAJI $^{A20-/-,\ TAX1BP1-/-}$. As expected, $A20^{S254R}$ and $TAX1BP1^{L307I}$ cells exhibited more persistent and stronger NF-kB activity compared to wild type or single mutant cells. The cells with three different stimuli showed the same results in both 24 hour and 48 hour stimulation.

We investigated the possibility of biochemical interaction between both mutant proteins by co immunoprecipitation experiments. Our initial hypothesis was that A20 ^{S254R} or TAX1BP1 ^{L307I} may interrupt the formation of molecular complexes involving these two proteins, possibly as a result of conformational changes. The results were in contrast to this prediction, and revealed that the interaction between A20 ^{S254R} and TAX1BP1 ^{L307I} is enhanced relative to that between wildtype proteins. We observed a relatively weak the interaction between wildtype A20 and TAX1BP1 possibly due to stringent immunoprecipitation buffer. By contrast, we observed a robust coimmunoprecipitation of mutant proteins, suggesting a higher affinity interaction between the mutant proteins. Preferential interaction of mutant proteins, resulting in greater than expected incorporation of mutant A20, would therefore amplify the phenotypic consequences of mutant A20, which we showed exhibits defect deubiquitination.

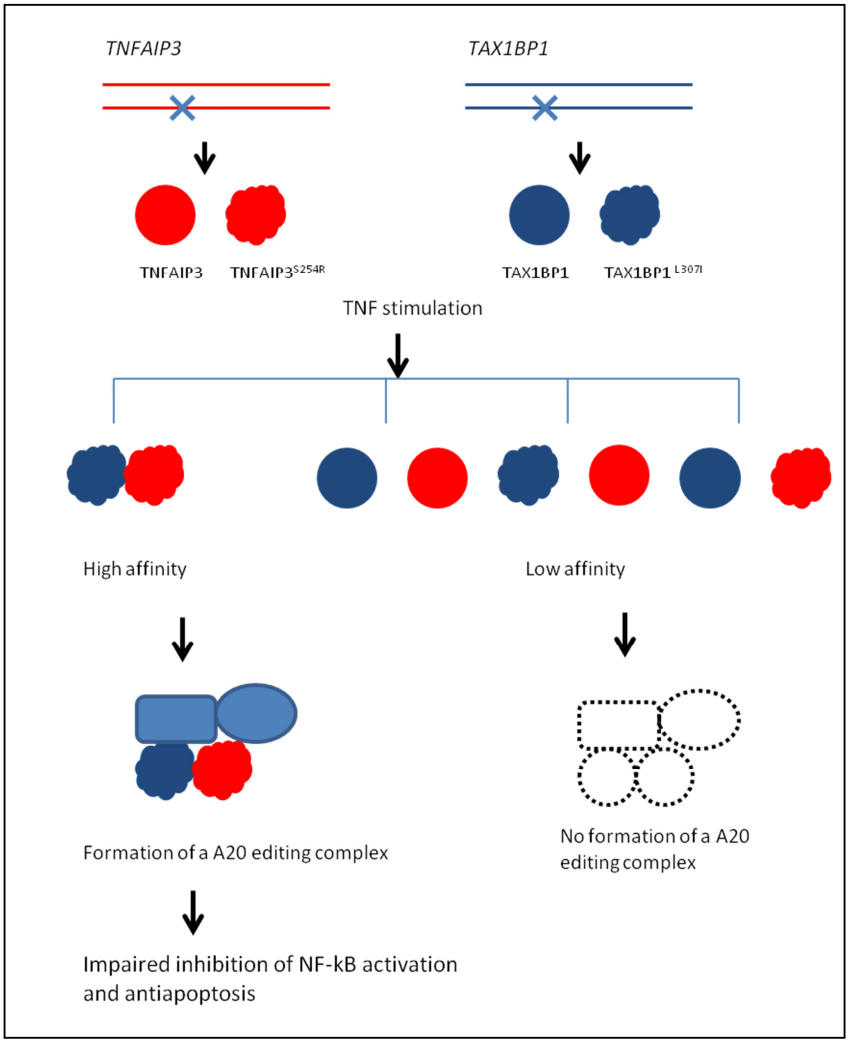

Figure 3.37 A theory of nonallelic noncomplementation discovered in this study

In conclusion, we report a novel mutant allele of A20 S254R that segregates with primary antibody deficiency. In vitro, $A20^{S254R}$ impairs DUB and inhibition of NF-kB. The mutation in TNFAIP3 appears to be in epistasis with a polymorphism of TAX1BP1, as the phenotypic consequences of the mutant A20 protein are accentutated by TAX1BP1 polymorphism. We present biochemical evidence of a preferential interaction between the two mutant proteins, consistent with the phenomenon of nonallelic noncomplementation, in which two different recessive mutations confer a phenotype because they encode proteins that act in the same pathway, or contribute to

the same macromolecular complex. In this particular case, the mutations increase the affinity of interaction between A20 and TAX1BP1 to amplify the consequences of a hypomorphic *TNFAIP3* allele.

Table 3.1 Summary of immunogical phenotype

		A.I.1	A.I.2	A.II.1	A.II.2	B.I.1	B.I.2	B.II.1	B.II.2	normal range
B cells (% of CD19+)	T1 B cells ($CD24^{+++}$ $CD38^{+++}$)	2.23	1.91	17.5	2.81	4.07	2.66	1.78	8.72	0.79-6.06
	T2 B cells ($CD24^{++}$ $CD38^{++}$)	6.31	7.36	18.5	4.72	12.7	8.09	6.05	15.3	2.87-11.5
	Naïve B cells ($CD24^{+}$ $CD38^{+}$)	57.1	55.4	18.8	43.3	72.8	47.7	76.8	54.7	41.3-68.7
	Memory B cells ($CD24^{++}CD38^{+}$)	21.3	22.8	5.98	26.7	8.41	36.1	13.6	17.7	7.47-39.3
	Plasma cells ($CD24^{-}CD38^{+++}$)	0.25	0.47	0.079	1.09	0.011	0.16	0.017	0.25	0.018-0.48
	Anergic B cells ($CD24^{-}$ $CD38^{-}$)	0.67	0.76	13.7	1.6	0.047	0.24	0.02	0.083	0.14-2.24
	$CD21^{low}$	14.57	13.54	46.61	18.18	9.31	6.6	7.13	7.67	3.7-17.6
T cell (% of CD4+)	CD4+ TEMRA ($CD4^{+}$ $CCR7^{-}$ $CD45RA^{+}$)	11.2	24.1	12.3	17.7	8.45	7.78	17.8	20.5	3.27-11.4
	CD4+ Naïve ($CD4^{+}$ $CCR7^{+}$ $CD45RA^{+}$)	15.5	47.2	1.48	37	32.5	23.8	44.6	58.4	8.47-55.4
	CD4+ TCM ($CD4^{+}$ $CCR7^{+}$ $CD45RA^{-}$)	15.1	10.3	6.72	14.3	33.4	14.5	9.33	5.67	14.7-31.1
	CD4+ TEM ($CD4^{+}$ $CCR7^{-}$ $CD45RA^{-}$)	58.2	18.3	79.5	31	25.7	54	28.4	15.4	18.9-45.3
	Treg ($CD4^{+}$ $CD25^{+}$ $CD127^{-}$ $FOXP3^{+}$)	3.86	4.29	0.58	3.35	3.2	3.63	2.9	3.65	4.13-7.47
	cTFH ($CD4^{+}$ $CXCR5^{+}$ $CD45RA^{-}$)	13.7	7.23	3.96	9.41	15.6	8.29	5.51	4.46	7.5-14
	TH1 ($CD4^{+}$ $CCR6^{-}$ $CXCR3^{+}$)	11.7	10.7	4.09	24.6	26.8	28.7	28.2	20.9	9.57-45.3
	TH2 ($CD4^{+}$ $CCR6^{-}$ $CXCR3^{-}$)	26.8	48.8	54.3	52.3	26.2	17.4	15.7	27.9	28.3-67.2
	TH17 ($CD4^{+}$ $CCR6^{+}$ $CXCR3^{-}$)	33.7	30.4	36.2	11.2	24.3	20.9	24.6	33.6	17.2-39.2
	CD57+	1.69	1.03	19.08	9.99	7.116	2.491	0.553	0.338	0.39-2.3
	PD1+	31.33	14.25	80.2	24.44	46.72	58.35	38.577	33.565	18.8-45.62
	CD57+ PD1+	0.83	0.45	14.7	5.44	6.22	2.35	0.477	0.265	0.22-1.62

4 Pedigree II

4.1 Results

4.1.1 Clinical history of our proband

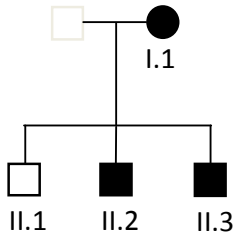

ID	DOB	Infections	autoimmune	Diagnosis	Sp Ab	IgG (g/L) (normal -> 6.2)	I gA (g/L) (normal -> 0.6)	IgM (g/L) (normal -> 0.48)
I.1	5/04/1958	Otitis media, Sinusitis, bronchitis, pleurisy, dental abscesses pneumonia Viral meningitis	Alopecia areata (age 11)	CVID (age 35)	N/A	5.53	0.18	0.009
II.1	14/02/1982	Nil	Nil	Well	N/A	11.4	1.86	0.66
II.2	29/08/1983	Sinusitis	Alopecia totalis (age 14)	CVID (age 20)	HIB 0 TetTex 0.16 PNab 7/14 = 0	2.7	0.1	0.4
II.3	3/12/1987	Pneumonia, bronchitis, sinusitis, otitis media, skin infections	Alopecia areata (age 8)	CVID (age 5)	N/A	1.64	0	0.05

Table 4.1 Clinical history of TCH128 family

We identified an individual (I.1) with complete B-cell deficiency from within a larger cohort of patients with primary immune deficiencies. She was not diagnosed with CVID until the age of 40 but had a long history of chronic sinusitis, bacterial pneumonia, recurrent intestinal giardiasis, and periodontitis. She also had alopecia areata at age 14 years. At the time of investigation, she was receiving intravenous immunoglobulin (IVIG) replacement. Further investigation of the kindred revealed 2 of 3 offspring with

hypogammaglobulinemia, 1 diagnosed at age 20 years (II.2) and the other in infancy (II.3) (Table 4.1). Both sons have a history of chronic sinusitis from childhood and remarkably, both have a history of childhood alopecia totalis. One is receiving IVIG, and the other remains healthy despite refusing immunoglobulin replacement therapy.

4.1.2 The cellular phenotype

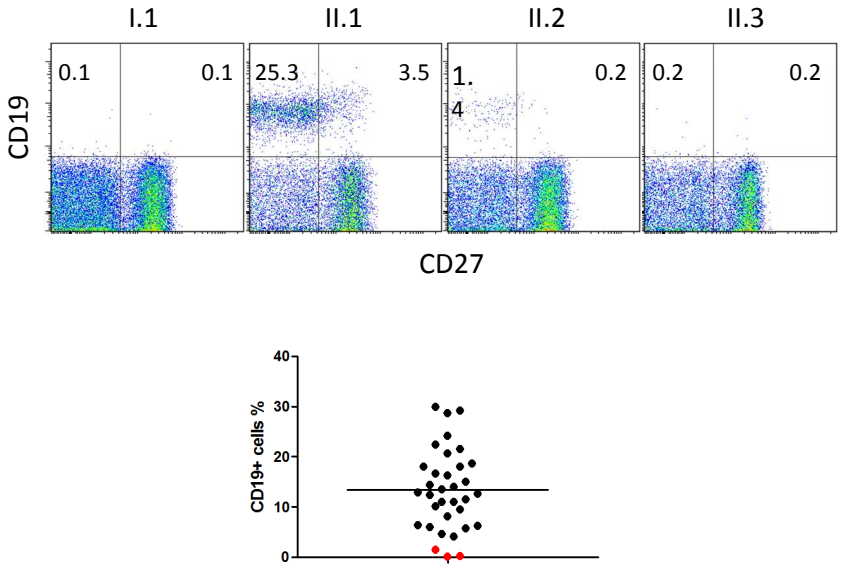

Figure 4.1 Analysis of circulating B cells and summary of B cell numbers relative to other CVID affected patients and healthy control CD19+CD27- cells represent naïve B cells CD19+ CD27+ cells indicate memory B cells.

Analysis of peripheral blood samples from A.I and all 3 offspring revealed severe B-cell deficiency (Figure 4.1). In all cases, B cells represented less than 2% of total lymphocytes, which is exception not only in healthy controls but also unrelated patients with hypogammaglobulinemia, where the average proportion of B cells was approximately 15% (Figure 4.1).

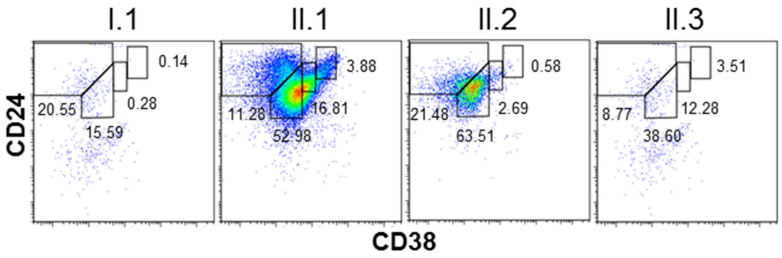

Figure 4.2 Analysis of transitional B cells in family members. They are CD19+ cells and CD24+++CD38++ cells represent transitional stage 2 B cells and CD24++ CD38 ++ cells represent transitional stage 1 B cells.

Each patient was also found to have severe deficiency of transitional stage 1 and 2 B cells (defined according to CD19, CD24 and CD38 expression) in the peripheral blood (Figure 4.2).

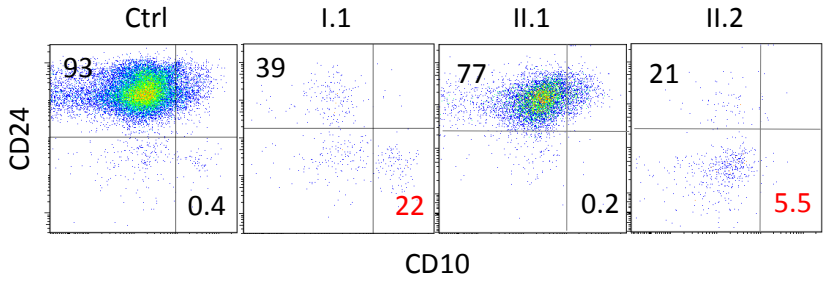

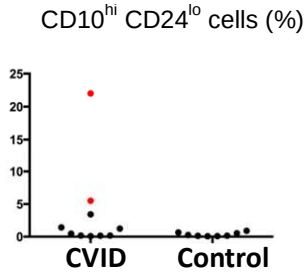

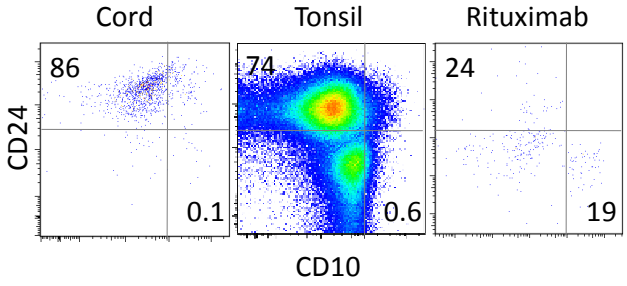

Figure 4.3 Distribution of CD24^{lo}and CD10^{hi} cells A. Analysis of CVID patients and healthy controls **B.** summary of the population C. Analysis of the population from Cord blood, Tonsile or ribuximab from patient with rituximab treatment.

Careful analysis of the few remaining CD19+ cells revealed a relative expansion in CD10^{hi} CD24^{lo} cells and this population, which is rare in cord blood and tonsil as well as adult peripheral blood, but is relatively prominent in patients who have received rituximab (anti-CD20) (Figure 4.3).

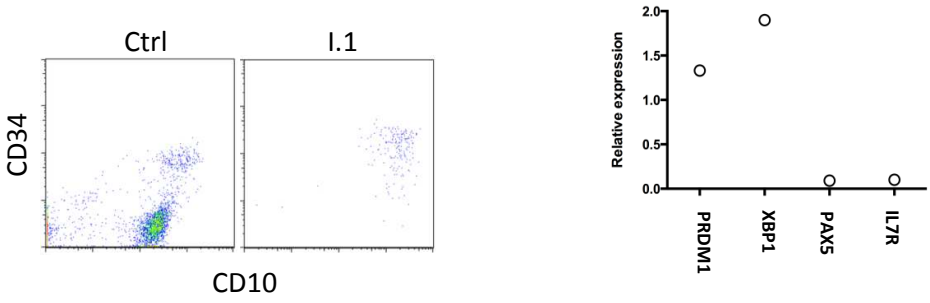

Figure 4.4 Analysis of bone marrow samples A. Pro B cells **(**CD10^{+} CD34^{+}) and Pre B cells (CD10^{+} CD34^{-}) were analysed **B.** Expression of indicated transcripts from I.1 relative to their expressions in two normal control marrows. Ctrl, control

Consistent with these findings, reanalysis of an archival bone marrow biopsy obtained a decade earlier from I.1 revealed an arrest in early B cell ontogeny (pro-B cells) (Figure 4.4).

Despite profound B cell deficiency, serum Ig was measurable. Furthermore, antibodies to specific antigens were also detected (tetanus toxoid and 7/14 pnemococcal polysaccharides, Table 4.1). Consistent with this finding, analysis of transcripts prepared form the aspirate are consistent with the presence of plasma cells (Figure 4.1).

In order to investigate abnormalities in plasmablast induction, B cells were stimulated with CD40L and IL-21, or CpG and IL-21 for 4 days in vitro. Remarkably, we observed a 4-12 fold increase in plasmablast (CD27 + CD38++) induction with CpG, IL-21 or CD40L, IL-21 in I.1 relative to controls (Figure 4.5). Thus, despite the profound B cell deficiency, plasmablast formation is preserved a finding consistent with the discordance between the observed B cell count and immunoglobulin levels.

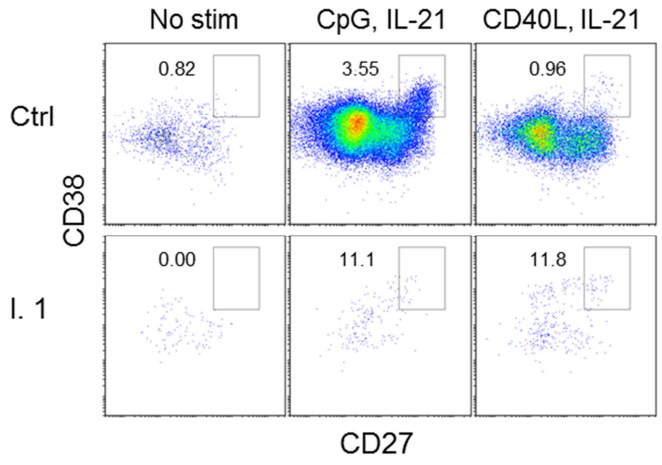

Figure 4.5 Flow cytometric analysis of plasmablast induction in vitro A. PBMCs were cultured with CD40L (1µg/ml) and IL-21 (50ng/ml) or CpG (2µM) and IL-21(50ng/ml) for 4 days. Then plasmablasts ($CD27^{++}$ $CD38^{+++}$) were enumerated. Ctrl, healthy control; I.1, proband

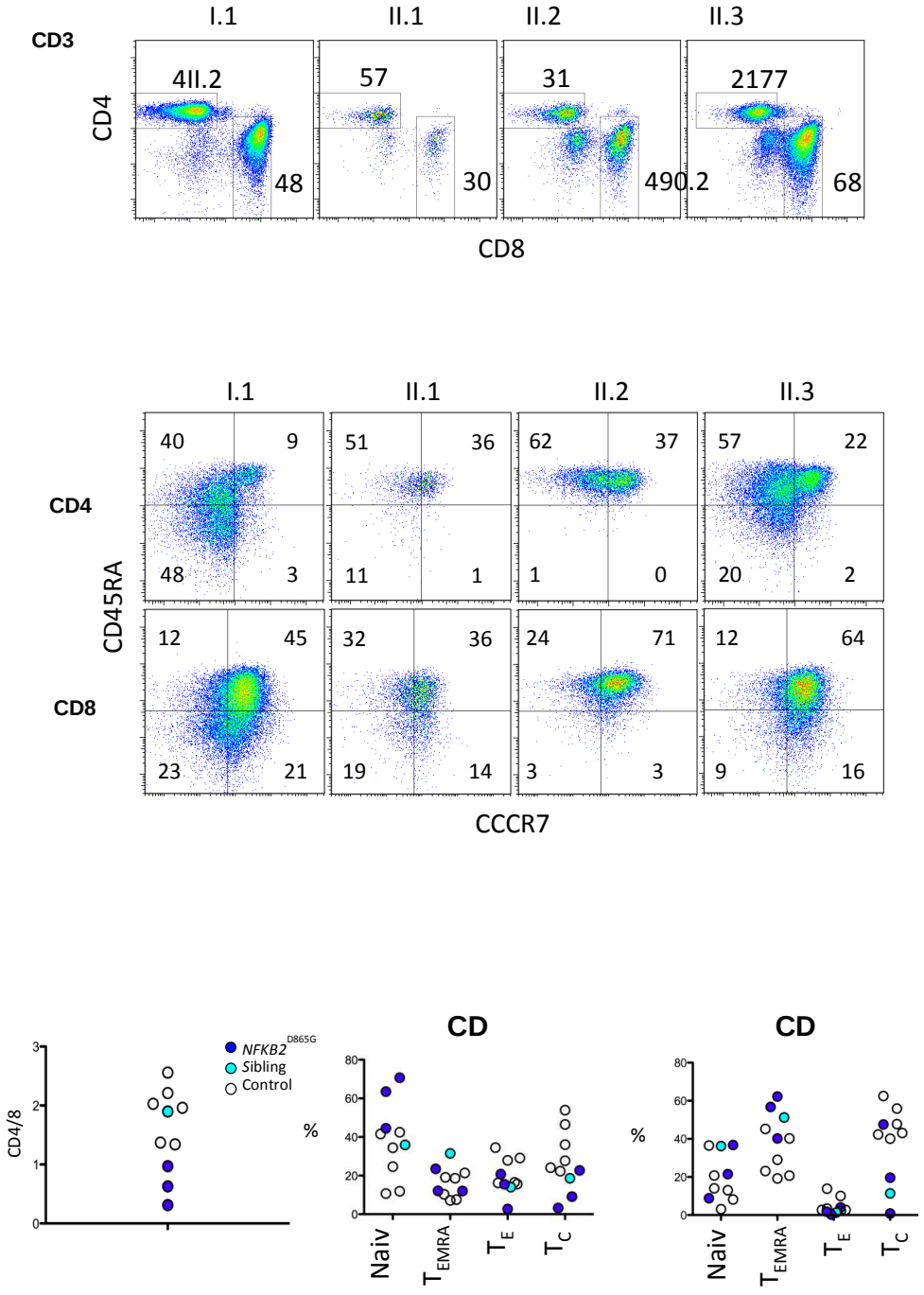

Figure 4.6 Flow cytometric analysis of circulating T lymphocytes Enumeration of memory and effector T cells. Representative profiles and summary data. TCM, central memory T cells; TEM, effector memory T cells; TEMRA, CD45RA+ effector memory T cells.

All family members had normal numbers of circulating T cells (Figure 4.6). Analysis of the T-cell compartment revealed an inversion of the normal CD4/8 ratio in patients and the affected individuals seems to have more naïve T cells in CD4 compartment however, we found no substantial abnormality of T-cell differentiation to memory cells or CD4 effector cells (Figure 4.6).

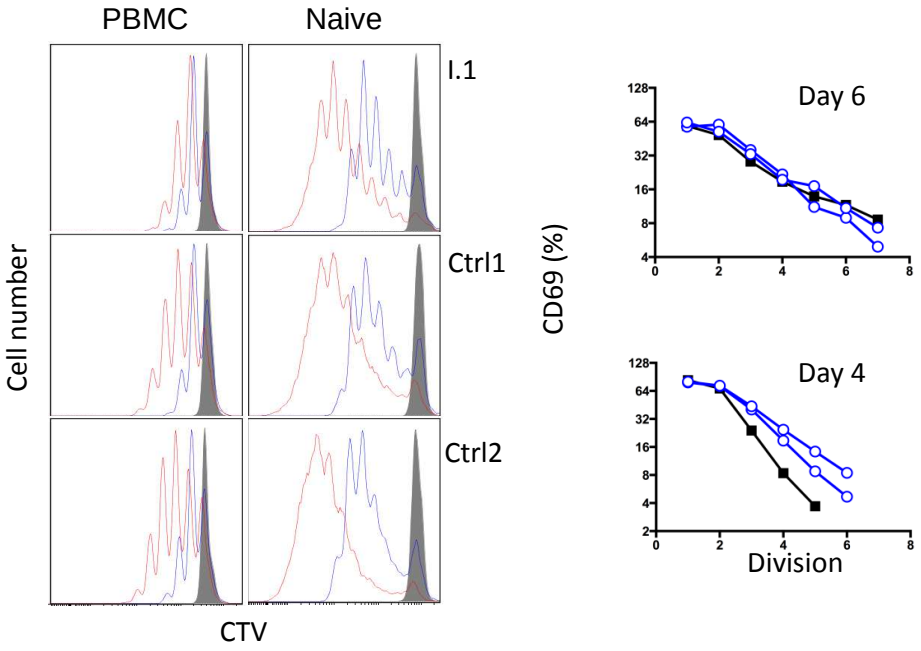

Figure 4.7 T cell activation and proliferation Either naive CD4+ T cells separated by negative selection with magnetic beads or CD4+ T cells with PBMC were analysed by dilution of cell trace violet after simulation with CD3 CD28. Cells were harvested and analysed by flow cytometry on day 4 (blue) and day 6 (red). Histograms were gated on CD3 and CD4. Unstimulated control cells are shown (grey). In the same experiment, naïve CD4+ T cells were analysed for activation based on induction of CD69. The percentage of CD69+ cells at each division was determined and plotted (control2, open blue; I.1, black filled). CTV, cell trace violet

To test for abnormalities of T-cell activation, PBMCs and purified naive T cells were isolated from both proband and controls and activated with anti CD3 and CD28. Activation according to CD69 and CD25 induction and proliferation appeared similar in patients and controls (Figure 4.7).

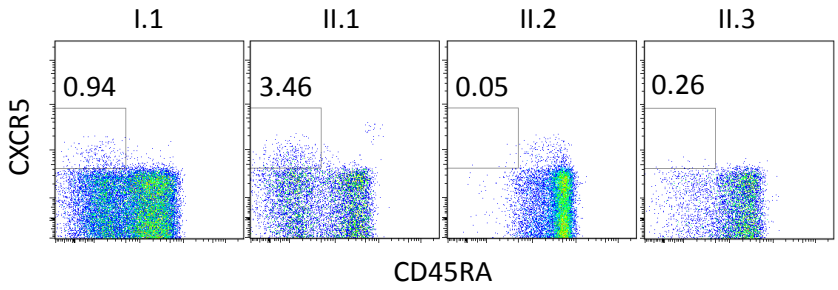

Figure 4.8. cTfh A. Peripheral blood flow cytometric analyses, gated on $CD4^+$ T cells and analyzed for Tfh-like cells (boxed as CXCR5+ CD45RA-). **B.** Frequencies of and circulating Tfh-like cells among CD4 T cells from healthy controls (open circles); healthy sibling (black-filled circles), ***P < 0.0001.

We did, however, identify a consistent reduction by approximately 20% in circulating CXCR5+ CD45RA- CD4+ T cells (P=0.0001; Figure4.8). This population is related to follicular helper T cells (Tfh), which are largely confined to secondary lymphoid organs here they provide crucial helper signals for B cells and antibody production. The mean frequency of natural regulatory T cells (FoxP3+) among CD4 cells was decreased to approximately 30% of normal in those affected (P=0.03; Figure 4.9).

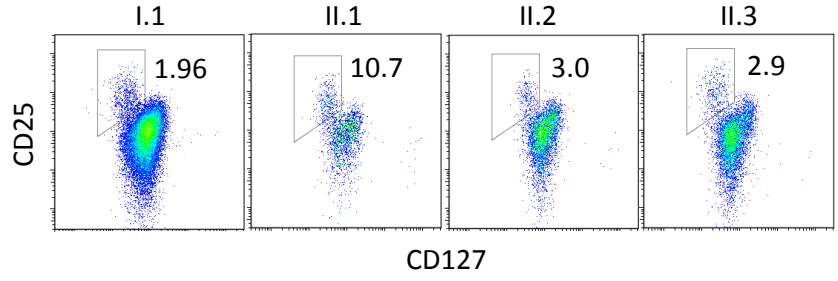

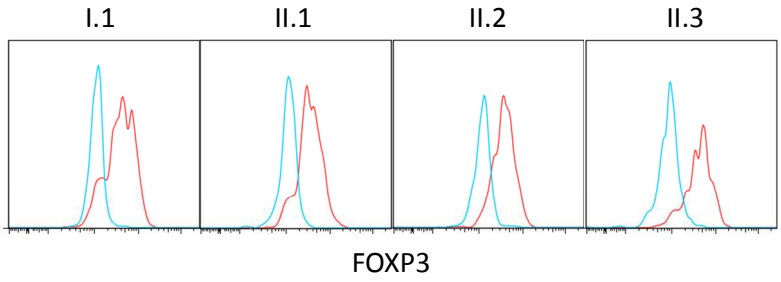

Figure 4.9 Regulatory T cells (boxed CD127low, CD25high) A. Percentage of CD4 T cells within the gated subsets is shown. **B.** Histograms show intracellular staining for Foxp3 expression in cells within the CD127low, CD25high gate (red histogram) and within the cells excluded from this gate (blue histogram). (C) Frequencies of and Tregs among CD4 T cells from healthy controls (open circles); healthy sibling (black-filled circles), *P=0.03

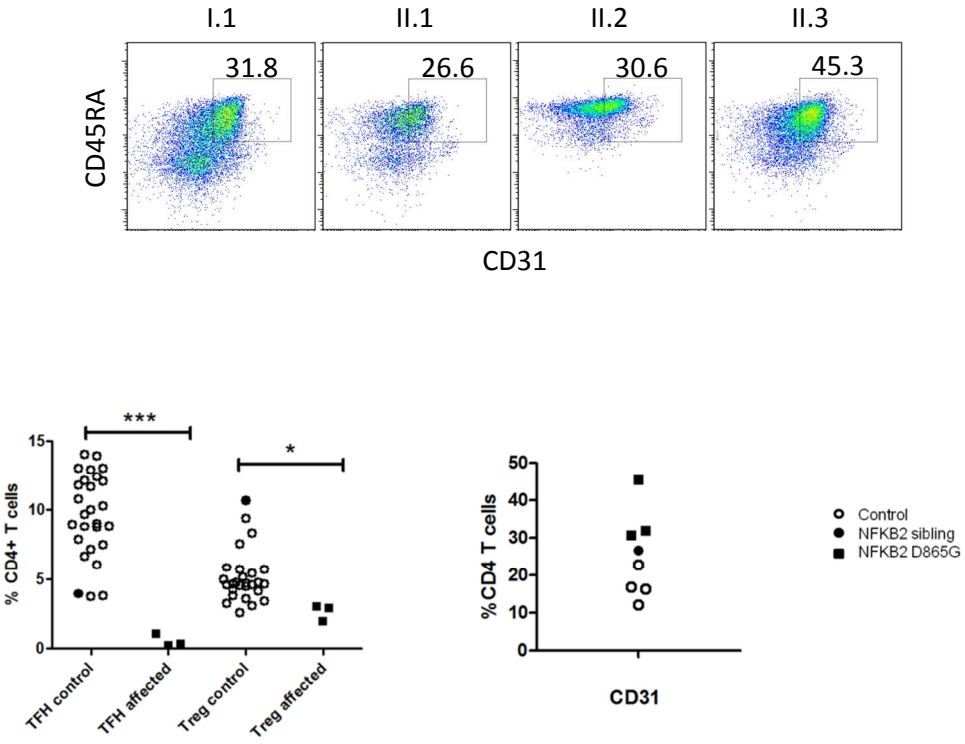

Figure 4.10 Recent thymic emigrants A. Flow cytometric analysis of peripheral blood mononuclear cells for recent thymic emigrants CD31+ CD45RA+). **B.** Frequencies of $CD31^{+}$ $CD4^{+}$ recent thymic emigrants among CD4 T cells from healthy controls (open circles); healthy sibling (black-filled circles); NFKB2 mutant siblings and parent (black-filled squares). (E)

We observed an increase in recent thymic emigrants, as determined by CD31+andCD45RA+cell expression (Figure 4.10), which raises the possibility of an abnormality in thymic function.

4.1.3 Mutation discovery

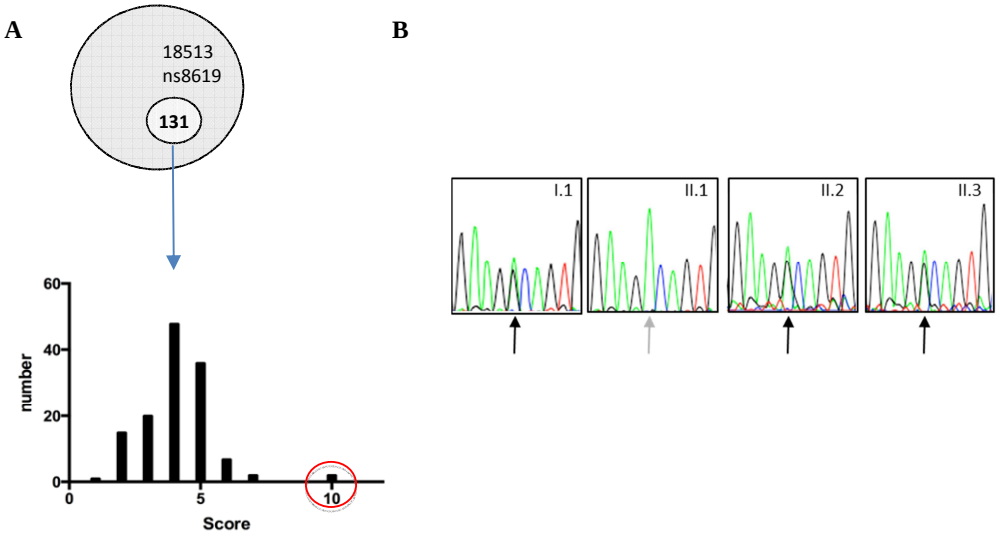

C

human	852	TRDKLPSTAEVKE**D**SAYGSQSVEQE
mouse	852	TRDKLPSTAEVKE**D**SAYGSQSVEQE
wolf	852	ARDKLPST-EVKE**D**SAYGSQSVEQE
cow	853	TQEKLPST-EVKE**D**SAYGSQSVEQE
chicken	859	PLEKLQST-EVKE**D**SAYGSESVEEE
zebrafish	870	PREDKQSS-DSTE**D**SGFGSQSIGEE
Xenopus	917	SPAEGKN**D**SAYESQSMEVDQS
Fugu	841	HNT–EATV**D**SGFSSQPMEEE
Elegans	no homologue	
Drosophila	no alignment	

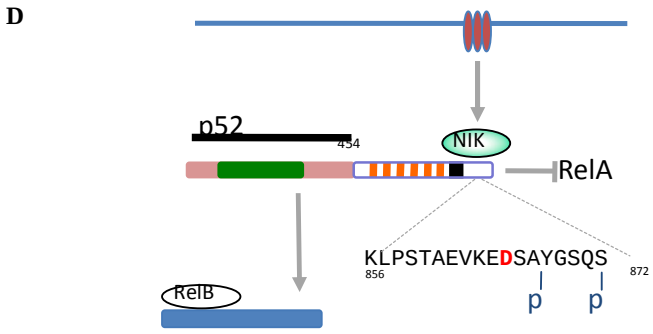

Figure 4.11 NFKB2 mutation. A. Frequency histogram of novel alleles according to filter based on tissue expression, phenotype of mice with mutations in orthologs, disease association, GO, and PolyPhen-2 scores (NFKB2 in red circle). **B**. Sanger sequencing of NFKB2 (according to pedigree in 4.1.1). **C**. Conservation of mutated residue of NF-kB2. **D**. Summary of p100 processing. Amino acid D in red indicates the location of D865G mutation, which is adjacent to one of the N-terminal phosphorylation sites (S866). Rel homology domain (green), ankyrin repeat domains (Jain, Ma et al.), death domain (Belot, Kasher et al.).

Table 4.2 Summary of the mutation

	NFKB2
Variant	Chr10; 104162024A>G g.2594 A>G; c.2594A>G;
Protein	D865G
Mutation taster	Disease causing P=0.999979076300663
SIFT	Damaging (0.04)
Poly Phen-2	Probably damaging 1.0 (sensitivity 0, Specificity 1.0)

Whole exome sequencing of the proband identified 131 novel mutations, which were then filtered according to pattern of tissue expression, GO pathways, phenotypes of mice harboring genetic mutations in orthologs, disease association (OMIM), and PolyPhen-2 score (Figure 4.11). From this analysis, 3 clear candidates emerged: *TNFRSF10A*, *TNFRSF1A*, and *NFKB2*. All 3 mutations were confirmed by Sanger

sequencing, but only the *NFKB2* mutation segregated with CVID phenotype and the B-cell phenotype. Furthermore, during the course of the project, 2 other kindreds with dominant antibody deficiency were described.

Members of the kindred described here have a heterozygous missense mutation encoding an amino acid substitution of aspartate to glycine at position 865 (*NFKB2*^{D865G}) (Figure 4.11, Table 4.2). Based on interrogation of dbSNP, 1000 Genomes Project, Human Genome Mutation Database, and ClinVar databases as well as other CVID kindreds within our cohort, this appears to be a novel mutation. Aspartate 865 is located in the NF-kB–inducing kinase (NIK)- responsive domain of the p100 protein product of NFKB2 and is absolutely conserved in vertebrates from humans to fish (Figure 4.11). The substitution with glycine is predicted to be damaging by 3 different in silico tests (Table 4.2).

4.1.4 Effect of NFKB2 ^{D865G} on P100 processing

Signaling via the noncannoical NF-kB pathway depends on accumulation of NIK (*MAP3K14*), a serine/threonine protein kinase that becomes stabilized after engagement of several TNF super family receptors including lymphotoxin α1β2, BAFF and CD40. NIK cooperates with another serine kinase, IkB kinase α (IKKα), to bind the full-length NF-kB2 (p100) protein and phosphorylate it on 2

A

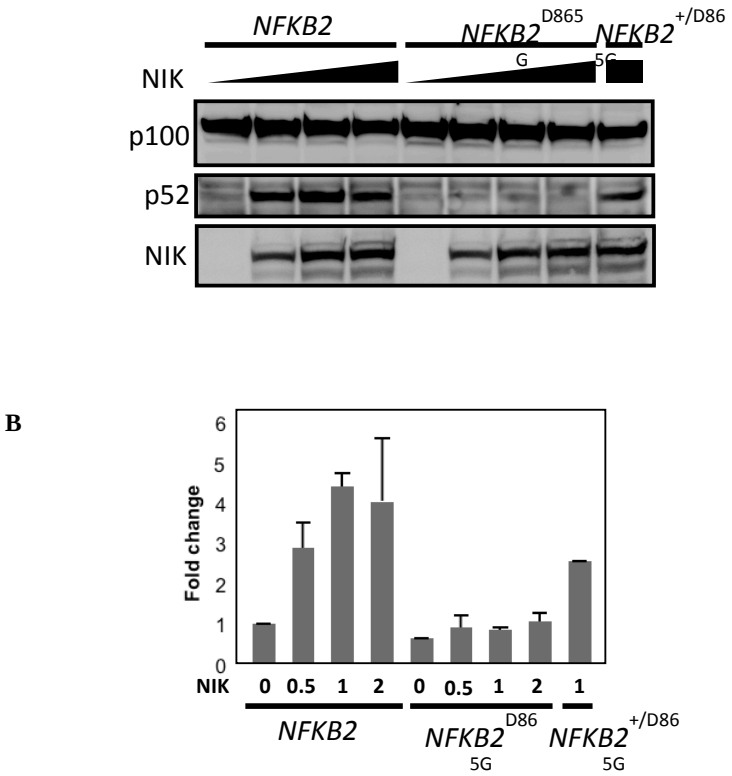

Figure 4.12 Effect of D865 > G mutation on NIK induced p100 processing HEK293 cells were co-transfected with expression vectors encoding wild-type (WT) or D865 . G mutant NFKB2 together with varying amounts of MAP3K14 expression vector encoding NIK. **A**. p100 and p52 detection by western blot **B**. Summary of relative expression of p100 and p52 determined as determined in (**A**).

critical serines, S866 and S870, in the C-terminal processing inhibitory domain. Phosphorylation of these sites allows binding of the ubiquitin ligase SCFbTrCP and polyubiquitination of lysine 855, tagging the p100 protein for limited proteasomal processing to yield the transcriptionally active p52 subunit of NF-kB2.The D865G mutation is located immediately adjacent to the critical S866 phosphorylation site. We investigated the effect of the D865G animo acid substitution on p100 processing. First, we transfected HEK293 cells with vectors expressing either wild-type or D865G mutant NFKB2 alleles. Analysis of cell lysates demonstrated dose-dependent processing of

normal p100 stimulated by co-transfected NIK. By contrast, NFkB2^{D865G} exhibited near-absence of p100 processing after NIK co-transfection (Figure 4.12). Only a small residual p52 band was detected, which is probably accounted for by endogenous NF-kB2 in the cell line. Co-transfection of mutant and normal alleles (NFKB2+/D865G) resulted in approximately 50% of normal processing to p52. The defect in NFKB2D865Gp100 processing was not corrected by stimulation with lymphotoxin-α. Processing of wild type p100 was blocked by MG132, a prteasome inhibitor, confirming its dependence on the proteasome (AppendixVI).

Next, we demonstrated that the D865G substitution affects p100 phosphorylation (Figure 4.13), even though this mutation does not involve a serine residue. This would appear to account for the loss of p100 processing.

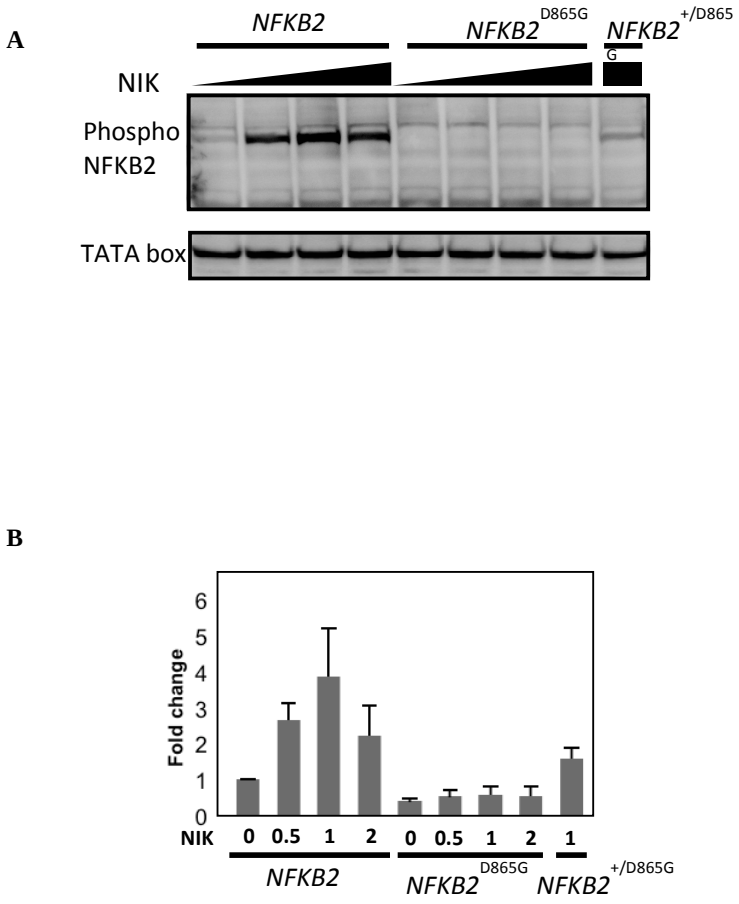

Figure 4.13 Effect of D865>G mutation on NIK induced p100 phosphorylation. HEK293 cells were co-transfected with expression vectors encoding wild-type (WT) or D865G mutant NFKB2 together with varying amounts of MAP3K14 expression vector encoding NIK. **A** phosphorylation of serines 867 and 870 in response to increasing dose of NIK **B**. Summary of relative expression of phosphor-NFKB2 as determined in (**A**).

Finally, we examined p100 processing in patient cells. B cells are too few in affected patients to examine for a biochemical defect in response to CD40L. Instead, we

generated dendritic cells in vitro from donor monocytes (DCMC). DCMC were then stimulated with CD40L; this revealed a similar defect in p100 processing as we had observed in transfectants (Figure 4.14).

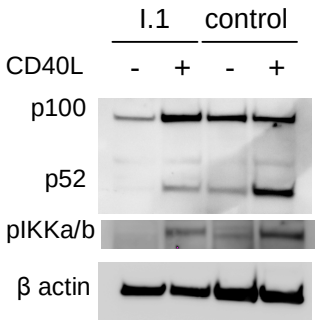

Figure 4.14 p100 processing in response to CD40L in monocyte derived dendritic cells (MDDC) Monocytes from I.1 or a healthy control were incubated with IL-4, GM-CSF and β-mecaptoethanol for 7 days to induce dendritic cells in vitro (MDDC). MDDCs were stimulated with CD40L (1ug/ml) for 3 days and p52 and p100 expression were measured by western blot. pIKKα and β-actin were used for non canonical activation and loading control, respectively

4.1.5 Effect of NFKB2 D865G on canonical NF-kB activity

p100 is thought to exert an IkB-like action on the canonical pathway, which prompted us to investigate whether the accumulation of p100 exerts a dominant negative action that contributes to the severity of the B-cell phenotype in this syndrome.

To directly test the effect of the mutation on both canonical and noncanonical pathways, we compared the actions of CD40L, which is considered a noncanonical stimulus, but also activates the canonical pathway, and anti-Ig (a canonical stimulus) for their abilities to activate rare peripheral B cells from an affected individual (Figure 4.15), according to

expression of surface antigens generally considered to be NF-kB–responsive (CD86, CD69, andCD83). B cells

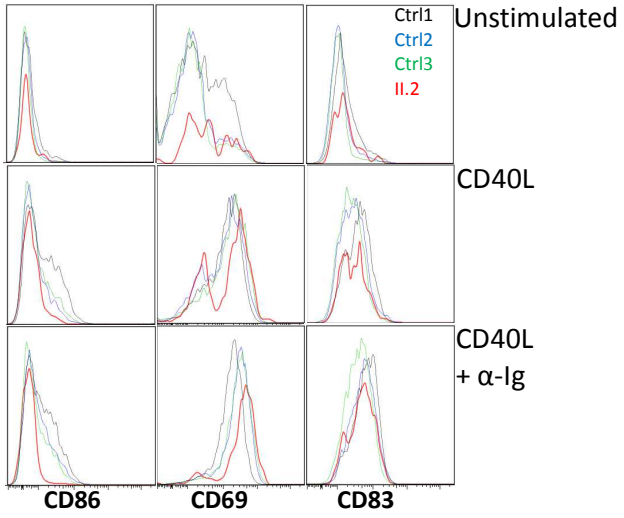

Figure 4.15 B cell activation Analysis of B cells from II.2 relative to controls for expression of CD86, CD69, and CD83 after 24 hours of treatment with indicated stimuli.

from patient II.2 exhibit much less CD86 induction but preserved CD69 expression withCD40L compared with healthy controls; the difference was more pronounced with CD40L and anti-Ig stimulation. These findings are consistent with defects in both canonical and noncanonical pathways. Activation of the canonical pathway results in translocation of p65 to the nucleus, where it regulates gene transcription. To further explore the possible action of p100 on canonical pathway signaling, we examined the location of p65 in cells transfected with NIK plus either wild-type or wild-type and D865G NFKB2. NIK alone results in activation of the noncanonical pathway and processing of p100, which causes abundant nuclear translocation of p65 in response to a

canonical stimulus (TNF). A similar response is observed in the presence of NF-kB2 *with NIK*, whereas D865G NF-kB2 *with NIK* results in cytoplasmic retention of p65.

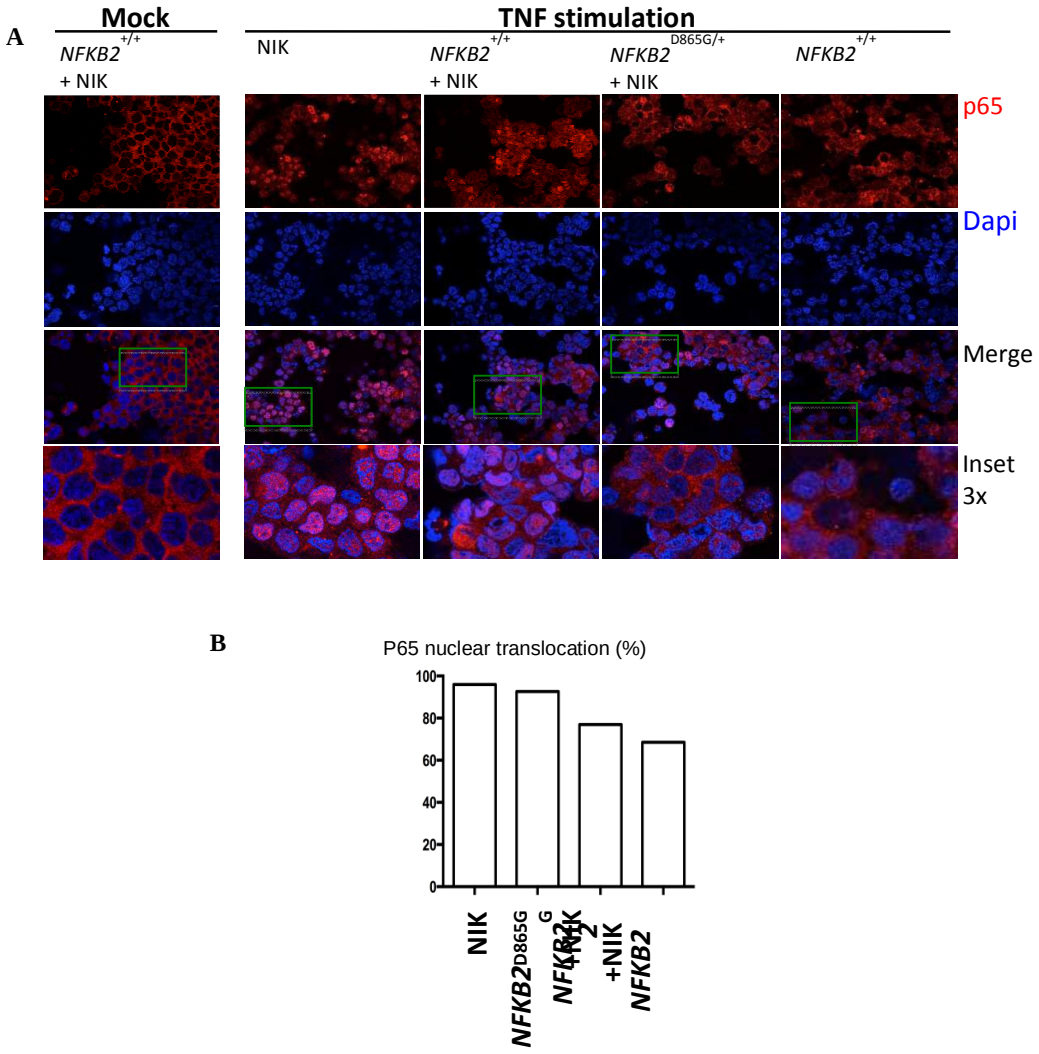

Figure 4.16 Inhibition of canonical NFKB pathway by investigation of p65 translocation Dapi is used for nuclei staining. TNFα (50ng/ml) was used for 1 hour to stimulate canonical NF-kB pathway Nuclear translocation of p65(red) in HEK293 cells transfected with the indicatedconstructs after stimulation with TNF. A 4,6 diamidino-2-phenylindole counterstain identifies cell nuclei. **A**. Image and **B**. Summary of p65 translocation of immunofluorescence confocal.

To determine the effect of our mutation on the canonical pathway, we looked at p65 translocation (Figure 4.16). We transfected HEK293 with vectors expressing either

wildtype or D865G mutant alleles of *NFKB2* with NIK. After 48 hours post transfection cells were stimulated with TNF alpha for 1 hour. p65 and nuclei were stained for translocation. This first column in Figure 4,16 shows that most of the p65 was cytoplasmic after mock stimulation. In cells transfected with NFKB2 and stimulated with TNF alone, p65 was distributed in both the cytoplasm and nuclei, as expected if p100 partially blocks the canonical pathway. In cells transfected with NIK alone, the majority of p65 translocated to the nucleus. In cells transfected with NFKB2 + NIK the majority of p65 was also found in the nucleus, although the effect was less pronounced compared to NIK alone. This is because in the absence of transfected NIK, transfected p100 may not have been completely processed, and may have bound to p65. Since the mutation described in the kindred is heterozygous mutation, we also investigated a possible dominant negative action. We transfected cells with wildtype and mutant *NFKB2* expressing vectors together with NIK. We observed that inhibition of p65 translocation was much more pronounced in heterozygous mutant culture compared to wildtype.

Next, we investigated how these changes in NFKB2 signalling would affect B cell activation. This experiment was made difficult by the severe B cell deficiency exhibited by patients. B cells were stimulated B cells with CD40L or CD40L+anti Ig. We found that II.2 showed much less CD86 induction with CD40L compared with healthy controls, and the effect was pronounced with CD40L and anti Ig stimulation. This result was similar to the p65 translocation in the heterozygous transfectant experiment. By contrast, we found no abnormalities CD83 or CD69 expression. This is consistent with

other evidence that CD86, Cd83 and CD69 responses can be discordant in the presence of defects in the canonical NF-kB pathway (Snow, Xiao et al. 2012).

4.2 Discussion

Our findings reveal the importance of D865 for NF-kB2 (p100) phosphorylation and processing to p52 for maintaining both integrity of noncanonical NF-kB signaling and efficiency of canonical NF-kB signaling for maintaining normal numbers of human B cells. Several previous lines of evidence have identified the importance of the noncanonical NF-kB pathway for human B-cell survival. NF-kB2 is known to be activated by signals from TNFRSF members lymphotoxin-b receptor, BAFFR, RANKL (receptor activator of NF-kB), and CD40 (Claudio, Brown et al. 2002; Coope, Atkinson et al. 2002; Kayagaki, Yan et al. 2002; Derudder, Dejardin et al. 2003; Novack, Yin et al. 2003). Of these, CD40 and BAFFR are thought to provide B-cell survival signals (Locksley, Killeen et al. 2001; Schiemann, Gommerman et al. 2001). Mutations in CD40 and CD40LG both confer a phenotype of hyper-IgM, with absent germinal centers and absence of class switch recombination (DiSanto, Bonnefoy et al. 1993; Conley, Larche et al. 1994; Morrison, Reiley et al. 2005). BAFF acts relatively selectively on the noncanonical NF-kB pathway (Morrison, Reiley et al. 2005). BAFFR deficiency has been reported to cause a primary antibody deficiency syndrome, based on the phenotypes of 2 siblings, both of whom presented relatively late in life (CVID4, OMIM 606269) (Warnatz, Salzer et al. 2009). In one of these individuals, there was an arrest of peripheral B-cell development at the transitional stage of B-cell ontogeny, and a significant deficiency of IgG. In the other sibling, the defect appeared to be milder

with detectable mature B cells. Similarly, antibody-mediated blockade of BAFF in humans is an approved therapy but induces a surprisingly gradual decrease in naive circulating B cells (Wallace, Stohl et al. 2009).

Finally, truncation mutations of NFKB2 have been reported to cause antibody deficiency but normal levels of circulating B cells.20 The phenotype of NFKB2D865G/1 is significantly different from that described for human mutations in CD40, CD40LG, and TNFRSF13C (BAFFR), and indeed for truncation mutations ofNFKB2.20 NFKB2D865G missense mutation results in unprocessable p100 and consistent and severe B-cell deficiency. Chen et al reported small reductions inBcells in 2 of 4 patients with truncation mutations (855X or 853X), but the mean reduction in total B-cell count is 30-fold greater in patients with the missense mutation described here (5.23% vs 0.16% of PBMCs). We demonstrate defects in B-cell activation via the canonical pathway and reduced nuclear translocation of p65 (Figure 4.16); we propose that the profound reduction in B cells conferred by NFKB2D865G mutation could be accounted for by the combined effects of reduced noncanonical signaling plus inhibition of the canonical pathway by unprocessed p100.

p100 exhibits IkB-like activity, which serves to inhibit assembly of the p50/RelA complex of the canonical NF-kB pathway as well as RelB/p52 itself and sequester the complexes in the cytoplasm (Basak, Kim et al. 2007; Tucker, O'Donnell et al. 2007). In other words, unprocessable p100 acts in a dominant negative manner to impair canonical signaling, while simultaneously compromising noncanonical signaling by haploinsufficiency. Consistentwith this possibility, mice deficient for both NFKB1 and

NFKB2 have more severe B-cell deficiency and profound maturation arrest than mice with either single deficiency, (Franzoso, Carlson et al. 1998; Claudio, Saret et al. 2009) although not as severe as the human deficiency observed here. By contrast, Nfkb2$^{-/-}$mice exhibit subtle reductions in B-cell numbers, normal Ig apart from IgA, but abnormal splenic white pulp architecture with failure of germinal center formation (Caamano, Rizzo et al. 1998).

Consistent with the dominant negative action proposed for the human mutation reported here, mice with an Nfkb2 truncating mutation 2 residues distal to D865 exhibit failure of p100 processing but have a relatively mild decrease in mature B cells even in homozygous state, although they have a deficit in lymph node development (Miosge, Blasioli et al. 2002; Tucker, O'Donnell et al. 2007). Defects in B-cell survival and differentiation have been reported in patients with mutations affecting BAFFR, NEMO, CD40, and CD40L as well as truncationmutations ofNFKB2, but none of these cause B-cell deficiency as severe as we report here. (DiSanto, Bonnefoy et al. 1993; Conley, Larche et al. 1994; Caamano, Rizzo et al. 1998; Warnatz, Salzer et al. 2009; Chen, Coonrod et al. 2013). This is likely because NFKB2D865G disrupts noncanonical signaling normally activated by several ligands, and because the mutation results in impaired canonical NF-kB signaling as well.

The noncanonical defect in p52 production is a defect in response to the combined actions of CD40L, CD27, and BAFF—all ligands that normally signal via the noncanonical pathway to maintain B-cell homeostasis. p100 not only functions as a precursor of p52, but also as the fourth IkB protein (along with IkBa, b, and g

[NEMO]), which inhibits nuclear translocation of RelA/p50 by the canonical pathway (Basak, Kim et al. 2007). Thus, noncanonical stimuli result in p100 processing to reduce the restraint on canonical signaling as well. Accumulation ofp100 conferred by NFKB2D865G appears to result in enhanced IkB activity, based on dampened response to canonical stimuli (anti-Ig) and reduced nuclear translocation of p65. As in mice, in which combined Nfkb1 and Nfkb2 defects cause much more severe defects than either defect alone, the combined effects on both canonical and noncanonical pathways are likely to explain the comparative severity of the B-cell phenotype. Two possible explanations emerge to account for differences in B-cell phenotype between truncation and missense mutations.

First, D865G results in more profound inhibition of the noncanonical pathway than the truncation mutant. For example, p100 protein translated from the missense mutation fails to undergo either phosphorylation or processing and might sequester IKKa, thereby reducing phosphorylation and processing of the protein product of the normal allele. Second, the full-length nonprocessable D865G p100 inhibits canonical signaling more effectively than the truncated protein. Our data favor the latter possibility. Co-transfection of normal and mutant alleles into HEK293 cells resulted in approximately 50% reduction in p52, arguing against a dominant negative action on the noncanonical pathway (Figure 4.12). Although the most obvious phenotype of the NFKB2 mutation described here is B-cell deficiency, all 3 affected individuals exhibited alopecia areata, with no other evidence of other autoimmunity. Taken together with findings reported by Chen et al, we confirm the autosomal-dominant syndrome of antibody deficiency and alopecia arising from NFKB2 mutation. We found no evidence for other autoimmunity

(including no ACTH deficiency). This independent confirmation would appear to substantiate an autosomal-dominant syndrome of antibody deficiency and alopecia areata as a consequence of NFKB2 mutation. Further studies will be necessary to delineate the cause for alopecia.Mouse models have established that NF-kB2 is important for central T-cell tolerancemediated by negative selection and Treg induction (Zhu, Chin et al. 2006; Venanzi, Gray et al. 2007; Seach, Ueno et al. 2008).

Noncanonical NF-kB signaling downstream of RANK and LTbR is necessary for normal maturation of the thymic medullary epithelial cells that express AIRE. We observed a significant reduction in natural Tregs. Consistent with this postulate, mutations in AIRE are the most penetrant genetic defects associated with alopecia so far (Wengraf, McDonagh et al. 2008). Either way, abnormalities in the noncanonical signaling provide a new mechanism to account for the curious and well-established coincidence of autoimmunity and primary antibody deficiency, and the occurrence of Treg deficiency in some cases of CVID. NF-kB2 is also important for cell migration by transactivating genes encoding chemokines and their ligands, including CCL19, andCCL21, which are important for thymic retention of T cells. This pathway could account for the increase in recent thymic emigrants in the peripheral blood. We also observed a deficiency of CXCR51 T cells in the periphery. Although the precise ontogeny of this T-cell subset remains uncertain, there is evidence that they have an enhanced capacity to provide help to B cells when compared with CXCR5- memory T-cell counterparts, (Morita, Schmitt et al. 2011) and mouse studies have shown their dependence on Nfkb2. It is also plausible, however, that this Tfh defect reflects the

absence of peripheral blood B cells because B cells are known to provide important trophic signals for this T-cell compartment (Martini, Enright et al. 2011).

Finally, this phenotype of the patients reported here is remarkable for the discordance between B-cell deficiency and antibody deficiency. Other examples of late-onset B-cell deficiency have been described in which the phenotype is more consistent with XLA. In XLA, however, there is usually a good correlation between the B-cell deficiency and the severity of the antibody deficiency. By contrast, the D865G NFKB2 mutation appears to cause profound B-cell deficiency, in which Ig levels including antigen-specific antibodies, remain detectable. The persistence of specific antibody in the absence of B cells raises the possibility that medium to long-livedplasma cells can form independently of NF-kB2. It is also possible that mimicking the effect of this mutation to obtain a partial reduction in NF-kB2 might offer therapeutic approaches for B-cell– and antibody-mediated disease, in which the objective is to eliminate ongoing aberrant immune responses while preserving protective immunity already established.

5 References

Adzhubei, I. A., S. Schmidt, et al. (2010). "A method and server for predicting damaging missense mutations." Nat Methods **7**(4): 248-249.

Alangari, A., A. Alsultan, et al. (2012). "LPS-responsive beige-like anchor (LRBA) gene mutation in a family with inflammatory bowel disease and combined immunodeficiency." The Journal of allergy and clinical immunology **130**(2): 481-488 e482.

Amir, R. E., H. Haecker, et al. (2004). "Mechanism of processing of the NF-kappa B2 p100 precursor: identification of the specific polyubiquitin chain-anchoring lysine residue and analysis of the role of NEDD8-modification on the SCF(beta-TrCP) ubiquitin ligase." Oncogene **23**(14): 2540-2547.

Basak, S., H. Kim, et al. (2007). "A fourth IkappaB protein within the NF-kappaB signaling module." Cell **128**(2): 369-381.

Bateman, E. A., L. Ayers, et al. (2012). "T cell phenotypes in patients with common variable immunodeficiency disorders: associations with clinical phenotypes in comparison with other groups with recurrent infections." Clin Exp Immunol **170**(2): 202-211.

Baumert, E., G. Wolff-Vorbeck, et al. (1992). "Immunophenotypical alterations in a subset of patients with common variable immunodeficiency (CVID)." Clin Exp Immunol **90**(1): 25-30.

Bellail, A. C., J. J. Olson, et al. (2012). "A20 ubiquitin ligase-mediated polyubiquitination of RIP1 inhibits caspase-8 cleavage and TRAIL-induced apoptosis in glioblastoma." Cancer Discov **2**(2): 140-155.

Belot, A., P. R. Kasher, et al. (2013). "Protein kinase cdelta deficiency causes mendelian systemic lupus erythematosus with B cell-defective apoptosis and hyperproliferation." Arthritis Rheum **65**(8): 2161-2171.

Blonska, M., Y. You, et al. (2004). "Restoration of NF-kappaB activation by tumor necrosis factor alpha receptor complex-targeted MEKK3 in receptor-interacting protein-deficient cells." Mol Cell Biol **24**(24): 10757-10765.

Bohgaki, M., T. Tsukiyama, et al. (2008). "Involvement of Ymer in suppression of NF-kappaB activation by regulated interaction with lysine-63-linked polyubiquitin chain." Biochim Biophys Acta **1783**(5): 826-837.

Boisson, B., E. Laplantine, et al. (2015). "Human HOIP and LUBAC deficiency underlies autoinflammation, immunodeficiency, amylopectinosis, and lymphangiectasia." J Exp Med **212**(6): 939-951.

Boisson, B., E. Laplantine, et al. (2012). "Immunodeficiency, autoinflammation and amylopectinosis in humans with inherited HOIL-1 and LUBAC deficiency." Nat Immunol **13**(12): 1178-1186.

Boone, D. L. (2004). "The ubiquitin-modifying enzyme A20 is required for termination of Toll-like receptor responses." Nature Immunol. **5**: 1052-1060.

Bosanac, I., I. E. Wertz, et al. (2010). "Ubiquitin binding to A20 ZnF4 is required for modulation of NF-kappaB signaling." Mol Cell **40**(4): 548-557.

Brohl, A. S., J. R. Stinson, et al. (2015). "Germline CARD11 Mutation in a Patient with Severe Congenital B Cell Lymphocytosis." J Clin Immunol **35**(1): 32-46.

Burns, K., S. Janssens, et al. (2003). "Inhibition of interleukin 1 receptor/Toll-like receptor signaling through the alternatively spliced, short form of MyD88 is due to its failure to recruit IRAK-4." J Exp Med **197**(2): 263-268.

Caamano, J. H., C. A. Rizzo, et al. (1998). "Nuclear factor (NF)-kappa B2 (p100/p52) is required for normal splenic microarchitecture and B cell-mediated immune responses." J Exp Med **187**(2): 185-196.

Castigli, E., S. Wilson, et al. (2007). "Reexamining the role of TACI coding variants in common variable immunodeficiency and selective IgA deficiency." Nat Genet **39**(4): 430-431.

Catrysse, L., L. Vereecke, et al. (2014). "A20 in inflammation and autoimmunity." Trends in immunology **35**(1): 22-31.

Charbonnier, L. M., E. Janssen, et al. (2015). "Regulatory T-cell deficiency and immune dysregulation, polyendocrinopathy, enteropathy, X-linked-like disorder caused by loss-of-function mutations in LRBA." The Journal of allergy and clinical immunology **135**(1): 217-227.

Chen, K., E. M. Coonrod, et al. (2013). "Germline mutations in NFKB2 implicate the noncanonical NF-kappaB pathway in the pathogenesis of common variable immunodeficiency." American journal of human genetics **93**(5): 812-824.

Chen, Z. J. (2005). "Ubiquitin signalling in the NF-kappaB pathway." Nature cell biology **7**(8): 758-765.

Chu, Y., J. C. Vahl, et al. (2011). "B cells lacking the tumor suppressor TNFAIP3/A20 display impaired differentiation and hyperactivation and cause inflammation and autoimmunity in aged mice." Blood **117**(7): 2227-2236.

Chun, A. C., Y. Zhou, et al. (2000). "Coiled-coil motif as a structural basis for the interaction of HTLV type 1 Tax with cellular cofactors." AIDS Res Hum Retroviruses **16**(16): 1689-1694.

Claudio, E., K. Brown, et al. (2002). "BAFF-induced NEMO-independent processing of NF-kappa B2 in maturing B cells." Nature immunology **3**(10): 958-965.

Claudio, E., S. Saret, et al. (2009). "Cell-autonomous role for NF-kappa B in immature bone marrow B cells." J Immunol **182**(6): 3406-3413.

Compagno, M. (2009). "Mutations of multiple genes cause deregulation of NF-[kappa]B in diffuse large B-cell lymphoma." Nature **459**: 717-721.

Conley, M. E., M. Larche, et al. (1994). "Hyper IgM syndrome associated with defective CD40-mediated B cell activation." J Clin Invest **94**(4): 1404-1409.

Coope, H. J., P. G. Atkinson, et al. (2002). "CD40 regulates the processing of NF-kappaB2 p100 to p52." The EMBO journal **21**(20): 5375-5385.

Coornaert, B., M. Baens, et al. (2008). "T cell antigen receptor stimulation induces MALT1 paracaspase-mediated cleavage of the NF-kappaB inhibitor A20." Nat Immunol **9**(3): 263-271.

Corn, R. A., C. Hunter, et al. (2005). "Opposing roles for RelB and Bcl-3 in regulation of T-box expressed in T cells, GATA-3, and Th effector differentiation." J Immunol **175**(4): 2102-2110.

Cullen, S. P., C. M. Henry, et al. (2013). "Fas/CD95-induced chemokines can serve as "find-me" signals for apoptotic cells." Molecular cell **49**(6): 1034-1048.

Cunningham-Rundles, C. (1989). "Clinical and immunologic analyses of 103 patients with common variable immunodeficiency." J Clin Immunol **9**(1): 22-33.

Cunningham-Rundles, C. (2002). "Hematologic complications of primary immune deficiencies." Blood Rev **16**(1): 61-64.

Cunningham-Rundles, C. and C. Bodian (1999). "Common variable immunodeficiency: clinical and immunological features of 248 patients." Clinical immunology **92**(1): 34-48.

Cunningham-Rundles, C., F. P. Siegal, et al. (1987). "Incidence of cancer in 98 patients with common varied immunodeficiency." J Clin Immunol **7**(4): 294-299.

Daniel, S., M. B. Arvelo, et al. (2004). "A20 protects endothelial cells from TNF-, Fas-, and NK-mediated cell death by inhibiting caspase 8 activation." Blood **104**(8): 2376-2384.

De Valck, D., D. Y. Jin, et al. (1999). "The zinc finger protein A20 interacts with a novel anti-apoptotic protein which is cleaved by specific caspases." Oncogene **18**(29): 4182-4190.

Dejardin, E. (2006). "The alternative NF-kappaB pathway from biochemistry to biology: pitfalls and promises for future drug development." Biochemical pharmacology **72**(9): 1161-1179.

Demchenko, Y. N., O. K. Glebov, et al. (2010). "Classical and/or alternative NF-kappaB pathway activation in multiple myeloma." Blood **115**(17): 3541-3552.

Derudder, E., E. Dejardin, et al. (2003). "RelB/p50 dimers are differentially regulated by tumor necrosis factor-alpha and lymphotoxin-beta receptor activation: critical roles for p100." The Journal of biological chemistry **278**(26): 23278-23284.

DiSanto, J. P., J. Y. Bonnefoy, et al. (1993). "CD40 ligand mutations in x-linked immunodeficiency with hyper-IgM." Nature **361**(6412): 541-543.

Dong, H., S. E. Strome, et al. (2002). "Tumor-associated B7-H1 promotes T-cell apoptosis: a potential mechanism of immune evasion." Nature medicine **8**(8): 793-800.

Duwel, M., V. Welteke, et al. (2009). "A20 negatively regulates T cell receptor signaling to NF-kappaB by cleaving Malt1 ubiquitin chains." J Immunol **182**(12): 7718-7728.

Ea, C. K., L. Deng, et al. (2006). "Activation of IKK by TNF[alpha] requires site-specific ubiquitination of RIP1 and polyubiquitin binding by NEMO." Mol. Cell **22**: 245-257.

Fang, D., C. Elly, et al. (2002). "Dysregulation of T lymphocyte function in itchy mice: a role for Itch in TH2 differentiation." Nat Immunol **3**(3): 281-287.

Fazilleau, N., L. Mark, et al. (2009). "Follicular helper T cells: lineage and location." Immunity **30**(3): 324-335.

Feng, B., S. Cheng, et al. (2004). "NF-kappaB inducible genes BCL-X and cyclin E promote immature B-cell proliferation and survival." Cellular immunology **232**(1-2): 9-20.

Fong, A. and S. C. Sun (2002). "Genetic evidence for the essential role of beta-transducin repeat-containing protein in the inducible processing of NF-kappa B2/p100." The Journal of biological chemistry **277**(25): 22111-22114.

Fong, A., M. Zhang, et al. (2002). "S9, a 19 S proteasome subunit interacting with ubiquitinated NF-kappaB2/p100." The Journal of biological chemistry **277**(43): 40697-40702.

Franzoso, G., L. Carlson, et al. (1998). "Mice deficient in nuclear factor (NF)-kappa B/p52 present with defects in humoral responses, germinal center reactions, and splenic microarchitecture." J Exp Med **187**(2): 147-159.

Gardam, S., V. M. Turner, et al. (2011). "Deletion of cIAP1 and cIAP2 in murine B lymphocytes constitutively activates cell survival pathways and inactivates the germinal center response." Blood **117**(15): 4041-4051.

Garibyan, L., A. A. Lobito, et al. (2007). "Dominant-negative effect of the heterozygous C104R TACI mutation in common variable immunodeficiency (CVID)." J Clin Invest **117**(6): 1550-1557.

Geha, R. S., L. D. Notarangelo, et al. (2007). "Primary immunodeficiency diseases: an update from the International Union of Immunological Societies Primary Immunodeficiency Diseases Classification Committee." The Journal of allergy and clinical immunology **120**(4): 776-794.

Gentle, I. E., W. W. Wong, et al. (2011). "In TNF-stimulated cells, RIPK1 promotes cell survival by stabilizing TRAF2 and cIAP1, which limits induction of non-canonical NF-kappaB and activation of caspase-8." J Biol Chem **286**(15): 13282-13291.

Gerlach, B., S. M. Cordier, et al. (2011). "Linear ubiquitination prevents inflammation and regulates immune signalling." Nature **471**(7340): 591-596.

Gerondakis, S., R. Grumont, et al. (2006). "Unravelling the complexities of the NF-kappaB signalling pathway using mouse knockout and transgenic models." Oncogene **25**(51): 6781-6799.

Gerondakis, S. and U. Siebenlist (2010). "Roles of the NF-kappaB pathway in lymphocyte development and function." Cold Spring Harb Perspect Biol **2**(5): a000182.

Ghosh, S. and M. Karin (2002). "Missing pieces in the NF-kappaB puzzle." Cell **109 Suppl**: S81-96.

Graham, R. R., C. Cotsapas, et al. (2008). "Genetic variants near TNFAIP3 on 6q23 are associated with systemic lupus erythematosus." Nat Genet **40**(9): 1059-1061.

Grech, A. P., M. Amesbury, et al. (2004). "TRAF2 differentially regulates the canonical and noncanonical pathways of NF-kappaB activation in mature B cells." Immunity **21**(5): 629-642.

Greil, J., T. Rausch, et al. (2013). "Whole-exome sequencing links caspase recruitment domain 11 (CARD11) inactivation to severe combined immunodeficiency." The Journal of allergy and clinical immunology **131**(5): 1376-1383 e1373.

Greten, F. R., M. C. Arkan, et al. (2007). "NF-kappaB is a negative regulator of IL-1beta secretion as revealed by genetic and pharmacological inhibition of IKKbeta." Cell **130**(5): 918-931.

Grey, S. T., M. B. Arvelo, et al. (1999). "A20 inhibits cytokine-induced apoptosis and nuclear factor kappaB-dependent gene activation in islets." J Exp Med **190**(8): 1135-1146.

Grimbacher, B., A. Hutloff, et al. (2003). "Homozygous loss of ICOS is associated with adult-onset common variable immunodeficiency." Nat Immunol **4**(3): 261-268.

Grossmann, M., D. Metcalf, et al. (1999). "The combined absence of the transcription factors Rel and RelA leads to multiple hemopoietic cell defects." Proc Natl Acad Sci U S A **96**(21): 11848-11853.

Gupta, K., D. Ott, et al. (2000). "A human nuclear shuttling protein that interacts with human immunodeficiency virus type 1 matrix is packaged into virions." J Virol **74**(24): 11811-11824.

Gurung, R., A. Tan, et al. (2003). "Identification of a novel domain in two mammalian inositol-polyphosphate 5-phosphatases that mediates membrane ruffle

localization. The inositol 5-phosphatase skip localizes to the endoplasmic reticulum and translocates to membrane ruffles following epidermal growth factor stimulation." J Biol Chem **278**(13): 11376-11385.

Hammer, G. E., E. E. Turer, et al. (2011). "Expression of A20 by dendritic cells preserves immune homeostasis and prevents colitis and spondyloarthritis." Nat Immunol **12**(12): 1184-1193.

Han, J. W., H. F. Zheng, et al. (2009). "Genome-wide association study in a Chinese Han population identifies nine new susceptibility loci for systemic lupus erythematosus." Nat Genet **41**(11): 1234-1237.

Hayden, M. S. and S. Ghosh (2008). "Shared principles in NF-kappaB signaling." Cell **132**(3): 344-362.

Hayden, M. S. and S. Ghosh (2011). "NF-kappaB in immunobiology." Cell research **21**(2): 223-244.

He, J. Q., B. Zarnegar, et al. (2006). "Rescue of TRAF3-null mice by p100 NF-kappa B deficiency." J Exp Med **203**(11): 2413-2418.

Hermaszewski, R. A. and A. D. Webster (1993). "Primary hypogammaglobulinaemia: a survey of clinical manifestations and complications." Q J Med **86**(1): 31-42.

Hettmann, T., J. DiDonato, et al. (1999). "An essential role for nuclear factor kappaB in promoting double positive thymocyte apoptosis." J Exp Med **189**(1): 145-158.

Heyninck, K., D. De Valck, et al. (1999). "The zinc finger protein A20 inhibits TNF-induced NF-kappaB-dependent gene expression by interfering with an RIP- or TRAF2-mediated transactivation signal and directly binds to a novel NF-kappaB-inhibiting protein ABIN." The Journal of cell biology **145**(7): 1471-1482.

Hjelmeland, A. B., Q. Wu, et al. (2010). "Targeting A20 decreases glioma stem cell survival and tumor growth." PLoS Biol **8**(2): e1000319.

Holm, A. M., E. A. Sivertsen, et al. (2004). "Gene expression analysis of peripheral T cells in a subgroup of common variable immunodeficiency shows predominance of CCR7(-) effector-memory T cells." Clin Exp Immunol **138**(2): 278-289.

Hu, Y., V. Baud, et al. (1999). "Abnormal morphogenesis but intact IKK activation in mice lacking the IKKalpha subunit of IkappaB kinase." Science **284**(5412): 316-320.

Hymowitz, S. G. and I. E. Wertz (2010). "A20: from ubiquitin editing to tumour suppression." Nat Rev Cancer **10**(5): 332-341.

Iha, H., J. M. Peloponese, et al. (2008). "Inflammatory cardiac valvulitis in TAX1BP1-deficient mice through selective NF-kappaB activation." EMBO J **27**(4): 629-641.

Ikeda, F., Y. L. Deribe, et al. (2011). "SHARPIN forms a linear ubiquitin ligase complex regulating NF-kappaB activity and apoptosis." Nature **471**(7340): 637-641.

Jabara, H. H., T. Ohsumi, et al. (2013). "A homozygous mucosa-associated lymphoid tissue 1 (MALT1) mutation in a family with combined immunodeficiency." The Journal of allergy and clinical immunology **132**(1): 151-158.

Jain, A., C. A. Ma, et al. (2004). "Specific NEMO mutations impair CD40-mediated c-Rel activation and B cell terminal differentiation." J Clin Invest **114**(11): 1593-1602.

Janssens, S., K. Burns, et al. (2003). "MyD88S, a splice variant of MyD88, differentially modulates NF-kappaB- and AP-1-dependent gene expression." FEBS letters **548**(1-3): 103-107.

Jimi, E., R. J. Phillips, et al. (2005). "Activation of NF-kappaB promotes the transition of large, CD43+ pre-B cells to small, CD43- pre-B cells." Int Immunol **17**(6): 815-825.

Jin, Z. (2009). "Cullin3-based polyubiquitination and p62-dependent aggregation of caspase-8 mediate extrinsic apoptosis signaling." Cell **137**: 721-735.

Kanayama, A., R. B. Seth, et al. (2004). "TAB2 and TAB3 activate the NF-kappaB pathway through binding to polyubiquitin chains." Mol Cell **15**(4): 535-548.

Karin, M. and F. R. Greten (2005). "NF-kappaB: linking inflammation and immunity to cancer development and progression." Nat Rev Immunol **5**(10): 749-759.

Kato, H., T. Ishii, et al. (2009). "Prevalence of linked angina and gastroesophageal reflux disease in general practice." World J Gastroenterol **15**(14): 1764-1768.

Kawai, T. and S. Akira (2007). "Signaling to NF-kappaB by Toll-like receptors." Trends Mol Med **13**(11): 460-469.

Kayagaki, N., M. Yan, et al. (2002). "BAFF/BLyS receptor 3 binds the B cell survival factor BAFF ligand through a discrete surface loop and promotes processing of NF-kappaB2." Immunity **17**(4): 515-524.

Kim, J. Y., M. Morgan, et al. (2011). "TNFalpha induced noncanonical NF-kappaB activation is attenuated by RIP1 through stabilization of TRAF2." J Cell Sci **124**(Pt 4): 647-656.

Kishimoto, H., C. D. Surh, et al. (1998). "A role for Fas in negative selection of thymocytes in vivo." J Exp Med **187**(9): 1427-1438.

Klionsky, D. J., F. C. Abdalla, et al. (2012). "Guidelines for the use and interpretation of assays for monitoring autophagy." Autophagy **8**(4): 445-544.

Kobayashi, K., L. D. Hernandez, et al. (2002). "IRAK-M is a negative regulator of Toll-like receptor signaling." Cell **110**(2): 191-202.

Komander, D. and D. Barford (2008). "Structure of the A20 OTU domain and mechanistic insights into deubiquitination." Biochem J **409**(1): 77-85.

Kool, M., G. van Loo, et al. (2011). "The ubiquitin-editing protein A20 prevents dendritic cell activation, recognition of apoptotic cells, and systemic autoimmunity." Immunity **35**(1): 82-96.

Krishna, S., D. Xie, et al. (2012). "Chronic activation of the kinase IKKbeta impairs T cell function and survival." J Immunol **189**(3): 1209-1219.

Kuehn, H. S., J. E. Niemela, et al. (2013). "Loss-of-function of the protein kinase C delta (PKCdelta) causes a B-cell lymphoproliferative syndrome in humans." Blood **121**(16): 3117-3125.

Kuijpers, T. W., R. J. Bende, et al. (2010). "CD20 deficiency in humans results in impaired T cell-independent antibody responses." J Clin Invest **120**(1): 214-222.

Lahtela, J., H. O. Nousiainen, et al. (2010). "Mutant CHUK and severe fetal encasement malformation." The New England journal of medicine **363**(17): 1631-1637.

Lamkanfi, M., N. Festjens, et al. (2007). "Caspases in cell survival, proliferation and differentiation." Cell Death Differ **14**(1): 44-55.

Lee, E. G., D. L. Boone, et al. (2000). "Failure to regulate TNF-induced NF-kappaB and cell death responses in A20-deficient mice." Science **289**(5488): 2350-2354.

Lee, J. J., I. Rauter, et al. (2009). "The murine equivalent of the A181E TACI mutation associated with common variable immunodeficiency severely impairs B-cell function." Blood **114**(11): 2254-2262.
Lee, S. H. and M. Hannink (2002). "Characterization of the nuclear import and export functions of Ikappa B(epsilon)." J Biol Chem **277**(26): 23358-23366.
Lee, S. H., M. S. Shin, et al. (1999). "Point mutations and deletions of the Bcl10 gene in solid tumors and malignant lymphomas." Cancer Res **59**(22): 5674-5677.
Li, H. and R. Durbin (2010). "Fast and accurate long-read alignment with Burrows-Wheeler transform." Bioinformatics **26**(5): 589-595.
Li, H. and A. Seth (2004). "An RNF11: Smurf2 complex mediates ubiquitination of the AMSH protein." Oncogene **23**(10): 1801-1808.
Li, L., D. W. Hailey, et al. (2008). "Localization of A20 to a lysosome-associated compartment and its role in NFkappaB signaling." Biochimica et biophysica acta **1783**(6): 1140-1149.
Li, Q. and I. M. Verma (2002). "NF-kappaB regulation in the immune system." Nat Rev Immunol **2**(10): 725-734.
Li, Q. and I. M. Verma (2002). "NF-kappaB regulation in the immune system." Nature reviews. Immunology **2**(10): 725-734.
Li, Z. W., W. Chu, et al. (1999). "The IKKbeta subunit of IkappaB kinase (IKK) is essential for nuclear factor kappaB activation and prevention of apoptosis." J Exp Med **189**(11): 1839-1845.
Liang, C., M. Zhang, et al. (2006). "beta-TrCP binding and processing of NF-kappaB2/p100 involve its phosphorylation at serines 866 and 870." Cell Signal **18**(8): 1309-1317.
Liao, G. and S. C. Sun (2003). "Regulation of NF-kappaB2/p100 processing by its nuclear shuttling." Oncogene **22**(31): 4868-4874.
Liao, G., M. Zhang, et al. (2004). "Regulation of the NF-kappaB-inducing kinase by tumor necrosis factor receptor-associated factor 3-induced degradation." J Biol Chem **279**(25): 26243-26250.
Ling, L. and D. V. Goeddel (2000). "T6BP, a TRAF6-interacting protein involved in IL-1 signaling." Proc Natl Acad Sci U S A **97**(17): 9567-9572.
Liston, P., W. G. Fong, et al. (2003). "The inhibitors of apoptosis: there is more to life than Bcl2." Oncogene **22**(53): 8568-8580.
Liuwantara, D., M. Elliot, et al. (2006). "Nuclear factor-kappaB regulates beta-cell death: a critical role for A20 in beta-cell protection." Diabetes **55**(9): 2491-2501.
Locksley, R. M., N. Killeen, et al. (2001). "The TNF and TNF receptor superfamilies: integrating mammalian biology." Cell **104**(4): 487-501.
Lohr, N. J., J. P. Molleston, et al. (2010). "Human ITCH E3 ubiquitin ligase deficiency causes syndromic multisystem autoimmune disease." American journal of human genetics **86**(3): 447-453.
Lopez-Herrera, G., G. Tampella, et al. (2012). "Deleterious mutations in LRBA are associated with a syndrome of immune deficiency and autoimmunity." American journal of human genetics **90**(6): 986-1001.
Lu, T. T., M. Onizawa, et al. (2013). "Dimerization and ubiquitin mediated recruitment of A20, a complex deubiquitinating enzyme." Immunity **38**(5): 896-905.
Ma, A. and B. A. Malynn (2012). "A20: linking a complex regulator of ubiquitylation to immunity and human disease." Nature reviews. Immunology **12**(11): 774-785.

Makris, C., V. L. Godfrey, et al. (2000). "Female mice heterozygous for IKK gamma/NEMO deficiencies develop a dermatopathy similar to the human X-linked disorder incontinentia pigmenti." Mol Cell **5**(6): 969-979.

Martin, M. U. and H. Wesche (2002). "Summary and comparison of the signaling mechanisms of the Toll/interleukin-1 receptor family." Biochim Biophys Acta **1592**(3): 265-280.

Martini, H., V. Enright, et al. (2011). "Importance of B cell co-stimulation in CD4(+) T cell differentiation: X-linked agammaglobulinaemia, a human model." Clin Exp Immunol **164**(3): 381-387.

Matmati, M., P. Jacques, et al. (2011). "A20 (TNFAIP3) deficiency in myeloid cells triggers erosive polyarthritis resembling rheumatoid arthritis." Nat Genet **43**(9): 908-912.

Matsushima, A., T. Kaisho, et al. (2001). "Essential role of nuclear factor (NF)-kappaB-inducing kinase and inhibitor of kappaB (IkappaB) kinase alpha in NF-kappaB activation through lymphotoxin beta receptor, but not through tumor necrosis factor receptor I." J Exp Med **193**(5): 631-636.

McKinnon, M. L., J. Rozmus, et al. (2014). "Combined immunodeficiency associated with homozygous MALT1 mutations." The Journal of allergy and clinical immunology **133**(5): 1458-1462, 1462 e1451-1457.

Mebius, R. E. and G. Kraal (2005). "Structure and function of the spleen." Nature reviews. Immunology **5**(8): 606-616.

Miosge, L. A., J. Blasioli, et al. (2002). "Analysis of an ethylnitrosourea-generated mouse mutation defines a cell intrinsic role of nuclear factor kappaB2 in regulating circulating B cell numbers." J Exp Med **196**(8): 1113-1119.

Morita, R., N. Schmitt, et al. (2011). "Human blood CXCR5(+)CD4(+) T cells are counterparts of T follicular cells and contain specific subsets that differentially support antibody secretion." Immunity **34**(1): 108-121.

Morrison, M. D., W. Reiley, et al. (2005). "An atypical tumor necrosis factor (TNF) receptor-associated factor-binding motif of B cell-activating factor belonging to the TNF family (BAFF) receptor mediates induction of the noncanonical NF-kappaB signaling pathway." The Journal of biological chemistry **280**(11): 10018-10024.

Nielsen, C., M. A. Jakobsen, et al. (2014). "Immunodeficiency associated with a nonsense mutation of IKBKB." J Clin Immunol **34**(8): 916-921.

Nilsson, J., B. Schoser, et al. (2013). "Polyglucosan body myopathy caused by defective ubiquitin ligase RBCK1." Ann Neurol **74**(6): 914-919.

Novack, D. V. (2011). "Role of NF-kappaB in the skeleton." Cell Res **21**(1): 169-182.

Novack, D. V., L. Yin, et al. (2003). "The IkappaB function of NF-kappaB2 p100 controls stimulated osteoclastogenesis." J Exp Med **198**(5): 771-781.

Opipari, A. W., Jr., M. S. Boguski, et al. (1990). "The A20 cDNA induced by tumor necrosis factor alpha encodes a novel type of zinc finger protein." The Journal of biological chemistry **265**(25): 14705-14708.

Opipari, A. W., Jr., H. M. Hu, et al. (1992). "The A20 zinc finger protein protects cells from tumor necrosis factor cytotoxicity." J Biol Chem **267**(18): 12424-12427.

Pannicke, U., B. Baumann, et al. (2013). "Deficiency of innate and acquired immunity caused by an IKBKB mutation." The New England journal of medicine **369**(26): 2504-2514.

Park, I. H., P. H. Lerou, et al. (2008). "Generation of human-induced pluripotent stem cells." Nat Protoc **3**(7): 1180-1186.

Paxian, S., H. Merkle, et al. (2002). "Abnormal organogenesis of Peyer's patches in mice deficient for NF-kappaB1, NF-kappaB2, and Bcl-3." Gastroenterology **122**(7): 1853-1868.

Perry, W. L., C. M. Hustad, et al. (1998). "The itchy locus encodes a novel ubiquitin protein ligase that is disrupted in a18H mice." Nature genetics **18**(2): 143-146.

Pham, L. V., L. Fu, et al. (2011). "Constitutive BR3 receptor signaling in diffuse, large B-cell lymphomas stabilizes nuclear factor-kappaB-inducing kinase while activating both canonical and alternative nuclear factor-kappaB pathways." Blood **117**(1): 200-210.

Pickart, C. M. (2001). "Mechanisms underlying ubiquitination." Annu. Rev. Biochem. **70**: 503-533.

Plenge, R. M., C. Cotsapas, et al. (2007). "Two independent alleles at 6q23 associated with risk of rheumatoid arthritis." Nat Genet **39**(12): 1477-1482.

Qing, G., Z. Qu, et al. (2007). "Endoproteolytic processing of C-terminally truncated NF-kappaB2 precursors at kappaB-containing promoters." Proceedings of the National Academy of Sciences of the United States of America **104**(13): 5324-5329.

Rebeaud, F., S. Hailfinger, et al. (2008). "The proteolytic activity of the paracaspase MALT1 is key in T cell activation." Nat Immunol **9**(3): 272-281.

Romberg, N., N. Chamberlain, et al. (2013). "CVID-associated TACI mutations affect autoreactive B cell selection and activation." J Clin Invest **123**(10): 4283-4293.

Rothe, M., M. G. Pan, et al. (1995). "The TNFR2-TRAF signaling complex contains two novel proteins related to baculoviral inhibitor of apoptosis proteins." Cell **83**(7): 1243-1252.

Ruddle, N. H. and E. M. Akirav (2009). "Secondary lymphoid organs: responding to genetic and environmental cues in ontogeny and the immune response." J Immunol **183**(4): 2205-2212.

Rudolph, D., W. C. Yeh, et al. (2000). "Severe liver degeneration and lack of NF-kappaB activation in NEMO/IKKgamma-deficient mice." Genes & development **14**(7): 854-862.

Ruland, J. (2011). "Return to homeostasis: downregulation of NF-kappaB responses." Nat Immunol **12**(8): 709-714.

Salvesen, G. S. and C. S. Duckett (2002). "IAP proteins: blocking the road to death's door." Nat Rev Mol Cell Biol **3**(6): 401-410.

Salzer, E., E. Santos-Valente, et al. (2013). "B-cell deficiency and severe autoimmunity caused by deficiency of protein kinase C delta." Blood **121**(16): 3112-3116.

Salzer, U., H. M. Chapel, et al. (2005). "Mutations in TNFRSF13B encoding TACI are associated with common variable immunodeficiency in humans." Nat Genet **37**(8): 820-828.

Salzer, U., A. Maul-Pavicic, et al. (2004). "ICOS deficiency in patients with common variable immunodeficiency." Clinical immunology **113**(3): 234-240.

Salzer, U., K. Warnatz, et al. (2012). "Common variable immunodeficiency: an update." Arthritis Res Ther **14**(5): 223.

Samuel, T., K. Welsh, et al. (2006). "Distinct BIR domains of cIAP1 mediate binding to and ubiquitination of tumor necrosis factor receptor-associated factor 2 and second mitochondrial activator of caspases." J Biol Chem **281**(2): 1080-1090.

Schaffer, A. A., U. Salzer, et al. (2007). "Deconstructing common variable immunodeficiency by genetic analysis." Curr Opin Genet Dev **17**(3): 201-212.

Schiemann, B., J. L. Gommerman, et al. (2001). "An essential role for BAFF in the normal development of B cells through a BCMA-independent pathway." Science **293**(5537): 2111-2114.

Schulze-Luehrmann, J. and S. Ghosh (2006). "Antigen-receptor signaling to nuclear factor kappa B." Immunity **25**(5): 701-715.

Seach, N., T. Ueno, et al. (2008). "The lymphotoxin pathway regulates Aire-independent expression of ectopic genes and chemokines in thymic stromal cells." J Immunol **180**(8): 5384-5392.

Sen, R. and D. Baltimore (1986). "Multiple nuclear factors interact with the immunoglobulin enhancer sequences." Cell **46**(5): 705-716.

Senftleben, U., Y. Cao, et al. (2001). "Activation by IKKalpha of a second, evolutionary conserved, NF-kappa B signaling pathway." Science **293**(5534): 1495-1499.

Shembade, N., N. S. Harhaj, et al. (2007). "Essential role for TAX1BP1 in the termination of TNF-alpha-, IL-1- and LPS-mediated NF-kappaB and JNK signaling." EMBO J **26**(17): 3910-3922.

Shembade, N., N. S. Harhaj, et al. (2008). "The E3 ligase Itch negatively regulates inflammatory signaling pathways by controlling the function of the ubiquitin-editing enzyme A20." Nature immunology **9**(3): 254-262.

Shembade, N., N. S. Harhaj, et al. (2007). "The human T-cell leukemia virus type 1 Tax oncoprotein requires the ubiquitin-conjugating enzyme Ubc13 for NF-kappaB activation." J Virol **81**(24): 13735-13742.

Shembade, N., A. Ma, et al. (2010). "Inhibition of NF-[kappa]B signaling by A20 through disruption of ubiquitin enzyme complexes." Science **327**: 1135-1139.

Shembade, N., K. Parvatiyar, et al. (2009). "The ubiquitin-editing enzyme A20 requires RNF11 to downregulate NF-[kappa]B signalling." EMBO J. **28**: 513-522.

Shembade, N., R. Pujari, et al. (2011). "The kinase IKKalpha inhibits activation of the transcription factor NF-kappaB by phosphorylating the regulatory molecule TAX1BP1." Nat Immunol **12**(9): 834-843.

Shinkura, R., K. Kitada, et al. (1999). "Alymphoplasia is caused by a point mutation in the mouse gene encoding Nf-kappa b-inducing kinase." Nat Genet **22**(1): 74-77.

Skaug, B., J. Chen, et al. (2011). "Direct, noncatalytic mechanism of IKK inhibition by A20." Mol Cell **44**(4): 559-571.

Snow, A. L., W. Xiao, et al. (2012). "Congenital B cell lymphocytosis explained by novel germline CARD11 mutations." J Exp Med.

Speliotes, E. K., C. J. Willer, et al. (2010). "Association analyses of 249,796 individuals reveal 18 new loci associated with body mass index." Nat Genet **42**(11): 937-948.

Stepensky, P., B. Keller, et al. (2013). "Deficiency of caspase recruitment domain family, member 11 (CARD11), causes profound combined immunodeficiency in human subjects." The Journal of allergy and clinical immunology **131**(2): 477-485 e471.

Sudol, M., H. I. Chen, et al. (1995). "Characterization of a novel protein-binding module--the WW domain." FEBS letters **369**(1): 67-71.

Sun, L., L. Deng, et al. (2004). "The TRAF6 ubiquitin ligase and TAK1 kinase mediate IKK activation by BCL10 and MALT1 in T lymphocytes." Mol Cell **14**(3): 289-301.

Sun, S. C. (2011). "Non-canonical NF-kappaB signaling pathway." Cell research **21**(1): 71-85.

Sun, S. C., P. A. Ganchi, et al. (1993). "NF-kappa B controls expression of inhibitor I kappa B alpha: evidence for an inducible autoregulatory pathway." Science **259**(5103): 1912-1915.

Sun, S. C., P. A. Ganchi, et al. (1994). "Autoregulation of the NF-kappa B transactivator RelA (p65) by multiple cytoplasmic inhibitors containing ankyrin motifs." Proc Natl Acad Sci U S A **91**(4): 1346-1350.

Tavares, R. M., E. E. Turer, et al. (2010). "The ubiquitin modifying enzyme A20 restricts B cell survival and prevents autoimmunity." Immunity **33**(2): 181-191.

Thiel, J., L. Kimmig, et al. (2012). "Genetic CD21 deficiency is associated with hypogammaglobulinemia." The Journal of allergy and clinical immunology **129**(3): 801-810 e806.

Tokunaga, F., H. Nishimasu, et al. (2012). "Specific recognition of linear polyubiquitin by A20 zinc finger 7 is involved in NF-kappaB regulation." EMBO J **31**(19): 3856-3870.

Torres, J. M., R. Martinez-Barricarte, et al. (2014). "Inherited BCL10 deficiency impairs hematopoietic and nonhematopoietic immunity." J Clin Invest **124**(12): 5239-5248.

Tsukiyama, T., M. Matsuda-Tsukiyama, et al. (2012). "Ymer acts as a multifunctional regulator in nuclear factor-kappaB and Fas signaling pathways." Mol Med **18**: 587-597.

Tucker, E., K. O'Donnell, et al. (2007). "A novel mutation in the Nfkb2 gene generates an NF-kappa B2 "super repressor"." Journal of immunology **179**(11): 7514-7522.

Turvey, S. E., A. Durandy, et al. (2014). "The CARD11-BCL10-MALT1 (CBM) signalosome complex: Stepping into the limelight of human primary immunodeficiency." The Journal of allergy and clinical immunology **134**(2): 276-284.

Ulrich, M., S. Seeber, et al. (2007). "Tax1-binding protein 1 is expressed in the retina and interacts with the GABA(C) receptor rho1 subunit." Biochem J **401**(2): 429-436.

Vallabhapurapu, S. and M. Karin (2009). "Regulation and function of NF-kappaB transcription factors in the immune system." Annual review of immunology **27**: 693-733.

Vallabhapurapu, S., A. Matsuzawa, et al. (2008). "Nonredundant and complementary functions of TRAF2 and TRAF3 in a ubiquitination cascade that activates NIK-dependent alternative NF-kappaB signaling." Nat Immunol **9**(12): 1364-1370.

van de Pavert, S. A. and R. E. Mebius (2010). "New insights into the development of lymphoid tissues." Nature reviews. Immunology **10**(9): 664-674.

van Zelm, M. C., I. Reisli, et al. (2006). "An antibody-deficiency syndrome due to mutations in the CD19 gene." The New England journal of medicine **354**(18): 1901-1912.

van Zelm, M. C., J. Smet, et al. (2010). "CD81 gene defect in humans disrupts CD19 complex formation and leads to antibody deficiency." J Clin Invest **120**(4): 1265-1274.

Varfolomeev, E., J. W. Blankenship, et al. (2007). "IAP antagonists induce autoubiquitination of c-IAPs, NF-kappaB activation, and TNFalpha-dependent apoptosis." Cell **131**(4): 669-681.

Varfolomeev, E., S. M. Wayson, et al. (2006). "The inhibitor of apoptosis protein fusion c-IAP2.MALT1 stimulates NF-kappaB activation independently of TRAF1 AND TRAF2." J Biol Chem **281**(39): 29022-29029.

Vaux, D. L. and J. Silke (2005). "IAPs, RINGs and ubiquitylation." Nat Rev Mol Cell Biol **6**(4): 287-297.

Venanzi, E. S., D. H. Gray, et al. (2007). "Lymphotoxin pathway and Aire influences on thymic medullary epithelial cells are unconnected." J Immunol **179**(9): 5693-5700.

Vendrell, J. A., S. Ghayad, et al. (2007). "A20/TNFAIP3, a new estrogen-regulated gene that confers tamoxifen resistance in breast cancer cells." Oncogene **26**(32): 4656-4667.

Venuprasad, K., M. Zeng, et al. (2015). "Multifaceted role of the ubiquitin ligase Itch in immune regulation." Immunol Cell Biol **93**(5): 452-460.

Vereecke, L., R. Beyaert, et al. (2009). "The ubiquitin-editing enzyme A20 (TNFAIP3) is a central regulator of immunopathology." Trends in immunology **30**(8): 383-391.

Verhelst, K., I. Carpentier, et al. (2012). "A20 inhibits LUBAC-mediated NF-kappaB activation by binding linear polyubiquitin chains via its zinc finger 7." EMBO J **31**(19): 3845-3855.

Verstrepen, L., I. Carpentier, et al. (2009). "ABINs: A20 binding inhibitors of NF-kappa B and apoptosis signaling." Biochemical pharmacology **78**(2): 105-114.

Verstrepen, L., K. Verhelst, et al. (2011). "TAX1BP1, a ubiquitin-binding adaptor protein in innate immunity and beyond." Trends in biochemical sciences **36**(7): 347-354.

Vince, J. E., W. W. Wong, et al. (2007). "IAP antagonists target cIAP1 to induce TNFalpha-dependent apoptosis." Cell **131**(4): 682-693.

Wagner, K. W., E. A. Punnoose, et al. (2007). "Death-receptor O-glycosylation controls tumor-cell sensitivity to the proapoptotic ligand Apo2L/TRAIL." Nature medicine **13**(9): 1070-1077.

Wallace, D. J., W. Stohl, et al. (2009). "A phase II, randomized, double-blind, placebo-controlled, dose-ranging study of belimumab in patients with active systemic lupus erythematosus." Arthritis Rheum **61**(9): 1168-1178.

Wang, K., M. Li, et al. (2010). "ANNOVAR: functional annotation of genetic variants from high-throughput sequencing data." Nucleic Acids Res **38**(16): e164.

Warnatz, K., U. Salzer, et al. (2009). "B-cell activating factor receptor deficiency is associated with an adult-onset antibody deficiency syndrome in humans." Proc Natl Acad Sci U S A **106**(33): 13945-13950.

Wehr, C., T. Kivioja, et al. (2008). "The EUROclass trial: defining subgroups in common variable immunodeficiency." Blood **111**(1): 77-85.

Weih, D. S., Z. B. Yilmaz, et al. (2001). "Essential role of RelB in germinal center and marginal zone formation and proper expression of homing chemokines." J Immunol **167**(4): 1909-1919.

Wengraf, D. A., A. J. McDonagh, et al. (2008). "Genetic analysis of autoimmune regulator haplotypes in alopecia areata." Tissue Antigens **71**(3): 206-212.

Wertz, I. E., K. M. O'Rourke, et al. (2004). "De-ubiquitination and ubiquitin ligase domains of A20 downregulate NF-kappaB signalling." Nature **430**(7000): 694-699.

Willis, T. G., D. M. Jadayel, et al. (1999). "Bcl10 is involved in t(1;14)(p22;q32) of MALT B cell lymphoma and mutated in multiple tumor types." Cell **96**(1): 35-45.

Won, M., K. A. Park, et al. (2010). "Novel anti-apoptotic mechanism of A20 through targeting ASK1 to suppress TNF-induced JNK activation." Cell Death Differ **17**(12): 1830-1841.

Wu, H., S. A. Boackle, et al. (2007). "Association of a common complement receptor 2 haplotype with increased risk of systemic lupus erythematosus." Proc Natl Acad Sci U S A **104**(10): 3961-3966.

Wu, M., H. Lee, et al. (1996). "Inhibition of NF-kappaB/Rel induces apoptosis of murine B cells." EMBO J **15**(17): 4682-4690.

Wu, W. and X. Zhang (2007). "Characterization of a Rab GTPase up-regulated in the shrimp Peneaus japonicus by virus infection." Fish Shellfish Immunol **23**(2): 438-445.

Xiao, G., A. Fong, et al. (2004). "Induction of p100 processing by NF-kappaB-inducing kinase involves docking IkappaB kinase alpha (IKKalpha) to p100 and IKKalpha-mediated phosphorylation." The Journal of biological chemistry **279**(29): 30099-30105.

Xiao, G., E. W. Harhaj, et al. (2001). "NF-kappaB-inducing kinase regulates the processing of NF-kappaB2 p100." Mol Cell **7**(2): 401-409.

Xie, P., L. L. Stunz, et al. (2007). "Tumor necrosis factor receptor-associated factor 3 is a critical regulator of B cell homeostasis in secondary lymphoid organs." Immunity **27**(2): 253-267.

Yang, H., S. C. Masters, et al. (2001). "The proapoptotic protein Bad binds the amphipathic groove of 14-3-3zeta." Biochim Biophys Acta **1547**(2): 313-319.

Yilmaz, Z. B., D. S. Weih, et al. (2003). "RelB is required for Peyer's patch development: differential regulation of p52-RelB by lymphotoxin and TNF." The EMBO journal **22**(1): 121-130.

Zarnegar, B., S. Yamazaki, et al. (2008). "Control of canonical NF-kappaB activation through the NIK-IKK complex pathway." Proc Natl Acad Sci U S A **105**(9): 3503-3508.

Zarnegar, B. J., Y. Wang, et al. (2008). "Noncanonical NF-kappaB activation requires coordinated assembly of a regulatory complex of the adaptors cIAP1, cIAP2, TRAF2 and TRAF3 and the kinase NIK." Nature immunology **9**(12): 1371-1378.

Zhang, X., H. Wang, et al. (2007). "A role for the IkappaB family member Bcl-3 in the control of central immunologic tolerance." Immunity **27**(3): 438-452.

Zhou, Q., H. Wang, et al. (2016). "Loss-of-function mutations in TNFAIP3 leading to A20 haploinsufficiency cause an early-onset autoinflammatory disease." Nat Genet **48**(1): 67-73.

Zhu, M., R. K. Chin, et al. (2006). "NF-kappaB2 is required for the establishment of central tolerance through an Aire-dependent pathway." J Clin Invest **116**(11): 2964-2971.

Zhu, M. and Y. Fu (2010). "The complicated role of NF-kappaB in T-cell selection." Cell Mol Immunol **7**(2): 89-93.

6 Appendex

Appendex I. DNA sequences

A20 cDNA

```
   1 TGCCTTGACCAGGACTTGGGACTTTGCGAAAGGATCGCGGGGCCCGGAGAGGTGTTGGAG
  61 AGCACAATGGCTGAACAAGTCCTTCCTCAGGCTTTGTATTTGAGCAATATGCGGAAAGCT
 121 GTGAAGATACGGGAGAGAACTCCAGAAGACATTTTTAAACCTACTAATGGGATCATTCAT
 181 CATTTTAAAACCATGCACCGATACACACTGGAAATGTTCAGAACTTGCCAGTTTTGTCCT
 241 CAGTTTCGGGAGATCATCCACAAAGCCCTCATCGACAGAAACATCCAGGCCACCCTGGAA
 301 AGCCAGAAGAAACTCAACTGGTGTCGAGAAGTCCGGAAGCTTGTGGCGCTGAAAACGAAC
 361 GGTGACGGCAATTGCCTCATGCATGCCACTTCTCAGTACATGTGGGGCGTTCAGGACACA
 421 GACTTGGTACTGAGGAAGGCGCTGTTCAGCACGCTCAAGGAAACAGACACACGCAACTTT
 481 AAATTCCGCTGGCAACTGGAGTCTCTCAAATCTCAGGAATTTGTTGAAACGGGGCTTTGC
 541 TATGATACTCGGAACTGGAATGATGAATGGGACAATCTTATCAAAATGGCTTCCACAGAC
 601 ACACCCATGGCCCGAAGTGGACTTCAGTACAACTCACTGGAAGAAATACACATATTTGTC
 661 CTTTGCAACATCCTCAGAAGGCCAATCATTGTCATTTCAGACAAAATGCTAAGAAGTTTG
 721 GAATCAGGTTCCAATTTCGCCCCTTTGAAAGTGGGTGGAATTTACTTGCCTCTCCACTGG
 781 CCTGCCCAGGAATGCTACAGATACCCCATTGTTCTCGGCTATCACAGCCATCATTTTGTA
 841 CCCTTGGTGACCCTGAAGGACAGTGGGCCTGAAATCCGAGCTGTTCCACTTGTTAACAGA
 901 GACCGGGGAAGATTTGAAGACTTAAAAGTTCACTTTTTGACAGATCCTGAAAATGAGATG
 961 AAGGAGAAGCTCTTAAAAGAGTACTTAATGGTGATAGAAATCCCCGTCCAAGGCTGGGAC
1021 CATGGCACAACTCATCTCATCAATGCCGCAAAGTTGGATGAAGCTAACTTACCAAAAGAA
1081 ATCAATCTGGTAGATGATTACTTTGAACTTGTTCAGCATGAGTACAAGAAATGGCAGGAA
1141 AACAGCGAGCAGGGGAGGAGAGAGGGGCACGCCCAGAATCCCATGGAACCTTCCGTGCCC
1201 CAGCTTTCTCTCATGGATGTAAAATGTGAAACGCCCAACTGCCCCTTCTTCATGTCTGTG
1261 AACACCCAGCCTTTATGCCATGAGTGCTCAGAGAGGCGGCAAAAGAATCAAAACAAACTC
1321 CCAAAGCTGAACTCCAAGCCGGGCCCTGAGGGGCTCCCTGGCATGGCGCTCGGGGCCTCT
1381 CGGGGAGAAGCCTATGAGCCCTTGGCGTGGAACCCTGAGGAGTCCACTGGGGGGCCTCAT
1441 TCGGCCCCACCGACAGCACCCAGCCCTTTTCTGTTCAGTGAGACCACTGCCATGAAGTGC
1501 AGGAGCCCCGGCTGCCCCTTCACACTGAATGTGCAGCACAACGGATTTTGTGAACGTTGC
1561 CACAACGCCCGGCAACTTCACGCCAGCCACGCCCCAGACCACACAAGGCACTTGGATCCC
1621 GGGAAGTGCCAAGCCTGCCTCCAGGATGTTACCAGGACATTTAATGGGATCTGCAGTACT
1681 TGCTTCAAAAGGACTACAGCAGAGGCCTCCTCCAGCCTCAGCACCAGCCTCCCTCCTTCC
1741 TGTCACCAGCGTTCCAAGTCAGATCCCTCGCGGCTCGTCCGGAGCCCCTCCCCGCATTCT
1801 TGCCACAGAGCTGGAAACGACGCCCCTGCTGGCTGCCTGTCTCAAGCTGCACGGACTCCT
1861 GGGGACAGGACGGGGACGAGCAAGTGCAGAAAAGCCGGCTGCGTGTATTTTGGGACTCCA
1921 GAAAACAAGGGCTTTTGCACACTGTGTTTCATCGAGTACAGAGAAAACAAACATTTTGCT
1981 GCTGCCTCAGGGAAAGTCAGTCCCACAGCGTCCAGGTTCCAGAACACCATTCCGTGCCTG
2041 GGGAGGGAATGCGGCACCCTTGGAAGCACCATGTTTGAAGGATACTGCCAGAAGTGTTTC
2101 ATTGAAGCTCAGAATCAGAGATTTCATGAGGCCAAAAGGACAGAAGAGCAACTGAGATCG
2161 AGCCAGCGCAGAGATGTGCCTCGAACCACACAAAGCACCTCAAGGCCCAAGTGCGCCCGG
2221 GCCTCCTGCAAGAACATCCTGGCCTGCCGCAGCGAGGAGCTCTGCATGGAGTGTCAGCAT
2281 CCCAACCAGAGGATGGGCCCTGGGGCCCACCGGGGTGAGCCTGCCCCCGAAGACCCCCCC
2341 AAGCAGCGTTGCCGGGCCCCCGCCTGTGATCATTTTGGCAATGCCAAGTGCAACGGCTAC
2401 TGCAACGAATGCTTTCAGTTCAAGCAGATGTATGGCTAACCGGAAACAGGTGGGTCACCT
2461 CCTGCAAGAAGTGGGGCCTCGAGCTGTCAGTCATCATGGTGCTATCCTCTGAACCCCTCA
```

TAX1BP1cDNA

```
   1 GGAAGAGACCGCCCCGTGGGCGGAAGTGACGCAAGGCCTACTGTCGGCTGGGAGGGGAGG
  61 TGTAGCCGGTCTTTGGGGGTAGGCGGTAGTGGCGGAAGAGGTTCGGCGGCTGATGGCGGA
 121 TCAGGATCGGAAGCCTGCGTAACTTTCTCCCTTGATCCGGGAGTCTTTCCACTGGATTCA
 181 CAATGACATCCTTTCAAGAAGTCCCATTGCAGACTTCCAACTTTGCCCATGTCATCTTTC
 241 AAAATGTGGCCAAGAGTTACCTTCCTAATGCACACCTGGAATGTCATTACACCTTAACTC
 301 CATATATTCATCCACATCCAAAAGATTGGGTTGGTATATTCAAGGTTGGATGGAGTACTG
 361 CTCGTGATTATTACACGTTTTTATGGTCCCCTATGCCTGAACATTATGTGGAAGGATCAA
 421 CAGTCAATTGTGTACTAGCATTCCAAGGATATTACCTTCCAAATGATGATGGAGAATTTT
 481 ATCAGTTCTGTTACGTTACCCATAAGGGTGAAATTCGTGGAGCAAGTACACCTTTCCAGT
 541 TTCGAGCTTCTTCTCCAGTTGAAGAGCTGCTTACTATGGAAGATGAAGGAAATTCTGACA
 601 TGTTAGTGGTGACCACAAAAGCAGGCCTTCTTGAGTTGAAAATTGAGAAAACCATGAAAG
 661 AAAAAGAAGAACTGTTAAAGTTAATTGCCGTTCTGGAAAAAGAAACAGCACAACTTCGAG
 721 AACAAGTTGGGAGAATGGAAAGAGAACTTAACCATGAGAAAGAAAGATGTGACCAACTGC
 781 AAGCAGAACAAAAGGGTCTTACTGAAGTAACACAAAGCTTAAAAATGGAAAATGAAGAGT
 841 TTAAGAAGAGGTTCAGTGATGCTACATCCAAAGCCCATCAGCTTGAGGAAGATATTGTGT
 901 CAGTAACACATAAAGCAATTGAAAAAGAAACCGAATTAGACAGTTTAAAGGACAAACTCA
 961 AGAAGGCACAACATGAAAGAGAACAACTTGAATGTCAGTTGAAGACAGAGAAGGATGAAA
1021 AGGAACTTTATAAGGTACATTTGAAGAATACAGAAATAGAAAATACCAAGCTTATGTCAG
1081 AGGTCCAGACTTTAAAAAATTTAGATGGGAACAAAGAAAGCGTGATTACTCATTTCAAAG
1141 AAGAGATTGGCAGGCTGCAGTTATGTTTGGCTGAAAAGGAAAATCTGCAAAGAACTTTCC
1201 TGCTTACAACCTCAAGTAAAGAAGATACTTGTTTTTTAAAGGAGCAACTTCGTAAAGCAG
1261 AGGAACAGGTTCAGGCAACTCGGCAAGAAGTTGTCTTTCTGGCTAAAGAACTCAGTGATG
1321 CTGTCAACGTACGAGACAGAACGATGGCAGACCTGCATACTGCACGCTTGGAAAACGAGA
1381 AAGTGAAAAAGCAGTTAGCTGATGCAGTGGCAGAACTTAAACTAAATGCTATGAAAAAAG
1441 ATCAGGACAAGACTGATACACTGGAACACGAACTAAGAAGAGAAGTTGAAGATCTGAAAC
1501 TCCGTCTTCAGATGGCTGCAGACCATTATAAAGAAAAATTTAAGGAATGCCAAAGGCTCC
1561 AAAAACAAATAAACAAACTTTCAGATCAATCAGCTAATAATAATAATGTCTTCACAAAGA
1621 AAACGGGGAATCAGCAGAAAGTGAATGATGCTTCAGTAAACACAGACCCAGCCACTTCTG
1681 CCTCTACTGTAGATGTAAAGCCATCACCTTCTGCAGCAGAGGCAGATTTTGACATAGTAA
1741 CAAAGGGGCAAGTCTGTGAAATGACCAAAGAAATTGCTGACAAAACAGAAAAGTATAATA
1801 AATGTAAACAACTCTTGCAGGATGAGAAAGCAAAATGCAATAAATATGCTGATGAACTTG
1861 CAAAAATGGAGCTGAAATGGAAAGAACAAGTGAAAATTGCTGAAAATGTAAAACTTGAAC
1921 TAGCTGAAGTACAGGACAATTATAAAGAACTTAAAAGGAGTCTAGAAAATCCAGCAGAAA
1981 GGAAAATGGAAGATGGAGCAGATGGTGCTTTTTACCCAGATGAAATACAAAGGCCACCTG
2041 TCAGAGTCCCCTCTTGGGGACTGGAAGACAATGTTGTCTGCAGCCAGCCTGCTCGAAACT
2101 TTAGTCGGCCTGATGGCTTAGAGGACTCTGAGGATAGCAAAGAAGATGAGAATGTGCCTA
2161 CTGCTCCTGATCCTCCAAGTCAACATTTACGTGGGCATGGGACAGGCTTTTGCTTTGATT
2221 CCAGCTTTGATGTTCACAAGAAGTGTCCCCTCTGTGAGTTAATGTTTCCTCCTAACTATG
2281 ATCAGAGCAAATTTGAAGAACATGTTGAAAGTCACTGGAAGGTGTGCCCGATGTGCAGCG
2341 AGCAGTTCCCTCCTGACTATGACCAGCAGGTGTTTGAAAGGCATGTGCAGACCCATTTTG
2401 ATCAGAATGTTCTAAATTTTGACTAGTTACTTTTTTATTATGAGTTAATATAGTTTAGCAG
2461 TAAAAAAAAAAAAAAAAA
```

NIK cDNA

```
    ATGAGCACAAGCCTGGGAGATGGCAGTGAT
 121 GGAAATGGCCTGCCCAGGTGCCCCTGGCTCAGCAGTGGGGCAGCAGAAGGAACTCCCCAA
 181 AGCCAAGGAGAAGACGCCGCCACTGGGGAAGAAACAGAGCTCCGTCTACAAGCTTGAGGC
 241 CGTGGAGAAGAGCCCTGTGTTCTGCGGAAAGTGGGAGATCCTGAATGACGTGATTACCAA
 301 GGGCACAGCCAAGGAAGGCTCCGAGGCAGGGCCAGCTGCCATCTCTATCATCGCCCAGGC
 361 TGAGTGTGAGAATAGCCAAGAGTTCAGCCCCACCTTTTCAGAACGCATTTTCATCGCTGG
 421 GTCCAAACAGTACAGCCAGTCCGAGAGTCTTGATCAGATCCCCAACAATGTGGCCCATGC
 481 TACAGAGGGCAAAATGGCCCGTGTGTGTTGGAAGGGAAAGCGTCGCAGCAAAGCCCGGAA
 541 GAAACGGAAGAAGAAGAGCTCAAAGTCCCTGGCTCATGCAGGAGTGGCCTTGGCCAAACC
 601 CCTCCCCAGGACCCCTGAGCAGGAGAGCTGCACCATCCCAGTGCAGGAGGATGAGTCTCC
 661 ACTCGGCGCCCCATATGTTAGAAACACCCCGCAGTTCACCAAGCCTCTGAAGGAACCAGG
 721 CCTTGGGCAACTCTGTTTTAAGCAGCTTGGCGAGGGCCTACGGGCTCTGCCTCGATCAGA
 781 ACTCCACAAACTGATCAGCCCCTTGCAATGTCTGAACCACGTGTGGAAACTGCACCACCC
 841 CCAGGACGGAGGCCCCCTGCCCCTGCCCACGCACCCCTTCCCCTATAGCAGACTGCCTCA
 901 TCCCTTCCCATTCCACCCTCTCCAGCCCTGGAAACCTCACCCTCTGGAGTCCTTCCTGGG
 961 CAAACTGGCCTGTGTAGACAGCCAGAAACCCTTGCCTGACCCACACCTGAGCAAACTGGC
1021 CTGTGTAGACAGTCCAAAGCCCCTGCCTGGCCCACACCTGGAGCCCAGCTGCCTGTCTCG
1081 TGGTGCCCATGAGAAGTTTTCTGTGGAGGAATACCTAGTGCATGCTCTGCAAGGCAGCGT
1141 GAGCTCAGGCCAGGCCCACAGCCTGACCAGCCTGGCCAAGACCTGGGCAGCAAGGGGCTC
1201 CAGATCCCGGGAGCCCAGCCCCAAAACTGAGGACAACGAGGGTGTCCTGCTCACTGAGAA
1261 ACTCAAGCCAGTGGATTATGAGTACCGAGAAGAAGTCCACTGGGCCACGCACCAGCTCCG
1321 CCTGGGCAGAGGCTCCTTCGGAGAGGTGCACAGGATGGAGGACAAGCAGACTGGCTTCCA
1381 GTGCGCTGTCAAAAAGGTGCGGCTGGAAGTATTTCGGGCAGAGGAGCTGATGGCATGTGC
1441 AGGATTGACCTCACCCAGAATTGTCCCTTTGTATGGAGCTGTGAGAGAAGGGCCTTGGGT
1501 CAACATCTTCATGGAGCTGCTGGAAGGTGGCTCCCTGGGCCAGCTGGTCAAGGAGCAGGG
1561 CTGTCTCCCAGAGGACCGGGCCCTGTACTACCTGGGCCAGGCCCTGGAGGGTCTGGAATA
1621 CCTCCACTCACGAAGGATTCTGCATGGGGACGTCAAAGCTGACAACGTGCTCCTGTCCAG
1681 CGATGGGAGCCACGCAGCCCTCTGTGACTTTGGCCATGCTGTGTGTCTTCAACCTGATGG
1741 CCTGGGAAAGTCCTTGCTCACAGGGGACTACATCCCTGGCACAGAGACCCACATGGCTCC
1801 GGAGGTGGTGCTGGGCAGGAGCTGCGACGCCAAGGTGGATGTCTGGAGCAGCTGCTGTAT
1861 GATGCTGCACATGCTCAACGGCTGCCACCCCTGGACTCAGTTCTTCCGAGGGCCGCTCTG
1921 CCTCAAGATTGCCAGCGAGCCTCCGCCTGTGAGGGAGATCCCACCCTCCTGCGCCCCTCT
1981 CACAGCCCAGGCCATCCAAGAGGGGCTGAGGAAAGAGCCCATCCACCGCGTGTCTGCAGC
2041 GGAGCTGGGAGGGAAGGTGAACCGGGCACTACAGCAAGTGGGAGGTCTGAAGAGCCCTTG
2101 GAGGGGAGAATATAAAGAACCAAGACATCCACCGCCAAATCAAGCCAATTACCACCAGAC
2161 CCTCCATGCCCAGCCGAGAGAGCTTTCGCCAAGGGCCCCAGGGCCCCGGCCAGCTGAGGA
2221 GACAACAGGCAGAGCCCCTAAGCTCCAGCCTCCTCTCCCACCAGAGCCCCCAGAGCCAAA
2281 CAAGTCTCCTCCCTTGACTTTGAGCAAGGAGGAGTCTGGGATGTGGGAACCCTTACCTCT
2341 GTCCTCCCTGGAGCCAGCCCCTGCCAGAAACCCCAGCTCACCAGAGCGGAAAGCAACCGT
2401 CCCGGAGCAGGAACTGCAGCAGCTGGAAATAGAATTATTCCTCAACAGCCTGTCCCAGCC
2461 ATTTTCTCTGGAGGAGCAGGAGCAAATTCTCTCGTGCCTCAGCATCGACAGCCTCTCCCT
2521 GTCGGATGACAGTGAGAAGAACCCATCAAAGGCCTCTCAAAGCTCGCGGGACACCCTGAG
2581 CTCAGGCGTACACTCCTGGAGCAGCCAGGCCGAGGCTCGAAGCTCCAGCTGGAACATGGT
2641 GCTGGCCCGGGGGCGGCCCACCGACACCCCAAGCTATTTCAATGGTGTGAAAGTCCAAAT
2701 ACAGTCTCTTAATGGTGAACACCTGCACATCCGGGAGTTCCACCGGGTCAAAGTGGGAGA
2761 CATCGCCACTGGCATCAGCAGCCAGATCCCAGCTGCAGCCTTCAGCTTGGTCACCAAAGA
2821 CGGGCAGCCTGTTCGCTACGACATGGAGGTGCCAGACTCGGGCATCGACCTGCAGTGCAC
2881 ACTGGCCCCTGATGGCAGCTTCGCCTGGAGCTGGAGGGTCAAGCATGGCCAGCTGGAGAA
2941 CAGGCCCTAACCCTGCCCTCCACCGCCGGCTCCAC
```

NFKB2 from BIOMATIK

```
gctagcATGGAGAGTTGCTACAACCCAGGTCTGGATGGTATTATTGAATATGATGATTTCAAATTGAACTCCTC
CATTGTGGAACCCAAGGAGCCAGCCCCAGAAACAGCTGATGGCCCCTACCTGGTGATCGTGGAACAGCCTAAGC
AGAGAGGCTTCCGATTTCGATATGGCTGTGAAGGCCCCTCCCATGGAGGACTGCCCGGTGCCTCCAGTGAGAAG
GGCCGAAAGACCTATCCCACTGTCAAGATCTGTAACTACGAGGGACCAGCCAAGATCGAGGTGGACCTGGTAAC
ACACAGTGACCCACCTCGTGCTCATGCCCACAGTCTGGTGGGCAAGCAATGCTCGGAGCTGGGGATCTGCGCCG
```

TTTCTGTGGGGCCCAAGGACATGACTGCCCAATTTAACAACCTGGGTGTCCTGCATGTGACTAAGAAGAACATG
ATGGGGACTATGATACAAAAACTTCAGAGGCAGCGGCTCCGCTCTAGGCCCCAGGGCCTTACGGAGGCCGAGCA
GCGGGAGCTGGAGCAAGAGGCCAAAGAACTGAAGAAGGTGATGGATCTGAGTATAGTGCGGCTGCGCTTCTCTG
CCTTCCTTAGAGCCAGTGATGGCTCCTTCTCCCTGCCCCTGAAGCCAGTCATCTCCCAGCCCATCCATGACAGC
AAATCTCCGGGGGCATCAAACCTGAAGATTTCTCGAATGGACAAGACAGCAGGCTCTGTGCGGGGTGGAGATGA
AGTTTATCTGCTTTGTGACAAGGTGCAGAAAGATGACATTGAGGTTCGGTTCTATGAGGATGATGAGAATGGAT
GGCAGGCCTTTGGGGACTTCTCTCCCACAGATGTGCATAAACAGTATGCCATTGTGTTCCGGACACCCCCCTAT
CACAAGATGAAGATTGAGCGGCCTGTAACAGTGTTTCTGCAACTGAAACGCAAGCGAGGAGGGGACGTGTCTGA
TTCCAAACAGTTCACCTATTACCCTCTGGTGGAAGACAAGGAAGAGGTGCAGCGGAAGCGGAGGAAGGCCTTGC
CCACCTTCTCCCAGCCCTTCGGGGGTGGCTCCCACATGGGTGGAGGCTCTGGGGGTGCAGCCGGGGGCTACGGA
GGAGCTGGAGGAGGTGGCAGCCTCGGTTTCTTCCCCTCCTCCCTGGCCTACAGCCCCTACCAGTCCGGCGCGGG
CCCCATGGGCTGCTACCCGGGAGGCGGGGGCGGGGCGCAGATGGCCGCCACGGTGCCCAGCAGGGACTCCGGGG
AGGAAGCCGCGGAGCCAAGCGCCCCCTCCAGGACCCCCCAGTGCGAGCCGCAGGCCCCGGAGATGCTGCAGCGA
GCTCGAGAGTACAACGCGCGCCTGTTCGGCCTGGCGCAGCGCAGCGCCCGAGCCCTACTCGACTACGGCGTCAC
CGCGGACGCGCGCGCGCTGCTGGCGGGACAGCGCCACCTGCTGACGGCGCAGGACGAGAACGGAGACACACCAC
TGCACCTAGCCATCATCCACGGGCAGACCAGTGTCATTGAGCAGATAGTCTATGTCATCCACCACGCCCAGGAC
CTCGGCGTTGTCAACCTCACCAACCACCTGCACCAGACGCCCCTGCACCTGGCGGTGATCACGGGGCAGACGAG
TGTGGTGAGCTTTCTGCTGCGGGTAGGTGCAGACCCAGCTCTGCTGGATCGGCATGGAGACTCAGCCATGCATC
TGGCGCTGCGGGCAGGCGCTGGTGCTCCTGAGCTGCTGCGTGCACTGCTTCAGAGTGGAGCTCCTGCTGTGCCC
CAGCTGTTGCATATGCCTGACTTTGAGGGACTGTATCCAGTACACCTGGCAGTCCGAGCCCGAAGCCCTGAGTG
CCTGGATCTGCTGGTGGACAGTGGGGCTGAAGTGGAGGCCACAGAGCGGCAGGGGGGACGAACAGCCTTGCATC
TAGCCACAGAGATGGAGGAGCTGGGGTTGGTCACCCATCTGGTCACCAAGCTCCGGGCCAACGTGAACGCTCGC
ACCTTTGCGGGAAACACACCCCTGCACCTGGCAGCTGGACTGGGGTACCCGACCCTCACCCGCCTCCTTCTGAA
GGCTGGTGCTGACATCCATGCTGAAAACGAGGAGCCCCTGTGCCCACTGCCTTCACCCCCTACCTCTGATAGCG
ACTCGGACTCTGAAGGGCCTGAGAAGGACACCCGAAGCAGCTTCCGGGGCCACACGCCTCTTGACCTCACTTGC
AGCACCAAGGTGAAGACCTTGCTGCTAAATGCTGCTCAGAACACCATGGAGCCACCCCTGACCCCGCCCAGCCC
AGCAGGGCCGGGACTGTCACTTGGTGATACAGCTCTGCAGAACCTGGAGCAGCTGCTAGACGGGCCAGAAGCCC
AGGGCAGCTGGGCAGAGCTGGCAGAGCGTCTGGGGCTGCGCAGCCTGGTAGACACGTACCGACAGACAACCTCA
CCCAGTGGCAGCCTCCTGCGCAGCTACGAGCTGGCTGGCGGGGACCTGGCAGGTCTACTGGAGGCCCTGTCTGA
CATGGGCCTAGAGGAGGGAGTGAGGCTGCTGAGGGGTCCAGAAACCCGAGACAAGCTGCCCAGCACAGCAGAGG
TGAAGGAAGACAGTGCGTACGGGAGCCAGTCAGTGGAGCAGGAGGCAGAGAAGCTGGGCCCACCCCCTGAGCCA
CCAGGAGGGCTCTGCCACGGGCACCCCCAGCCTCAGGTGCACTGAggatcc

Appendix II. Antibody cocktail mix

1. B cells

Marker	Fluorescent	Ratio	volume
CD19	Pecy7	1:80	12.5
CD3	APC	1:10	100
CD27	FITC	1:20	50
CD38	V450	1:300	3.3
FACS wash			834.2

2. 10 colour B cells

	Marker	Fluorescent	Ratio	volume
1st staining	CD19	Pecy7	1:80	12.5
	CD3	AF700	1:50	20
	CD27	APC	1:80	12.5
	CD21	PerCP Cy5.5	1:100	10
	CD38	V450	1:160	6.25
	CD24	CF594	1:20	50
	IgM	FITC	1:120	8.3
	IgD	PE	1:80	12.5
	IgA	Biotin	1:320	3.1
	FACS wash			864.8
2nd staining	Streptavidin	V500	1:1600	0.63
	FACS wash			999.4

3. Transitional B cells

Marker	Fluorescent	Ratio	volume
CD19	Pecy7	1:80	12.5
CD3	FITC	1:100	10
CD27	APC	1:80	12.5
CD21	PeCy5	1:100	10
CD10	PE	1:20	50
FACS wash			905

4. T cell distribution

Marker	Fluorescent	Ratio	volume
CD3	FITC	1:100	10
CD4	PerCP	1:20	50
CD8	PE	1:200	5
CD45RA	Pacific Blue	1:300	3.3
CCR7	Pecy7	1:20	50
FACS wash			876.7

5. Tfh and Effector T cells

Marker	Fluorescent	Ratio	volume
CD3	APC	1:10	100
CD4	PerCP	1:20	50
CD45RA	FITC	1:10	100
CXCR3	BV510	1:40	25
CCR6	PE	1:20	50
CCR7	Pecy7	1:20	50
FACS wash			625

6. Treg

	Marker	Fluorescent	Ratio	volume
Surface	CD4	PerCP	1:50	20
	CD25	APC	1:6	167
	CD127	FITC	1:20	50
	FACS wash			763
intercellular	FoxP3	PE	1:6	167
	FACS wash			833

Appendix III Gene lists

NF-kB target genes

AHR, BANK1, BATF, BCL2, BCL2A1, BCL2L1, BIRC2, BIRC3, BUB1B, CCL2, CCL22, CCL3, CCL4, CCND2, CCR4, CCR7, CD36, CD40, CD40LG, CD44, CD69, CD82, CD83, CFLAR, CISH, CSF2, CX3CL1, CXCL1, CXCL10, CXCL13, CXCL2, CXCL9, CXCR7, DUSP1, DUSP2, EBI3, EGR1, ELL2, EMR1, FAS, FGF12, FNDC3A, GADD45B, HLA-F, HSPA1L, ICAM1, ID2, IER2, IER3, IL10, IL15RA, IL1B, IL2, IL2RA, IL32, IL6, IL8, IRF1, IRF4, JUNB, KLF10, LSP1, LTA, LYN, MAP3K1, MAP3K8, MYB, NCL, NFKB1, NFKB2, NFKBIA, NFKBIE, PASK, PIM1, PIM2, PLEK, PRKCD, PRPF4B, PTGS2, PTPN1, PTPN3, RASGRP1, REL, RELB, RET, RFTN1, RGS1, RRAS2, SDC4, SELL, SLAMF7, SLC2A5, SMAD7, SMARCA2, SOCS2, SOD2, SPI1, STAT1, STAT5A, STX4, TNF, TNFAIP3, TNIP2, TPMT, TRAF1, VIM, WTAP, ZFP36L1

BLK pathway genes

ABL1, B4GALT1, CL2L1, BCL2L11, BLK, BLNK, BMX, BTK, CBL, CBLB, CD19, CD72,CD79A, CD79B, DAPP1, DCLRE1C, ECSIT, EPO, FADD, FASLG, FCER1A, FCER1G, FGR, FOS, FYN, GAPDH, GP6, GRAP2, GRB2, GTF2I, HCK, HRAS, IBTK, IGHE, INPP5D, IRAK1, IRAK2, IRAK3, IRAK4, ITK, ITPR3, JAK1, JAK2, JUN, KHDRBS1, KIT, LCK, LYN, MAP3K1, MYD88, NCK1, PIK3AP1, PIK3CA, PIK3CB, PIK3CD, PIK3CG, PIK3R1, PIK3R2, PIK3R3, PIK3R5, PIP4K2A, PLCG1, PLCG2, PLCG2, PLEK, PRKCA, PRKCB, PRKCE, PRKCQ, PRKCZ, PRKD1, PTPN6, RAC1, RELA, RPS6KB1, SH3BP5, SH3KBP1, SIGIRR, SOS1, SRC, STAT5A, SYK, TEC,

TIRAP, TLR4, TLR6, TLR8, TLR9, TNFRSF11A, TP53, TRAF6, TREM2, TYROBP, VAV1, VAV2, VAV3, WAS, ,YES1, ZAP70

A20 interacting gene list from BioGrid and string

ALDH9A1, ARRDC3, AXIN1, BECN1,BioGRid A20, BioGRid A20, BIRC2, BIRC3, CASP8, CCDC50, CHUK, CNKSR2, FADD, FBXO3, GIT2, GLDC, HSP90AA1, IKBKB, IKBKE, IKBKG, IL17A, IL17RA, IRAK1, IRAK2, IRF7, ITCH, KIF11, LAMP1, LAPTM5, LMP1, LRRC47, MALT1, MAP3K5, MCM6, NAF1, NDUFS1, NFKB1, NFKB2, NFKBIA, NXF1, OCLN, OLIG3, PPP2R1B, PPP6R3, PTPN22, RARRES3, RBCK1, RELA, RIPK1, RIPK2, RLIM, RNF11, RNF114, RNF31, RNF5, RNH1, RPS27A, SHARPIN, STAT4, TAX1BP1, TBK1, TICAM1, TNF, TNFAIP3, TNFRSF10B, TNFRSF1A, TNFSF10, TNIP1, TNIP2, TNIP3, TP53, TRADD, TRAF1, TRAF2, TRAF6, TRIM2, TRIM23, TRIM3, TRIM8, UBC, UBE2D1, UBE2N, YWHAB, YWHAE, YWHAG, YWHAH, YWHAQ, YWHAZ

Appendix VI Supplementary experiments

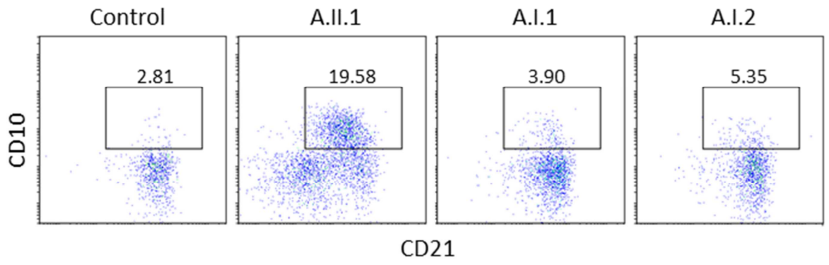

Supplementary Figure 1 Analysis of transitional B cells in A.II.1 and his family members. CD21 and CD10 were gated on CD19+ cells and CD21+ CD10+ cells represent transitional B cells

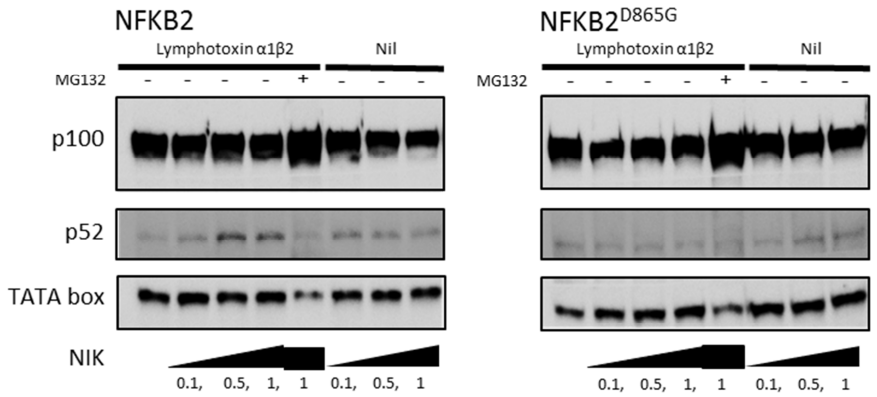

Supplementary Figure 2 Effect of D865>G mutation on NIK induced p100 processing with lympotoxin α1β2 stimulation. HEK293 cells were co-transfected with expression vectors encoding wild-type (WT) or D865 . G mutant NFKB2 together with varying amounts of MAP3K14 expression vector encoding NIK and after 24hours cells were simulated with lympotoxin α1β2 or PBS. Six hours prior to the stimulation MG132 was added and p100 and p52 detection by western blot